CHEMICAL REACTIVITY OF MICA SURFACES

A thesis submitted for the degree of
Doctor of Philosophy of the University of London

K.G. Bhattacharyya

Department of Chemistry
Imperial College
London SW7 2AY

NOVEMBER 1984

ABSTRACT

The chemical reactivity of air-cleaved and vacuum-cleaved mica surfaces has been studied with the expectation that mica might prove to be a useful model for solid acid catalysts. A carbonaceous overlayer was always present on the air-cleaved surface and this had to be removed by bombardment with hydrogen-atoms before adsorption experiments were commenced. The adsorption of carbon dioxide and ammonia on the clean mica surface was studied by temperature programmed desorption and X-ray photoelectron spectroscopy (XPS). Low energy electron diffraction and other techniques were also used to characterize the clean surface.

With carbon dioxide, a reversible state of chemisorption was observed, which desorbed at temperatures around 390K with second order kinetics, the activation energy being 94 $kJmol^{-1}$. However XPS measurements showed that most of the adsorbed carbon dioxide was held irreversibly up to a temperature of 670K. A mechanism in which carbon dioxide is adsorbed at hydroxylated silicon atoms to form a carbonate complex and a mobile proton has been proposed. Anomalous C1s photoemission peaks were observed when mica was cleaved in carbon dioxide and these are attributed to mosaic charge fields built up on the mica surface.

Two states of adsorption of ammonia were observed with activation energies for desorption of 76 and 122 $kJ\ mol^{-1}$ respectively. The kinetics of desorption was first order for both states. The XPS spectra showed a single, broad N1s peak at a binding energy of 400eV. The adsorption of ammonia at acidic sites on the mica surface has been described by a model similar to that used with zeolites and silica-

aluminas.

Mica flakes have been found to be active in catalyzing the isomerization of cyclopropane. Finally, it was found at the end of the work that potassium ions in the mica surface could be exchanged with ammonium ions by cleaving the mica under aqueous ammonia and keeping immersed in it.

ACKNOWLEDGEMENTS

I am very much indebted to my supervisor Dr D.O. Hayward for his guidance, encouragement and co-operation throughout the course of this work. Without his help it would have been impossible to complete this project on time.

I also wish to thank Dr M.A. Morris for his valuable assistance with the ESCALAB work. My thanks are also due to all my co-workers in Room 534 for constant encouragement and help.

I am particularly grateful to Mr C. Smith of the glass workshop of the Chemical Engineering Department for constructing the glass cell and for his ready assistance in modifications and various repair jobs.

My thanks are also due to all the members of the departmental glass, mechanical and electronic workshops for their co-operation during the course of this work and particularly to Mr B. Ratnasekara for constructing the Linear Temperature Control Unit. I am very grateful also to Mr G. Millhouse for preparing all the photographs for this thesis.

This work would not have been possible without a Commonwealth Academic Staff Scholarship from the Commonwealth Scholarship Commission in the U.K. and I am grateful to the Commission and to the British Council for the help they have offered during the stay in London. I also express gratitude to the University of Gauhati, Assam for granting me study-leave to take up this scholarship.

Finally, I like to thank Miss Tina Richardson for her prompt and careful typing of the manuscript.

CONTENTS

Page

Page

F I G U R E S

CHAPTER ONE

INTRODUCTION

1.1 DEVELOPMENT OF CATALYTIC CRACKING

Catalytic cracking of petroleum hydrocarbons has played a very important role in the development of present-day industries and in providing infra-structure for a lot more. New catalytic materials have been synthesized and developed to make the cracking process progressively more effective, producing a variety of products. Much work has also been done to understand the activity of the cracking catalysts and the cracking process itself.

The early stages of development of these catalysts was reviewed by Ryland, Tamele and Wilson (1960). As described by the authors, introduction of clay-minerals as catalysts during the late 1930's not only boosted the whole cracking process, but also made it possible to get a host of new products, not obtained in ordinary thermal cracking. The catalyst, however, gets deactivated rapidly through coke-formation and sulphur-deposition from the petroleum crude. Increasing the temperature of cracking simply accelerates the deactivation process. A suitable cracking catalyst would need to regenerate its active surface fairly easily, but such regeneration was difficult in case of clay-minerals.

After Loper (1955) reported the use of a new cracking catalyst, composed of a mixture of silica and alumina in the ratio 3:1, various concoctions of silica and alumina soon replaced the clay-minerals as principal cracking catalysts. With the silica-

aluminas, it was possible either to slow down or control the rate of coke-formation. A completely new dimension in catalytic cracking was opened up by Eastwood and co-workers (1962a, 1962b) with the use of synthetic zeolites as catalysts. The zeolite 'super-lattice' has a very wide range of distribution of cations with pores of different dimensions, cavities, windows and channels. Breck (1974) has shown that it is possible to prepare a zeolite framework meeting almost any requirement in catalytic cracking. According to Heinemann (1981), the zeolite structure can be tailored to meet the different requirements of heterogeneous catalysis by selective adsorption and reaction. Such versatility has given the zeolites almost a 90% share of the present-day market of cracking catalysts. The Y-faujasites, with their sodium cations replaced by hydrogen, rare-earth or alkaline-earth cations, have been known to be the best cracking catalysts after the work of Plank, Rosinsky and Hawthorne (1964). The introduction of ZSM-5 zeolites by Anganer and Landolt (1972) has further extended the use of zeolite catalysts.

1.2 CHOICE OF MICA AS A MODEL CATALYST

Natural mica, mainly muscovite, with the ideal formula $KAl_2Si_3AlO_{10}(OH)_2$, is an important clay-mineral and because of its excellent insulating properties, it has been used extensively in the electronic and electrical industries. Mica is, however, not known for any of the activities usually associated with the clay-minerals. The mica surface was thought to be very inert because of the presence of potassium ions, which are required to balance

the negative charge arising from substitution of silicon by aluminium in the mica structure.

The silicon-aluminium ratio of muscovite is nearly 1.00. This ratio is very small compared to that of the conventional cracking catalysts. In the case of zeolites, silica-aluminas or clay-mineral catalysts, it is now generally recognized that the main source of activity is the acidic sites, created by tetrahedral aluminium atoms. Whether similar acidic sites are generated by aluminium in tetrahedral positions in mica is not known. Even if generated, the difficulty remains about the accessibility of such acidic sites through the layer of potassium ions.

After prolonged heating, muscovite tends to lose some potassium as well as aluminium. For example, Löffler, Haller and Fenn (1979) noticed a decrease of the surface aluminium-silicon ratio of muscovite to 0.60 from near 1.00 after a long heating period at 873K or above. A corresponding decrease in potassium-content was also observed. Whether the apparent enhancement of silicon on the surface and loss of potassium was accompanied by an increase in activity was not studied. The nature of the hydroxyl groups in mica is also not known. The mica surface contains adsorbed water and it is possible that some of the potassium ions exist in the hydrated form. Whether dehydration can generate acidic sites on mica, as is common in the case of silica-aluminas or clay-mineral catalysts, has not been investigated.

The development of synthetic mica-montmorillonites (SMM), which have high catalytic activity for cracking reactions, put new emphasis on the need to evaluate the properties of the mica surface. Wright, Granquist and Kennedy (1972) have shown that SMM is comparable

to zeolites in catalytic activity. Surprisingly, the SMM structure is quite similar to the muscovite structure, the only difference being in the interlayer ions: while muscovite has potassium ions balancing the layer charge SMM has ammonium ions. On heating SMM, ammonia is released and an 'acidic' surface is obtained. As potassium depletion takes place from the muscovite surface on heating, it would be interesting to know in what form potassium leaves the surface and whether protons are generated to maintain charge-balance. Such a surface would be expected to be fairly active.

It is therefore possible that under suitable circumstances, the muscovite surface will emulate some of the properties of a conventional cracking catalyst. One interesting facet of the high activity of SMM is the role of edge effects; Wright, Granquist and Kennedy have suggested that the edges of SMM platelets are catalytically more active than the surface. Such effects may be equally likely in mica. If, under suitable conditions, mica does have some active sites, it will be an ideal model for the verification of many aspects of catalysis by clay-minerals, silica-aluminas as well as zeolites, particularly under UHV conditions. Muscovite mica is readily obtainable in single crystal form. The plate-like structure with perfect cleavage properties ensures that a clean surface can be obtained easily by cleavage in UHV. The difficulties in designing a suitable holder for powdered samples of zeolites, silica-aluminas or clay-minerals is also non-existent with mica. Mica, thus, stands as an ideal choice to model the complex aluminosilicate materials which have found so much application in today's industries. To present mica as a model catalyst, it is, however, necessary to

have a broad understanding of the nature and source of activity of this group of solid catalysts.

1.3 SURFACE ACIDITY OF SOLID CATALYSTS

1.3.1 DEFINITION OF A SOLID ACID

A number of industrially important reactions are catalyzed by clay-minerals, silica-aluminas and zeolites; these include cracking, isomerization, alkylation, polymerization, etc. All these reactions have one common feature: they are thought to proceed through a carbonium ion mechanism, as first proposed by Whitmore (1934). These reactions exhibit remarkable similarities to reactions catalyzed by mineral acids and also to reactions catalyzed by known acidic catalysts such as boron trifluoride and aluminium chloride. The acidic nature of catalysis by silica-alumina, clay-minerals and zeolites is further substantiated by the rapid deactivation of these materials by basic substances.

A solid acid is defined as one having a tendency to donate a proton (Brönsted acid) or to accept an electron pair (Lewis acid). The Brönsted acids generally consist of protons associated with surface anions and Lewis acids consist of incompletely coordinated surface ions.

Forni (1974) has shown that acidity of a solid surface can be described in toto by a knowledge of the acid strengths of all the available sites, the density of such sites on the surface and the nature of such sites in terms of Brönsted and Lewis acidity. Because of interdependence of strength and density of acid sites on each other and because of heterogeneous surface distribution of such sites,

it is often impossible to have an adequate description of surface acidity of a solid.

1.3.2 ACID STRENGTH

Walling (1950) defined the acid strength of a solid as its ability to convert a neutral base, adsorbed on its surface, into the corresponding conjugate acid. If this acid-base reaction takes place through the transfer of a proton from the solid surface to the adsorbed molecule (Brönsted acidity), the acid strength is given by the well-known Hammett function, H_o

$$H_o = - \log a_{H+} f_B / f_{BH^+}$$

or

$$H_o = pK_a + \log[B]/[BH^+] \qquad (1)$$

where a_{H+} is the proton activity, [B] and $[BH^+]$ are concentrations of the neutral base and its conjugate acid respectively, f_B and f_{BH^+} the corresponding activity coefficients and K_a is the dissociation constant of the acid. However, if the reaction takes place by means of electron pair transfer from the adsorbate to the solid surface, the Hammett function is given by

$$H_o = pK_a + \log[B]/[AB] \qquad (2)$$

where [AB] is the concentration of the addition product formed by the adsorption of the base B on the Lewis acid site of the solid surface.

While acid strengths of different materials containing only pure Brönsted acid sites may be compared, the same is not true for Lewis acid sites. Brown and Johanneson (1953), and also Brown and Kanner (1953) showed that strengths of Lewis acids depended on steric factors as well as on intrinsic coordinating abilities of atoms. The comparison of Lewis acids is also influenced by the particular base used. Because of these reasons, Benesi and Winquist (1978) remarked that the generalized Hammett function H_o has only limited application for the Lewis acids and therefore, equation (2) should be applied sparingly for such cases.

1.3.3 DETERMINATION OF SURFACE ACIDITY

The methods to determine acidity of solid surfaces have been extensively described and reviewed by Goldstein (1968), Tanabe (1970), Forni (1974) and Benesi and Winquist (1978). As in the case of mineral acids, solid acids can be titrated directly with a dilute base in an aqueous suspension. The disadvantages of this simple method are numerous. Water forms H_3O^+ with all Brönsted acid sites having an acid strength greater than that of H_3O^+, making it impossible to discriminate among Brönsted acid sites of different strengths. Water also creates new Brönsted acid sites by reacting with incompletely coordinated metal atoms and it may alter drastically the structural properties of many solids, including clay-minerals and zeolites.

A rapid qualitative estimate of acid strength is often made by adding a Hammett indicator to a nonaqueous suspension of the solid. Hammett indicators are organic bases having distinctive acid and base colours. Sufficient number of such indicators covering the whole range of solid acids are not always available and sometimes these indicators produce colour by processes other than proton addition. Leftin and Hobson (1963) and Drushel and Sommers (1966) have extended the useful range of Hammett indicators by applying spectrophotometric determination of the absorbances of a series of indicator-solid acid mixtures. From such absorbance measurements, Kotsarenko, Karakchiev and Dzisko (1968) have given the following order of relative acid strengths among the metal oxide-silica mixtures:

$$Al_2O_3.SiO_2 > ZrO_2.SiO_2 > Ga_2O_3.SiO_2 > BeO.SiO_2 \sim MgO.SiO_2 > Y_2O_2.SiO_2 > La_2O_3.SiO_2 > SnO.SiO_2 \sim PbO.SiO_2.$$

Johnson (1955), Benesi (1957) and Hirschler (1963) developed the amine-titration method for determining total acidity of a solid, using a suitable indicator. Benesi (1973) also showed that if a sterically hindered amine was used for titration, the Lewis acid sites could be selectively prevented from reaction, and Brönsted acidity alone could be measured. As Take, Nomizo and Yoneda (1973), and many other workers have shown, the direct titration of a solid acid with an amine generally yields higher acidity values than the actual number of acid sites.

1.3.4 INFRA-RED SPECTROSCOPIC METHOD

Complete characterization of surface-acidity, including determination of the number, strength and type of acid sites, is achieved with the infra-red spectroscopic method. The relative amounts of Brönsted and Lewis acid sites are determined from the relative intensities of absorption bands arising from the protonated and coordinated forms of an adsorbed amine. Relative strengths of the acid sites can also be determined from measurement of band intensities for a series of amines of different basicity.

Mapes and Eischens (1954) studied ammonia absorption on a silica-alumina cracking catalyst with the IR technique to show that the catalyst contained both Brönsted and Lewis acid sites. Pyridine is now preferred over ammonia for such determinations; pyridine, being a weak base, selectively attacks the strong acid sites and the pyridine-bands are comfortably away from the O-H stretching and H-O-H bending bands of water which often interfere with the ammonia bands. Piperidine, aniline, diethylamine, quinoline, butylamine and other bases are also equally used. The infra-red method has been widely used to determine the acidity of solid surfaces and a large literature has grown up on the subject.

1.3.5 GASEOUS BASE ADSORPTION METHOD

The acid strength of a catalyst surface is directly proportional to the strength with which a gaseous base is adsorbed on the surface. The general method consists in first eliminating volatile impurities from a solid surface by evacuation and heating or

flushing in an inert gas flow, and then exposing the surface to a gaseous base like ammonia or pyridine. The solid surface is then heated to desorb the gaseous base. The amount of gas desorbed will be a direct measure of the surface acidity and the desorption temperature will indicate the strength of the acidic sites. Before exposing the surface to the base, it is sometimes necessary to heat the solid in a flow of hydrogen or oxygen to get rid of less volatile impurities from the surface. The main advantage of this method is that acidity can be estimated under conditions similar to those under which the solid is used as a catalyst. There is a source of error, however, that can sometimes affect the measurements; besides actual chemisorption of the base on acidic sites, other types of surface reactions can occur which may make the results inaccurate. For example, Peri (1965) showed that while ammonia was mostly held undissociatively on a γ-alumina surface, some of the base molecules reacted with surface oxide ions, forming NH_2^- + OH^- ion-pairs.

It is however not always possible to relate the surface acidity values determined by this gaseous base adsorption method to the catalytic activity of a solid. Clark, Holm and Blackburn (1962) showed that for a series of silica-aluminas, the isosteric heat of adsorption dropped rapidly as coverage for ammonia increased, and at low coverages, the isosteric heat was highest for pure γ-alumina. On this basis γ-alumina is expected to have maximum activity for acid-catalysis. On the contrary, as Holm and Clark (1963) have later shown, the catalytic activity of the silica-aluminas for O-xylene isomerization and other reactions actually increases with rising silica content, reaching a maximum for approximately 85% silica, 15% alumina. These typical results are shown in Fig. 1a

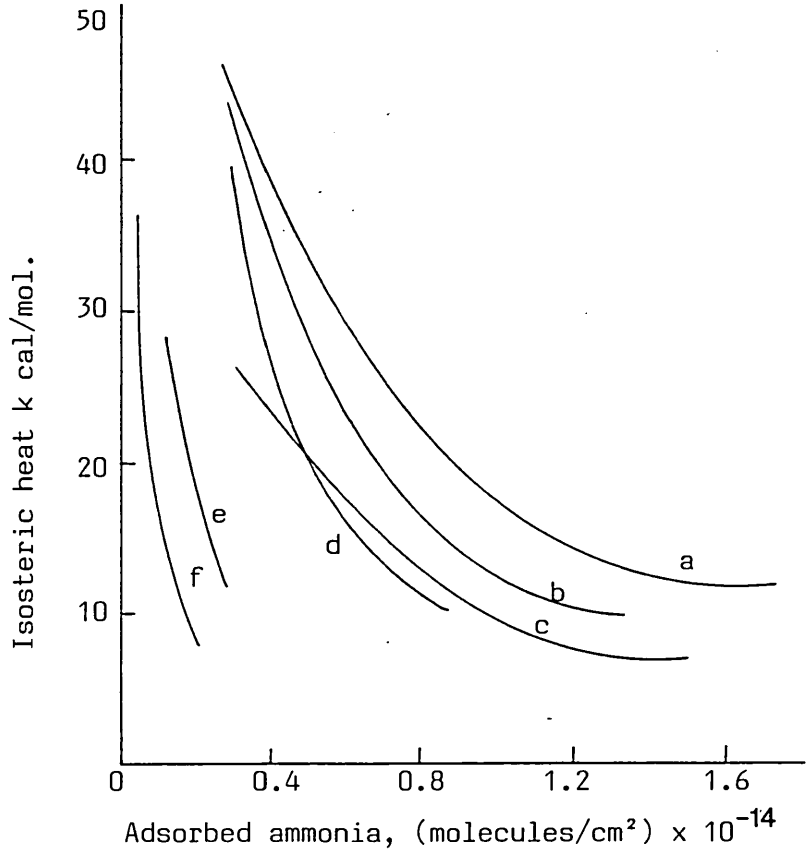

(a)

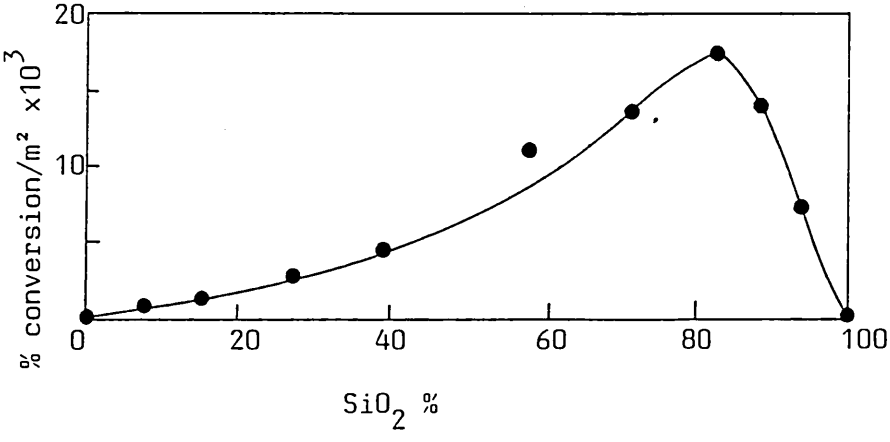

(b)

FIG. 1: (a) Variation of isosteric heats of adsorption with coverage of ammonia on silica-aluminas: a - pure alumina, b - 15% silica, c - 70% silica, d - 90% silica, e - 98% silica, f - pure silica. (After Clark et al. (1962)).

b) Activity versus composition of silica-aluminas for xylene-isomerization. (After Holm & Clark, 1963).

and 1b. Benesi and Winquist (1978) commented that this discrepancy might be due to a substantial amount of the base attaching itself to catalytically inactive sites on the solid surface.

Acid strength determination by ammonia-desorption for various silica-alumina catalysts was pioneered by Kubokawa (1963); Amenomiya and Cvetanovic (1963); Adams, Kimberlin and Shoemaker (1964); Amenomiya, Chenier and Cvetanovic (1964); and others. Quinoline, pyridine, piperidine, trimethylamine, n-butylamine and pyrrole are also equally used along with ammonia. During desorption, a base adsorbed on weak acid sites comes off first. This fact has led to the development of the Temperature Programmed Desorption (TPD) technique for studying acidity of solid catalysts. Cvetanovic and Amenomiya (1967) described a gas-chromatographic TPD method to characterize alumina and silica-alumina surfaces by adsorption of ethylene, propylene and trans-butene-2. Recent applications of the technique will be discussed later for specific solids.

1.3.6 METHOD OF MODEL CATALYTIC REACTIONS

Simple reactions, which are well-known as being catalyzed by acids, are often used to estimate relative surface acidity of solid catalysts. Commonly used reactions are cracking of cumene, and isomerization of cyclopropane and xylene. Ward and Hansford (1969) were among the first to show that conversion of o-xylene to p- and m-xylenes over a series of silica-alumina catalysts followed the acidity strengths of these materials, which had been independently determined by IR methods.

In what is known as catalytic titration, a model reaction is stopped by gradually poisoning the acid sites of a catalyst with addition of a base. The amount of base required exactly to stop the reaction represents the acid amount of the catalyst. Goldstein and Morgan (1970) used quinoline to inhibit cumene-cracking over CeY-zeolite. Benesi (1973) suggested that the weak base 2,6-dimethyl pyridine could be a very effective poison, because this base selectively adsorbs on the Brönsted acid sites, while the Lewis acid sites remain inaccessible due to steric hindrance.

1.3.7 PHOTOELECTRON SPECTROSCOPIC METHOD

Electron spectroscopic methods, mainly X-ray and Ultraviolet Photoelectron Spectroscopy (XPS and UPS) give a direct measure of the electron energy levels existing at the surface and hence provide useful information about surface bonding. This should be ideal for studying surface acidity through adsorption of bases. However, experimental difficulties associated with the problem of charging for insulating substances and the resultant uncertainties in binding energy assignments have made these electron-spectroscopic techniques less attractive for application to cracking catalysts. Defosse and Canesson (1976) were the first to apply XPS to the study of acidity of NH_4-Y zeolites from pyridine adsorption. The zeolite samples, activated at 300-400°C prior to pyridine exposure, showed a N(1s) peak which was resolved into two components, one high intensity peak at 399.6eV and a low intensity peak at 397.5eV. The samples activated at 500-600°C similarly produced

two components, the high intensity one at 398.3eV and the low intensity one at 400.5eV. Whatever the activation temperature, the N(1s) peak had two components with a binding energy difference of ~ 2eV. Defosse and Canèsson attributed the low binding energy peak to pyridine on Lewis acid sites and the high binding energy ones to pyridine adsorbed on Brönsted acid sites. The relative acidity contributions of the two types of site were also calculated from the relative intensities of the two N(1s) peaks. The comparison with the IR data on the same samples showed that when the XPS data were taken at -90°C after pyridine exposure, the correlation was satisfactory, but room temperature XPS results were not in agreement with the IR measurements.

Vinek, Latzel, Noller and Ebel (1978) used XPS to measure the basicity of magnesium oxide and the authors proposed as a general rule that the O(1s) binding energy would be higher for acidic oxides than for basic oxides. Earlier Vinek, Noller, Ebel and Schwarz (1977) utilized the XPS binding energies of the 2p electrons associated with Mg^{2+}, Zn^{2+}, Al^{3+} and O^{2-} ions in a number of oxides and zeolites as a measure of the Lewis acid-base characteristics of these ions in the substances considered.

UPS, XPS and Work function measurements were used by Rogers, Campbell, Hance and White (1980) to study the adsorption and bonding of NH_3 on clean and oxidized aluminium. The authors found that the amount of Lewis acidity of an oxidized Al surface increased with increase in the extent of oxidation, and there was no evidence for any NH_4^+ type species on the surface, indicating absence of Brönsted acidity.

There has been an increase recently in the use of XPS for general surface characterization of zeolites and other acidic catalysts. Some of these will be considered later under the appropriate section.

1.3.8 OTHER METHODS

Gay and Liang (1976) have shown that ^{13}C NMR spectroscopy can be used to determine surface-acidity of SiO_2, Al_2O_3 and SiO_2-Al_2O_3 from amine-adsorption. Pearson (1977), on the other hand, has demonstrated that ^{1}H NMR spectroscopy can be applied to estimate Brönsted acidity quantitatively. The method used by Pearson was to adsorb deuterated pyridine on the Brönsted acid site. The proton, which becomes associated with the pyridine, appears as the sole narrow line in the NMR spectrum. By this method, Pearson has proved that alumina does contain some Brönsted acid sites.

Mizuno, Take and Yoneda (1976) showed that UV absorption spectra of p-nitroaniline chemisorbed on silica-alumina gave two peaks, corresponding to Brönsted and Lewis acid sites.

Some authors have used thermogravimetric studies and differential thermal analysis to characterize acidic sites. These methods have not found wide application and generally they serve to complement either IR studies or gas-adsorption methods.

1.4 SOURCE OF SURFACE ACIDITY, STRUCTURE OF ACIDIC SITES AND CATALYTIC ACTIVITY

The literature is flooded with reports on the study of acidic

sites of alumina, silica, silica-aluminas, zeolites and clay-minerals. A few interesting and relevant results are summarized below.

1.4.1 ALUMINA

Acid-base properties of alumina were discussed by Peri (1965), Medema and co-workers (1972), Knözinger and Ratnasamy (1978), Vit, Vala and Malek (1983), and many others. Uncalcined alumina is known to be catalytically inactive because of absence of almost any acidity. Ito and co-workers (1969) have found interesting results on the effect of calcination temperature on acidic properties of pure alumina prepared from aluminium isopropoxide. This is shown in Fig. 2. Two acidity maxima are obtained at 500°C and at 700-800°C with an unusual minimum at 600°C. Parry (1963) has found that most of the hydroxyl groups in alumina are removed when calcined at 500°C, the few remaining did not show any acidity. One particular type of hydroxyl group on the surface of alumina was identified by Fink (1967) and Parkyns (1971) because it reacted as a base with carbon dioxide. Parkyns concluded that several types of oxide ions existed on alumina surfaces. These ions differ from one another on the basis of the nature and number of nearest neighbours.

Hindlin and Weller (1956) showed that each new oxide ion was formed from the condensation of two hydroxyl groups according to the following scheme:-

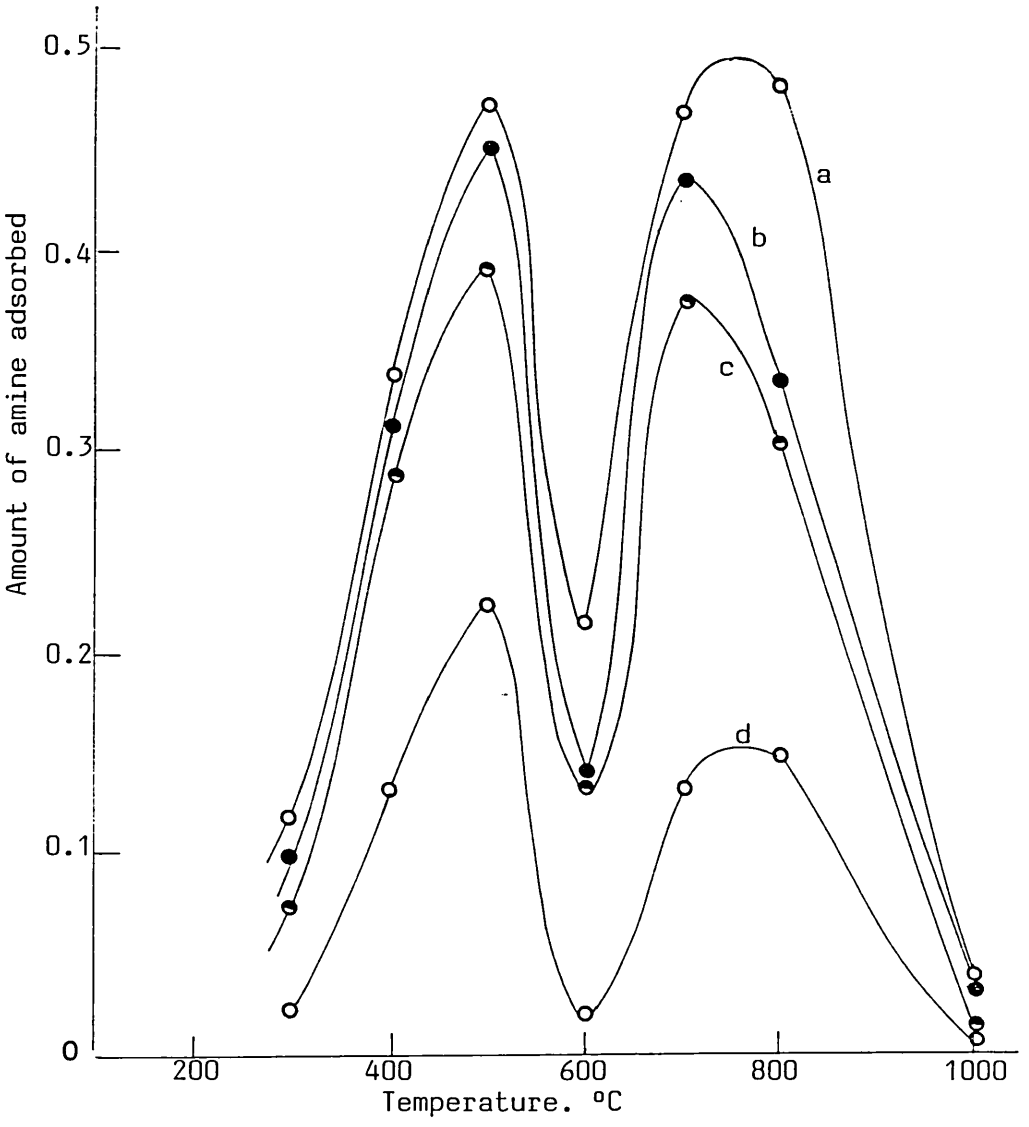

FIG.2: Total acidity of alumina, determined from n-butylamine adsorption, at various acid strengths against temperature of calcination. (After Itoh et al., 1969).

a: acid strength $H_o \leqslant 3.3$

b: $H_o \leqslant 1.5$

c: $H_o \leqslant -3.0$

d: $H_o \leqslant -5.6$

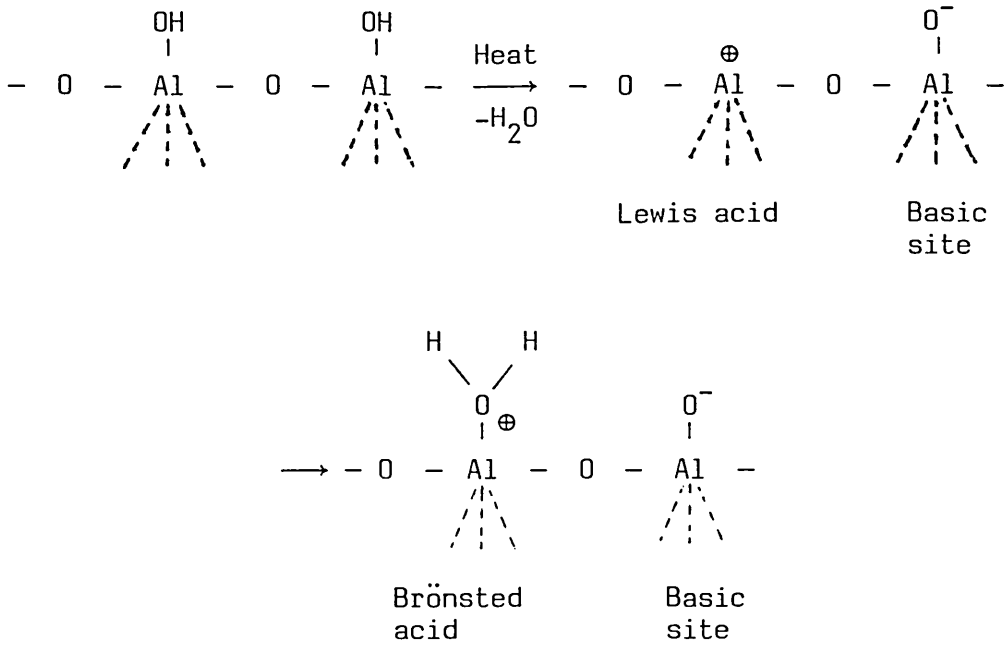

The incompletely coordinated aluminium acts as the Lewis acid and the negatively charged oxygen as the basic site. A Lewis acid site becomes a very weak Brönsted acid by adsorbing moisture.

Pure activated alumina catalyzes many isomerization reactions. Pines and Haag (1969a and b) showed that the isomerization of cyclohexane and 3,3-dimethylbutene-1 over alumina proceeded via carbonium ion-formation. Both these reactions were poisoned by ammonia. However, the location of the exact sites for the isomerization still remains a matter of controversy. Medema, Van Bokhoven and Kuiper (1972) and many others point to the Lewis acid sites as the active centres. On the other hand, Peri (1966) showed that the isomerization can take place at the basic oxide ions, and Gati and Knözinger (1973) as well as Ghorbel, Hoang-Van and Teichner (1974) have maintained that the isomerization proceeded with some assistance from the oxide ions. The evidence in support of the Lewis acid sites, at present, seems overwhelming. In a probe reaction, Lunsford, Zingery and Rosynek (1975) found that hydrogen sulphide selectively adsorbed on Al-ions

and this prevented isomerization of butene-1 over γ-alumina.

Morterra, Chiorino, Chiotti and Garrone (1979) showed that the surface acidity of alumina increases with increasing activation temperature, because more and more Lewis acid sites with incompletely coordinated Al are generated. As Mochida and co-workers (1978) showed, the acidic properties predominate on the surface of dehydrated alumina, whereas basic properties predominate on hydrated alumina. They observed that the surface basicity was increased by sorbed water rather than by oxide ions. In a more comprehensive experiment, Vit and co-workers (1983) have established that acidity of alumina is connected with the dehydrated part of the surface and chemisorbed water behaves as a poison to catalysis by acid sites. With adjustment to the extent of dehydration, alumina can be made to act both as a basic and an acidic catalyst.

The acidity of alumina increases markedly with addition of foreign ions like fluoride, chloride and phosphate, and also in combination with other oxides. Such addition produces strong Brönsted acid sites which catalyse a large number of reactions.

1.4.2 SILICA

Pure silica gel is only feebly acidic as shown by West, Haller and Burwell (1973). An infra red study carried out by Morimoto, Imai and Nagao (1974) has proved the existence of very weak Brönsted acid sites on the surface of silica gel which react with n-butylamine but not with pyridine. Young (1958) has established that the surface of silica gel contains varying amounts of silanol $\geqslant$Si-OH groups

and siloxane $\geqslant$Si-O-Si$\leqslant$ bridges depending upon thermal treatment and exposure to water. The silanol groups are acidic enough to form surface silicates with cations and methoxy groups with methanol, but do not have appreciable catalytic activity. On silica gel exposed to ammonia, Benesi and Winquist (1978) identified IR bands corresponding to ammonium ions which disappeared even when the gel was degassed at room temperature. When heated above 500°C, silica gel loses most of the surface $\geqslant$Si-OH groups and hence the Brönsted acidity. In a thorough investigation, Morrow and Cody (1975, 1976a and 1976b) found that more and more Lewis acid sites were generated on the silica surface by dehydroxylation up to 1500K in vacuum. These sites could chemisorb H_2O, NH_3, and CH_3OH, but were inert towards O_2, H_2, CH_4, C_2H_4 and HCN. This dehydroxylated silica is however, not a good catalyst, because reactants are either too strongly adsorbed or the inactive silanol groups are regenerated.

The inactive silica becomes very active when trace amounts of acid-producing impurities are present. West, Haller and Burwell (1973) showed that addition of 0.012% aluminium to silica gel increases its efficiency for hexene-1 isomerization at 100°C by 10,000-fold.

1.4.3 SILICA-ALUMINA

Incorporation of silica into alumina produces one of the most important classes of acid catalysts. Shiba and co-workers (1964) have determined the Brönsted and Lewis acid amounts of a number of silica-alumina mixtures. These results are shown in Fig. 3. It is evident that pure alumina is a strong Lewis acid with almost

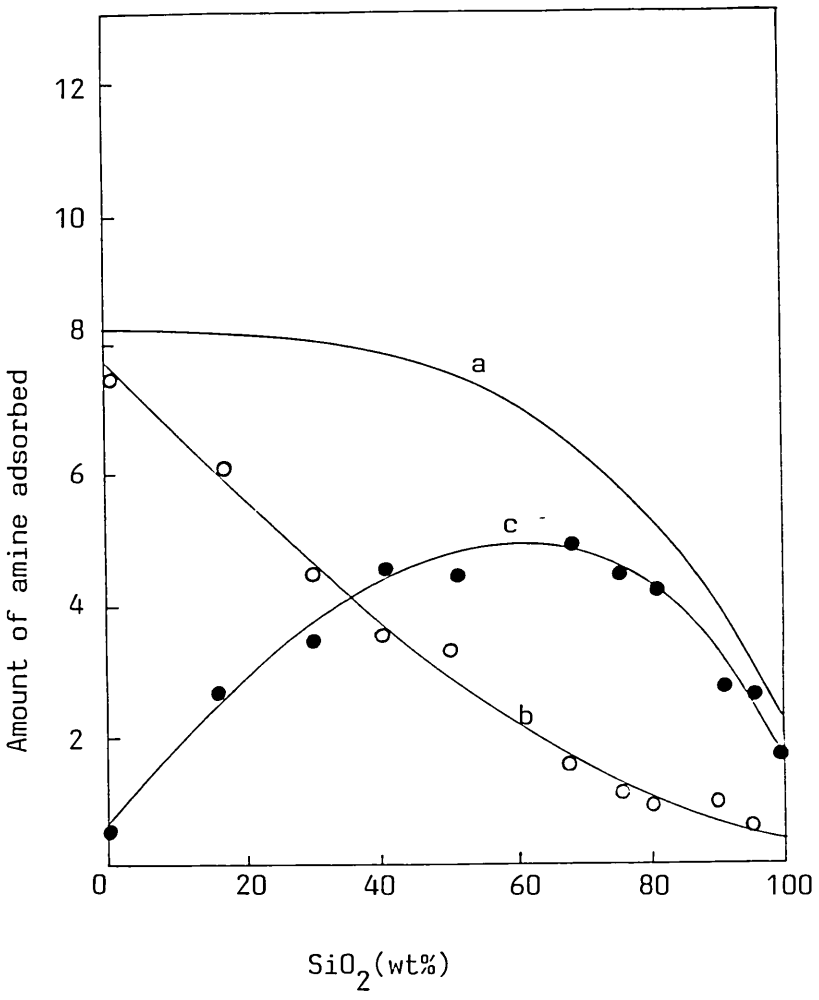

FIG.3: Acidity of silica-aluminas versus silica content (After Shiba et al., 1964).

a: total acidity at $H_o \leq 1.5$ as determined from amounts of n-butylamine adsorption,

b: Lewis acidity, determined by amounts of chlorotriphenylmethane adsorption,

c: Brönsted acidity obtained by subtracting b from a.

no Brönsted acidity, but as the silica content increases, Brönsted acidity increases reaching a maximum with about 70% silica, and then starts to fall again. These authors have also shown that coprecipitated silica-alumina has generally more Lewis acidity and less Brönsted acidity than the ones obtained by simply mixing silica and alumina.

The acidic properties of silica-aluminas are determined by (a) method of preparation, (b) proportion of silica, (c) temperature of dehydration and (d) method of acidity estimation. Infra-red studies by a host of workers have established the existence of both Brönsted and Lewis acid centres on silica-alumina. From deuterium exchange reactions and NMR spectra, which showed that the hydrogen on the surface of silica-alumina is chemically similar to that in alcohols, Hall and co-workers (1963) suggested that most of the hydrogen remained as either SiOH or AlOH.

The structure of acidic sites on silica-alumina is a matter of contention. Basila, Kantner and Rhee (1964) drew the conclusion that primary acid sites consisted of surface Al-atoms which were of Lewis type. The Brönsted acid sites were produced by second order interaction between a molecule chemisorbed on a Lewis acid site and an adjacent surface-hydroxyl group. Bourne, Cannings and Pitkethly (1970) used the IR method to study two extreme cases of acidity on silica-alumina. They found that when a very low concentration of Al-atoms was incorporated on the surface of silica gel, the dehydrated sample behaved only as a Lewis acid to pyridine. On the other hand, when the same concentration of Al-atoms was incorporated within the silica lattice, the dehydrated sample showed only Brönsted acidity. IR and thermogravimetric studies on the chemi-

sorption of pyridine on both untreated and dealuminated silica-alumina by Ballivet, Barthomeuf and Pichat (1972) indicated that the strong acidic sites were retained down to 2.4 wt% Al_2O_3, but a sample containing only 0.1% alumina did not adsorb pyridine at all, showing that it had neither kind of acidity.

Following the works of Thomas (1949), Tamele (1950) and Hansford (1952), it is now generally recognized that the acid sites in silica-alumina result from isomorphous substitution of trivalent aluminium for tetravalent silicon. Leonard and co-workers (1971) postulated that defect structures might also produce acidity in these substances.

Morimoto, Imai and Nagao (1974) found that pyridine had greater affinity for Lewis acid sites than Brönsted acid sites. On the other hand, Schwarz (1975) observed that pyridine bonded to the Lewis acid sites of silica-alumina could not be converted to pyridinium ions (pyridine + Brönsted acid) by exposing the surface to water. Takahaski, Iwasawa and Ogasawara (1976) made a detailed TPD investigation of the behaviour of silica-aluminas towards pyridine and n-butylamine. Two types of adsorption site were found with n-butylamine, only one of which was catalytically active. On these active sites, constituting about one fifth of the total number of acid sites, the amine decomposed at temperatures above 300°C. Pyridine desorption produced only one peak, indicating that only one type of site, presumably the Lewis acid site, was involved. No decomposition of pyridine was seen even above 400°C.

Schwarz, Russell and Harnsberger (1978) used both the IR method and TPD to study acidic sites on silica-alumina from pyridine adsorption. The authors established first order desorption kinetics for pyridine adsorbed on either Lewis or Brönsted acid sites. The

IR data showed the Brönsted acid site density to be quite low, thus accounting for the absence of structure in the TPD spectra.

The overwhelming evidence, according to Spencer and Whittam (1980), points to the presence of two types of hydroxyl group on the surface of hydrated silica-aluminas of low aluminium content. One of them is similar to the silanol groups on silica and is catalytically inactive. The other hydroxyl group is associated with tetrahedral aluminium, is much more acidic (up to $H_o \leqslant -13.3$), and is the source of most catalytic activity. Dehydration produces Lewis acid sites.

Zhixing and co-workers (1983) developed a theoretical model of the silica-alumina surface. Using the CNDO/2-FA method, the authors assigned the structure Al-OH-Si to the strong Brönsted acid site, and Si-OH in combination with a four-coordinated aluminium to a moderate acid site. Kawakami, Yoshida and Yonezawa (1984), on the other hand, applied the molecular orbital approach to find out the origin of Brönsted acidity on solid surfaces. It was suggested that an isolated $\geqq$Si-OH or $\geq$Al-OH species would be too stable to loose a proton and would be non-acidic. On the other hand, a Lewis acid site may produce a Brönsted acid by interacting with a nearby hydroxyl group. A structure consisting of a surface tri-coordinated silicon and an adjacent tetra-coordinated aluminium under the surface was shown as being capable of generating very strong acidity.

1.4.4 ZEOLITES

The nature of acidic sites in zeolites was first comprehensively studied by Uytterhoeven, Christner and Hall (1965). From IR studies, the authors proposed that when an ammonium-zeolite was heated the protons remaining after the release of ammonia attacked lattice oxygen and became attached to a particular oxygen atom rather than remaining mobile. The following scheme was suggested:

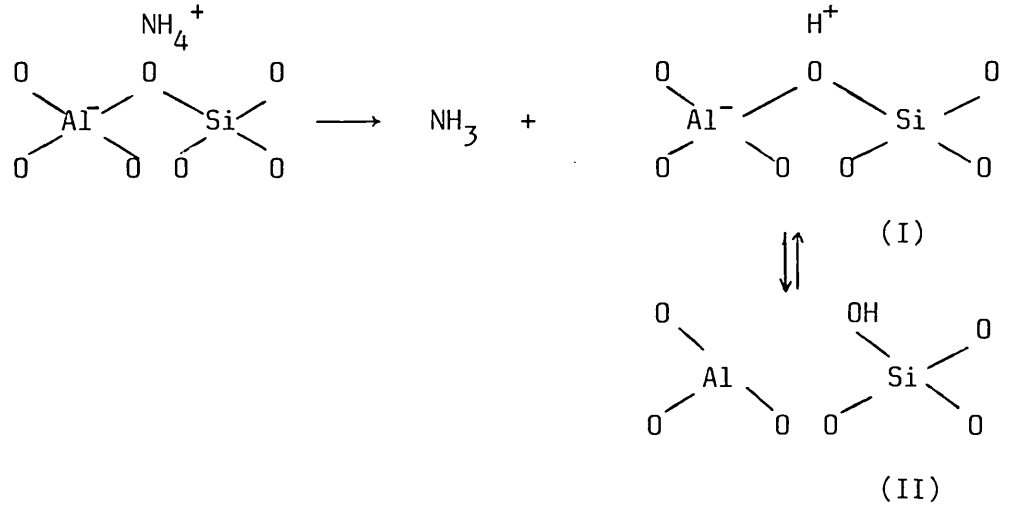

As IR measurements showed, the typical Brönsted acid (I) was not present in substantial quantities at room temperature. At the approach of a base, a proton would be supplied by the equilibrium. The authors showed that the trigonal aluminium in (II) would behave as a Lewis acid, depending upon accessibility of the aluminium to the base. On dehydroxylation, (II) could produce other kinds of site, as shown below:

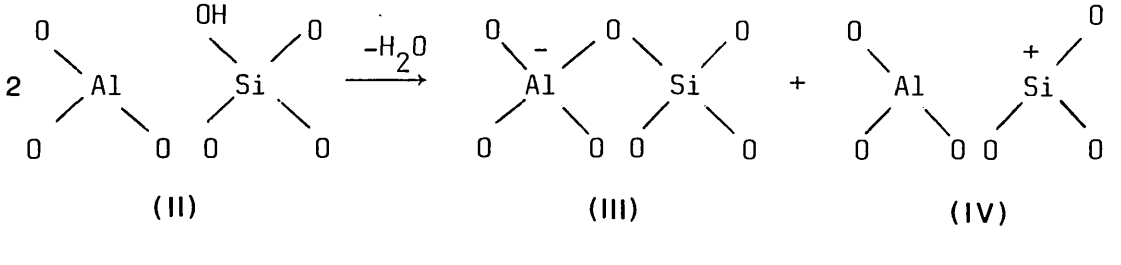

The tetrahedron is closed again in (III), while in (IV), easily accessible trigonal aluminium is formed adjacent to positively charged trigonal silicon. Works of Angell and Schaffer (1965), Ward (1967), Hughes and White (1967) and many others support the above scheme. Ward (1967) applied the IR method to pyridine chemisorption on decationized Y-zeolites in order to measure both the Brönsted and Lewis acidity and found that the concentration of Brönsted acid sites increased up to a calcination temperature of 350°C, remained constant to 500°C and then decreased rapidly. On the other hand, the Lewis acid site concentration increased slowly from a temperature of about 450°C to 550°C and then, rapidly built up until at 700°C, there were equal concentrations of both types of acid sites. At 800°C, the zeolite was shown to be essentially a pure Lewis acid. These results are shown in Fig. 4. Hughes and White (1967) have obtained similar results.

Following Uytterhoeven et al (1965), both groups of workers, mentioned above, explained the increase in Lewis acidity with temperature on the basis of dehydroxylation through conversion of (II) to (III) and (IV) in the scheme shown above. Kuhl (1977) has shown however that X-ray spectrometry of Y-zeolites could not detect any tricoordinated silicon even after dehydroxylation, neither was tricoordinated aluminium observed. X-ray data showed most of the aluminium atoms in tetracoordinated form with about 19% in the hexacoordinated state which was suggested as the possible source of Lewis acidity.

Both the acidity and catalytic activity of zeolites depend upon many other factors besides calcination temperature: some of these factors are type of zeolite, nature of cations present, decationization and cation-exchange levels, etc. The complex nature of activity of

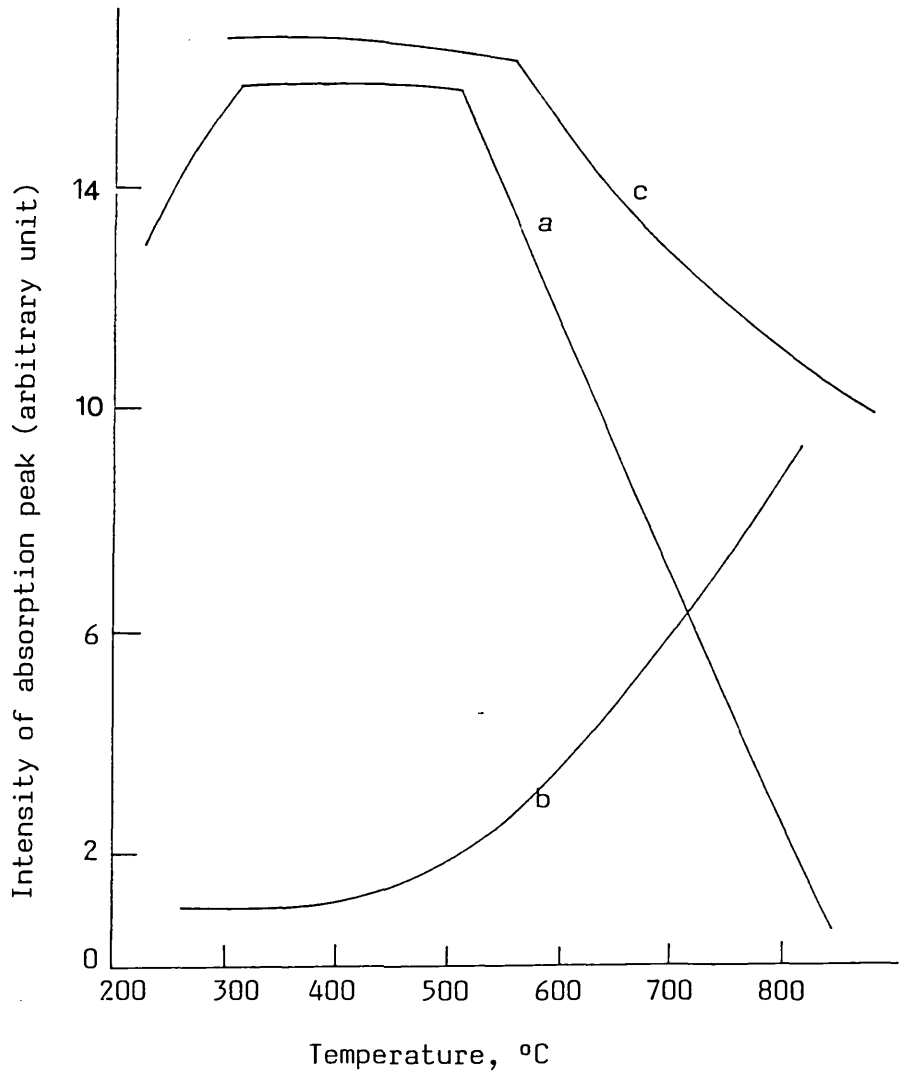

FIG.4: Change in Brönsted and Lewis acidity of decationated Y-zeolite with temperature of calcination. Acidity measurements were done from intensity measurements of IR absorption bands for chemisorbed pyridine.

a: Brönsted acidity from the intensity of the 1545cm^{-1} IR band,

b: Lewis acidity from the intensity of the 1451cm^{-1} IR band,

c: total acidity from a+b. (After Ward, J.W., 1967).

the zeolites has been discussed in detail by Ward (1976), Poutsma (1976), Minachev and Isakov (1976),Rabo (1984), Barthomeuf (1984a) and many others. Chu (1976) has shown that for maximum catalytic activity, ammonium zeolites need to be activated at temperatures just above that at which ammonia evolution stops. The activity decreases considerably if the hydrogen-zeolite obtained after removal of ammonia is further heated above dehydroxylation temperature. This observation agrees well with Benesi's (1967) view that Brönsted acid sites rather than Lewis acid sites (formed through dehydroxylation) are the seat of activity in zeolites.

The distribution of active sites in zeolites is thought to be a function of the silica/alumina ratio, but attempts to quantitatively correlate activity or acidity with this ratio have not been a complete success. Haag, Lago and Weisz (1984) have shown that the catalytic site for acid catalysis on all aluminosilicates can be identified quantitatively with concentration of protonated aluminium atoms in the silica framework. These aluminium atoms are shown to be highly reactive even at very low levels of parts per million. In ZSM-5 zeolites, it is shown that only about 1 out of 1,000 aluminium atoms found from chemical analysis is actually effective in catalysis.

It was suggested by Poutsma (1976) that the activity of zeolites was governed by two opposing factors; increasing SiO_2/Al_2O_3 ratio enhances the acid strength per site but decreases the number of sites. Bierenbaum et al (1971) as well as Satterfield and George (1978) have shown that the catalytic activity of zeolites at first increases with rising silica/alumina ratio, reaches a maximum at a silica/alumina ratio of 10-40 and then declines with higher ratios.

Parra, Ballivet and Barthomeuf (1975) prepared a series of L-zeolites with varying potassium, hydrogen and aluminium contents, and showed that both the total acidity, measured by butylamine titration, and the catalytic activity reached maximum values when about half the potassium ions were removed, but became almost zero on complete removal. This exemplifies the fact that the acidity and activity not only depend upon the silica/alumina ratio, but also on the actual structure of the zeolite, its composition, and the nature of exchangeable cations.

An XPS study of Ce-Y zeolites by Tempere, Delafosse and Contour (1975) revealed that the Si/Al ratio at the surface was twice the value of that in the bulk. It was suggested that the Al-O-Si-Al-O-Si bonds might have terminated with Si-OH groups, leading to depletion of Al at the surface. A similar conclusion was reached by Knecht and Stork (1977), e.g. the XPS showed a surface Na/Al/Si ratio of 0.99/0.65 /1.00 in one of their zeolite-A samples compared to a bulk ratio of 0.96/0.99/1.00. Barr (1983) also demonstrated an enrichment of the Si/Al ratio on the surface for a number of zeolites from XPS intensity data, but the enhancement was not as pronounced as that observed by Tempere and co-workers (1975). Finster and Lorenz (1977) also made similar observations for Si/Al ratios in A-, Y-zeolites and mordenites. However, Suib, Stucky and Blattner (1980) reported that an AES study of single crystalline and powdered, natural and synthetic zeolites revealed no difference between surface and bulk Si/Al ratios. No proper explanation for the divergence between the XPS and AES results was given, although it was thought that surface-charging might be responsible for the discrepancy. In another contrasting result, Gross and co-workers (1984) recently

showed that their XPS intensity measurements showed no difference in the Al/Si and Na/Si ratios between bulk and surface for Na-Y and NH_4-Na-Y zeolites. The thermochemically dealuminated zeolites, on the other hand, showed Al/Si ratios on the surface (at high temperatures) up to three times higher than that in the bulk, the enrichment of Al being interpreted as an accumulation of non-framework species on the surface.

Various sources of protons, like water, alcohol, hydrogen chloride, hydrogen sulphide, etc., are known to promote zeolite activity. Mirodatos and co-workers (1976a and b) found that the activities of MgY and CaY zeolites for iso-octane cracking increased reversibly with the addition of CO_2 to the reaction mixture. The following model was suggested by Haynes (1978) on the basis of infra-red and ESR studies as well as n-butylamine titration:

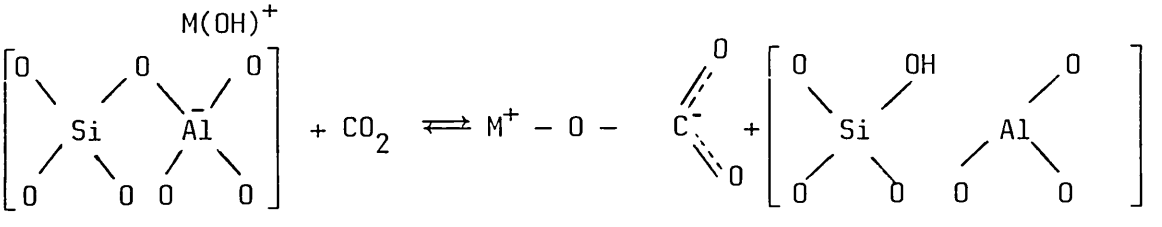

(I)

The formation of Brönsted acid (I) promotes activity.

Recently, Khulbe, Mann and Manoogian (1983) investigated the effect of activation temperature on the electron-accepting and donating properties of Na-Y zeolites by studying the adsorption of phenothiazine and tetracyanoethylene. Phenothiazine and tetracyanoethylene are known to react respectively with electron acceptors and electron donors to producecationic and anionic radicals.

Both kinds of sites were found on the zeolite surface from ESR measurements, with the electron accepting (acid) sites being greater than the electron donating (basic) sites. The number of cation-forming sites (acid) decreased with higher activation temperature, while the number of anion sites (basic) have increased. These changes were however not proportionate. The authors also observed the formation of SO_2^- anions and CO^+ cations on the zeolite surface from interaction between sulphur dioxide and carbon monoxide.

Barthomeuf (1984b) has studied conjugate acid-base pairs on X,Y,L, mordenite and ZSM-5 zeolites by using pyridine adsorption for acid sites and pyrrole adsorption for basic sites. Oxygen atoms are proposed as the basic sites whose basicity increases with the increase in the negative charge on the oxygen atoms. The acid-base properties depend upon the nature of exchangeable cation and also upon the aluminium content. For the case where aluminium Lewis acid sites are inaccessible or absent, a model has been proposed in which conjugate acid-base pairs result from the dipole moment induced by the asymmetrically positioned cations.

Hidalgo and co-workers (1984) used TPD of ammonia to determine the acidity of a number of different H-zeolites. The adsorption was carried out at 373K. Mordenites and ZSM-5 zeolites gave two TPD peaks while Y-zeolites gave only one broad peak. From the peak maximum temperature of the high temperature peak around 680K, the acid strengths were shown to be in the order of H-mordenite > H-ZSM-5 > H-Y. The authors also showed that the amount of ammonia desorbed would be a measure of the amount of acid on the zeolite surface. Ammonia adsorption also showed that the strong acid sites were preferentially poisoned by cation-exchange whereas

dealumination reduced all types of acidic sites. TPD of ammonia has also been used by a large number of other workers, including Topsøe (1981), Post and van Hooff (1984), Chao and co-workers (1984), Mirodatos and Barthomeuf (1981).

A considerable number of model reactions have been used to measure the activity of various zeolites. Cumene-cracking activity of the zeolites serves as a convenient way to measure the catalytic efficiency. The cracking of n-hexane was also established as a suitable model reaction by the early works of Myers (1968), Kerr (1970) and their co-workers. The isomerization of cyclopropane has also become a common test reaction for catalytic activity of zeolites following the works of George and Habgood (1970), Nguyen, Cooney and Curthoys (1976), and Kiricsi and co-workers (1980). Recently Förster and Seebode (1983) used this isomerization reaction over A-zeolites to propose a model in which the cations, acting as Lewis acids, polarize the π-bonds of the cyclopropane molecule to undergo isomerization. Itoh and co-workers (1984) used the conversion of methanol to hydrocarbons as a probe of the acid property of various zeolites.

1.4.5 CLAY MINERALS

The two main groups of clays, kaolin and montmorillonite, both have layered structures consiting of parallel sheets of oxide and hydroxide ions coordinated to qua drivalent silicon and trivalent aluminium. Benesi (1956, 1957) measured the acidity of a number of clays, finding that the H-forms of the clays were the strongest acids with $-5.6 \leqslant pKa \leqslant -8.2$. Benesi explained the acidity of

dried Na- and NH_4-forms of kaolinite and montmorillonite, which were completely neutralized in aqueous suspensions, by suggesting that new acid sites were exposed when water was removed from highly solvated cations. Kaolinite has strong, but relatively few, acid sites whereas montmorillonite contains a large number of acid sites with slightly lesser strength. Solomon and co-workers (1971, 1972) demonstrated that kaolinite dried at 110°C had acid strength equal to 90% H_2SO_4, but the strength rapidly decreased if the kaolinite was exposed to water vapour. From IR spectra of adsorbed ammonia on montmorillonite, Mortland and co-workers (1963, 1968a and b) proposed that strongly polarized water molecules in the vicinity of exchangeable cations dissociated to provide protons and hydroxyl ions according to the scheme

$$M^{z+}(H_2O)_{ads} + NH_3 \rightarrow (M^{z+})_{ads} + (OH^-)_{ads} + (NH_4^+)_{ads} \quad .$$

For a bentonite clay, it was found that the ability to protonate ammonia decreased roughly in the order of polarizing power of the exchangeable cations, Al = Mg > Ca > Li > Na > K at low humidity and Al > Mg > Ca = Li > Na = K at high humidity. A similar correlation was observed also by Frenkel (1974).

The interest in clay minerals as acidic catalysts has been renewed after Wright, Granquist and Kennedy (1972) reported the high catalytic activity of a synthetic clay, termed synthetic mica montmorillonite (SMM). This clay has remarkable structural similarity to muscovite mica and the infra-red spectra of the two materials were shown to be almost identical. Minor differences were attributed to the lower aluminium content and higher fluoride/

hydroxyl substitution in SMM, and the greater silicon/aluminium ordering in muscovite. Both muscovite and SMM were shown to have the same unit cell formula,

$$[(Al_4)^{octahedral}(Si_{8-x}Al_x)^{tetrahedral}O_{20}(OH,F)_4]^{x-} \cdot \frac{x}{n} M^{n+} .$$

For muscovite, $x \approx 2$ and $M = K^+$, while for SMM, M is predominantly NH_4^+, and probably some Al(OH) species. The SMM consists of platelets of average diameter 1000Å and the nitrogen BET surface area at an outgassing temperature of 200°C was found to be about 160m²/g. Wright et al showed that the large amount of edge area present in SMM had probably the most catalytic activity. Activation of SMM by heating up to 600°C results in loss of ammonia and structural dehydroxylation. During this process, protons are released to the SMM framework, and, in subsequent exposure to ammonia, IR spectra showed ammonium ions as well as ammonia bound to Lewis acid sites. Pyridine also produced a small amount of pyridinium ions and at least two Lewis acid species. Wright and his co-workers also showed that, although the acidic site density was much lower in SMM compared to the zeolites, the two types of catalysts had comparable activity because of the greater accessibility of the layered clay surface.

The mechanism of isomerization of cyclopropane, methyl-cyclopropane and n-butenes over SMM was investigated by Hattori, Milliron and Hightower (1973). The hydrogen atoms on the surface of SMM were found to be quite labile, judged from the rate of exchange with deuterium, and the rate-determining step in all the reactions appeared to be the formation of carbonium ions through

transfer of a labile proton from the surface. These labile protons make the SMM more active than the silica-aluminas.

The catalytic activity of SMM increased even further with substitution of nickel or cobalt ions into the structure during synthesis. Nickel ions are thought to occupy octahedral positions, two aluminium ions being replaced by three nickel ions. The activity of such Ni-SMM has been studied by Swift and Black (1974), Giannetti and Fisher (1975), Bercik et al (1978) and Heinerman et al (1983). Heinerman et al (1983) showed that Ni-SMM could catalyze pentane isomerization only when the lattice Ni^{2+} ion was reduced to zero-valent Ni. The activity was shown to have decreased when the metallic Ni was made inaccessible through adsorption of carbon monoxide. Robschlager and co-workers (1984) recently reported that the high activity of Ni-SMM was due to formation of strong Brönsted acid sites during reduction of lattice Ni^{2+} ions and the isomerization of n-alkanes probably was a bifunctional reaction, involving both the metal and the acidic sites.

For the common 2:1 layer silicates, Davidtz (1976) found that the acid activity was proportional to the surface concentration of tetrahedrally coordinated aluminium atoms. From the study of catalytic decomposition of t-butyl alcohol, the author was able to show that the octahedral sites were quite inactive. Frenkel and Heller-Kallai (1983) on the other hand, showed from the transformation of limonene on montmorillonite that the rate of transformation depended on the interlayer cations, with Na < Mg < Al < H. With a suitable choice of the interlayer cation, the reaction could be directed to either isomerization, disproportionation or oxidation.

Seyama and Soma (1984) recently studied montmorillonite with

XPS and X-ray induced AES and came to the conclusion that the bonding of exchangeable cations in montmorillonite was identical to that of corresponding cations in typical ionic compounds. Thus the cations which compensate for the negative charge arising from the substitution of silicon by aluminium in the tetrahedral layer were shown to form nearly pure ionic bonds in the mineral.

1.5 AIM OF THE PRESENT WORK

In this work, both air-cleaved and vacuum-cleaved surfaces of muscovite mica were investigated for acidic sites using temperature programmed desorption (TPD) of gaseous bases. Ammonia was mainly used, although a few experiments were done with pyridine as well. The general reactivity of mica surfaces towards carbon monoxide and carbon dioxide, water, and methanol were also studied with TPD. Some casual observations on the reactivity of mica surfaces can be found in the literature, but no thorough study has ever been reported. This will be discussed in the next chapter.

Significant differences were noticed between the air-cleaved and vacuum-cleaved surfaces of mica with respect to carbon contamination. A surface cleaved in air picked up carbon almost immediately while the vacuum cleaved surface remained carbon-free for a long time. This carbon contamination of mica surfaces was investigated in some detail.

The surface-composition and other characteristics were investigated with X-ray Photoelectron Spectroscopy (XPS). Some of the results of the TPD study were confirmed through XPS analysis.

The effects of surface charging on the binding energies of principal constituent peaks of the mica surface through the processes of cleaving, heat-treatment and exposure to gases were also studied. The mica surface was also characterized by means of Low Energy Electron Diffraction (LEED) patterns.

Finally, the activity of the mica surface as a model catalyst was studied with respect to cyclopropane isomerization, in a fixed-bed pulse reactor.

CHAPTER TWO

LITERATURE REVIEW ON MICA

2.1 STRUCTURE, COMPOSITION AND GENERAL PROPERTIES OF MICA

The crystal structure of mica has been well established through the pioneering works of Mauguin (1927,1928), Pauling (1930), and Jackson and West (1930, 1933). Structures of different varieties of mica and related matters have been thoroughly reviewed by Deer, Howie and Zussman (1962), Bragg, Claringbull and Taylor (1965), and more recently by Bailey (1980).

Mica can be conveniently described as a hydrous aluminosilicate having a composite layer structure, consisting of three layers: one layer of octahedrally coordinated metal atoms sandwiched between two identical tetrahedral layers with the vertices of both pointing inward. Each tetrahedral sheet has the composition $(Si,Al)_2 O_5$ in which individual tetrahedra are linked together through three of the four corners to form a hexagonal mesh pattern. Thus, all the three basal oxygens are shared among neighbouring tetrahedra. This is shown in Fig. 5.

The fourth set of tetrahedral corners consist of the apical oxygens which are normal to the tetrahedral sheet and form part of the octahedral sheet where the octahedra are linked together laterally by sharing edges as shown in Fig. 6. The common plane of junction between the tetrahedral and octahedral sheets contains the shared apical oxygens and unshared OH groups. The OH groups lie at the centre of each tetrahedral six-fold ring formed by the basal oxygens,

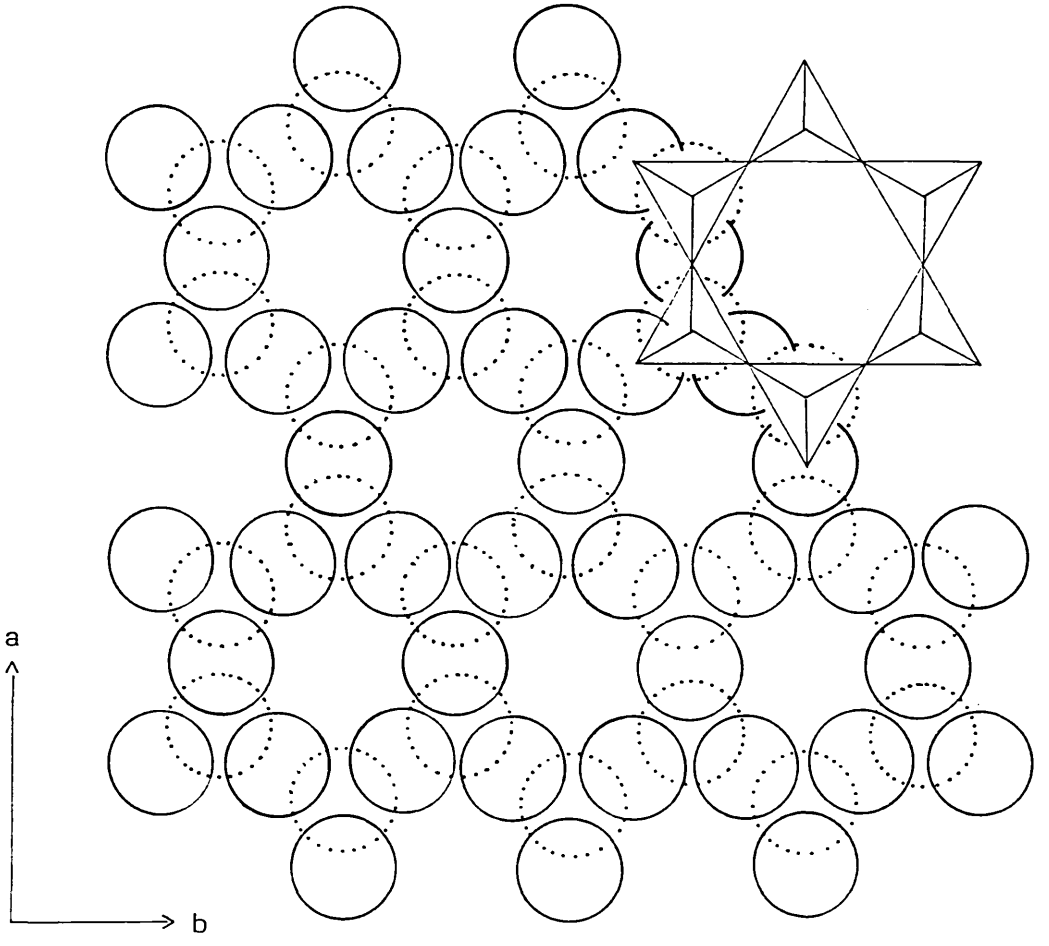

FIG. 5: Plan view of the tetrahedral sheet of mica showing the hexagonal holes formed by the basal oxygens (silicon and aluminium atoms are not shown). The dotted circles represent apical oxygen atoms.

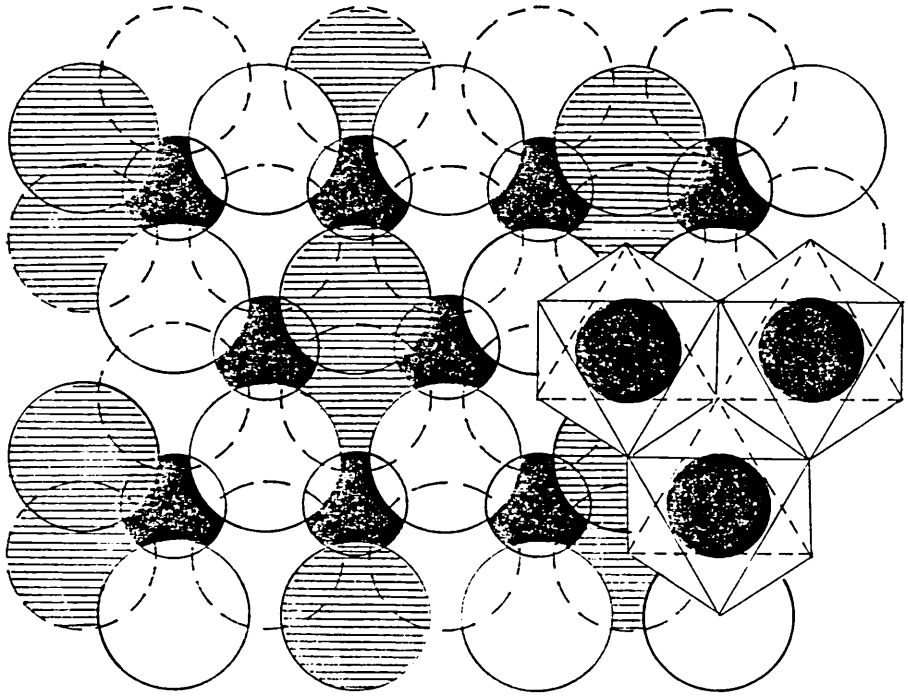

FIG.6: View of the octahedral sheet. Black circles represent aluminium atoms, shaded circles hydroxyl groups and unshaded circles oxygen atoms. Closed circles show outer and broken circles inner hydroxyl and oxygen. (After Bailey, 1980).

but remain in the same plane as the apical oxygens.

Another tetrahedral sheet is joined to the octahedral sheet from the other side with the apical oxygens again pointing towards the octahedral sheet. The combination of three sheets together produces what is known as a 2:1 layer silicate. The octahedral positions are normally occupied by Mg, Al, Fe (II and III), and also to a small extent by Li, Ti, V, Cr, Mn, Co, Ni, Cu and Zn. The hydroxyl groups in some species are substituted partly by fluorine. The smallest structural unit consists of three octahedra and the mica is known as trioctahedral or dioctahedral depending upon whether all three or only two of the octahedral sites are occupied. The 2:1 layer is not electrically neutral because of one or more of the following reasons:

(i) substitution of a trivalent atom (primarily Al, Fe or Cr) for quadrivalent silicon in the tetrahedral layer; this requires a residual negative charge on the trivalent substituent,

(ii) substitution of monovalent or divalent atoms for di- or trivalent atoms respectively in the octahedral positions, or

(iii) additional vacancies in octahedral positions.

The resultant layer charge is generally -1.00, which is neutralized by interlayer cations, normally by potassium ions, but also by sodium, rubidium and cesium ions. A divalent interlayer cation, such as calcium, produces the brittle micas. The edge-on-view of the mica structure is shown in Fig. 7, where all the octahedral positions are

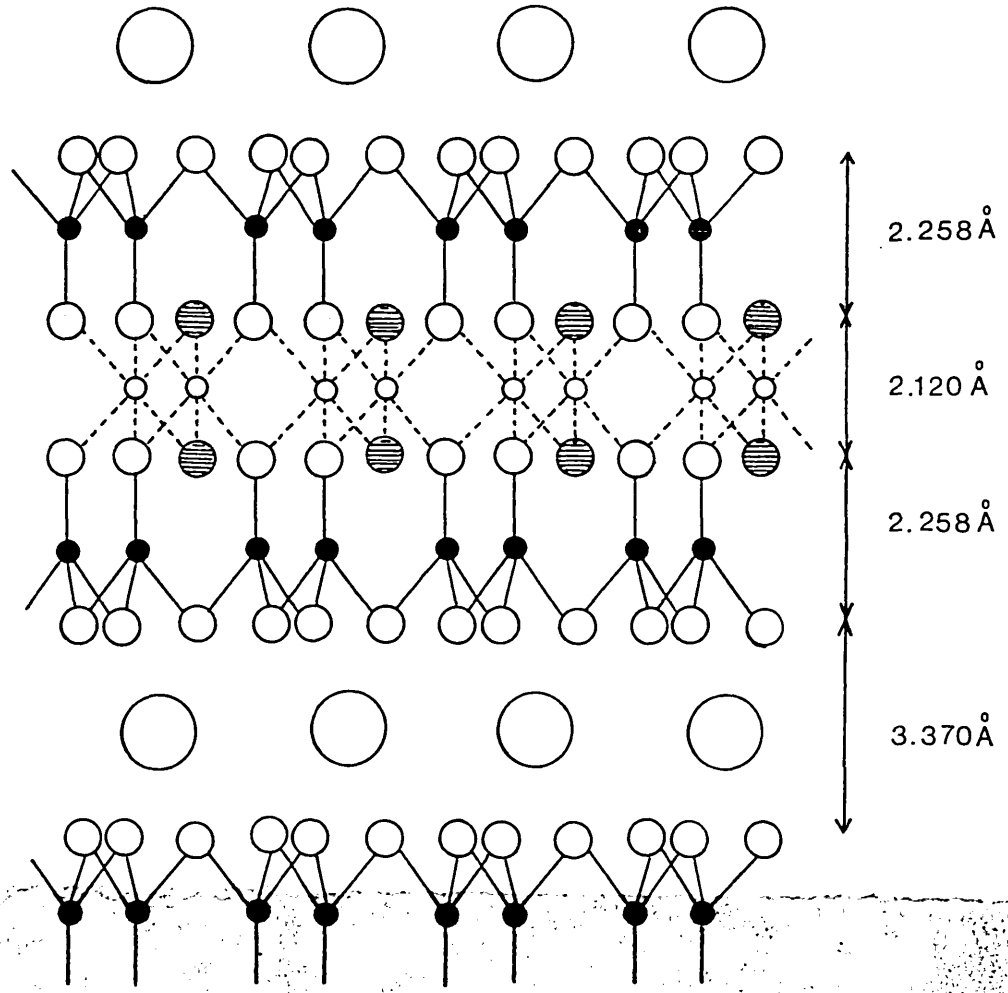

FIG. 7: Edge-on view of the muscovite structure. Large circles represent potassium ions, medium unshaded circles oxygen atoms, shaded circles hydroxyl groups, small black circles silicon and aluminium tetrahedral atoms, and small unshaded circles aluminium octahedral atoms. (After Deer, Howie & Zussman, 1962).

shown as occupied.

A variety of metal atoms can occur in the octahedral configuration and these result in different classes of mica. For example, muscovite has aluminium as the main octahedral atom while phlogopite has magnesium; both of them have potassium as the inter layer cation. In biotite, octahedral positions are filled by magnesium, iron and aluminium while lithium and aluminium are the octahedral atoms in lepidolite.

Yoder and Eugster (1955) have found the following cell dimensions for a $2M_1$ polymorph of muscovite with C2/c space group:-

$a = 5.189 \pm 0.010A$, $b = 8.995 \pm 0.020A$

$c = 20.097 \pm 0.005A$

Monoclinic angle, $\beta = 95°11' \pm 5'$

This unit cell has four formula units $KAl_2(Si_3Al)O_{10}(OH)_2$. The density of muscovite on this basis is $2.83 g.cm^{-3}$. One quarter of the tetrahedral sites are occupied by aluminium but there is conflicting evidence about ordering of silicon and aluminium in the tetrahedral layer. Generally, it is thought that two kinds of tetrahedral sites are present, one fully occupied by Si and the other by $Si_{\frac{1}{2}}Al_{\frac{1}{2}}$ on the average. The basal planes of the (Si_3Al) tetrahedra are symmetrically opposed, as if mirror images, creating a large cavity between the two opposing hexagons of oxygens. Potassium ions fill these cavities apparently in 12-fold coordination. The K-O bond length is 3.09Å on the average, which is larger than the sum of their ionic radii, 2.95Å approximately. Thus, potassium may not be in true 12-fold coordination.

Some interesting deviations from the ideal structure of muscovite were revealed by the rigorous X-ray analysis of Gatineau and Méring (1958). The silicon and aluminium atoms in the tetrahedral layer were found to lie in different planes parallel to (001), the Si-plane being 0.12Å closer to the octahedral plane. The apical oxygens and the hydroxyl groups also exist in two different planes with a separation of 0.06Å. In the octahedral layer, two-thirds of the sites are occupied by Al while the other one-third is vacant. The 12-fold coordination positions between composite layers are all occupied by potassium ions and the stacking of successive layers gives rise to the most common $2M_1$ polymorph. For the ideal structure there should be no X-ray reflections of order (06ℓ) with ℓ = odd, but muscovite gives quite strong (06ℓ) reflections indicating that the structure is highly distorted. Also the monoclinic angle of 95°30′ instead of 94°55′ for the ideal structure points to a distorted structure.

Despite the perfect hexagonal symmetry of the tetrahedral sheets, muscovite symmetry is only monoclinic. The hexagonal symmetry of each tetrahedral sheet is lost when two such sheets are linked by aluminium atoms to form a double sheet as shown in Fig. 8. The hydroxyl groups lie at the centre of each hexagon but since they are not opposite each other because of close-packing, it is not possible to have true hexad axes common to the double sheet. The staggering of the tetrahedral sheets leads to a lower symmetry (i.e. monoclinic) for micas. Fig. 9 shows a model of muscovite mica.

The distortions in the muscovite structure were studied in detail by Radoslovich and co-workers (1959, 1960, 1962a,b, 1963). It has been suggested that the opposing basal oxygen surfaces in micas

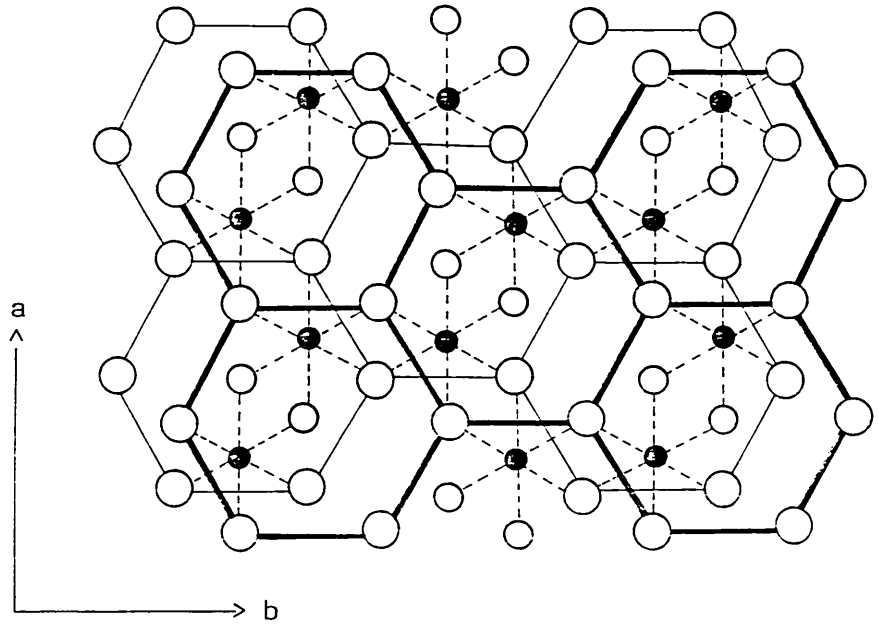

Apical oxygen atom

Hydroxyl group

Octahedral aluminium atom

FIG. 8: The central double sheet of the muscovite structure. The hexagonal nets represent the sheets of vertices of (Si_3Al) tetrahedra on either side of the octahedral sheet of aluminium atoms. The hydroxyl groups lie at the centres of hexagons. The lines outlining the hexagons do not represent bonds. (After Bragg, Claringull & Taylor, 1965).

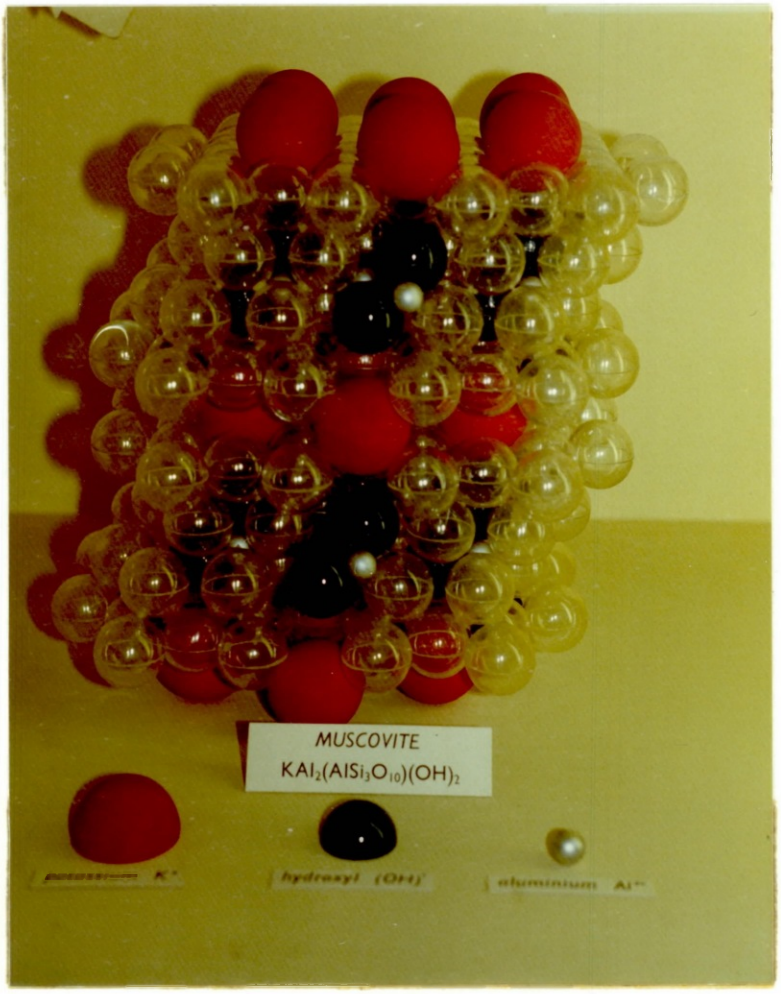

FIG. 9: A model of muscovite mica

are distorted from hexagonal to trigonal or ditrigonal symmetry as a result of tetrahedral rotation. This tetrahedral rotation moves every other basal oxygen towards the centre of each ring, reducing the opening between the two sheets of basal oxygens facing each other. The potassium ions push the two layers slightly apart, thus neutralizing to some extent the effect of tetrahedral rotation. The large potassium ions also stretch the octahedral sheet laterally. Radoslovich (1960) showed that the potassium ions were not at the geometric centres of the oxygen-hexagons, but that they were displaced towards the unfilled octahedral sites above and below their positions. The interlayer cations have only six nearest oxygen neighbours instead of twelve and these six oxygens form a stable octahedral coordination around the interlayer cation.

The composition of mica depends upon the source of natural occurrence and is seldom stoichiometric. Radoslovich (1960)'s data for a natural muscovite sample, yields the formula

$$(K_{0.94}Na_{0.06})(Al_{1.83}Fe^{3+}_{0.12}Mg_{0.06})(Si_{3.11}Al_{0.89})O_{10}(OH)_2$$

which has the following composition:

K_2O 10.91%, SiO_2 46.20%, Al_2O_3 34.28%, Fe_2O_3 2.29%, MgO 0.60%, Na_2O 0.44% and water 5%.

The thickness of tetrahedral and octahedral sheets, and interlayer separation in muscovite are respectively 2.258Å, 2.120Å and 3.370Å. These are shown in Fig. 7. Radoslovich also recognised two kinds of tetrahedral sites: site(I) is half occupied by silicon and half

by aluminium, while site (II) is occupied by silicon alone. The mean Si_I-O bond length (1.695Å) is significantly longer than the mean Si_{II}-O bond length (1.612Å). Within each tetrahedron, the bond to the apical oxygen is larger than the bond to the basal oxygens, by 0.02Å approximately. The potassium ions are nearer to one oxygen layer (with mean K-O bond length of 2.812Å) than to the other (mean K-O bond length of 3.389Å). The mean Al-O and Al-OH bond lengths are 1.954Å. Considerable variations are found to exist among O-O and O-OH distances in both tetrahedral and octahedral layers. These distances are generally determined by packing considerations. The average value of 2.769Å for O-O and O-OH distances is close to twice the ionic radius of oxygen.

Smith and Yoder (1956) suggested that the distortion in the oxygen network of muscovite might be due to the misfit between a tetrahedral sheet and an octahedral sheet. For an ideal tetrahedral layer with silicon-aluminium ratio of 3:1, b should be 9.30 ± 0.06Å. In muscovite, b is only 8.995Å. This indicates considerable contraction of the tetrahedral sheet, which is necessary to accommodate the octahedral sheet. The overall effect would be to stretch the octahedral layer laterally, resulting in its contraction in the perpendicular direction. Thus the octahedral sheet in muscovite is 2.12Å thick, while in gibbsite, for example, a similar octahedral sheet without a tetrahedral sheet, has a thickness of 2.53Å. Radoslovich (1960) suggested that a rotation of about 13° by the Si,Al tetrahedra would produce the necessary contraction required for fitting into the octahedral sheet. The direction of rotation is possibly determined by the small residual charges on the surface oxygens and octahedral Al-atoms, according to Radoslovich.

Muscovite, like the other forms of mica, can exist in several polymorphic forms because of a stagger of a/3 in the octahedral region of each composite sheet. Smith and Yoder (1956) showed six possible polymorphs for muscovite and other micas. Takeda and co-workers (1966, 1969, 1971), on the other hand suggested many more complex polymorphs. Muscovite polymorphs of 1M, $2M_1$ and 3T have been observed, but $2M_1$ is the most common one.

Cleavage in mica takes place very readily along the (001) plane in the potassium layer. Electrical neutrality requires that the potassium ions are divided equally between the two cleaved faces. The cleaved faces are often not of equal thickness all over, but have a series of steps. Tolansky (1948) showed such steps to have a thickness of about 10Å or its multiple. The preferred orientation of crystals of ammonium iodide and other substrates grown on a freshly cleaved mica surface, demonstrates the existence of these steps.

All micas have a water-content to the extent of 4-5 per cent. Ganguly (1951), and Brown and Norrish (1952) suggested that some of the water might exist as H_3O^+ ions replacing potassium ions from the interlayer positions.

The ordering of the metal atoms in micas has been recently reviewed by Bailey (1984). Ordering of the tetrahedral species, silicon and aluminium, is not observed in muscovite $2M_1$, phlogopite 1M and biotite 1M, which are the most common micas. It is shown that an apical oxygen attached to a tetrahedral silicon and two octahedral aluminium atoms has its negative charge exactly balanced. If the tetrahedral atom is also aluminium, then an excess negative charge remains. Ordering would require, as Güven (1971) has shown, that two apical oxygens with negative charge remain diagonally along

an octahedral edge common to two octahedral aluminium atoms. Such ordering is not found in muscovite mica because of the instability of the structure due to repulsion between the two apical oxygens.

XPS and X-ray photoelectron diffraction (XPD) have been used in recent years to determine the composition and structural details of natural aluminosilicates by Adams and co-workers (1977, 1978) as well as by Evans and co-workers (1977, 1978, 1979a, 1979b, 1982). Assuming the extents of substitution in the tetrahedral and octahedral layers of muscovite to be respectively 'x' and 'y', Evans, Adams and Thomas (1979b) give the following general formula to muscovite:

$$M^{I}_{(x+y)/(4-x)}[M^{III}_{(2-y)/(4-x)}M^{II}_{y/(4-x)}][Si_{1.00}M^{III}_{x/(4-x)}]O_{10/(4-x)}(OH,F)_{2/(4-x)}$$

on the basis of Si = 1.00. On XPS analysis, the actual formula comes out to be

$$M^{I}_{1.1}[Al_{1.62}Fe^{III}_{0.24}Mg_{0.15}][Si_{3.05}Al_{0.95}]O_{10}(OH)_{1.98}F_{0.02} \ .$$

The authors did not find any compositional differences between the cleavage planes and the bulk. The total interlayer ion content (K+Na), obtained from XPS analysis, is slightly less than that obtained from chemical analysis; the authors attributed this to the presence of small quantities of Li, Cs, Rb below the XPS detection limit. Even fluorine could not be detected by XPS, only chemical methods were able to find its presence in muscovite. XPD data showed that the small number of sodium ions (normally about one-tenth of potassium ions) occupied positions close to one of the two opposing basal oxygen layers. This was attributed to the small size of the sodium ions.

The large potassium ions, on the other hand, would be expected to take up middle positions between the two oxygen layers.

The overall picture of the top three layers of a cleaved muscovite surface is shown in Fig. 10, following after Müller and Chang (1968), and Lewis and Anderson (1978). The first layer consists of half a monolayer of potassium ions with the other half being vacant after cleavage. Although the filled and vacant potassium positions are shown as ordered in Fig. 10, the evidence so far suggests a random distribution of these sites. The second layer consists of oxygen atoms from the basal plane of the Si, Al-tetrahedra. All the three oxygen atoms for a given tetrahedron, are shown as non-equivalent. The tetrahedral cations, silicon and aluminium, form the third layer. Two different types of silicons are shown; one with a neighbouring aluminium atom and the other without. The unit mesh and the distorted oxygen hexagon are also outlined in the figure.

2.2 OUTGASSING OF MICA

The first attempt to quantitatively estimate the amounts of gases released on heating mica was reported by Collins and Turnbull (1961). These authors found that a piece of muscovite pretreated at 400°C for 1 hour, gave off the following gases when heated continuously for 40 hours again at 400°C.

Hydrogen : 1.5 μℓ/g

$CO + N_2$: 0.2 μℓ/g

CO_2 : 0.3 μℓ/g

O_2 : 0.01 - 0.5 μℓ/g .

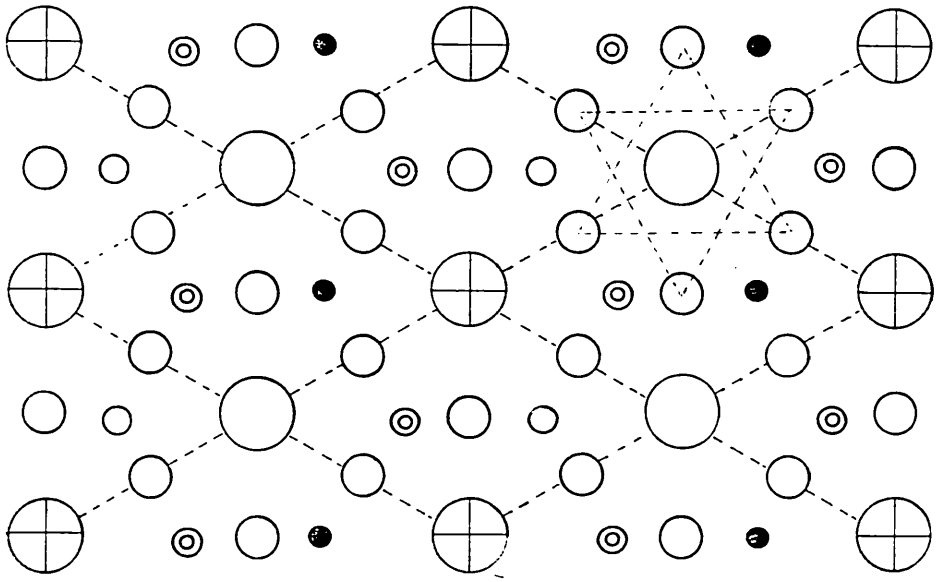

Sites filled with potassium ions

Sites previously occupied by potassium ions

Oxygen atoms

Silicon atom with an aluminium neighbour

Silicon atom without an aluminium neighbour

Tetrahedral aluminium atom

FIG. 10: Surface sites of mica. The unit mesh and the distorted oxygen hexagon are outlined. Half the potassium sites are empty. (After Müller & Chang, 1968 and Lewis and Anderson, 1978).

A considerable amount of water vapour was also evolved, together with mass 19, but the authors did not quantify these results. The variable amounts of oxygen evolution were attributed to trapping or occlusion of the gas in fissures between the layers on the cleavage plane. Why this does not happen with the other gases, particularly nitrogen, is not explained.

Lawson (1962) studied the outgassing of mica at above 500°C and noticed no change in physical appearance up to 750°C in vacuum. Above this temperature, muscovite mica shows interference colours and then gradually becomes opaque above 770°C accompanied by exfoliation of the sheets, and expansion to almost three times its original thickness. It was also found that the rate of gas evolution from mica between 650 - 950°C was almost linear. It was shown that water-evolution stopped at temperatures above 750°C and the rate of gas evolution was then determined by diffusion processes.

Thermal degassing of a UHV cleaved muscovite surface was investigated in some detail by Mercer (1967), from room temperature to about 300°C. Water was found to be the major desorbant starting from a temperature of ~ 70°C and proceeding to the end of the cycle, with a maximum around 250°C. It was estimated by Mercer that for every 2-5 potassium ions in the cleavage plane, there was one water molecule. Interestingly, the cleaved surface also desorbed N_2, CO, H_2 and CO_2 in smaller amounts and the desorption peaks, excepting that for N_2, had well-defined shoulders. The N_2-peak and the high-temperature shoulders for the others were considered to be due to a slow diffusion process from the interior. The first prominent peak shown by CO, H_2 and CO_2 was assigned to adsorption on the UHV-cleaved surface although the source of these gases was not known.

Adsorption strengths were given as CO_2 < CO < H_2,H_2O. The composition of the evolved gases was estimated roughly as water vapour, 70-80%: H_2 and CO, 10% each; and CO_2, 3%. The experimental results of Mercer are shown in Fig. 11.

Generally the trioctahedral micas, like phlogopite and biotite, are thermally more stable than the dioctahedral micas like muscovite. Thus,under ordinary conditions, muscovite decomposition starts at about 650°C while phlogopite decomposition takes place at above 1000°C. Vedder and Wilkins (1969) have commented that the vacant octahedral positions in muscovite may have contributed to its relative thermal instability, although no mechanism was suggested. These authors have shown that when muscovite is heated in air, the structural OH-groups are removed gradually at 600°C and above, through dehydroxylation. The dehydroxylation is not an equilibrium process. The process starts at the surface and gradually proceeds into the interior. Coloured striations are observed initially parallel to the a-axis, then as the temperature rises, water molecules begin to form inside the layers, and move to the edges where they escape. The dehydroxylated muscovite expands along both b and c axes, but no change in 'a' is observed. Dehydroxylation is a very slow process and, as shown by Vedder and Wilkins, a 1.35μm thick piece of mica requires 760 hours to lose 70% of its OH-content. On exposing this sample to water-vapours, up to 84% of the original OH-content was regained. IR spectra showed that the muscovite structure was distorted further during dehydroxylation, but these distortions were removed after rehydroxylation when the OH groups returned to their original positions.

Outgassing of mica in UHV was studied by Poppa and Lee (1976) who suggested a working temperature for mica of less than 550°C to

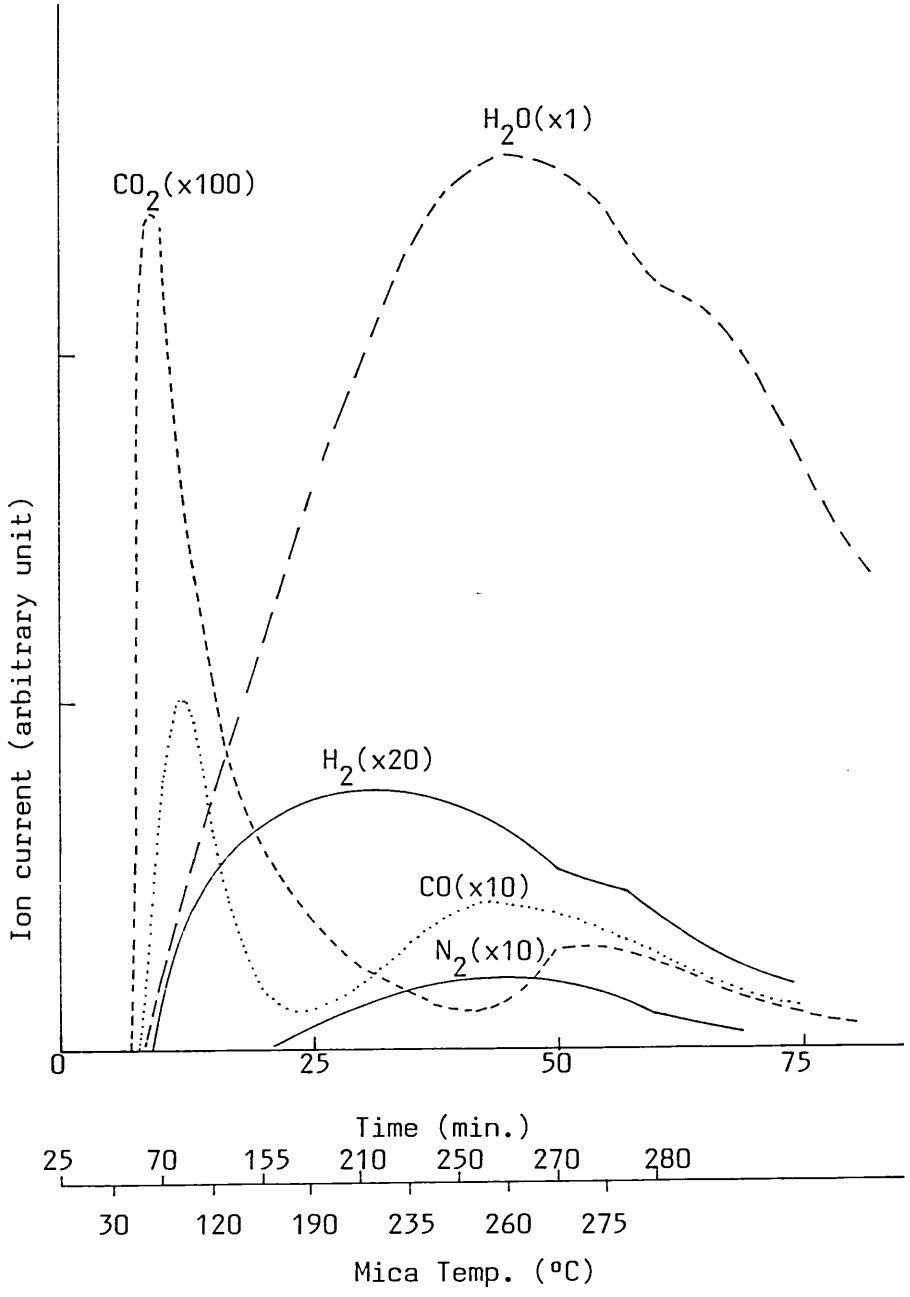

FIG. 11: Gases evolved on heating a freshly cleaved mica surface (after Mercer 1967).

prevent decomposition. Poppa and Lee noticed that all residual gas components except water could be removed by heating, but at temperatures $\geqslant$ 450°C dehydroxylation started to generate increasing amounts of water in short, characteristic bursts. A freshly cleaved surface after annealing is thus left with an equilibrium coverage of water, determined by the annealing temperature, water partial pressure and the pumping speed for the system. Poppa and Lee observed no change in the oxygen-signal on Auger analyses of the freshly cleaved surface and the annealed surface. The change in oxygen-Auger signal due to desorption of water was thought to be too small to be detected. Surprisingly, however, the Auger analysis of a freshly cleaved surface annealed for 30 minutes at different temperatures showed a depletion of potassium signal up to 40%. This was, however, not thoroughly investigated.

2.3 CLEAVAGE OF MICA

Cleavage of mica in air does not require much of a force, but in UHV, the force required is quite considerable. Bryant (1962) has observed that UHV-cleaving required as much as 30 times more energy than air-cleaving. In an experiment designed to test the effect of different components of air on the cleaving process, Bryant definitely established that water vapour helped cleaving by reducing the binding energy between mica layers in some manner. In a more detailed analysis, Bryant, Taylor and Gutshall (1963) attributed the large difference in cleavage energy of mica in air and in UHV to two possible mechanisms:

(i) A diffusion mechanism in which a gas, e.g. water vapour, enters deep into the solid, weakens bonds between atoms and promotes easy cleavage. In ultra-high vacuum, such a possibility is almost absent and cleaving requires tremendous force.

(ii) A charge mechanism in which the two new surfaces, generated upon cleavage, are assumed to have charge mosaics on them with a net attractive force. These charges are quickly neutralized by gas adsorption in air, and again, in UHV, charge neutralization is either not possible or liable to take a very long time.

Deryagin and Metsik (1960) had actually measured charge mosaics on freshly cleaved muscovite surfaces and Gaines and Tabor (1956) calculated the ionic binding energy of a muscovite surface to be 2,875 ergs/cm^2. Bryant and co-workers (1963), using a quartz deflection fibre, determined the energy necessary for cleaving muscovite at pressures of 10^{-10} torr to be 4,570 ergs/cm^2. All these results were explained on the basis of the charge mechanism of cleaving. It was shown that the energy required to cleave muscovite in UHV should be equal to the coulombic attraction between the positively charged potassium ions and the negative charge of the alumino-silicate framework. The calculated value of cleavage energy on the basis of charge mosaic agrees very well with the experimental values, as was shown by Bryant and co-workers.

On cleaving muscovite in vacuum, Mercer (1967) observed that all specimens released nitrogen and hydrogen with small amounts of carbon dioxide, carbon monoxide, methane, argon and oxygen. It was proposed that these gases were occluded in pockets or fissures,

restricted to the actual cleavage plane and the amount of gas released was determined by the number of such pockets or fissures. The number of gas molecules released was estimated at between 8.5×10^{12} to 2×10^{14} per cm² of cleaved surface for a number of different specimens. The maximum pressure rise observed was 7×10^{-5} torr in a static 1 litre volume. Müller and Chang (1969) on the other hand found a pressure burst in the 10^{-8} torr range in a 60 litre system during cleaving of muscovite, but synthetic phlogopite mica gave a pressure rise of less than 1×10^{-10} torr on cleaving. Müller and Chang's data differ from those of Mercer (1967) only in one respect, the former detected water vapour released by the cleavage process whereas the latter did not.

2.4 SURFACE STUDIES

Studies of mica surfaces have so far been directed at evaluating the suitability of the surface as a substrate for epitaxial vapour deposition. The advantages of mica as a substrate material were summarized by Poppa and Elliot (1971) as:-

(i) it can be cleaved easily to get a clean surface and samples as thin as a few hundred angstroms can be prepared,

(ii) mica is available in single crystal, high-grade natural and synthetic forms,

(iii) it has reasonable thermal stability up to 700°C, and

(iv) specimens for examination under the electron-microscope can be easily prepared by the mica stripping method.

Lewis and Anderson (1978) also recently reviewed the use of mica surfaces for thin-film epitaxy experiments. One of the important observations made by Jaeger, Mercer and Sherwood (1967) was that films deposited under identical conditions on air-cleaved and vacuum-cleaved mica surfaces had different structures. No epitaxy was seen on the air-cleaved surface; but after exposing the air-cleaved surface to water vapour, partial epitaxy was obtained. Water vapour might have a part to play, but no concrete reason was put forward.

Low Energy Electron Diffraction (LEED) patterns of mica show hexagonal unit mesh. This was reported by Müller (1966) and Deville, Eberhardt and Goldsztaub (1967a, 1967b). Müller and Chang (1968, 1969) studied LEED patterns produced by both the air-cleaved and the vacuum-cleaved muscovite surfaces. A vacuum-cleaved surface was shown to have charged to a potential greater than 1000V, whereas mica cleaved in 10 torr pressure of H_2, O_2, N_2, H_2O, CO, Ar, or air remained uncharged. The charge on the vacuum-cleaved surface could be removed by directing electrons of energy > 1000eV at the surface or by heating above 100°C. When exposed to an electron beam, both vacuum-cleaved and air-cleaved mica surfaces showed a secondary charging, the final potential being dependent on the energy of the beam. This energy must exceed a certain value (according to Müller and Chang, about 30 to 80V depending upon the sample) in order that a LEED pattern can be seen. The authors noticed that an air-cleaved mica surface showed the normal round spots which, however, gradually deteriorated and eventually were blanked out. The vacuum-cleaved surface, on the other hand, showed unusual patterns with triangular spots, three-winged stars, triple or double spots, or streaks - all

with similar orientation. The authors showed that surface disorder and imperfections were unlikely to be the cause of these abnormal patterns and instead they attributed them to the existence of dipole domains on the mica surface between the K^+ ions of the top layer and the atoms of the inner layers. The results also indicated a complete lack of ordering of the K^+ ions on the cleaved surface and correspondingly of the substitutional aluminium atoms in the tetrahedral layer.

The characterization of a clean mica surface and identification of contaminants was first reported by Poppa and Elliot (1971) from their Auger Electron Spectroscopic study of mica surfaces under different conditions. The principal contaminant of an air-cleaved surface was found to be carbon whereas a surface cleaved in UHV did not show any carbon. The source of this carbon-contamination was not definitely established. It was, however, shown that a mica sample cleaved in UHV did not take up any carbon when subsequently introduced to CO, CO_2 or CH_4. On the other hand, the UHV-cleaved surface picked up carbon when exposed to laboratory atmosphere. The conclusion drawn by the authors was that water vapour in air could, in some way, promote carbon-contamination.

Poppa and Elliot (1971) also demonstrated that a UHV-cleaved surface of mica remained clean through long heating periods in UHV and there was no diffusion of contaminants from the interior. The AES revealed only a depletion of potassium-content. The air-cleaved mica, on the other hand, showed much more depletion of potassium and enhancement of the silicon peak as well as the carbon peak. The

air-cleaved surface was made carbon-free by heating in 2 x 10^{-5} torr of oxygen at 450-500°C for 4 hours, but this reduced the amount of potassium on the surface. Bombarding the UHV-cleaved surface with 1KeV electrons, the authors concluded that quadrivalent silicon in the surface was reduced to elemental Si, and the potassium content was reduced greatly, but carbon-contamination reappeared.

Staib (1973) noticed that a low current density was needed for Auger analysis of mica surfaces to avoid charging problems and also to prevent electron impact desorption of surface potassium. The author carried out a depth analysis of vacuum cleaved muscovite surfaces, the top layers being successively sputtered away with a low energy (500eV) argon ion beam. The ion bombardment seemed to have destroyed the surface very rapidly, as no LEED patterns could be obtained after bombardment. According to the authors, the upper two layers of potassium and oxygen were completely destroyed and the sample became more insulating due to removal of the surface potassium ions. This was reflected in a shift of 6eV to higher energies for all Auger peaks. The bombardment also resulted in surface enrichment of silicon and aluminium, but as a whole the depth analysis by AES was made ambiguous by the ion-induced effects on the surface composition.

Static Secondary Ion Mass Spectroscopy (SIMS) analyses of the mica surface by Dowsett, King and Parker (1977, 1978) yielded identical results to the AES analyses, discussed above, for the surface contaminants of mica. The authors demonstrated the usefulness of SIMS in detecting all the major constituents of muscovite together with various isomorphous replacements. It was suggested that alkali halides were present on the air-cleaved surface as contaminants. The

major carbon-contamination was shown to be of hydrocarbon origin which resisted cleaning procedure by UHV-heating and ion-bombardment. The UHV-cleaved surface was shown to be the cleanest, although SIMS revealed a little carbon contamination even on this surface, which the authors described as being native to mica. The UHV-cleaved surface was also shown to pick up carbon-contamination through prolonged heating in UHV. The potassium depletion from the UHV-cleaved surface on heat treatment was estimated at one tenth. Elliot (1974) observed significant depletion of potassium from both surface and bulk on heating a mica specimen, the depletion proceeding rapidly at first and then tending to some stationary value.

SIMS was recently used in combination with AES and Ion Scattering Spectroscopy (ISS) to characterize mica surfaces by Baun (1980), and Baun and Solomon (1980). The results on matching cleaved surfaces definitely indicated that cleavage occurred along the potassium layer with potassium ions equally divided between the separated surfaces. The authors also showed the difference in potassium content between a freshly cleaved surface and a weathered surface.

While much work seems to have been done to characterize the mica surfaces and to evaluate effects of various heat treatments, no systematic work has been reported on the chemical reactivity of mica surface. The mica surface has been generally regarded as inert, but the carbon-contamination found by almost all workers on air-cleaved surfaces, points to a different picture. The exposure of the vacuum-cleaved surface to carbonaceous gases was reported by Müller and Chang (1969), Poppa and Elliot (1971), and others. These studies

however, appear not to be exhaustive and no conclusion could be drawn with any certainty about the source of carbon-contamination from the published data. Another commonly reported feature of mica surfaces is the loss of potassium from the surface as well as bulk on heating. The effects of this on the properties of mica havealso drawn very little attention.

As in the case of LEED and other surface techniques, application of XPS to mica has been plagued by the problem of surface charging. Castle, Hazell and West (1979), for example, found that the binding energies of mica-constituents were apparently increased by about 7.5eV due to charging. The authors investigated the effects of hydration on the silicon and aluminium peaks of muscovite and suggested that the XPS results indicated a greater degree of ionic bonding for both silicon and aluminium in the muscovite framework. The ionic bonding was attributed to the presence of water between the layers. A few XPS data on muscovite were also reported by Wagner and co-workers (1982).

2.5 REACTION STUDY ON MICA SURFACES

Isomerization of cyclopropane to propene has been a favourite test reaction for studying acidic sites of a catalyst. Prada-Silva and co-workers (1979) studied this reaction on a muscovite surface at temperatures between 700 and 900K, using a Recycled Molecular Beam Reactor. In this technique a beam of cyclopropane, which could be heated to different temperatures, was directed at the surface of mica

and the scattered gas was recycled. Although this work was aimed at elucidating the role of vibrational energy in isomerization of cyclopropane, the results indicated an activated adsorption of cyclopropane on the mica surface followed by desorption of propene. The authors reported that the initial aluminium to silicon ratio of 0.98 (from XPS peak intensities) of the muscovite sample changed to 0.60 after the experiments, indicating a considerable decrease in surface aluminium. A decrease in potassium and an increase in carbon were also observed. The authors also investigated another muscovite specimen, which had undergone ion-exchange with concentrated ammonium hydroxide solution and had then been calcined to give an "acidic" surface. The results with this surface were shown to be similar to those on the untreated mica. Because of the Molecular Beam technique, the isomerization must have actually occurred at the mica surface. The activation energy for the process was found by the authors to be 21k cal/mol, which is within the range of 15 to 35 k cal/mol., found by Hall, Lutinski and Gerberich (1964), and by Bassett and Habgood (1960) for the truly catalytic process on silica-alumina

Löffler, Haller and Fenn (1977) extended the Recycled Molecular Beam technique to study the isomerization and dehydrogenation of butene-1 on mica surface. The reaction was found to depend on the surface temperature of mica, rather than on the energy of the butene molecules. The authors found the activation energies for butene-1 to cis- and trans-butene 2, and butadiene-1,3 to be respectively 41.9, 48.1 and 58.2 kJ/mol. These values are lower than the values for homogeneous thermal isomerization and dehydrogenation, which are all above 250kJ/mol. The conclusion drawn was that the reaction was of a catalytic nature on mica surface, starting with the chemisorption

of butene molecules on to the mica surface at 650 to 850K, followed by transformation into products. The authors suggested that the results could very well be compared to those on silica-alumina by Gerberich and Hall (1966), despite the higher alumina content and the presence of potassium in mica. The muscovite sample was shown to retain its activity even after several runs. The authors, however, thought that the mica sample must have lost its crystallinity due to removal of aluminium and potassium.

No other study of catalytic reaction on mica surface has been found in the literature.

CHAPTER THREE

ADSORPTION/DESORPTION EXPERIMENTS IN THE GLASS ULTRA-HIGH VACUUM APPARATUS

3.1 THE APPARATUS

3.1.1 GENERAL DESCRIPTION

The adsorption/desorption measurements on mica surfaces were carried out in a glass ultra-high vacuum (UHV) apparatus which was originally used for molecular beam experiments on metal surfaces. The apparatus in its original form was described by Walters (1973) and also in varying forms by Chappell and Hayward (1972), and Hayward and Walters (1974). For the present work, a number of modifications were made to this apparatus. A description of the apparatus in its present form, therefore, seems necessary.

A schematic diagram of the apparatus is shown in Fig. 12. The apparatus was constructed from pyrex glass. It was pumped by a series of liquid nitrogen trapped mercury diffusion pumps (Z1, Z2 and Z3). The portion enclosed by the dotted lines is the Ultra-High Vacuum (UHV) section, a photograph of which is shown in Fig. 13. This section is bakeable and does not contain any greased stopcocks. Instead, magnetically operated ball and socket (dekker) valves (D1, D2, D3, D4, D5, D6, and DL) are used to isolate various parts of the system. The valve DL is a leak valve such that gas can be pumped at a known rate when this is closed. CT1 to CT5 are liquid nitrogen cooled cold traps.

C represents the cell containing the mica sample with

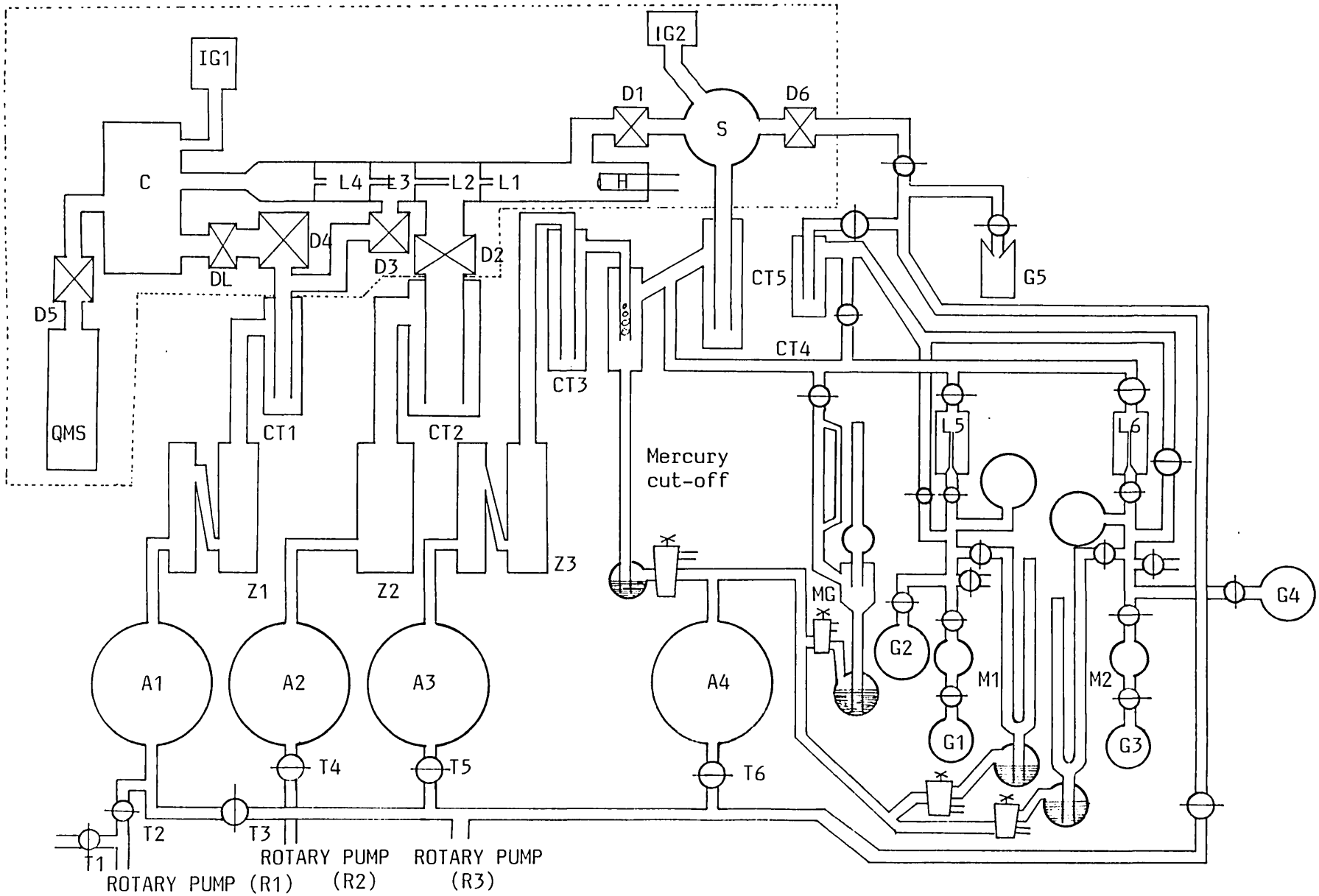

FIG. 12: The glass system for adsorption/desorption experiments (The bakeable portion is enclosed inside dotted line).

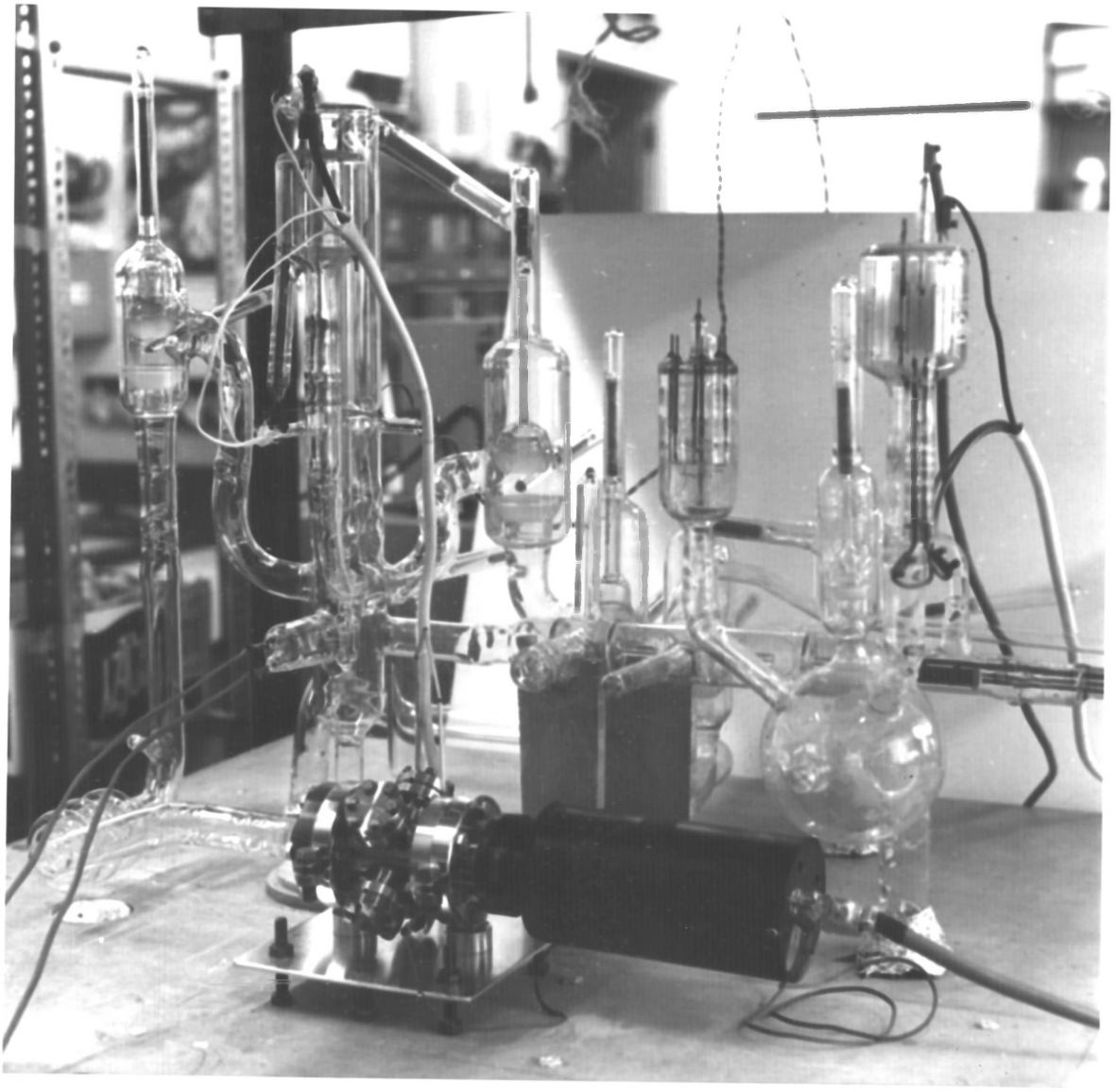

Fig. 13 The glass UHV system for adsorption/desorption experiments. View from the mass spectrometer side.

arrangements for cleaving and heating. The pressure in the cell is measured with an ionization gauge (IG1) or with the quadrupole mass spectrometer (QMS). Gas is stored in the bulb S where pressure is read with the ionization gauge (IG2). Gas is dosed into the cell via the four capillaries L1, L2, L3 and L4. Gases are stored in G1, G2, G3 and G4 and a constant pressure of gas at S is maintained by controlled leak of gas through either one of the capillaries L5 or L6.

3.1.2 PRELIMINARY DESIGN PROBLEMS FOR THE ADSORPTION/DESORPTION CELL

The design of a successful cell required much preliminary experimentation in order to satisfactorily meet the following needs:-

(a) an ability to cleave mica in situ,

(b) the provision of controlled heating and cooling of the mica sample for adsorption/desorption experiments, and

(c) an ability to measure the adsorption/desorption of small amounts of gases.

A glass-encapsulated soft-iron slug and hook arrangement, operated magnetically from outside, was considered the best possible way to cleave mica in a glass system. Initial experimentation showed that cleaving of mica in UHV required a tremendous force and unless the sample was rigidly supported at both ends, either it could not be cleaved at all or the whole piece of mica became detached from the holder during the cleaving process. The holder needed to be rotated so that both faces of the mica could be cleaved using the same hook

mechanism. Some vertical motion was also desirable to aid cleaving. The design of the cell is thus intricately linked with the design of the sample holder.

Mica, being a very bad conductor of heat, presents problems for design of a suitable heating or cooling arrangement. In initial designs, the sample-holder was such that it could be lowered into a finger at the bottom of the cell which could be heated or cooled externally. This method was abandoned when it was seen that neither heating nor cooling was adequate, and also the raising and lowering of the sample holder was seen to produce spurious pressure bursts.

In an alternative design of the cell, a heating filament in direct contact with the sample was used. This method of heating had the disadvantage that the mica closest to the filament decomposed before the bulk of the sample had reached the required temperature. Electron bombardment heating was then tried using an independent filament placed some distance from the mica to allow for the rotational movement of the sample. The emitted electrons were collected on a gold foil placed against the mica sample. With 8mA electron emission and a collector potential of 6kV, this method failed to give a temperature significantly higher than that produced by conduction from the hot filament alone without electron bombardment. The failure of this method of heating was probably due to poor thermal contact between the gold foil and the sample. This could possibly have been remedied by depositing a thin layer of gold on the back of the mica sample, but this would have prevented cleavage of both faces and might have interfered with the adsorption measurements.

Radiative heating with a tungsten filament near the mica sample was found to be the only suitable method of heating. With a supply

of 4A/14V to the filament, mica could be heated to 573K, which was sufficient for most of the experiments. The thermocouple for measuring the temperature was fixed by pushing it in between the mica-layers as no other way of fixing the thermocouple was found suitable.

3.1.3 THE WORKING CELL

The cell finally used in this work is much simpler than several originally tested. A side view of the cell is shown in Fig. 14 and a photograph of the cell is given in Fig. 15. All the results reported from the glass system were done on this cell.

The cell consists of a wide-bore glass tube of diameter 4.5cm and total height 47cm. The finger at the bottom was part of an earlier design. The tube T2 (diameter 1.2cm) was sealed concentrically to the cell and provided the rigid support to the sample holder, necessary during cleaving. The cleaving hook H is contained in a side-arm and can be moved by external magnets. The hook is made of 1.5mm diameter tungsten rod sealed to a glass-encapsulated iron slug M3. During cleaving, the hook engages a wire loop attached to the mica sample and the cleaved flake is deposited in the storage tube W.

The heating filament F was made from 0.3mm diameter tungsten wire and is introduced through two glass-to-metal seals at the centre of the cell. The cell has three additional glass-to-metal terminals; two were used for the thermocouple and the third was originally intended as a high tension lead for electron-bombardment.

Each time a new mica sample was introduced, the cell had to be

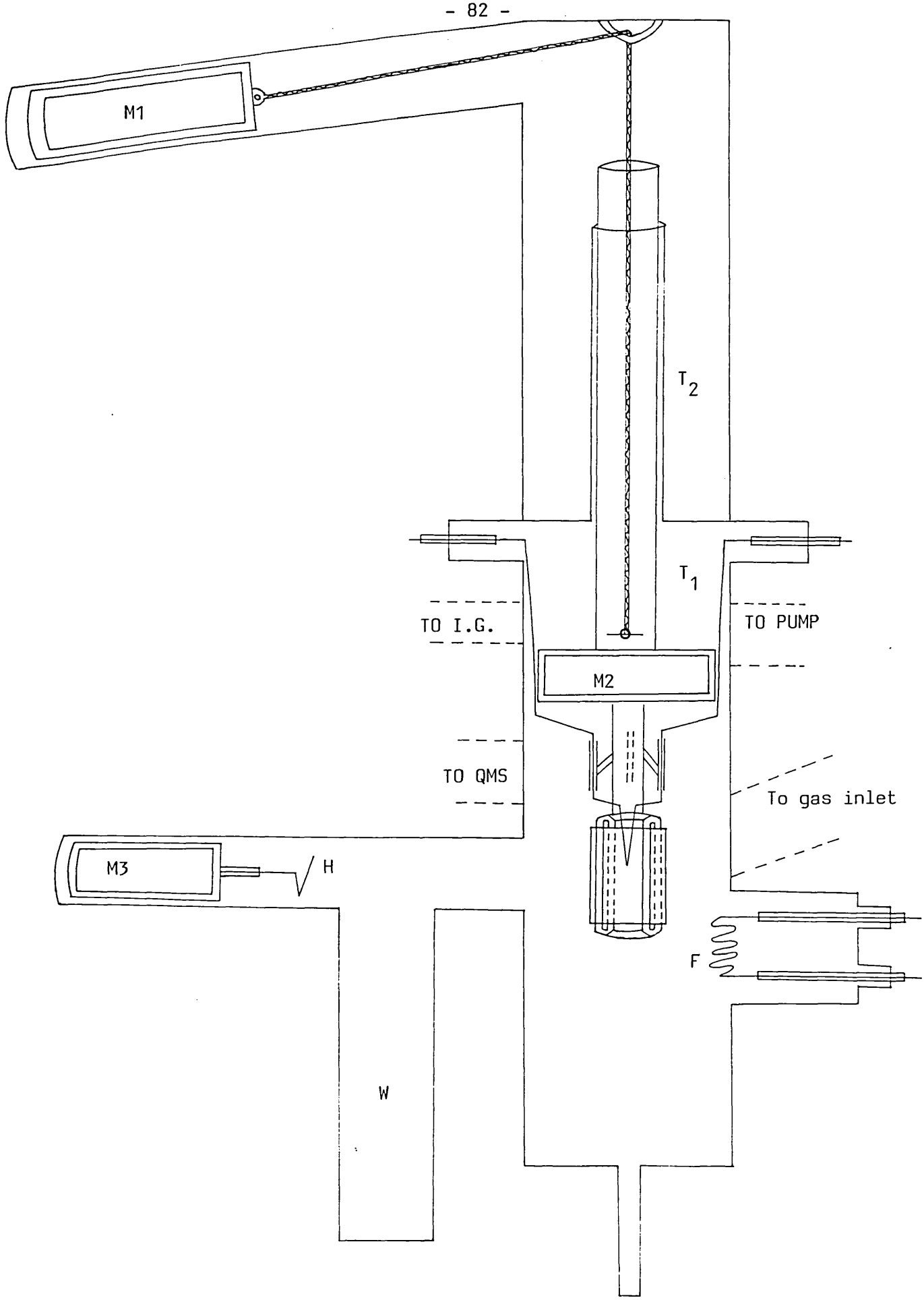

FIG. 14: The cell

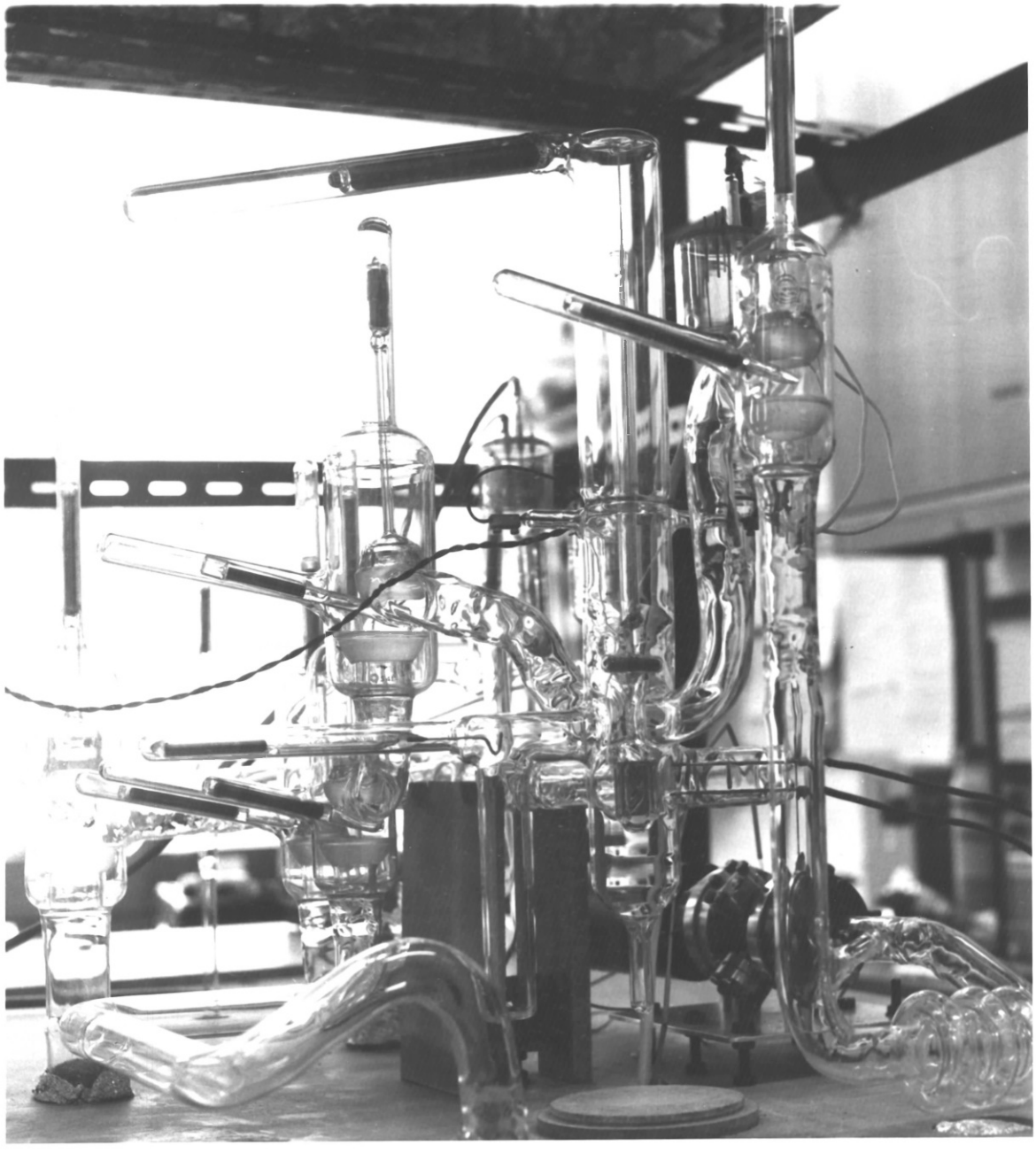

Fig. 15 Front view of the glass UHV system showing the adsorption/ desorption cell, the arrangement for cleaving, the sample holder with a mica sample and the heating filament.

broken above the hook arm and resealed.

3.1.4 THE SAMPLE HOLDER

The sample holder can be seen in Fig. 14 and also in the accompanying photograph, Fig. 15. The holder was made from 3mm diameter glass rods joined together with a narrow opening between them to form a cage which could hold a piece of mica. This cage is connected through a glass rod to a small glass-encapsulated iron slug M2. This glass rod also carries three small 3mm diameter glass tubes through which the two thermocouple leads and the high tension lead (not used) could be connected to the sample. A long glass tube T1 is connected to the top of the slug M2. The tube T1 can move freely inside the fixed tube T2. A sterling silver chain connects the sample holder to a large glass-encapsulated slug M1 which is contained in the top side-arm of the cell. The weight of this slug exactly balances the weight of the sample-holder assembly. The sample can be lowered or raised by moving the slug M1. The slug M2 helps to rotate the sample to make it face the cleaving hook, the gas-inlet or the filament, as required.

3.1.5 THE GAS-INLET SECTION

Gas was introduced to the cell via a molecular beam dosing line, although in this work it was not normally operated so as to give a molecular beam. The dosing line consists of four accurately aligned capillary tubes L1, L2, L3 and L4 of the same internal diameter,

but of different lengths. The intervening spaces between the capillaries are pumped by diffusion pumps. The chamber behind L1 is connected to the gas storage bulb S through the dekker valve D1. The chamber between L1 and L2 is pumped via wide bore tubing by the high speed mercury diffusion pump Z2, which is a Jencons H.134/2 pump with a reported speed of 30 litres/sec. at 10^{-6} torr. The section between L2 and L3 and the cell C are both pumped by the combined single and three stage Klemperer pumps Z1 via the dekker valves D3 and D4 respectively. For introducing the gas as a molecular beam, the dekkers D2 and D3 must be kept open so that gas not constituting the beam can be pumped away. In the present work, however, D2 and D3 were kept closed during gas-dosing. Gas was let into the cell by opening the dekker D1 and the cell was kept pumped during gas-dosing by keeping D4 open.

The RF heater H at the end of the beaming section was originally intended to provide an oven-source for the molecular beam, but was not used during the work.

Towards the end of the present work, the beaming section accidentally broke between L2 and L3, and the last experiments were carried out by connecting a direct dosing line from the storage section S, after D1, to the cell. This dosing line contained a 6cm long capillary of internal diameter 1mm. The section between the dekker D1 and the end of this capillary is pumped via D2 by the Jencons diffusion pump.

1.3.6 THE GAS-HANDLING SECTION

Schematically, this section can be seen in Fig. 12. Four gases can be stored at a time in the bulbs G1, G2, G3 and G4. Permanent gases can be let into the storage bulb S by one or other of two gas lines, each with its own manometer. Gas at a pressure of approximately 1cm mercury is introduced into either volume V1 or V2 and then allowed to pass through a calibrated capillary, either L5 or L6, at a known rate. The gas enters the storage bulb S via the cold trap CT4. The storage section as well as the gas handling lines are pumped by a set of Klemperer single and three-stage mercury diffusion pumps, Z3. The rate of pumping can be controlled by raising or lowering the mercury cut-off C1 to close or open one or more of the pumping holes. In this way, any desired pressure of a gas can be established at S.

For condensible gases, a new handling line had to be constructed to avoid gas pumping through the cold trap CT4. This line consists of the gas-generating bulb G5, stopcock T10 and the dekker valve D6.

3.1.7 PUMPING

The mercury diffusion pumps are backed by three rotary pumps, which also serve to rough-pump the system to give pressures in the 10^{-3} torr region. R1 backs the diffusion pumps, Z1, which pump the cell and the middle of the beaming section. R2 backs the Jencons pump, Z2, R3 backs the diffusion pumps Z3 for the storage section and all the gas-handling lines. The pumps R1 and R3 are kept isolated

(by closing T3) during gas-dosing to prevent back-diffusion of the gas to the cell. With the help of appropriate stopcocks, any part of the gas-handling section can be rough-pumped by the pump R3 while the diffusion pumps Z3 are kept isolated. Each rough pumping line is backed by a 5 litre volume (A1, A2, A3 and A4) which helps to maintain the vacuum even when the backing rotary pump is disconnected for several hours.

Each rotary pump is also fitted with a two litre bulb and a 13X-molecular sieve trap to prevent pump-oil vapours from entering the vacuum system.

3.1.8 PRESSURE MEASUREMENT AND RESIDUAL GAS ANALYSIS

Pressure in the cell and the storage bulb was measured with modified Mullard IOG-12 Bayard-Alpert type ionization gauges, in which an additional side-arm had been inserted containing a rhenium filament coated with lanthanum hexaboride. These low temperature cathodes were used in preference to the normal tungsten filaments because they cause less gas dissociation. The modifications are described in detail by Walters (1973). Freshly coated Re-LaB_6 filaments were prepared by the cataphoretic deposition method described by Hayward and Taylor (1966). Each filament was activated by heating to red heat for about one hour in UHV before being used for pressure measurement. These filaments are known to give a stable electron emission of 0.1mA at an operating temperature of 1400K. However, it was seen that if the filament was operated at more than 1mA emission, the hexaboride coating was gradually removed. The filament was thoroughly outgassed by maintaining at 0.1mA emission for many hours.

Residual gas analyses, as well as adsorption/desorption measurements, were carried out with a Vacuum Generators Anavac-2 quadrupole mass spectrometer which measures total and partial pressures over the range 2-60 a.m.u.

3.2 EXPERIMENTAL PROCEDURE

3.2.1 ATTAINMENT OF ULTRA-HIGH VACUUM

The ultimate vacuum in a glass system is governed by the dynamic equilibrium between the number of molecules being continuously removed by pumping and the number desorbed by the walls of the system. If the pressure goes below 10^{-10} torr, the diffusion of helium through the glass walls into the system also becomes a contributing factor to the overall vacuum. In the present system, the best vacuum obtained without a bake was in the region of 5×10^{-7} torr. This shows the very high rate of desorption of gas molecules from the unbaked glass walls. The main constituent of the residual gases under these conditions was water vapour.

Bakeout was done generally at 473K for a period of 18 hours or more. The glass itself is bakeable up to about 700K, but the quadrupole mass spectrometer and particularly, its ceramic feed-throughs could not be baked above 523K. The liquid nitrogen dewars around the cold traps were kept in position until the furnace reached its highest set temperature. They were then removed and the cold traps were outgassed with heating tapes. The dewars were replaced at least two hours before switching off the furnace. The furnace was raised while it was still hot and the ion gauges, the heating

filament and the mass spectrometer filament were outgassed. The Re-LaB_6 filaments could not be operated at emission currents above 1mA and these filaments therefore required prolonged outgassing at either 0.1 or 1mA emission. The mass spectrometer filament also required prolonged outgassing at its fixed 2mA emission current. It was thus impossible to complete all the outgassing operations while the glass walls remained hot enough to prevent readsorption. This often made it necessary to carry out another bake for attaining UHV.

If the mass spectrometer filament was not switched on after the bakeout, the ultimate vacuum obtained was of the order of 4×10^{-10} torr. However, with the mass spectrometer in operation, the vacuum was never better than 2×10^{-9} torr. The Anavac-2 spectrometer filament could not be outgassed completely and it was found that this filament acted as a source for continuous production of mass 28 (carbon monoxide). This became a limiting factor for the ultimate vacuum in the system.

After the use of condensible gases like ammonia and carbon dioxide, the vacuum slowly worsened and when the pressure in the system rose above 10^{-8} torr, the apparatus was baked again. This had to be repeated several times during the course of the present investigation.

The main constituents of the residual gas at 2×10^{-9} torr were observed to be masses 2 and 28, with small amounts of 44, 16, 18 and 17.

3.2.2 CALIBRATION OF ION GAUGES AND THE MASS SPECTROMETER

Calibration of the ion gauges over the pressure range 10^{-2} to 10^{-5} torr was done with the help of a McLeod gauge. The absolute pressure was calculated from the relation,

$$P = 3.112 \times 10^{-4} \times x^2 \text{ torr} \qquad (3.1)$$

where 'x' in cm is the difference in height of the two mercury columns when the outer column is level with the top of the capillary tube. The numerical factor was calculated from the dimensions of the capillary and the McLeod bulb.

In the calibrations, mercury vapour was prevented from entering the UHV section of the system by a liquid nitrogen cooled cold trap placed between the McLeod gauge and the ion gauge. Several authors, including Gaede (1913), Leck, (1964) and Gregory (1967) have commented upon the possible errors in the calibrations arising from a continuous streaming of mercury vapour from the McLeod gauge to the cold trap. However, as Walters (1973) has pointed out, such effects were minimized in the present system by putting a few 90° bends between the McLeod gauge and the cold trap. Streaming corrections were therefore ignored in calculating absolute pressures. The ion gauge (I.G.2) connected to the storage bulb was calibrated first. The dekkers D1 and D6 were kept closed and the mercury cut-off C1 was fully raised to stop all pumping. Carbon monoxide was used for calibration and a small amount of gas was let into the storage bulb. After a steady state had been reached, both ion gauge and McLeod readings were taken. The Re-LaB_6 filament of the ion gauge was

operated at 0.1mA emission to minimise pumping effects.

The sensitivity, s, of an ion gauge is defined by the relation,

$$\frac{i_+}{i_-} = s.P \qquad (3.2)$$

where i_+ is the ion current, i_- the emission current (= 0.1mA) and P is absolute pressure. If $\log(i_+/i_-)$ is plotted against log P, the gradient of the straight line obtained gives the sensitivity of the ion gauge.

A series of measurements of ion gauge pressure against McLeod pressure were made and the ion gauge pressure readings were converted to i_+/i_-, multiplying by the sensitivity setting of the control unit. The plot of $\log(i_+/i_-)$ versus log P is shown in Fig. 16, from which the sensitivity of the ion gauge is calculated to be

$$s = 14.3 \text{ per torr at } 298K \text{ for carbon monoxide.} \qquad (3.3)$$

The ion gauge (I.G.1) connected to the cell is similar in all respects to the ion gauge (I.G.2) and was found to give identical ion current readings at the same carbon monoxide pressure. The same sensitivity factor was therefore used for this ion gauge (I.G.1) as well.

The correction factor for the ion gauge readings for conversion to absolute pressures is thus

$$\frac{\text{Absolute pressure}}{\text{Observed pressure}} = \frac{\text{control unit sensitivity setting (= 25.00)}}{\text{Measured sensitivity (= 14.3)}}$$

$$= 1.75 \qquad (3.4)$$

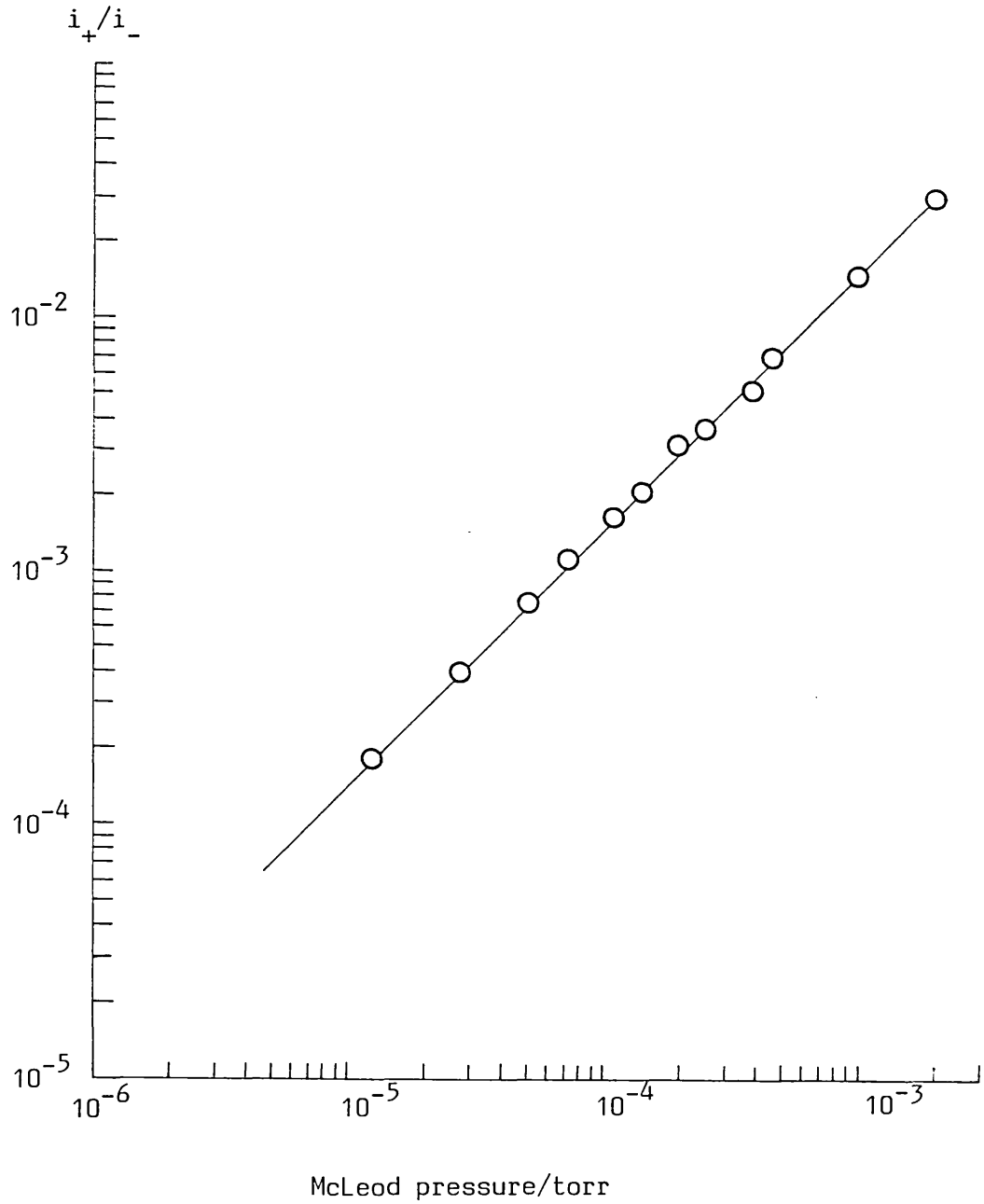

FIG. 16: Calibration curve for the modified Bayard-Alpert ionization gauge.

The factory calibration of the Anavac-2 mass spectrometer was checked in a series of experiments, in which carbon monoxide gas was introduced to the cell at different pressures. With the cell isolated from the pumps and the dekker D5 open, the total pressures read by the mass spectrometer as well as the ion gauge (I.G.1) were noted. The Anavac-2 readings were then plotted against corrected ion gauge readings. This is shown in Fig. 17. The Anavac-2 readings were only slightly higher than the corresponding absolute pressure values, and on the basis of the plot of Fig. 17, it was found that

$$\frac{\text{Total Pressure read by Anavac 2}}{\text{Absolute Pressure obtained from I.G.1}} = 1.14 \qquad (3.5)$$

with respect to carbon monoxide at 298K. All mass spectrometer readings can therefore be corrected utilizing equation (3.5).

Experimental calibration with respect to the condensible gases, carbon dioxide, ammonia, etc., was very difficult in the present system, because the cold trap CT4 could not be avoided. Also these gases are decomposed to some extent by the ion gauge filament. The experimental calibration factor for carbon monoxide can be used if the relative sensitivities of the various gases are known. Sensitivity values for carbon dioxide are summarized by Weston (1979), but no reliable data is available for ammonia. From the table of relative sensitivities given by Weston, a value of 1.4 for carbon dioxide relative to that of carbon monoxide was used in the present work and the same value was used also for ammonia.

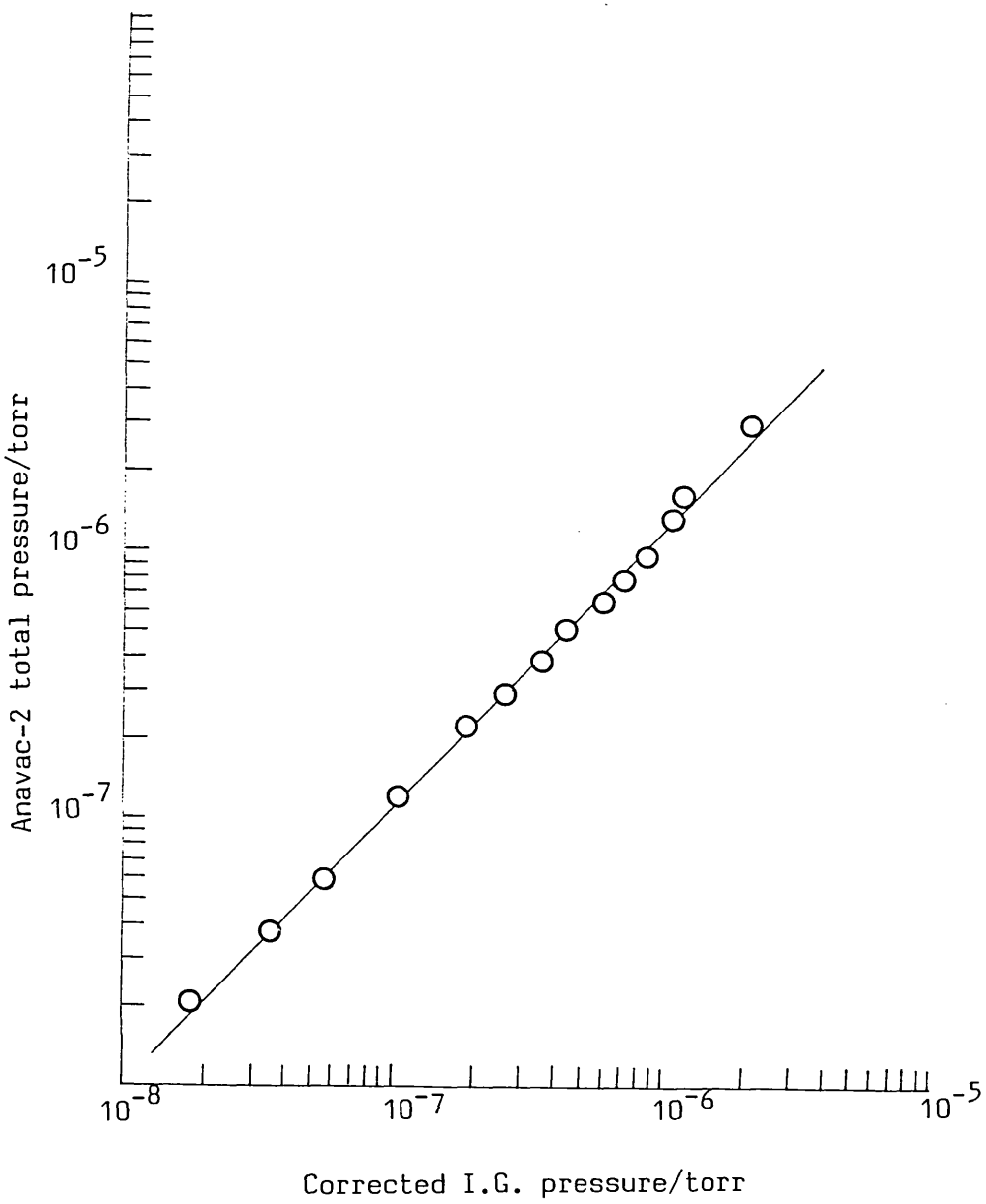

FIG. 17: Calibration curve for the Anavac-2 mass spectrometer

3.2.3 CALCULATION OF CAPILLARY CONDUCTANCES

In order to calculate the flux of molecules entering the cell from the known pressure of a gas in the storage bulb S, it is necessary to know the conductance of the four capillaries constituting the gas inlet line. An expanded view of the capillaries and the whole of gas inlet section is shown in Fig. 18. The conductances (F) of the capillaries were calculated using the well-known formula of Dushmann (1922),

$$F = \frac{ZA}{1 + \frac{3\ell}{8r}} \qquad (3.6)$$

where $Z = (2\pi mkT)^{-\frac{1}{2}}$, the Hertz-Knudsen collision factor and A is the cross-sectional area of a capillary of length ℓ and radius r. Dushmann showed the validity of this formula for $\ell/r > 10$, which is true in the present case. The absolute conductances of the capillaries and their dimensions are given in Table 1.

TABLE 1

Absolute conductances of the capillaries

CAPILLARY	RADIUS (cm)	LENGTH (cm)	Absolute conductance for hydrogen at 300K [molecules $(Nm^{-2})^{-1}s^{-1}$]
L1	0.084	1.0	4.37×10^{16}
L2	0.084	3.0	1.66×10^{16}
L3	0.084	2.0	2.41×10^{16}
L4	0.084	1.0	4.37×10^{16}

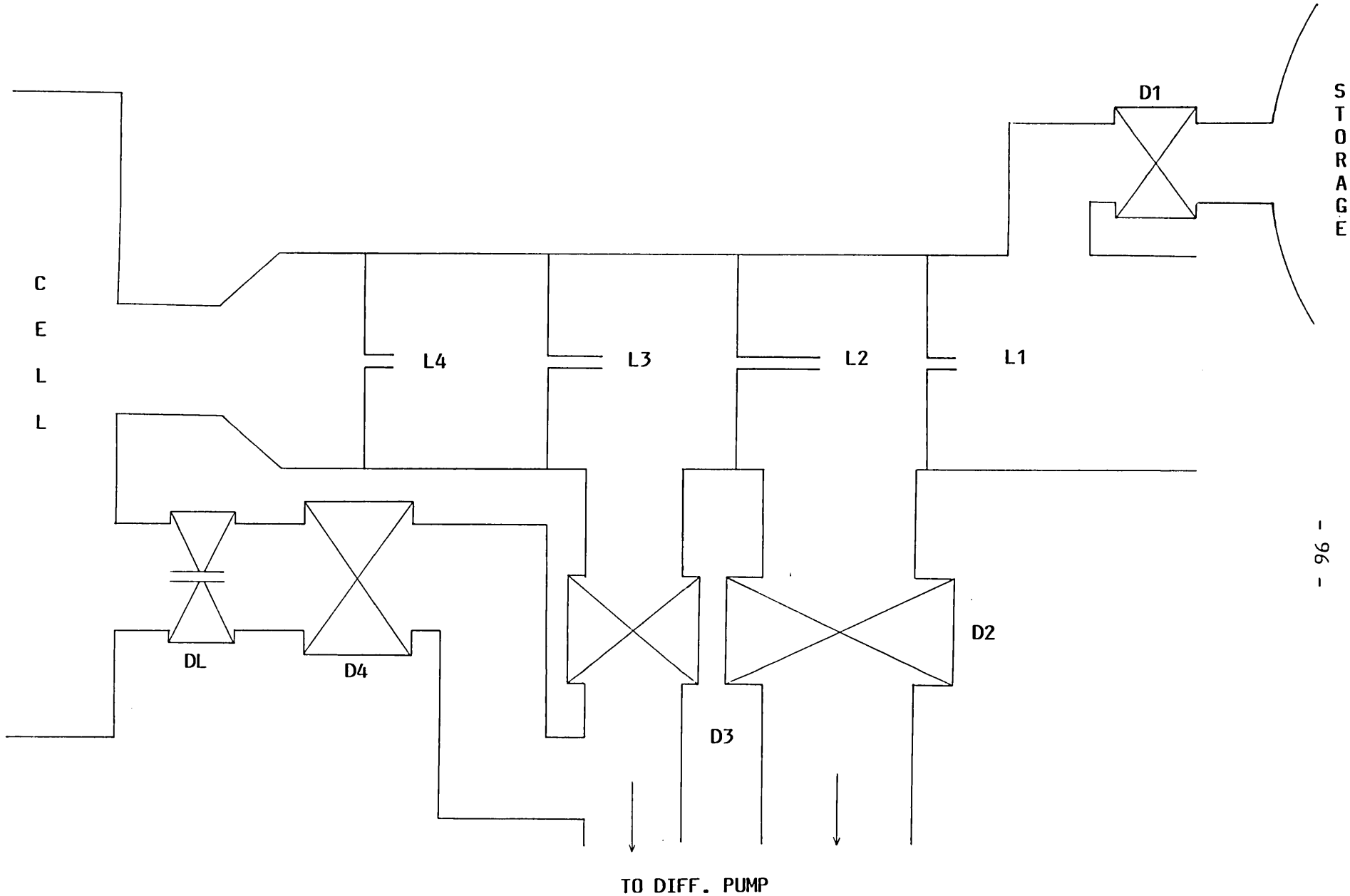

FIG. 18: The gas inlet line

3.2.4 DETERMINATION OF THE VOLUME OF THE CELL

The effective volume of the cell with all the side arms, the ion gauge and the mass spectrometer was determined experimentally. For this purpose, a calibrated bulb with a greased stopcock was connected between the cell and the mass spectrometer and after pumping the system down to a pressure of 10^{-6} torr, the bulb was filled with carbon monoxide gas to a pressure of approximately 10^{-3} torr. The gas was then allowed to expand to the main cell and from the difference in pressure (measured by the ion gauge), the volume was calculated. From a number of measurements, the volume of the cell was found to be

$$V = 2.98 \pm 0.09 \text{ litres} \qquad (3.7)$$

The calibrated bulb was later disconnected from the system.

3.2.5 DETERMINATION OF PUMPING SPEED

In a dynamic system, the rate of pumping, i.e. the number of molecules removed from the system per second, is directly proportional to the steady state pressure (P) of the gas. This is expressed by the relation

$$\frac{dn}{dt} = K.P \qquad (3.8)$$

where K is known as the pumping speed of the system, and n is the number of molecules in the system at time t. An accurate determination of 'K' is essential to express the results of the adsorption/desorption experiments in quantitative terms. This has been emphasized by

King (1975), Rhodin and Adams (1976) and many other authors.

Assuming that at low pressures, the equation of state for the gas can be written in terms of the ideal gas laws, the steady state pressure is given by

$$PV = nkT$$

where V is the volume of the cell, T the absolute temperature and k the Boltzmann constant. On differentiation with respect to time,

$$\frac{dP}{dt} = \frac{kT}{V}\frac{dn}{dt}$$

$$= \frac{kT}{V} KP \text{ , from (3.8) .}$$

Thus, $$K = \frac{V}{kT}\frac{d\ell nP}{dt} . \qquad (3.9)$$

From equation (3.2), $P = \frac{1}{s}\frac{i_+}{i_-}$, and since s and i_- are constants, equation (3.9) can be written as

$$K = \frac{V}{kT}\frac{d\ell ni_+}{dt} \qquad (3.10)$$

From the slope of the plot of $\ell n\ i_+$ against time, it is therefore possible to calculate the pumping speed of the system.

The pumping speed was determined with respect to carbon dioxide gas. It was not possible simply to isolate the cell from the gas supply and observe the logarithmic decay in pressure (or ion current) with time because gas present in the beam chambers slowly diffused into the cell. This resulted in erroneous values for the pumping speed. It was therefore necessary to adopt the procedure outlined below.

The dekkers D2 and D3 were kept closed and gas from the storage bulb at a pressure of approximately 10^{-5} torr was introduced to the cell by opening D1. The cell was continuously pumped via D4. When the pressure in the cell reached steady state, D1 was closed, followed immediately by closure of D4. This allowed time for the gas between the beam chambers to reach the cell. At the same time D2 was opened so that gas from the end of the beam could be pumped away. D4 was opened immediately afterwards and the exponential decay of ion current was monitored. The steady state base ion current (i_+^0) was noted and $\ell n(i_+^t - i_+^0)$ was plotted against time.

A typical i_+^t-t curve is shown in Fig. 19, while the logarithmic plot of the exponential decay of i_+^t is presented in Fig. 20. The logarithmic plot becomes somewhat nonlinear after about 10 seconds of pumping time which may be largely due to slow evolution of gas from the walls. From a series of similar experiments, the pumping speed was determined for carbon dioxide at 298K from the slopes of logarithmic plots, to be

$$K = (2.37 \pm 0.12) \times 10^{17} \text{ molecules } (Nm^{-2})^{-1}s^{-1} \quad .$$

Another series of determinations were done in the same way, but by monitoring the 44 m/e ion current with the mass spectrometer. The pumping speed with respect to carbon dioxide at 298K came out to be $(1.98 \pm 0.16) \times 10^{17}$ molecules $(Nm^{-2})^{-1}s^{-1}$. As the mass spectrometer was connected to the cell by a very long tube, there might be an appreciable delay in response to the pressure-changes in the cell and the systematically lower values of the pumping speed found with the mass spectrometer are attributed to this cause.

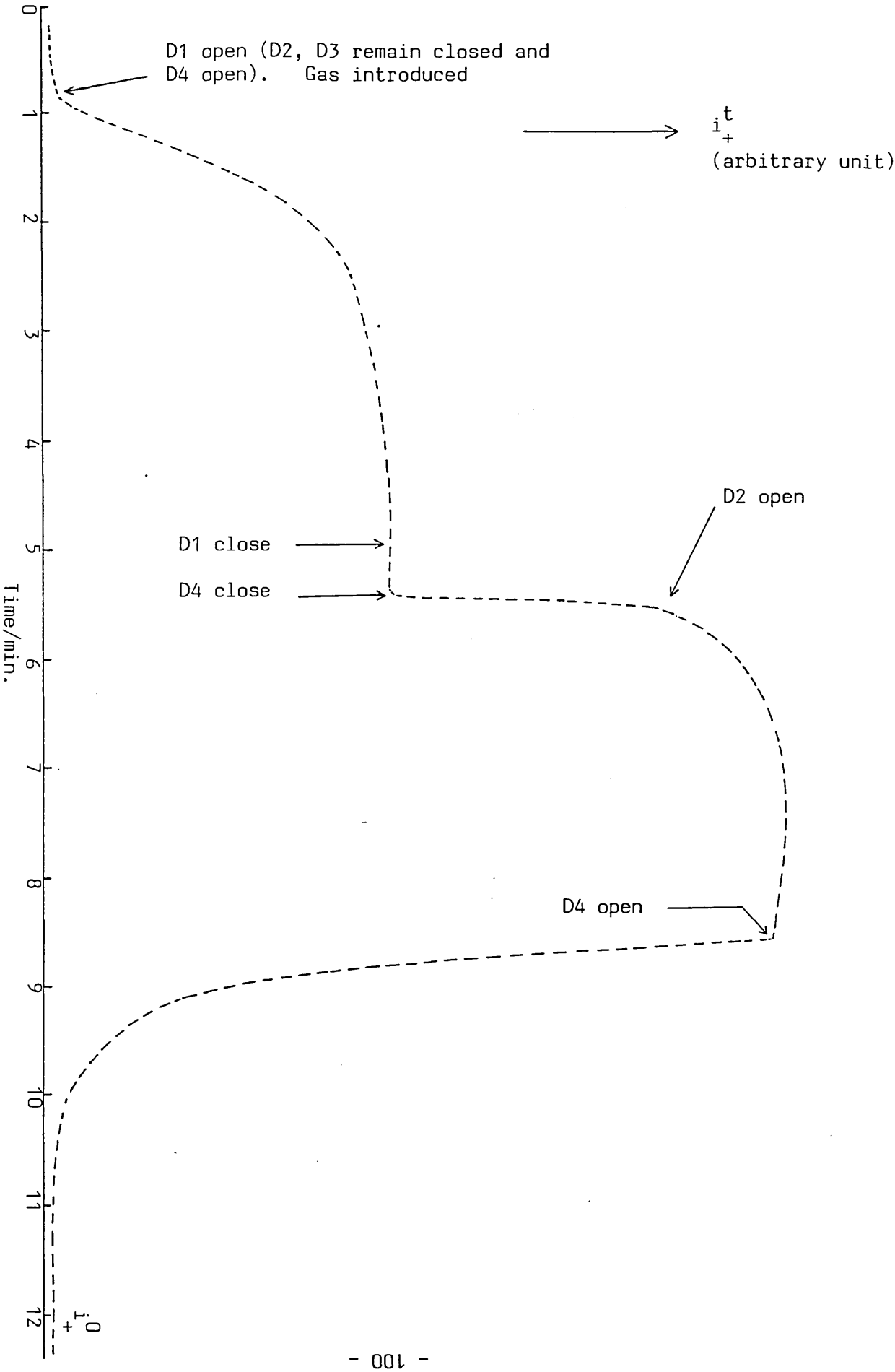

FIG. 19: Typical pumping curve for carbon dioxide pumping at room temperature.

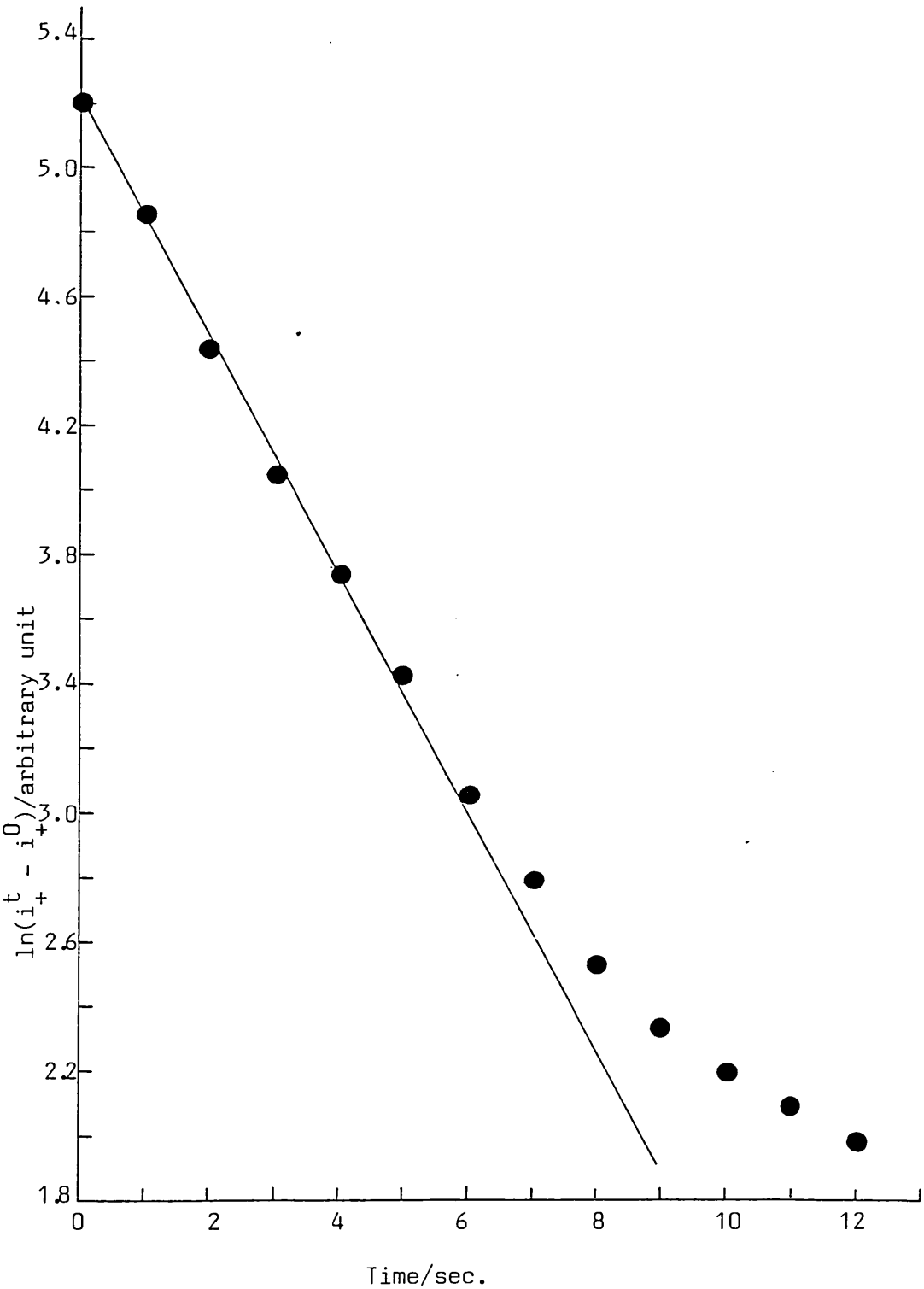

FIG. 20: Plot of $\ln(i_+^t - i_+^0)$ vs. time for carbon dioxide pumping at room temperature.

It is also possible to calculate the pumping speed by measuring the steady state pressure in the cell and the corresponding storage bulb pressure if the conductance of the inlet system is known. Provided that the storage bulb pressure (P_s) does not fluctuate during an experiment, the rate of influx of molecules into the cell is given by

$$\left(\frac{dn}{dt}\right)_i = F.P_s \qquad (3.11)$$

where F is the conductance of the inlet system.

When a steady state is established in the cell, the steady state pressure (P) is related to the rate of removal of molecules by pumping, by the relation

$$\left(\frac{dn}{dt}\right)_r = K.P \qquad (3.12)$$

where K is the pumping speed.

Under dynamic equilibrium,

$$\left(\frac{dn}{dt}\right)_i = \left(\frac{dn}{dt}\right)_r$$

and, $F.P_s = K.P.$

Thus, the pumping speed, $K = F.\ \frac{P_s}{P}$. (3.13)

Equation (3.13) gave unsatisfactory values of the pumping speed with the beaming system, probably because leakage through the dekker valves caused the calculated inlet conductance to be in error. This method was, however, successfully used in a later series of experiments in which the beaming section was replaced by a single capillary.

The conductance of this capillary (length 6cm, radius 0.5mm) calculated from the formula (3.6) for carbon dioxide at 298K was 3.98×10^{14} molecules $(Nm^{-2})^{-1}s^{-1}$, which gave a value of the pumping speed of

$$K = (2.45 \pm 0.11) \times 10^{17} \text{ molecules } (Nm^{-2})^{-1}s^{-1}$$

This value was in very good agreement with the value obtained from the logarithmic plots.

For ammonia, the above method yielded a value of $K = (3.91 \pm 0.14) \times 10^{17}$ molecules $(Nm^{-2})^{-1}s^{-1}$ while the logarithmic plots gave a value of $(3.68 \pm 0.12) \times 10^{17}$ molecules $(Nm^{-2})^{-1}s^{-1}$.

In all later calculations, a mean value of the pumping speed obtained from the two methods will be used.

3.2.6 EXPOSURES AND DESORPTION EXPERIMENTS

Although the gas inlet line consists of a molecular beam arrangement, it was very difficult to introduce the gas as a beam in the present investigation with condensible gases. If the dekkers D2 and D3 were kept open, most of the condensible gas went into the big cold traps and practically no gas reached the cell, even with 10^{-2} torr pressure of the gas in the storage bulb. For this reason, all exposures were done with no pumping of the beam chambers (i.e. D2 and D3 remained closed) while the cell was continuously pumped, (D4 remained open). After the gas-flow to the cell was stopped by closing D1, it was always necessary to open D2, otherwise the cell pressure continued to rise for a few seconds. This was because the

chambers between the capillaries acted as temporary reservoirs of the gas.

Before each exposure, the mica sample was outgassed at 540-573K for 15 minutes or more. Gas was then introduced for a known length of time and the storage bulb pressure was noted. After exposure, the cell was pumped to the base pressure and desorption was carried out by heating the sample. With ammonia and carbon dioxide, pumping had to be continued for as long as 30 minutes to 1 hour, before the pressure was low enough to do the desorption experiment. The mica sample required up to 30 minutes to come to room temperature after a desorption experiment when another exposure could be made.

As a general practice, the sample was kept facing the beaming section during gas exposure even though the beam component of the gas was known to be negligible. For desorption, the sample was normally turned to face the filament with the help of an external magnet. If the sample remained facing the beam (i.e. at right angles to the filament) during desorption, the thermocouple registered at least 50 degrees lower temperature than when it was facing the filament. In this position, one edge of the sample came very near to the filament and it was likely that this side of the sample would heat up more quickly, although the thermocouple would not register this. Thus, a desorption run with the sample at right angles to the filament could be a test to determine whether a certain desorbed gas originated from mica, or from the filament or the glass walls. If the desorption was from the filament, or the glass walls, the desorption peak would be expected to appear in the same position in the P-t curves (with the same heating rate) irrespective of whether the

sample was facing the filament or was at right angles to it.

A series of blank exposure and desorption experiments with the mica sample removed from the system were carried out to eliminate the possible artifacts created by the presence of the tungsten heating filament, the glass walls of the cell, and the glass sample-holder assembly. The results will be discussed later.

The condensible gases used in the experiments were generated in the following way:

Ammonia solution (BDH AnalaR grade with about 35% ammonia) was first cooled to liquid nitrogen temperature in G5 and the handling line was pumped down to a reasonable vacuum. The liquid nitrogen bath was then removed and ammonia was allowed to distil over into the cold trap CT5 where it was frozen again. After pumping the line once more, CT5 was allowed to thaw to room temperature and the released ammonia was stored in either G2 or G4. The rest of the gas in the line was then pumped out. Carbon dioxide was similarly generated from cardice.

3.2.7 TEMPERATURE MEASUREMENT AND HEATER CONTROL

A chromel-alumel thermocouple was used to measure the temperature of the mica. A correction was applied to allow for the fact that the cold junction was at room temperature rather than at 273K. The thermocouple was mounted by inserting the hot junction between two layers of the mica sample. This was not entirely satisfactory as it was found that significant differences in temperature could arise between the surface of the mica and its interior as a result of the

poor conduction properties of mica. Thus, in a simulated desorption cycle, performed in air, it was found that there was initially a 25K difference between the readings of a thermocouple touching the mica surface and another one inserted between the layers. This difference, however gradually diminished as the temperature rose.

The heating filament was controlled by a specially designed Linear Temperature Programmer unit. This design was a modification of a number of known circuits, specially that of Herz, Conrad and Küppers (1979). The voltage from the chromel-alumel thermocouple inserted in the mica sample was used to control a ramp generator supplying d.c. power to the filament. The unit has two power supplies with maximum outputs of 25V/10A and 150V/1A respectively. The initial and final temperature as well as slopes for different heating rates can all be preset.

The experimental heating rates for the mica sample are shown in Fig. 21. The heating cycles started at 298K and ended at 600K, but heating rates up to only 523K are shown. The initial nonlinearity of the curves is probably due to the delayed response of the thermocouple which was inserted inside the layers of the mica sample and was therefore effectively insulated from the front surface where the radiation was absorbed. The heating rates also became slightly nonlinear towards the end of the cycle, but as the desorption experiments were done below 523K, this was unlikely to affect the results.

During heating, the mica sample was about 15mm away from the filament and heating was by radiation alone. The filament required a current of 4A at 14V to give a final mica temperature of 600K. If, however, an aluminium foil was wrapped round the middle of the cell, the final temperature of the sample reached 673K with the same supplies

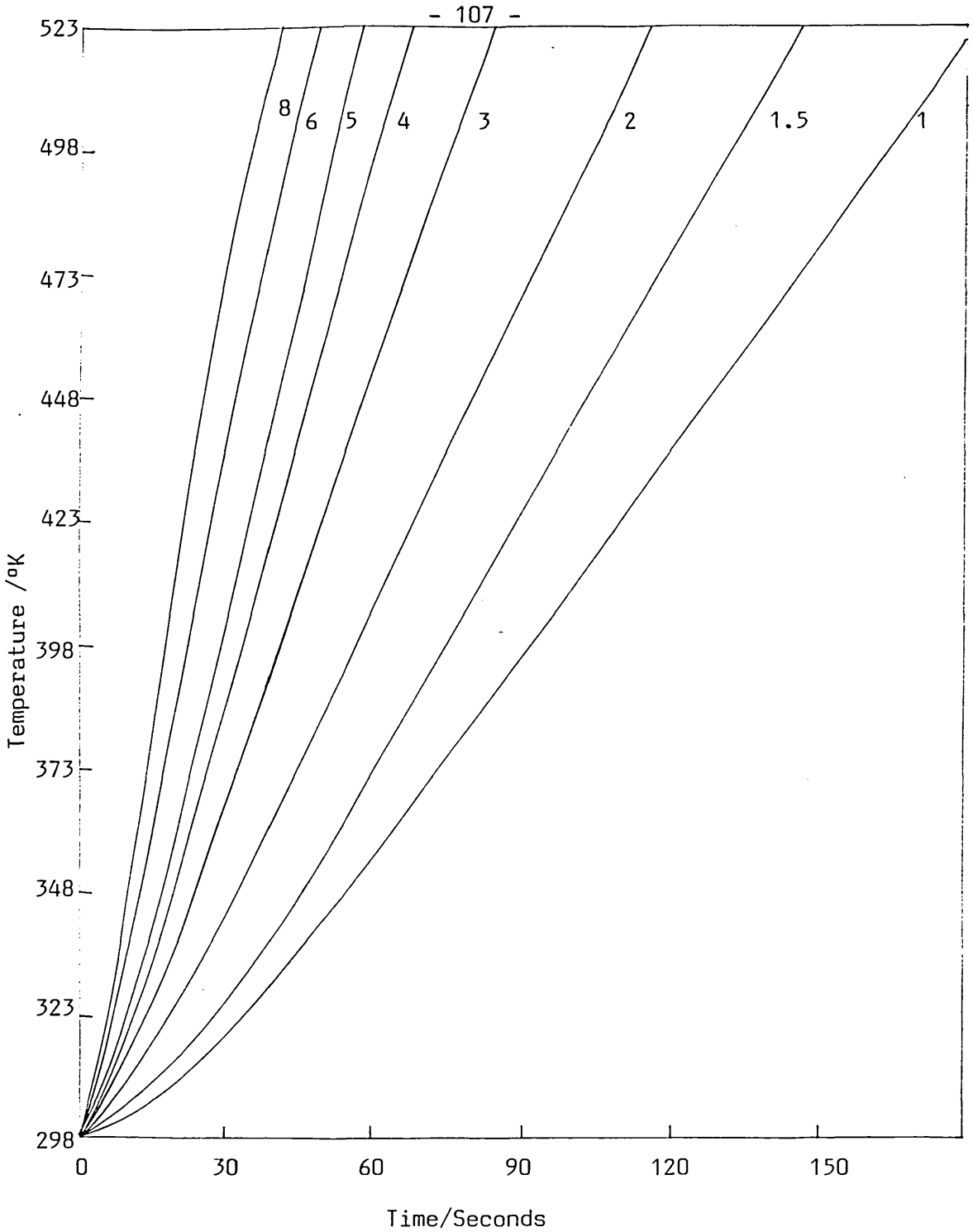

FIG.21: Performance of the Linear Temperature Programmer. Heating rates at different arbitrary slope settings (1, 1.5, 2,...,etc.) are shown. The final temperature obtainable under the constant current/voltage setting of the heater was 600K.

to the filament. This was useful for outgassing the sample. During this process, the surrounding glass walls reached a temperature as high as 400K, while normally the temperature of glass walls never went above 323K with a mica temperature of 600K.

3.2.8 SAMPLE PREPARATION AND CLEANING

Natural muscovite mica, grade 5, of Indian origin and supplied by Startin and Company (London, England) was used in all experiments. The thick pieces were light green in colour, but after a few cleavages in air, the thin pieces appeared colourless and transparent. All experimental samples were made from freshly air-cleaved pieces, which were less than 0.25mm in thickness. A 28mm x 23mm piece was carefully cut with a sharp razor blade avoiding partial opening of the edges as far as was practicable. A section of mica, 5mm wide, was cut away from the long edges on both sides of the sample leaving a thicker middle portion to be cleaved in vacuum. This is shown schematically in Fig. 22. Holes were made at the top of the middle portion on both sides of the mica and fine silver wire tags were inserted. These were later used during cleaving. The upper part of the sample (about 4mm) was unavoidably cleaved during this process. The thermocouple was inserted at the middle of the top edge of the sample through the layers. The sample fitted perfectly into the cage of the glass holder and no additional tags were necessary.

It is well known that an air-cleaved mica surface contains an appreciable carbon-contamination, but no satisfactory cleaning procedure has yet been devised. Poppa and Elliot (1971) have shown

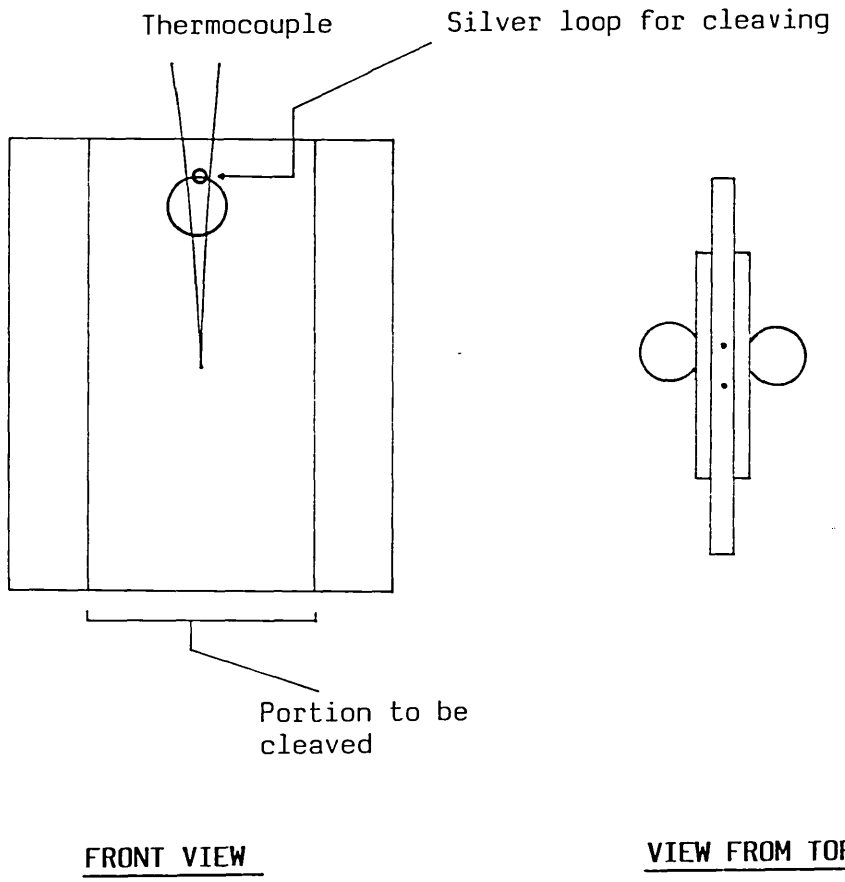

FIG. 22: Mica sample for adsorption/desorption experiments in the glass system.

that carbon can be removed by heating the mica in oxygen at temperatures above 770K, but since dehydroxylation of the mica surface as well as potassium depletion are known to occur under these conditions, this method was not used in the present work. Instead a cleaning procedure based on bombardment of the mica surface with hydrogen atoms was tried. This will be discussed later.

3.3 RESULTS AND DISCUSSION

3.3.1 GASES RELEASED ON HEATING THE MUSCOVITE MICA SAMPLE

As the UHV section of the apparatus had to go through one or more 18 hour bake-out cycles at a temperature of 470K, the mica was likely to lose most of the occluded gas during these cycles. It was thus not possible to determine quantitatively the amounts of gases released by the mica on heating. However, even after bakeout, the air-cleaved mica was found to outgass considerably when heated to a temperature of 520K or more in ultra high vacuum. Prolonged heating was necessary to outgass mica completely.

A typical residual gas spectrum after bakeout and outgassing of all filaments, but before any heat treatment of the mica, is shown in Fig. 23. At this stage the heating filament was turned to full power (4A/14V) to remove any absorbed gas whilst the mica was kept in the raised position where it did not heat up appreciably. On lowering the sample to face the filament, the mica temperature rose to 570K and the total pressure in the cell shot up from 2×10^{-9} to 1×10^{-7} torr. The residual gas spectrum taken immediately afterwards is shown in Fig. 24. The gas given off by the mica

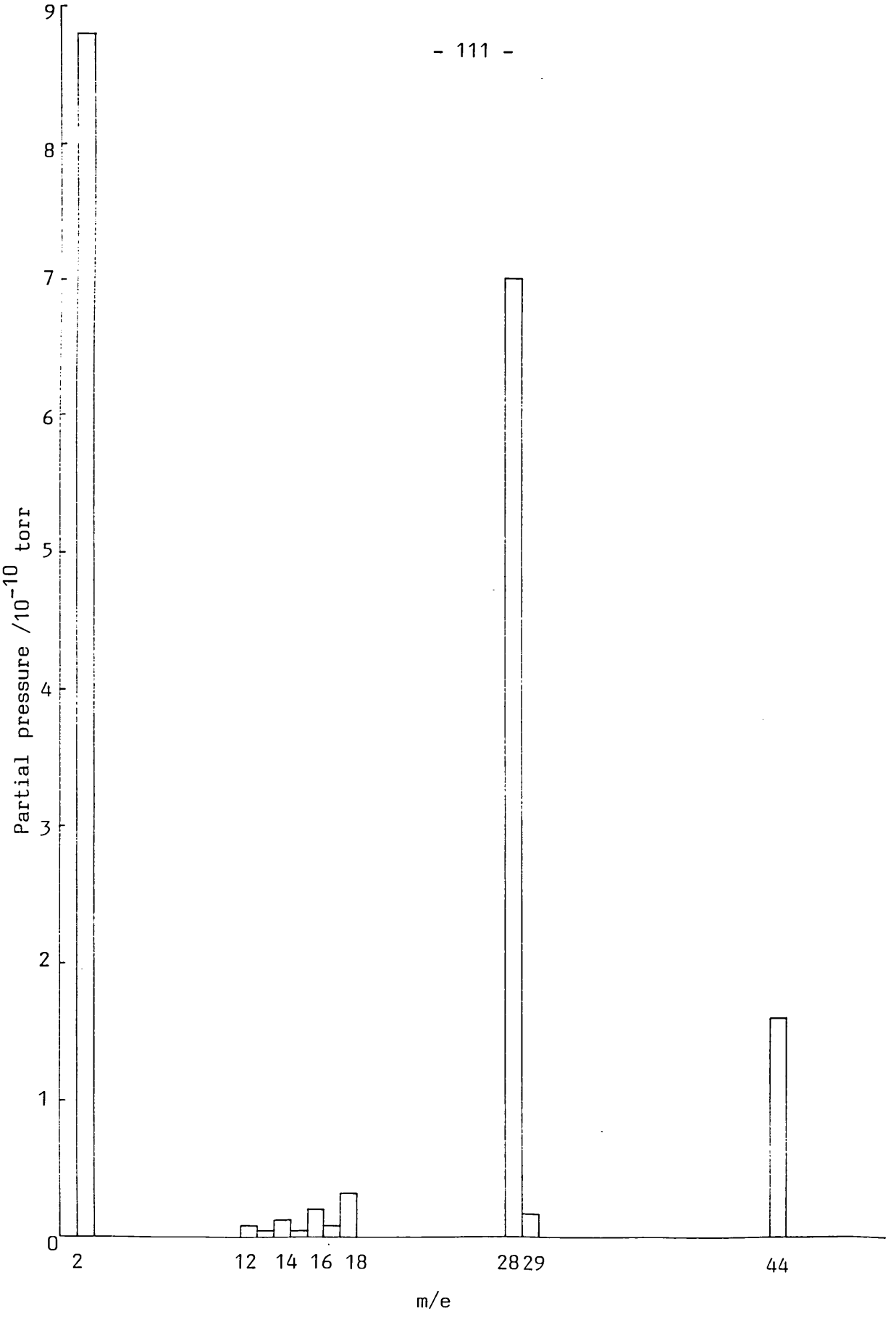

FIG. 23: Residual Gas Spectrum of the background after bakeout and outgassing of all filaments (Total pressure 2 x 10^{-9} torr).

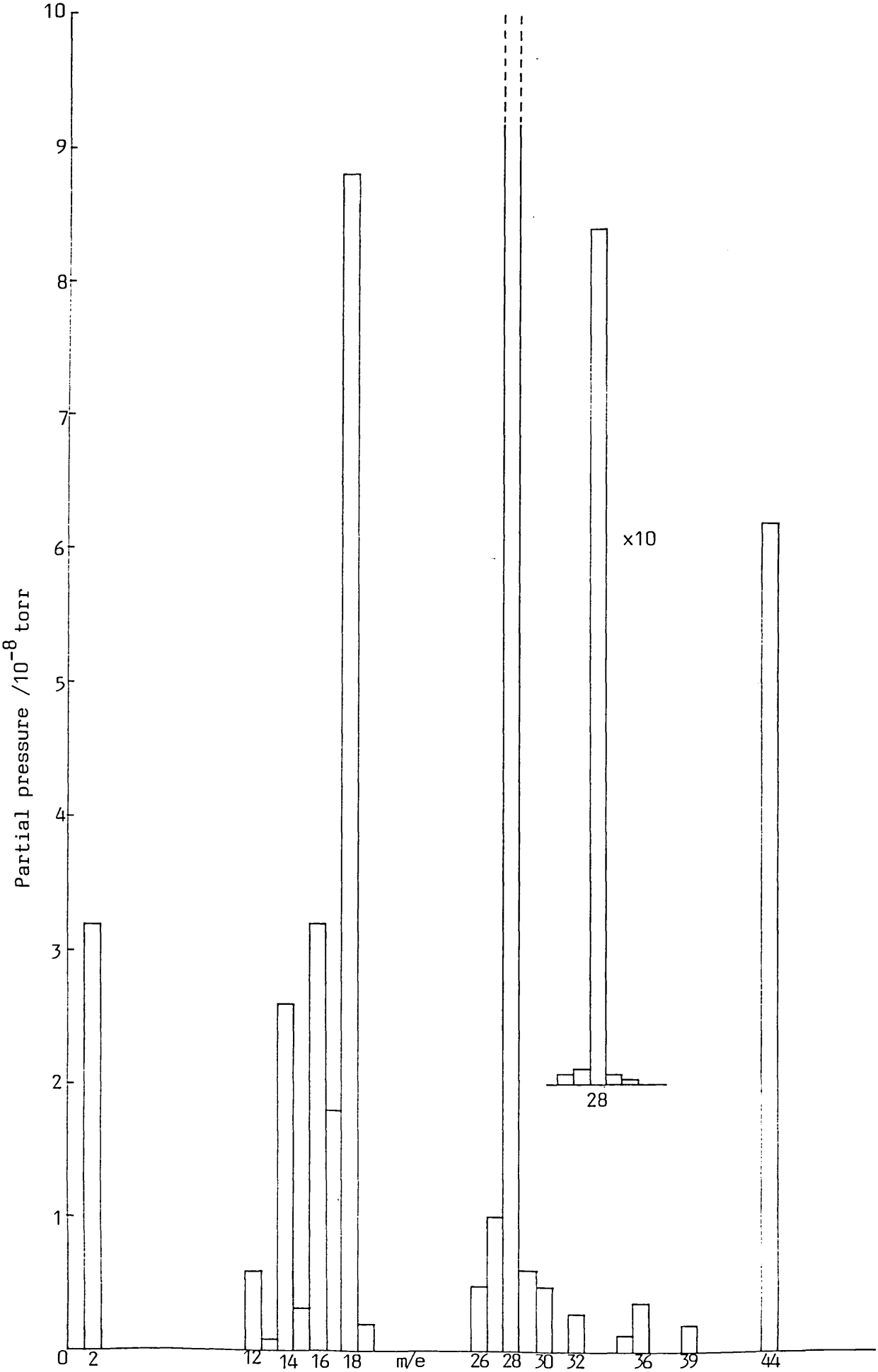

FIG. 24: Residual Gas Spectrum during heating the air-cleaved mica for the first time at 570K.

consisted mainly of water vapour (m/e 18), nitrogen (m/e 28 and m/e 14), carbon monoxide (m/e 28), carbon dioxide (m/e 44) and methane (m/e 16). Considerable evolution of hydrogen also occurred, but the true extent of hydrogen evolution was difficult to measure because of rapid pumping by the hot filament. Oxygen was also detected in the evolved gas. The increase in mass numbers 26, 27, 29 and 30 along with 28 was perhaps due to C2 hydrocarbon fragments given off by the mica. The appearance of peaks at masses 35, 36 and 39 may be due to other hydrocarbon species, although Poppa and Elliot have attributed mass 39 to potassium and masses 35 and 36 could conceivably be due to chlorine.

The pressures of all the residual gases, excepting water vapour, were found to come down rapidly, but water vapour continued to build up in the continuously pumped cell for half an hour or more if the mica was maintained at a temperature of 520K or above. After this first heat treatment of the mica, it was necessary to bake the system again to get rid of the water vapour.

Once the mica had been outgassed and ultra-high vacuum had been re-established, little gas was evolved on subsequent heating to temperatures below 520K. Above this temperature some water vapour was still detectable with the amount becoming less and less with each cycle of heating. It was found to be impossible to drive off all the water vapour from the mica by heating at temperatures below 620K (the highest temperature obtainable in the present work). Water vapour remaining between the layers of mica possibly comes to the surface by a very slow diffusion process and consequently requires a large number of heating cycles for complete removal.

An analysis of the gases evolved on heating the air-cleaved mica for the first time in UHV showed that all the major components of air were present in the mica as impurities. These results agree well with the works of Mercer (1967) and Poppa and Elliot (1971), but differ in one respect. No oxygen was detected by these workers. Mercer reported oxygen as one of the gases released on cleaving muscovite mica, but the freshly cleaved mica did not release any detectable amount of oxygen on subsequent heating in UHV to a temperature of about 570K. Poppa and Elliot, on the other hand, noticed a pressure rise from 5×10^{-9} to 2×10^{-8} torr in their large stainless steel chamber on heating a mica sample for the first time. Hydrogen, water and carbon dioxide were the main outgassing products in their work and while they detected a little mass 39 among the products, no oxygen was obtained. The appearance of m/e 32 in the present work on heating the mica for the first time may be assigned to the possible differences in source and origin of the specimen.

The SIMS work of Dowsett, King and Parker (1977) has shown the existence of alkali halide compounds as impurities on the air-cleaved surface, although the source of these impurities is uncertain. The presence of masses 35 and 36 in the residual gas spectrum after heating mica in the present work agrees with this observation. The presence of methane in the residual gas spectrum on heating mica for the first time in UHV may be attributed to two sources: (i) methane gas occluded between the layers or remaining chemisorbed on the surface and (ii) methane gas freshly produced by reduction of the surface carbon impurity with hydrogen atoms generated at the surface of the hot filament.

In the present investigation, the freshly vacuum-cleaved mica did not release appreciable amounts of gas (excepting water vapour above 520K) on subsequent heating. As the sample had gone through a number of bakeouts and innumerable heating cycles before being cleaved in UHV, this was not surprising.

3.3.2 CLEANING AIR-CLEAVED MICA BY HYDROGEN ATOM BOMBARDMENT

All mica samples, cleaved in air, were found to have a carbonaceous overlayer. This will be discussed later in connection with the XPS characterization of the mica surface. This carbonaceous layer may be totally or partly responsible for the chemical inactivity of air-cleaved mica surfaces. In fact, during this investigation, it was found that the air-cleaved surface did not show any appreciable activity even after prolonged outgassing at 520K. Elliot (1974) and Poppa and Elliot (1971) have reported partial or almost total removal of carbon contamination from air-cleaved mica surfaces by heating in a comparatively high pressure (about 10^{-5} torr) of oxygen at a temperature range of 770K to 870K for upto 4 hours. In the present work, an attempt was made to remove the carbon contamination from the mica surface by bombarding with hydrogen atoms.

For this purpose, the tungsten filament served as the atomisation source. Hydrogen was let into the cell to reach a steady state pressure of 2×10^{-6} torr, but once the filament was switched on, the hydrogen pressure fell due to atomisation. A maximum atomisation rate was achieved with the filament white hot, which corresponded to a supply of about 3A/10V to the filament. During the bombardment, the mica reached a temperature of 470K as compared

to 400K in the absence of hydrogen gas. The bombardment was continued for one hour.

The residual gas spectrum half-way through the hydrogen-atom bombardment is shown in Fig. 25. The major component of the residual gas was water vapour showing that surface oxygen had been reduced. There were also very substantial amounts of hydrocarbons and hydrocarbon fragments, shown by the abundance of peaks around masses 16 (C1), 28 (C2), and 40(C3). Considerable amounts of masses 19, 20, 22, 32, 35 and 36 were also evident in the residual gas. After bombardment, the water partial pressure remained in the 10^{-7} torr range and overnight pumping was required to bring it down to the acceptable levels of 10^{-10} torr range. It was also found to be necessary to temporarily isolate the UHV section so that the liquid nitrogen cooled cold traps could be warmed up and the condensed hydrocarbons pumped away.

Although it was not possible to determine the nature of reactions taking place at the mica surface under the influence of hydrogen-atom bombardment, the appearance of water vapour and a large number of hydrocarbons in the mass spectra showed that some drastic processes were taking place. When this experiment was repeated later in the ESCALAB system, subsequent XPS analysis of the bombarded surface showed almost total removal of the carbon contamination. The XPS showed no apparent change in the surface composition of the mica excepting the pronounced decrease in the C1s peak. This method of cleaning the mica surface is therefore a safer method as far as the mica surface composition is concerned. Cleaning by heating in a flow of oxygen at a temperature above 770K was shown by Poppa and Elliot (1971) to result in potassium depletion. Use of such a high temperature is also likely to cause dehydroxylation and corresponding reconstruction of

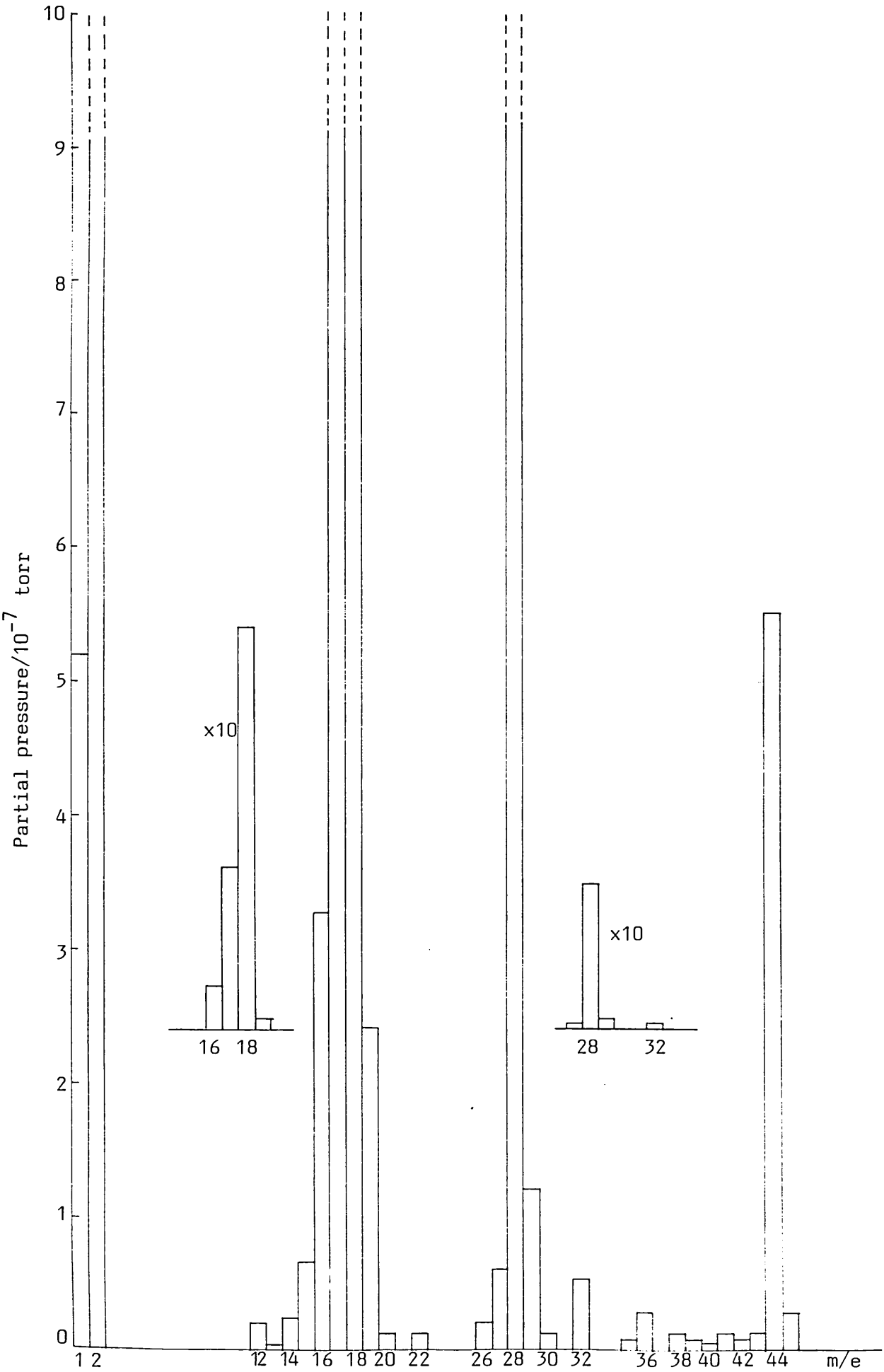

FIG. 25: Residual Gas Spectrum of the background halfway through the hydrogen-atom-bombardment.

the mica structure.

The origin of the carbonaceous overlayer on air-cleaved mica surfaces is not definitely established, but work by Dowsett, King and Parker (1977, 1978) and others has shown that upon ion-bombardment, this layer produces hydrocarbon fragments up to C_4H_n. On hydrogen-atom bombardment, however, no C_4H_n fragment was detected. Salmeron and Somorjai (1982) observed that when a metallic catalyst having a carbonaceous overlayer was heated in the absence of hydrogen, dehydrogenation of the hydrocarbons occurred leaving ultimately a graphitic layer on the surface. It was also shown that if the temperature was below 670K, the formation of the graphitic overlayer was delayed and most carbon contamination remained in the form of CH_2, C_2H and CH type fragments. Somorjai (1981) identified these fragments on various catalyst surfaces using High Resolution Electron Energy Loss Spectroscopy (HREELS). A similar situation may exist in the case of the mica where the large amount of hydrogen evolved on heating the air-cleaved mica in the UHV may be attributed to the dehydrogenation of hydrocarbons from the carbonaceous layer on the surface. It is not clear where the hydrocarbon layer comes from; it could have formed during the prolonged outgassing in vacuum and the long time required to obtain a good vacuum. Dehydrogenation of the hydrocarbon-contaminants is a more likely explanation for the large hydrogen evolution on heating the mica than any of the alternatives, namely that hydrogen remains chemisorbed on the surface or that it forms part of the occluded gas among the layers.

In the present work, the temperature of the mica seldom exceeded 570K and it was thus unlikely that the carbonaceous overlayer would be converted to an irreversibly held graphitic layer. After

initial heat-treatment, therefore, the mica surface would be likely to contain hydrogen deficient carbon skeletons. On subsequent treatment with hydrogen atoms, these were perhaps converted to methane (CH_4) and other hydrocarbon fragments and were released from the surface.

An explanation of the formation of water on hydrogen-atom treatment is not so straightforward. It is thought that some of the carbon contamination may be of the carbonate-bicarbonate type, formed as a result of the action of carbon dioxide and water vapour from air on the air-cleaved mica surface. These carbonate-bicarbonate species are likely to undergo reduction with atomic hydrogen forming water and more hydrocarbon fragments.

3.3.3 CLEAVING MICA IN UHV

The mica sample was cleaved at 2×10^{-9} torr total pressure. It was not possible to monitor the residual gas spectrum at the moment of cleavage because the movement of the magnets necessary for operating the cleaving hook produced artificial pressure fluctuations. The residual gas spectrum, taken immediately after cleavage, showed very little change excepting minor increases in the masses 14, 28 and 44. Both faces of the sample were cleaved.

Jaeger et al.(1967) noticed a pressure rise of between 10^{-8} torr and 10^{-6} torr on cleaving mica with an identical hook and slug arrangement in a glass cell. They did not mention the possible effects of the magnetic movements, but observed that the background pressure was restored in 2 to 3 seconds. Mercer (1967) reported a

pressure burst of up to 7×10^{-5} torr on cleaving a mica specimen in a static 1 litre glass system, again using a magnetically operated hook. In the 3 litre dynamic system used in the present work, it was routinely noticed that the movement of the glass-encapsulated slugs operated with external magnets produced momentary pressure bursts, sometimes up to 10^{-6} torr. On the other hand Bryant (1962) and Hines (1964) detected no gas evolution on cleaving mica in UHV. Similarly Poppa and Elliot (1971) recorded a pressure rise of less than 1×10^{-10} torr upon cleaving a preheated sample of mica in their stainless steel system with a line-of-sight mass spectrometer. In their work even a fresh sample produced a pressure rise of less than 1×10^{-9} torr upon cleavage. Goldstaub et al (1966) also observed a pressure rise of only about 2×10^{-10} torr on cleaving mica.

It is therefore not surprising that no appreciable gas evolution was detected on cleaving mica at 2×10^{-9} torr background pressure in this work. Firstly, the mica sample had undergone a large number of heating cycles and obviously very little gas would be expected to remain between the layers. Secondly, wide variations in gas content are reported depending upon the material used.

The mica used in this investigation was of the highest grade of natural muscovite and consequently the gas-content would be low.

3.3.4 CHEMISORPTION OF CARBON DIOXIDE ON THE MICA SURFACE

It will be shown later through the XPS measurements that muscovite surfaces, freshly cleaved in air, always pick up carbon contamination. The obvious carbonaceous agent in air is carbon dioxide. The air-cleaved mica surface after bakeout and with no further treatment showed almost no affinity towards carbon dioxide. After prolonged outgassing between 520 and 570K, however, the surface was a little more active, but the desorption peaks measured with the TPD technique, were too small to be meaningfully analysed. Only after hydrogen-atom bombardment did the surface become sufficiently active for reliable desorption spectra to be obtained.

In all adsorption/desorption experiments the partial pressure of CO_2 (mass 44) was monitored simultaneously with time and temperature.

Measurements were also done for carbon dioxide adsorption on a surface of the mica cleaved in the UHV. This surface was found to be almost as active as the hydrogen-atom bombarded surface of the air-cleaved mica.

After the surfaces were exposed to carbon dioxide at room temperature (298K), the cell was pumped down to the base pressure in the manner described earlier. This almost certainly removed any weakly held adsorbed species from the surface. Temperature Programmed Desorption (TPD) was then carried out with a known heating rate. Typical desorption spectra for the air-cleaved and the vacuum-cleaved surfaces are shown in Fig. 26. The spectra were very similar. Each of the spectra shows four distinct peaks, labelled A,B,C and D. The thermocouple had an initial delay of 5 to 10 seconds in recording a temperature rise, although the mica surface facing the filament would

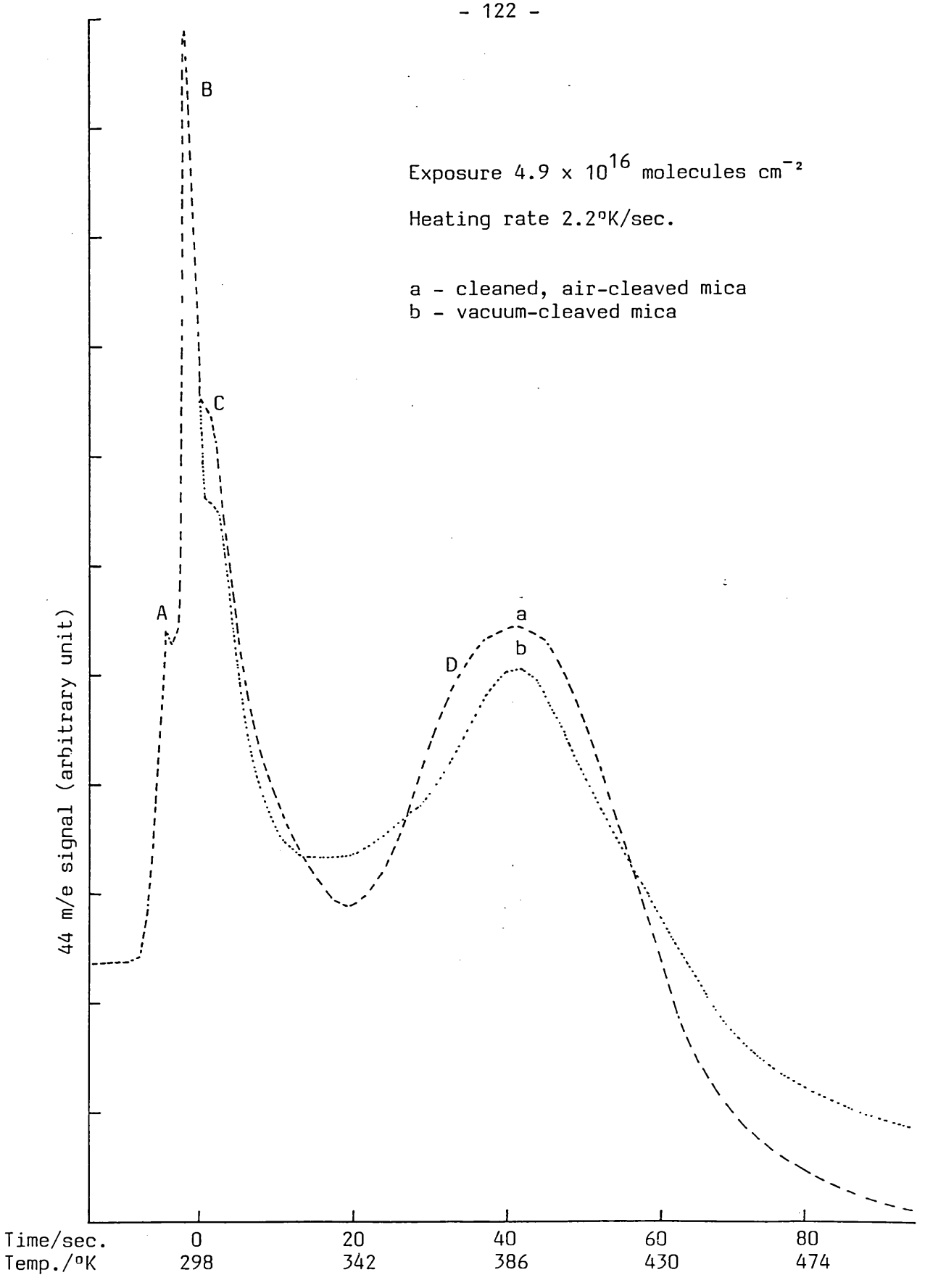

FIG. 26: Typical desorption spectra for carbon dioxide adsorbed at room temperature on mica surfaces.

have become hot as soon as the filament was switched on. In Fig. 26, both the time and temperature scales are shown to have started at the point where the thermocouple had recorded a rise in temperature of the mica. After desorption, the mass 44 partial pressure fell below the original base line which was possibly due to rapid pumping of the carbon dioxide by the filament.

The first two peaks, A and B, of the desorption spectra appeared before the temperature of the mica started to rise and are attributed to desorption from the tungsten filament, which rapidly became white hot. The peak C appeared just after the temperature of the mica began to rise and it was very difficult to isolate this peak from the filament desorption peaks. However it was noticed that when the mica sample was kept at some distance from the filament, so that its temperature rose more slowly, the peak C separated from the filament peaks. It thus appeared that there was a weakly held form of CO_2 on mica which desorbed just above room temperature. In an attempt to investigate this state in more detail, the mica was cooled prior to desorption by circulating liquid nitrogen through an aluminium tube wrapped round the middle of the cell. The mica could be cooled to 180K in this way while the glass envelope reached an even lower temperature. However, it was very difficult to maintain a constant temperature and the desorption spectra were masked by a slow evolution of CO_2 condensed on the cooler glass walls. This effect commenced as soon as the heating filament was switched on and made it impossible to give a quantitative analysis of the peak C.

The peak D was assigned to desorption of carbon dioxide from the mica surface. This was confirmed by a set of blank experiments in which the mica sample was removed from the cell leaving the holder and the chromel-alumel thermocouple in their normal positions, the

thermocouple dangling inside the cage of the holder. Adsorption/ desorption experiments were carried out with CO_2 under conditions identical to those when the mica was in place. The desorption spectrum for the blank experiment contained only two very sharp peaks - identical to the peaks A and B of Fig. 26. The effects of the hot filament, the glass walls, the holder and the thermocouple wires could be eliminated in this way and the peaks, C and D, could be assigned to the mica.

Desorption kinetics were determined using the well-known formulations of Redhead (1962). The rate of desorption from unit surface area may be written as

$$- \frac{d\sigma}{dt} = N_o \Theta^n \nu_n \exp\left(-\frac{E}{RT}\right) \qquad (3.14)$$

where n is the order of the desorption process,

σ is the surface coverage (molecules/cm^2),

N_o is the number of adsorption sites per cm^2,

Θ is the fractional surface coverage ($=\sigma/N_o$).

ν_n is the pre-exponential factor

and E is the activation energy of desorption.

In the present work, the temperature of the mica surface followed a simple linear relationship with time, i.e. $T = T_o + \beta t$, where β is the heating rate per second. With the assumptions that readsorption is negligible during the desorption cycle and that the activation energy of desorption does not vary with the surface coverage, the equation (3.14) can be solved to obtain the following relations:

$$\frac{E}{RT_p^2} = \frac{\nu_1}{\beta} \exp(-\frac{E}{RT_p}), \qquad \text{for } n = 1 \tag{3.15}$$

and $$\frac{E}{RT_p^2} = \frac{\sigma_0 \nu_2}{N_o \beta} \exp(-\frac{E}{RT_p}), \qquad \text{for } n = 2 \tag{3.16}$$

where T_p is the temperature corresponding to the desorption peak maximum and σ_0 is the initial surface coverage.

From equations (3.15) and (3.16), it follows that T_p depends upon the initial surface coverage for a second order desorption process, whereas it is independent of the initial surface coverage for a first order desorption process. T_p depends on the heating rate for both first and second order processes. The activation energy, E, and the pre-exponential factor, ν, can be obtained by taking a series of desorption measurements at different linear heating rates. Thus for both first and second order processes, a plot of $\ln(T_p^2/\beta)$ versus $(1/T_p)$ should be linear with slope equal to E/R. The pre-exponential factors can be obtained from the intercepts.

Alternatively, the activation energy for a second order process can be obtained from the variation of T_p with coverage at a constant heating rate. Equation (3.16) may be rewritten as-

$$\ln(\sigma_0 T_p^2) = \frac{E}{R}(\frac{1}{T_p}) + \ln \frac{\beta E N_o}{R\nu_2} \tag{3.17}$$

Hence a plot of $\ln(\sigma_0 T_p^2)$ versus $(1/T_p)$ should give a straight line for a second order desorption process with constant activation energy. The slope (E/R) of this straight line will give the activation energy of desorption and the intercept $(\ln \frac{\beta E N_o}{R\nu_2})$ may be used to calculate the pre-exponential factor (ν_2).

Although often difficult to use as a valid criterion, peak shapes may also be a rough guide to the order of a desorption process. Redhead (1962) has shown that for a linear heating rate, a first order desorption peak is asymmetric about T_p whereas a second order peak is always symmetric.

The peak D of interest in the present work for desorption of CO_2 from the mica surfaces was found to follow the second order kinetics on two counts, i.e.

(i) the peak was symmetrical around the peak maximum temperature, T_p, and

(ii) T_p varied with the surface coverage, a plot of $\ln(\sigma_0 T_p^2)$ versus $(1/T_p)$ yielding a straight line.

Fig. 27 shows the shift in the desorption peak maximum with coverage for a hydrogen-atom bombarded, air-cleaved muscovite surface. The spectra were obtained at a constant heating rate of 2.2°K/sec. Both time and temperature axes are shown in the figure. The vacuum-cleaved surface produced very similar data.

Table 2 summarises the variation of T_p with coverage for both the air-cleaved and the vacuum-cleaved mica surfaces. The table also shows the values of the activation energy and the pre-exponential factor obtained from the plots of $\ln(\sigma_0 T_p^2)$ versus $(1/T_p)$. These plots are given in Figs. 28 and 29, respectively for the air-cleaved and the vacuum-cleaved mica surfaces.

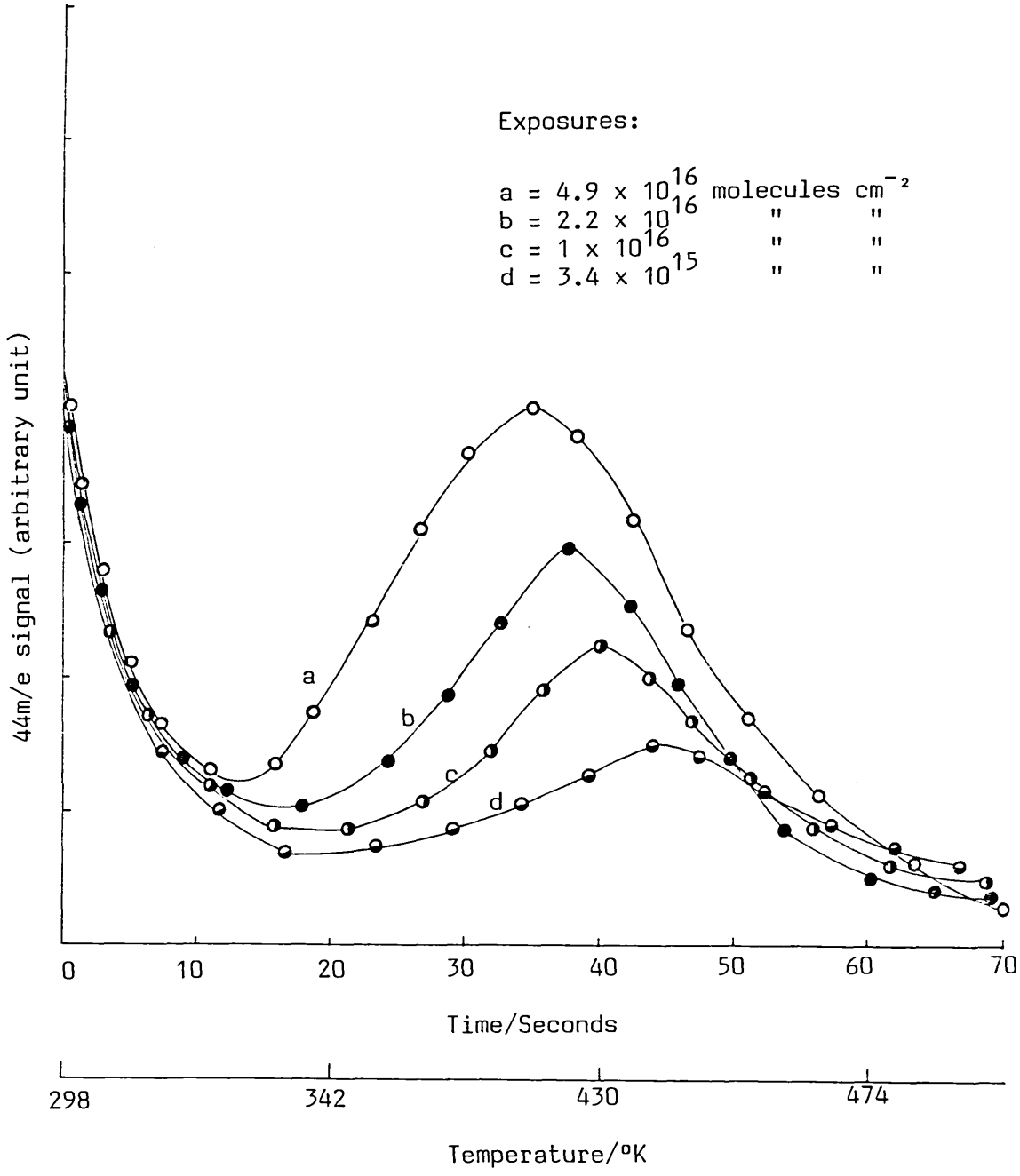

FIG. 27: Shift of desorption peak maximum with exposure for room temperature carbon dioxide adsorption on cleaned, air-cleaved mica surface. (Heating rate 2.2°K/sec.)

TABLE 2: Activation Energies of Desorption and Pre-exponential Factors for Carbon Dioxide adsorption on Muscovite Mica

Coverage σ_0/molecules cm^{-2}	Temperature of Peak Max. T_p/°K	Activation Energy of Desorption E/kJmol^{-1}	Pre-exponential Factor ν_2/sec^{-1}
A I R - C L E A V E D M I C A S U R F A C E			
8.82×10^{12}	372.8		
8.36×10^{12}	373.5		(i) 1.3×10^{12}
7.00×10^{12}	375.5		(ii) 1.98×10^{12}
4.88×10^{12}	380.5		
3.50×10^{12}	384.0	93.7	
3.15×10^{12}	385.5		
2.35×10^{12}	389.0		
1.48×10^{12}	394.5		
V A C U U M - C L E A V E D M I C A S U R F A C E			
4.52×10^{12}	381.0		
4.41×10^{12}	382.0		
4.07×10^{12}	382.5		
3.72×10^{12}	383.3		(i) 1.12×10^{12}
3.51×10^{12}	384.0		
3.31×10^{12}	385.0	94.4	(ii) 1.02×10^{12}
2.77×10^{12}	387.5		
2.14×10^{12}	390.5		
1.58×10^{12}	395.0		

(i) These values are calculated from the equation (3.16)
(ii) These values are calculated from the intercepts of the plots of $\ln(\sigma_0 T_p^2)$ versus $1/T_p$.

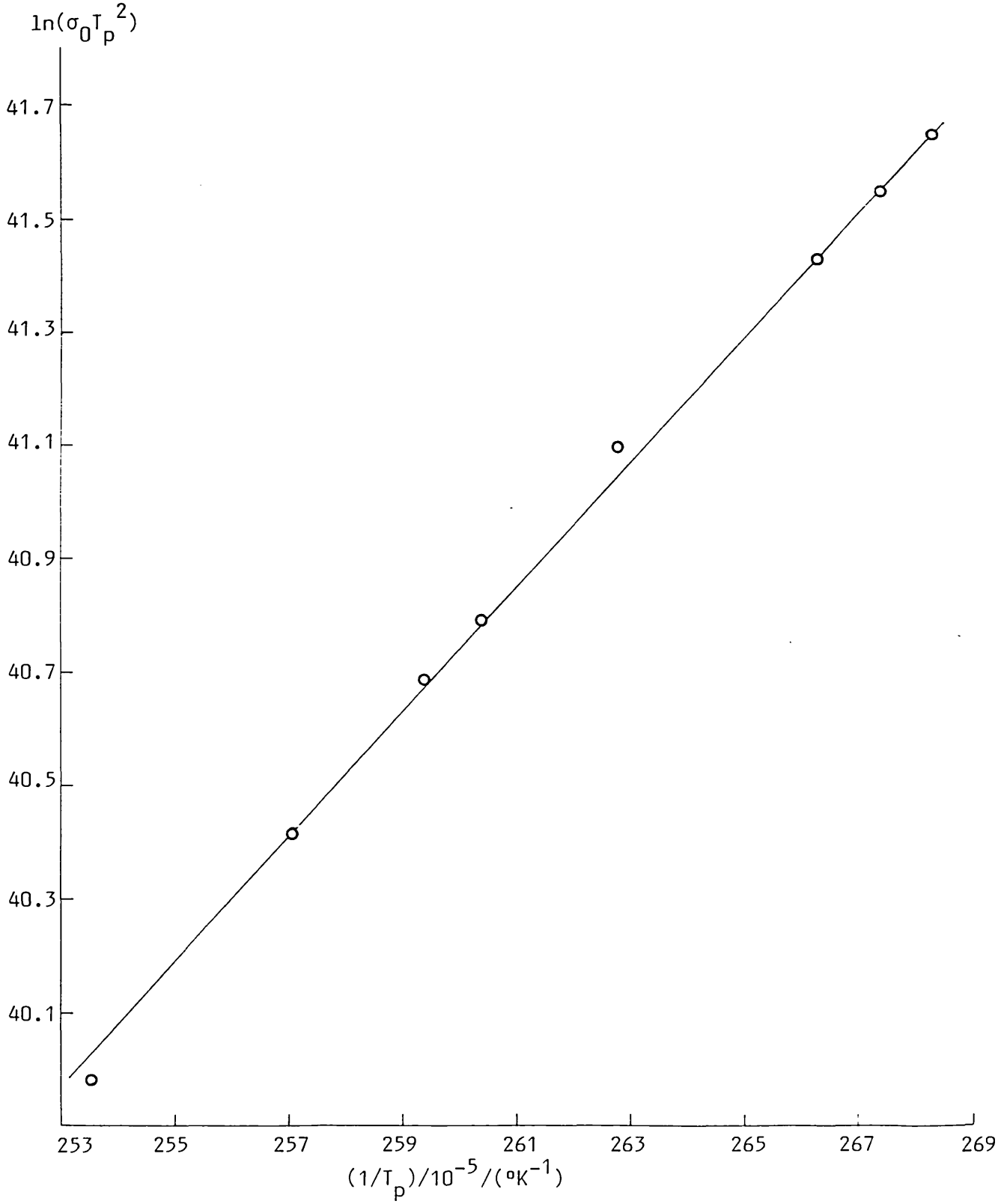

FIG. 28: Plot of $\ln(\sigma_0 T_p^2)$ versus $1/T_p$ for room temperature adsorption of carbon dioxide on the cleaned, air-cleaved mica surface.

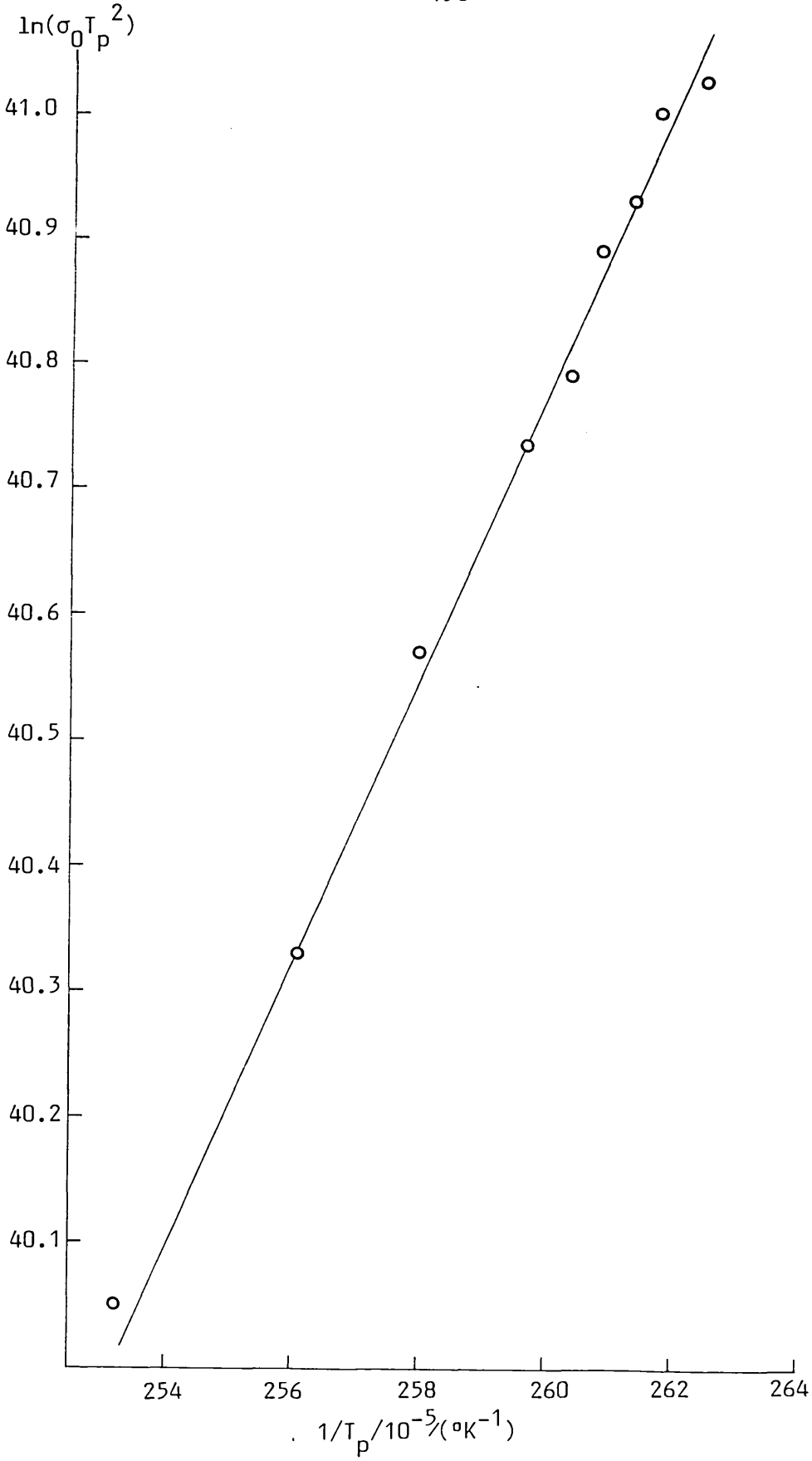

FIG. 29: Plot of $\ln(\sigma_0 T_p^2)$ versus $1/T_p$ for room temperature adsorption of carbon dioxide on the vacuum-cleaved mica surface.

In an adsorption/desorption experiment, the total gas exposure for each cm^2 area of the mica surface was calculated from the area under the P-t curve during the adsorption cycle using the following formula:

$$\text{Exposure per } cm^2 = z \int P dt \text{ molecules} \qquad (3.18)$$

where P is the pressure of the gas in the cell at time t, and $z = (2\pi mkT)^{-\frac{1}{2}}$, the Hertz-Knudsen collision factor for the gas (= 2.30×10^{18} molecules $(Nm^{-2})^{-1}$ $sec^{-1}cm^{-2}$ for carbon dioxide at 298K).

The initial surface coverage (σ_0) per cm^2 area of the mica surface was similarly calculated from the area under the desorption curve using the relation:

$$\sigma_0 = \frac{1}{A} K \int P dt \qquad (3.19)$$

where K is the pumping speed with respect to carbon dioxide and A is the geometric surface area of the sample in cm^2.

The exposure and coverage values were corrected for absolute pressure values in the manner described in section 3.2.

The plots of coverage versus exposure for both the air-cleaved and the vacuum-cleaved mica surfaces are shown in Fig. 30. From the figure, the saturation coverage of carbon dioxide on the vacuum-cleaved surface of the mica (~ 4.8×10^{12} molecules cm^{-2}) appears to be only half as much as that on the air-cleaved, hydrogen-atom bombarded surface (~ 9×10^{12} molecules cm^{-2}). These coverages are very small compared to those on active metal surfaces and the values thus reflect the small number of active sites on the mica surfaces.

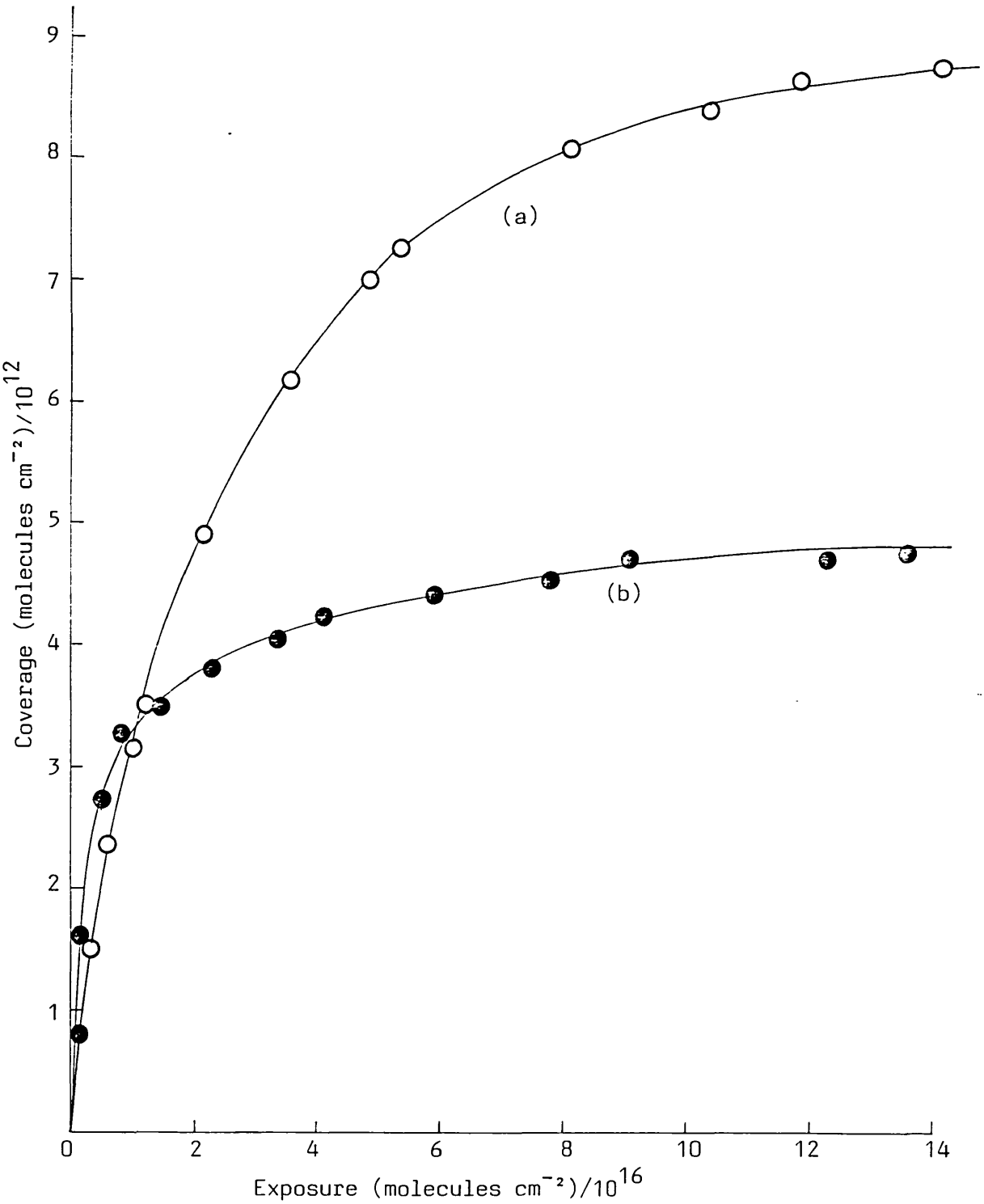

FIG. 30: Coverage versus exposure plots for room temperature adsorption of carbon dioxide on (a) cleaned, air-cleaved mica and (b) vacuum-cleaved mica.

The sticking probability (s), which is defined as the fraction of the incident adsorbate molecules adsorbed on the adsorbent surface, may be obtained from the slope of the coverage versus exposure plots. From Fig. 30, the following values are obtained:

Initial sticking probability of CO_2 on the vacuum-cleaved mica surface = 1.3×10^{-3},

Initial sticking probability of CO_2 on the air-cleaved mica surface = 3.8×10^{-4}

The vacuum-cleaved mica surface thus has a higher sticking probability for carbon dioxide than the air-cleaved surface. The low values of the sticking probability also indicate the slow nature of uptake of carbon dioxide by the mica surfaces.

The amount of adsorption of carbon dioxide on the mica surface did not appear to depend on the adsorption temperature. Thus, in a set of experiments where the mica surface was kept at 325K during gas dosing, the coverages were found to be similar to those obtained for adsorption at room temperature.

According to Barrer (1978), each oxygen hexagon in the surface of the mica has an area of 24Å^2. The potassium ions sit in these hexagons. On this basis, each cm^2 of the mica surface is capable of holding $\sim 4.2 \times 10^{14}$ potassium ions, but since on cleavage the potassium ions are presumed to be equally divided between the two faces, the number of these ions on a freshly cleaved surface is around $2.1 \times 10^{14} cm^{-2}$. If it is supposed that these are the adsorption sites on the mica surface, it can be seen that for the hydrogen-atom bombarded air-cleaved surface, only one in 23 sites is occupied

by carbon dioxide whilst for the vacuum-cleaved surface the occupation is even less at one in 44 sites.

The air-cleaved surface had gone through many heat-treatments as well as hydrogen-atom bombardments and therefore it is natural to assume that this surface had suffered at least some depletion of potassium compared to the vacuum-cleaved surface which had had very little treatment before being exposed to carbon dioxide. If the potassium ions were the adsorption sites, then the vacuum-cleaved surface is expected to have a higher saturation coverage of carbon dioxide than the air-cleaved surface. The fact that the reverse is true points to some other kind of adsorption site on the mica surface. It is possible that the active sites are below the potassium layer. In the air-cleaved surface, the loss of some potassium through repeated bakeouts and heating cycles was likely to make more sites (below the potassium layer) accessible to carbon dioxide and consequently this surface has a higher coverage.

Second order kinetics for desorption of carbon dioxide from the mica surface implies that the rate determining step is a random coming together of two surface species, both of which have a surface concentration proportional to the total reversible uptake of carbon dioxide. One possibility is that the carbon dioxide is dissociatively adsorbed as

$$CO_2(g) \rightleftharpoons CO(ads.) + O(ads.)$$

although it is not clear what type of site would be involved in such an adsorption. One species, at least, would need to be mobile and able to diffuse across the surface in order to produce second order

desorption kinetics. Since the conceivable sites for adsorption of these species are far apart on the mica surface, it is hard to see how the diffusion process would operate. Alternatively, the mobile species might be an electron or more likely a positive hole, in which case the rate determining step in the desorption process is likely to be

$$CO_2^-(ads.) + (e^+) \rightarrow CO_2(g) \ .$$

Another mechanism can be conceived where the mobile species is a proton. This mechanism will operate as follows:-

(i) The initial attack of carbon dioxide is at hydroxyl sites (I) on the mica surface to form a bicarbonate species (II),

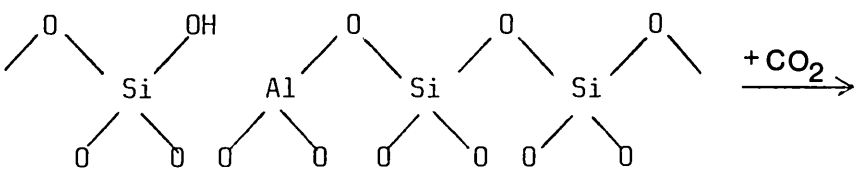

Hydroxylated tetrahedral layer of mica (I)

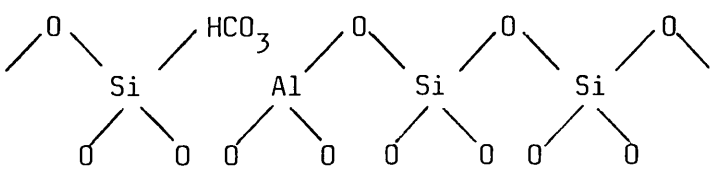

Bicarbonate (II)

(ii) The bicarbonate species (II) then dissociates into a carbonate (III) and a proton which migrates along the layer of oxygen atoms,

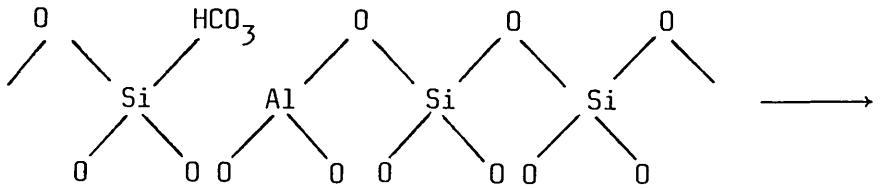

(II)

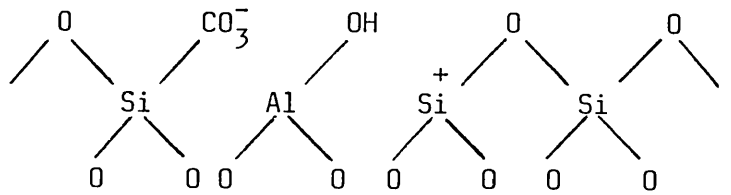

Carbonate (III)

Proton migration

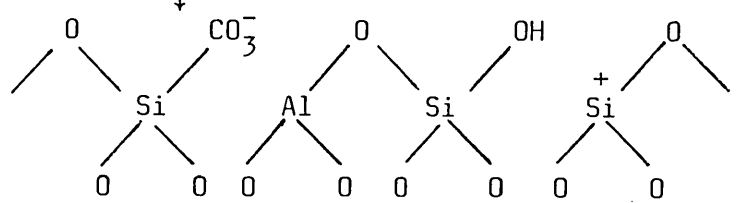

(IV)

(iii) Protons become stabilized at a quadrivalent aluminium site,

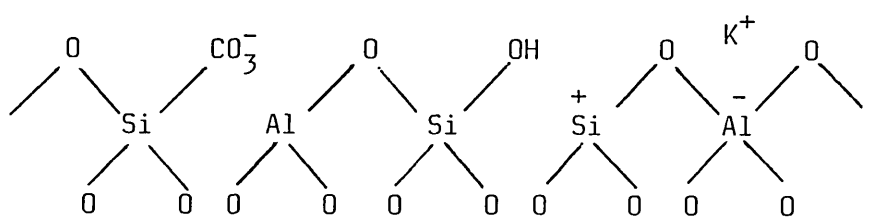

(IV)

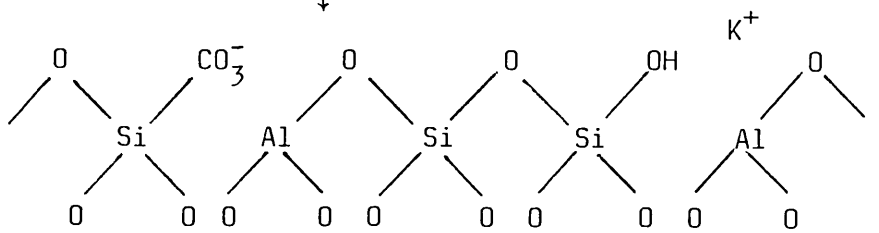

(V)

(iv) Desorption occurs when the carbonate and hydroxyl species come together again.

Formation of bicarbonate and carbonate complexes by reaction of CO_2 with M-O and M-OH bonds is well-known. The chemistry of carbonato and carbon dioxide complexes has recently been thoroughly reviewed by Palmer and van Eldik (1983). Bertsch and Habgood (1963) studied carbon dioxide adsorption on alkali and alkaline earth X-zeolites and detected carbonate type species from infra-red measurements. They found that the presence of small amounts of preadsorbed water greatly accelerated the CO_2 adsorption. According to their scheme, the CO_2 attacks a lattice oxygen normally bonded to a silicon or an aluminium atom. This weakens the Si-O or Al-O bond, but the formation of the carbonate does not require any major change in the position of the surface oxygen on the lattice. The authors have shown that carbonate formation is most likely with a surface oxygen adjacent to a positive ion (e.g. the exchangeable cations, Na^+, or K^+) whose positive field extending out would help to stabilize the carbonate. This scheme agreed with the later works of Ward and Habgood (1966), Angell and Howell (1969), Jacobs et al. (1973) and many others. Lerot and co-workers (1975), on the other hand, showed the formation of both bicarbonate and carbonate species on faujasite zeolites from infra-red data.

Morterra et al. (1977) have found two surface bicarbonate species by reacting CO_2 with η-alumina, the concentrations of the species depending on the thermal pretreatment. More recently Lercher, Colombier and Noller (1984) have studied adsorption of CO_2 on alumina, alumina-magnesia mixed oxides and magnesia by infra-red spectroscopy, and have proposed the following two species:

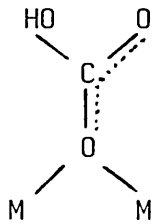

Surface bicarbonate

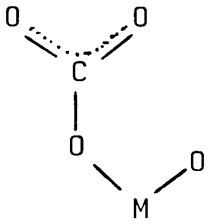

Surface monodentate carbonate

On the basis of these observations, it is quite reasonable to assume that carbon dioxide forms bicarbonate and carbonate species on the mica surface, as proposed in the mechanism above. The TPD is however not a suitable technique to probe for such species.

The existence of a hydroxylated tetrahedral layer (I) in the mica, where some of the basal oxygens are converted to hydroxyl groups, is also quite plausible. The mica surface, as was shown earlier, could never be freed of adsorbed water and it is possible that some of the water existed as hydroxonium (H_3O^+) ions replacing some of the potassium. On dehydration during heating the mica, the H_3O^+ ion is likely to form a surface hydroxyl as shown below:

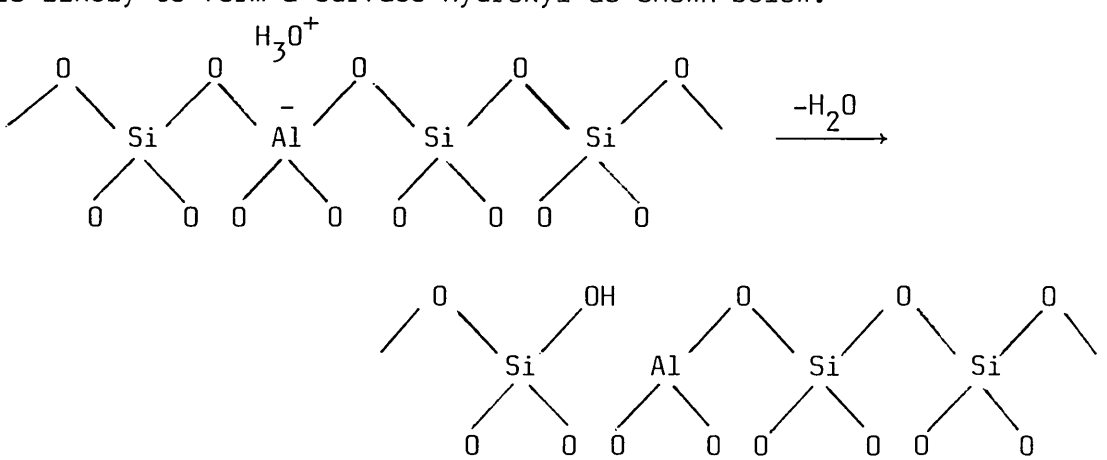

such surface hydroxylation is well-established in silica, alumina, silica-alumina and zeolites. With the air-cleaved mica, hydroxylation was also possible during hydrogen-atom bombardment. Haynes (1978)

has shown that zeolite surfaces can be hydroxylated through reduction with hydrogen.

In any case, the air-cleaved mica surface went through extended heat treatments as well as hydrogen-atom bombardment and therefore this surface was expected to have more hydroxyl groups than the relatively untreated vacuum-cleaved surface. This accounts for twice as much carbon dioxide being taken up by the air-cleaved mica.

The second order desorption kinetics rests on the ability of the proton in (III) to migrate across the basal oxygen layer of the mica, as from III to IV in the mechanism proposed above. Proton mobility on the zeolite surface is thought to be one of the reasons for high catalytic activity. Ward (1976) has discussed in detail the mobility and delocalization of protons in the zeolites. It was shown that interaction of the hydroxyl group with an adjacent aluminium atom led to proton mobility

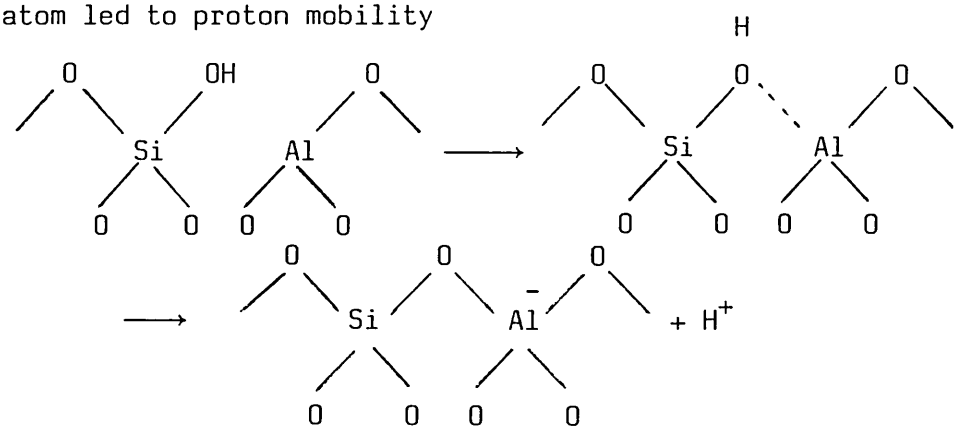

The proton can then attach itself to another surface oxygen, reverting aluminium to the trivalent state. Fripiat (1971) used various techniques including magnetic resonance measurements to conclude that the protons in a zeolite surface were mobile. Freude et al.(1974) have shown the proton jump frequency to be of the order of 2-10 x 10^4 sec^{-1} at 200°C with activation energies of 5-10kcal/mole.

The mechanism proposed for the second order kinetics of desorption

of CO_2 from mica thus appears reasonable. The formation of a trivalent silicon with a positive charge as in (III) is also a well-known postulation in zeolite chemistry. The tetrahedral layer in mica has three silicons to one aluminium on the average and it is known that the distribution of the aluminium atoms is random. Also there is much more aluminium in mica than in any zeolite. The random presence of aluminium in the lattice is thus likely to promote proton mobility.

Finally, as discussed above, the electrical field of the potassium ions is favourable to the formation of the carbonate species and therefore, the conversion of the bicarbonate to the carbonate form can be achieved easily.

3.3.5 ADSORPTION OF AMMONIA ON MICA SURFACES

No ammonia was found to adsorb on the air-cleaved mica surface when the gas was introduced to an untreated surface just after bakeout. The air-cleaved surface became active only after carbon contamination had been removed by the hydrogen-atom bombardment described earlier. The first experiments on the cleaned surface were performed with carbon dioxide, which is known from XPS measurements to deposit carbon, and it was necessary for the surface to be exposed to further hydrogen-atom bombardment for one hour at 2×10^{-6} torr pressure of hydrogen before commencing the ammonia work. Ammonia was also found to adsorb on the vacuum-cleaved surface.

Both ammonia adsorption and desorption were monitored in terms of the mass 17 partial pressure although desorption spectra were occasionally taken with mass 18 or mass 16 in order to distinguish

between ammonia and water vapour. It was not possible to calculate the total uptake of ammonia by the mica surface from the adsorption profile as this also contained the filament uptake. Following each exposure, the cell was pumped down to the base pressure (normally in the 10^{-9} torr range with respect to mass 17 partial pressure) before the desorption spectra were taken. Thus any very weakly adsorbed ammonia would have been pumped away before heating commenced.

A typical desorption spectrum with a linear temperature rise for an air-cleaved, hydrogen-atom bombarded surface is shown in Fig. 31. From the mass 17 desorption profile four different peaks can be distinguished. The first two sharp peaks, labelled A and B, appeared before the temperature of the mica started to rise. These two peaks were also the only peaks which appeared under identical experimental conditions in a blank run with the mica sample removed from the cell. It is therefore clear that these two peaks are caused by desorption from the tungsten filament.

The peaks, labelled C and D, appeared respectively in the temperature ranges 300-350K and 375-510K. Both of these peaks were absent in the blank test which shows that they represent genuine desorption from the mica surface. This was confirmed by noting the different times at which the peaks appeared when the orientation of the mica with respect to the filament was altered. If the ammonia had been desorbing from the glass walls or from the filament, the peak positions would have been dependent only on the filament temperature and would not have been expected to vary with the orientation of the mica surface.

It should be noted that the high temperature peak (peak D) is very broad and appears to have a shoulder on the low temperature side.

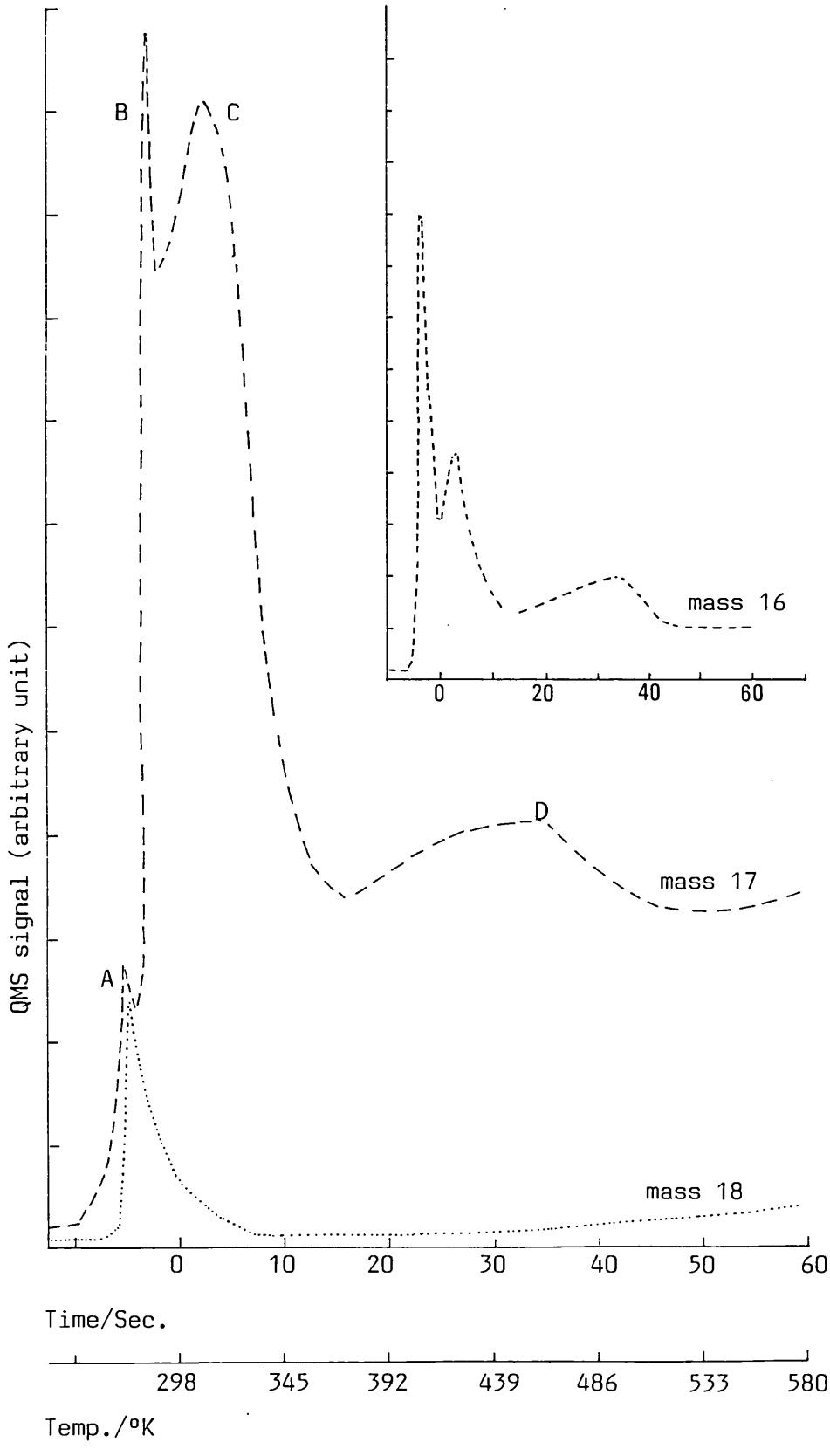

FIG. 31: Typical desorption spectra with respect to masses 17, 18 and 16 after room temperature adsorption of ammonia on muscovite mica. The background rose after the desorption as the surrounding glass walls became warm. (Heating rate 5.60°K/sec.).

It was however impossible to resolve this peak and all calculations were done taking this peak as a single state.

The ammonia used in these experiments was prepared from an aqueous solution of ammonia by a double freeze-pump-thaw process and was known to contain between 5 and 15% water vapour. It was therefore necessary to check that the desorption peaks were due to ammonia and not to water vapour. This was done by monitoring the mass 18 and the mass 16 signals. The cracking pattern of ammonia for the Anavac-2 mass spectrometer was found to consist of mass 17 (100%), mass 16 (80%) and negligible amounts of masses 15 and 14 whereas the cracking pattern for water vapour contained predominantly mass 18 (100%) and mass 17 (23%). Thus, mass 16 and mass 18 spectra should be representative of ammonia and water vapour respectively. The desorption spectra of masses 18 and 16 for an ammonia exposure identical to that used for the mass 17 spectrum are shown in Fig. 31. The single sharp peak in the mass 18 spectra appears before the temperature of the mica begins to rise and indicates that the peak A assigned to desorption from the tungsten filament in the mass 17 desorption pattern may be due to water vapour. The mass 16 spectrum confirms this conclusion, showing only three peaks, corresponding to peaks B, C and D of the mass 17 spectrum. The presence of only one ammonia desorption peak from the filament is in agreement with the recent observation of Reed and Lambert (1984) who obtained a single mass 17 peak for ammonia desorption from a (100) oriented polycrystalline tungsten specimen.

The slow rise in mass 17 and mass 18 signals at temperatures greater than 500K was found to be due to evolution of water from the interior of the mica, possibly through a slow diffusion process. Because of this, water could not be completely eliminated from the background.

The two peaks, C and D, attributed to desorption of ammonia from mica, were both found to follow first order desorption kinetics. This is based on the following evidence:-

(i) The temperatures of the peak maxima did not shift as the coverage of the ammonia was increased at constant heating rate. This is shown in Fig. 32 for the hydrogen-atom bombarded vacuum-cleaved surface. This behaviour is typical of first order desorption kinetics.

(ii) Peak D was found to be asymmetric about the peak maximum temperature in accordance with the normal shape of a first order desorption. The shape of peak C, on the other hand, is not easy to establish as most of the low temperature side of this peak is enclosed inside the filament desorption peaks.

For both chemisorbed states of ammonia on mica, the peak maxima shifted to higher temperatures as the heating rate was increased. Results are shown in Fig. 33 for a cleaned, air-cleaved mica surface. For the sake of clarity, the desorption profiles at three different heating rates only are shown. In actual practice, seven different heating rates from 2.2°K/sec to 7.5°K/sec were used. The temperatures at which the two peaks reached their maxima and the corresponding heating rates for both the air-cleaved and the vacuum-cleaved mica surfaces are summarized in Table 3. The heating rates and the temperatures for the air-cleaved surface have been corrected with reference to the values for the vacuum-cleaved surface in order to allow for the temperature gradient that existed between the mica surface and the thermocouple. After cleaving the thermocouple was much closer to the surface and no temperature correction was thought necessary. Table 3 shows that there are only slight differences between the corresponding

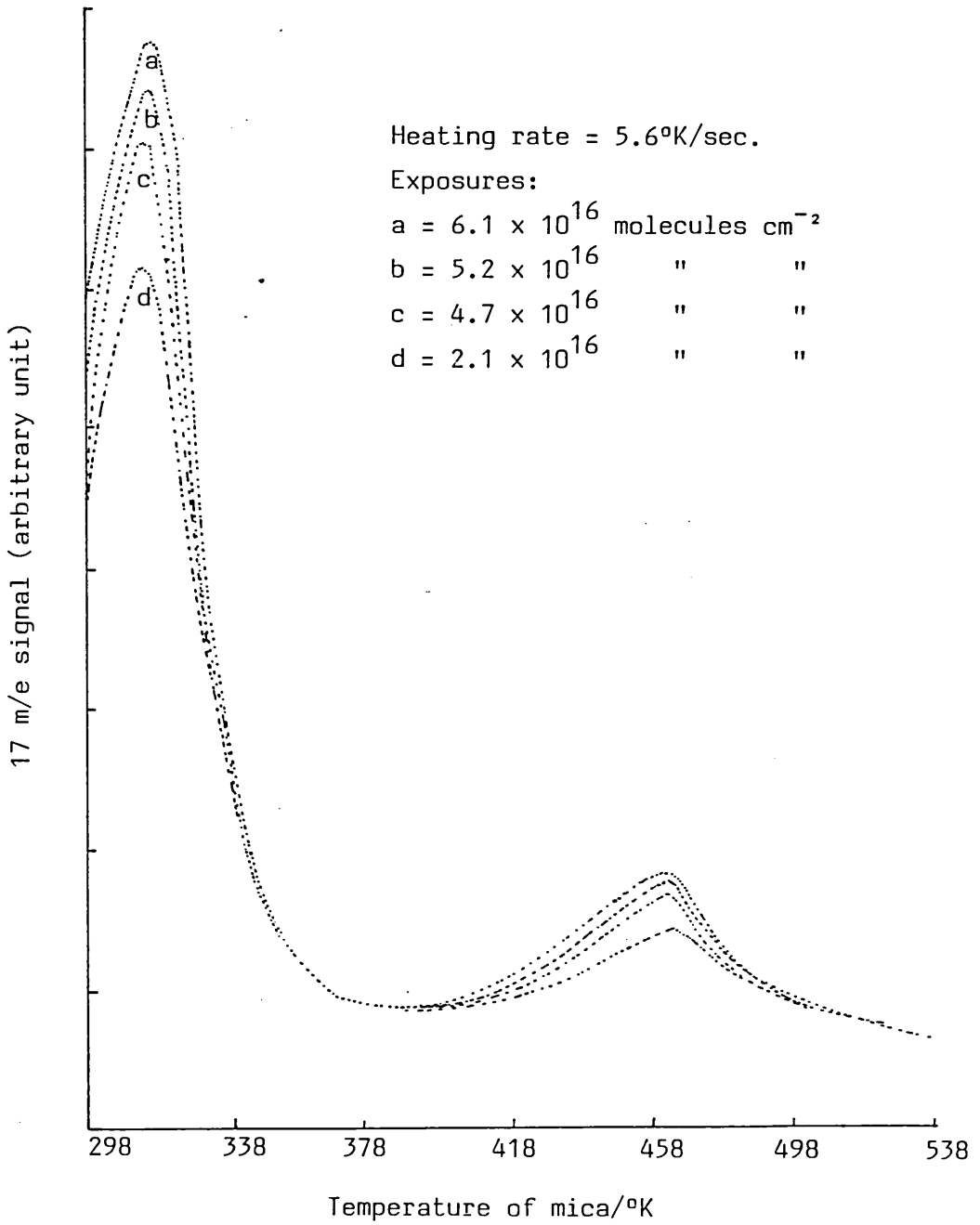

FIG. 32: Desorption spectra for ammonia adsorbed at room temperature on the vacuum-cleaved mica surface.

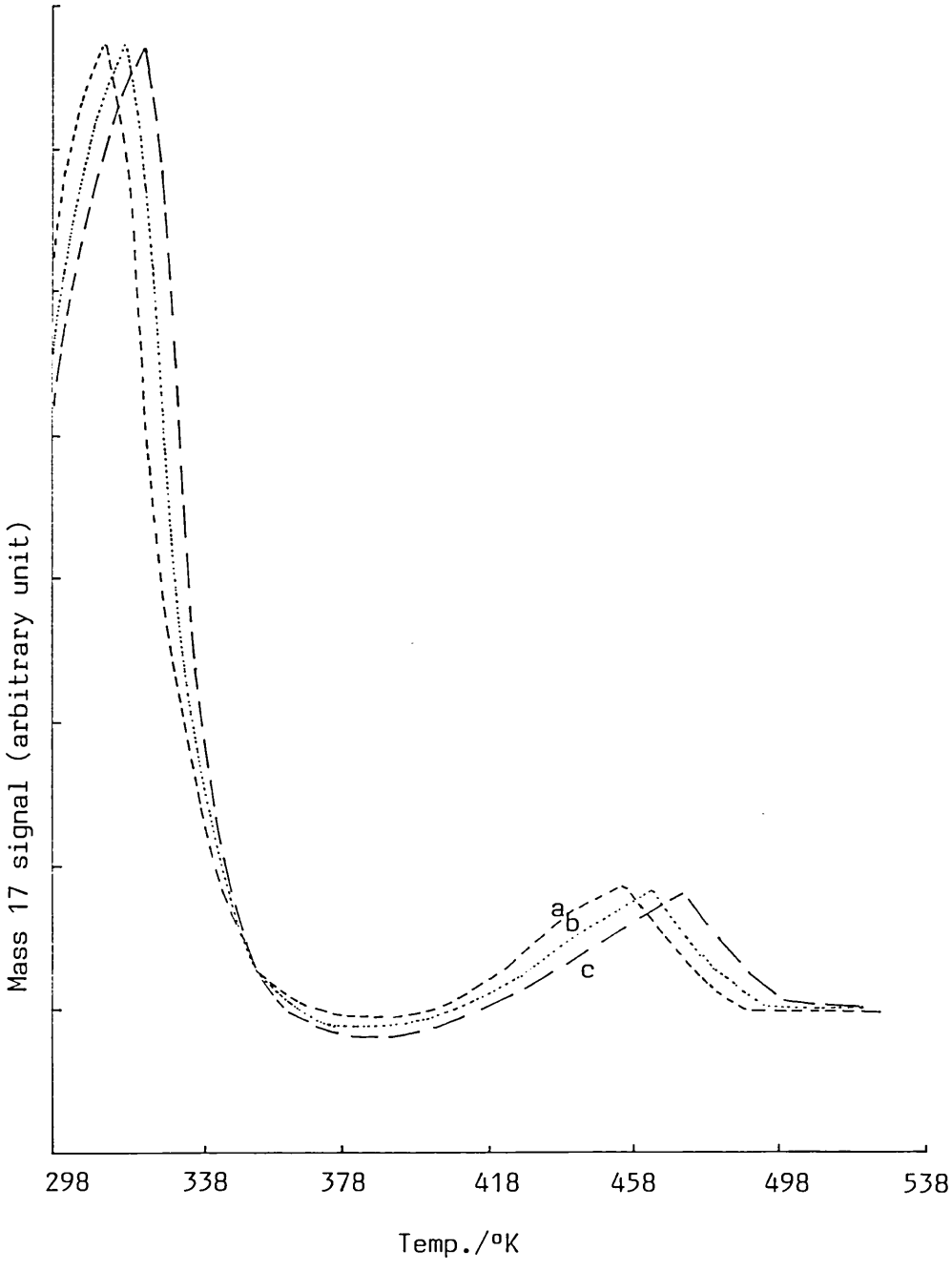

FIG. 33: Shift in the desorption peak maximum with heating rate for room temperature adsorpton of ammonia on the cleaned, air-cleaved mica.

a, 3.8°K/sec; b, 5.6°K/sec. and c, 7.5°K/sec.
Exposure 3.7×10^{16} molecules cm^{-2}.

'T_p' values for the air-cleaved and the vacuum-cleaved mica surfaces.

TABLE 3: Peak Maximum Temperature at Different Heating Rates

HEATING RATE $\beta/^oK sec^{-1}$	PEAK MAXIMUM TEMPERATURE, $T_p/^oK$			
	Low Temperature Peak		High Temperature Peak	
	Air-cleaved Mica	Vac -cleaved Mica	Air-cleaved Mica	Vac-cleaved Mica
2.2	310.5	310.0	450.5	451.0
3.0	313.0	312.0	453.0	453.0
3.8	315.0	315.0	455.0	455.5
4.7	317.5	316.8	457.8	458.0
5.6	319.0	318.5	460.5	461.0
6.0	321.0	320.8	463.0	462.5
7.5	323.0	322.5	465.5	464.0

For first order desorption kinetics with constant activation energy, E, and no appreciable readsorption, the variation of peak maximum temperature, T_p, with heating rate, β, should obey equation (3.15). This can be rewritten as

$$\ln\left(\frac{T_p^2}{\beta}\right) = \frac{E}{R}\left(\frac{1}{T_p}\right) + \ln\frac{E}{\nu_1 R} \qquad (3.20)$$

where ν_1 is the first order pre-exponential term. Plots of $\ln(T_p^2/\beta)$ versus $(1/T_p)$ for the low temperature and high temperature states of

ammonia on mica surfaces are shown respectively in Figs. 34 and 35. From the slopes and intercepts of the plots, the activation energies and the frequency terms given in Table 4 were calculated.

TABLE 4: Activation energies of desorption and pre-exponential factors for ammonia desorption from the mica surfaces

Low Temperature State		High Temperature State	
Activation Energy $E/kJmol^{-1}$	Pre-exponential Factor ν_1/sec^{-1}	Activation Energy $E/kJmol^{-1}$	Pre-exponential Factor ν_1/sec^{-1}
AIR-CLEAVED MICA			
76.6	1.2×10^{12}	121.3	1.8×10^{13}
VACUUM-CLEAVED MICA			
75.2	8.6×10^{11}	122.8	1.8×10^{13}

The exposures and the coverages were calculated using the formulae (3.18) and (3.19) respectively. However, there is an element of uncertainty in the exposure values calculated from the areas under the P-t curves for the ammonia dosing cycles. It was found that after the flow of gas was stopped the ammonia partial pressure went down rapidly at first, but after about 5 seconds it rose slightly and then fell again very slowly. Desorption of considerable amounts of weakly-held ammonia from the glass walls was thought to be responsible for this abnormal behaviour. In calculating exposures, the area under the P-t curve was taken up to the point where the sharp fall of mass 17

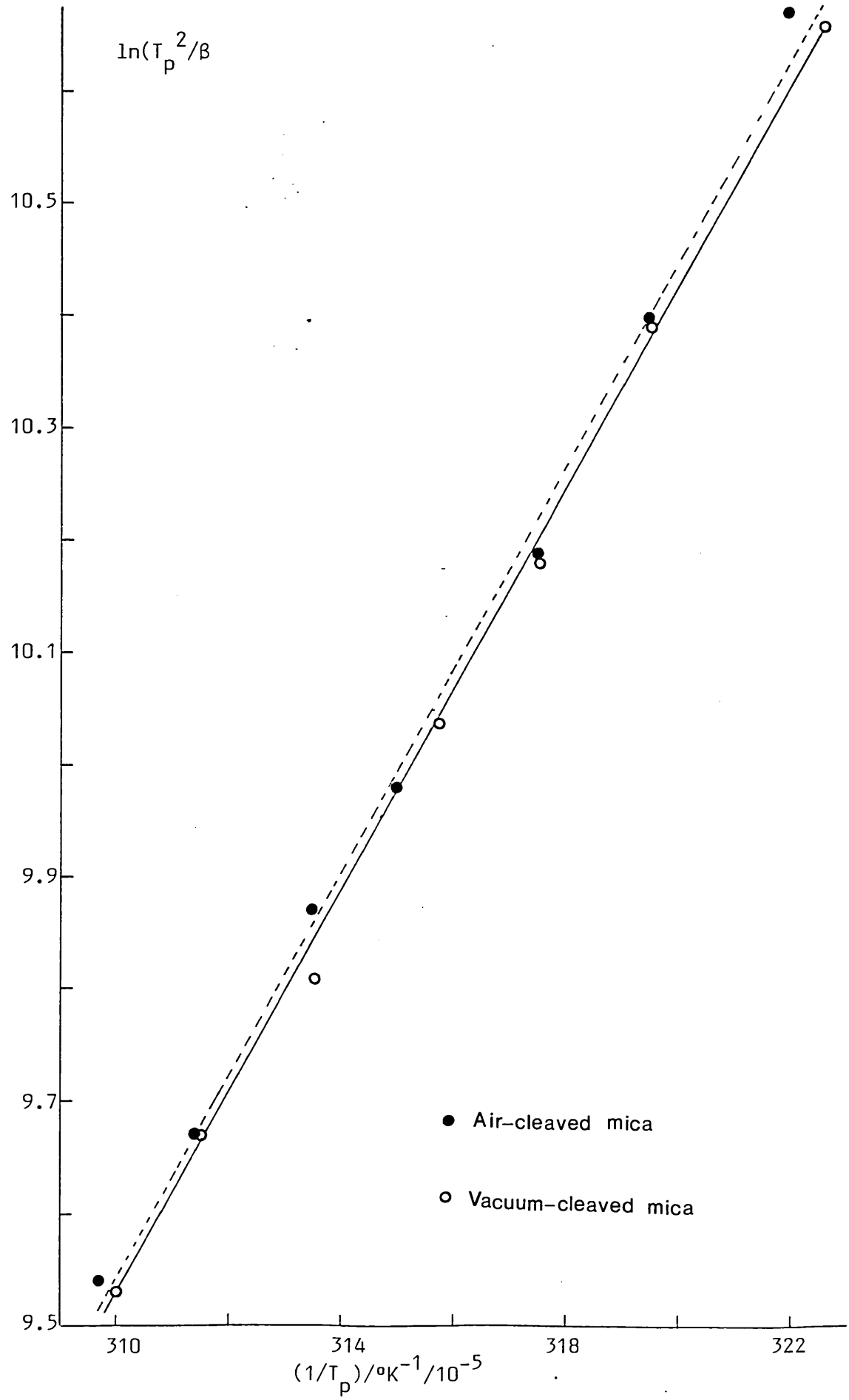

FIG. 34: Plot of ln T_p^2/β versus $(1/T_p)$ for the low temperature desorption peak of ammonia.

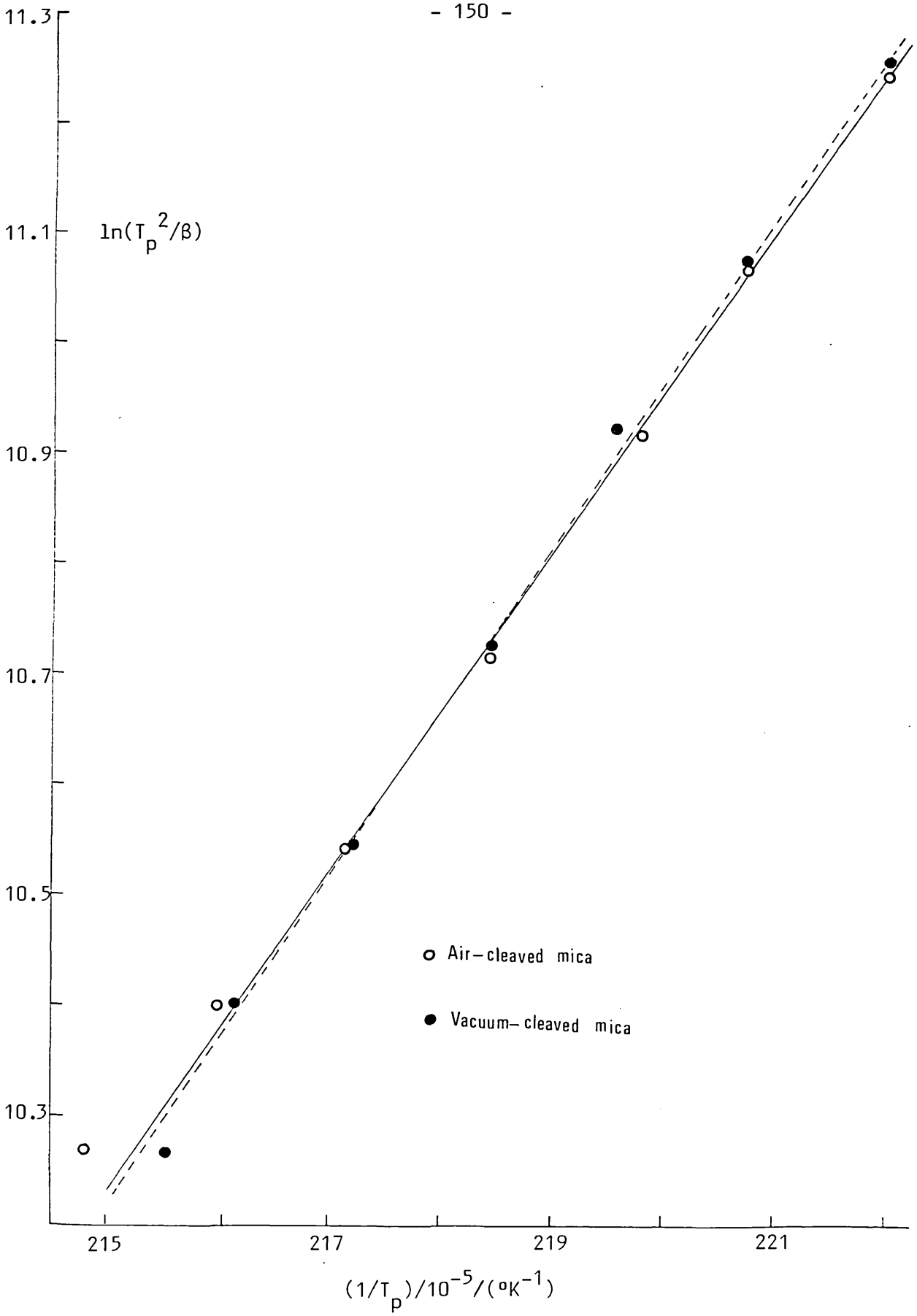

FIG. 35: Plot of $\ln(T_p^2/\beta)$ versus $(1/T_p)$ for the high temperature desorption peak of ammonia on the air-cleaved and vacuum cleaved mica surfaces.

partial pressure ended. The actual exposures were thus likely to be somewhat higher and therefore, the true sticking probability values will be lower than those obtained on the basis of the exposures calculated as described above.

The coverage versus exposure plots for the low and the high temperature states of ammonia, at a constant heating rate of 5.6°K/sec, are shown respectively in Figs. 36 and 37. Data for both the air-cleaved and the vacuum-cleaved surfaces are shown side by side. As the low temperature peak overlapped the filament desorption peaks, the peak area had to be calculated by assuming that it was twice the area between the peak maximum and the high temperature tail. This is unlikely to introduce any significant error.

The saturation coverages and the initial sticking probabilities found from the above plots are summarized in Table 5. It can be seen that the uptake of ammonia into the low temperature state of adsorption on the vacuum-cleaved surface has both a lower sticking probability and a lower saturation coverage than that on the air-cleaved surface. For the high temperature state of adsorption, the sticking probability is still lower on the vacuum-cleaved surface but the uptakes on both surfaces are similar.

Adsorption of ammonia on mica at room temperature must have many features in common with adsorption on the so-called acidic solids, namely the zeolites, silica-aluminas and the clay minerals. Ammonia is a relatively strong base and is known for its equal preference for both Lewis and Brönsted acid sites. Since ammonia desorption follows first order kinetics, dissociative adsorption to form $-NH_2$ and $=NH$ groups seems unlikely although it cannot be entirely ruled out. (If the products of dissociation remain on neighbouring sites,

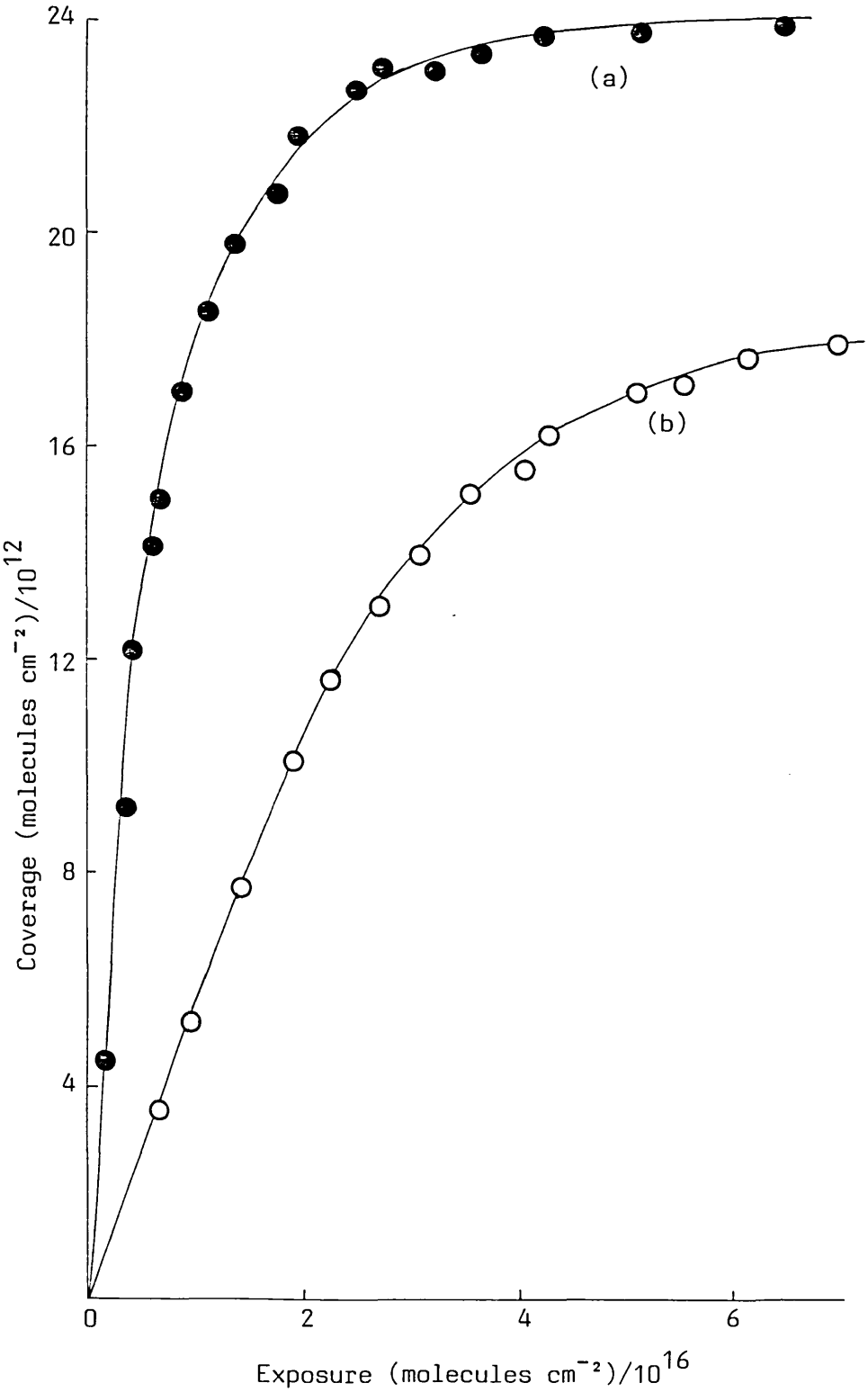

FIG. 36: Coverage versus exposure plots for the low temperature desorption peak of room temperature ammonia adsorption on (a) cleaned, air-cleaved mica and (b) vacuum-cleaved mica.

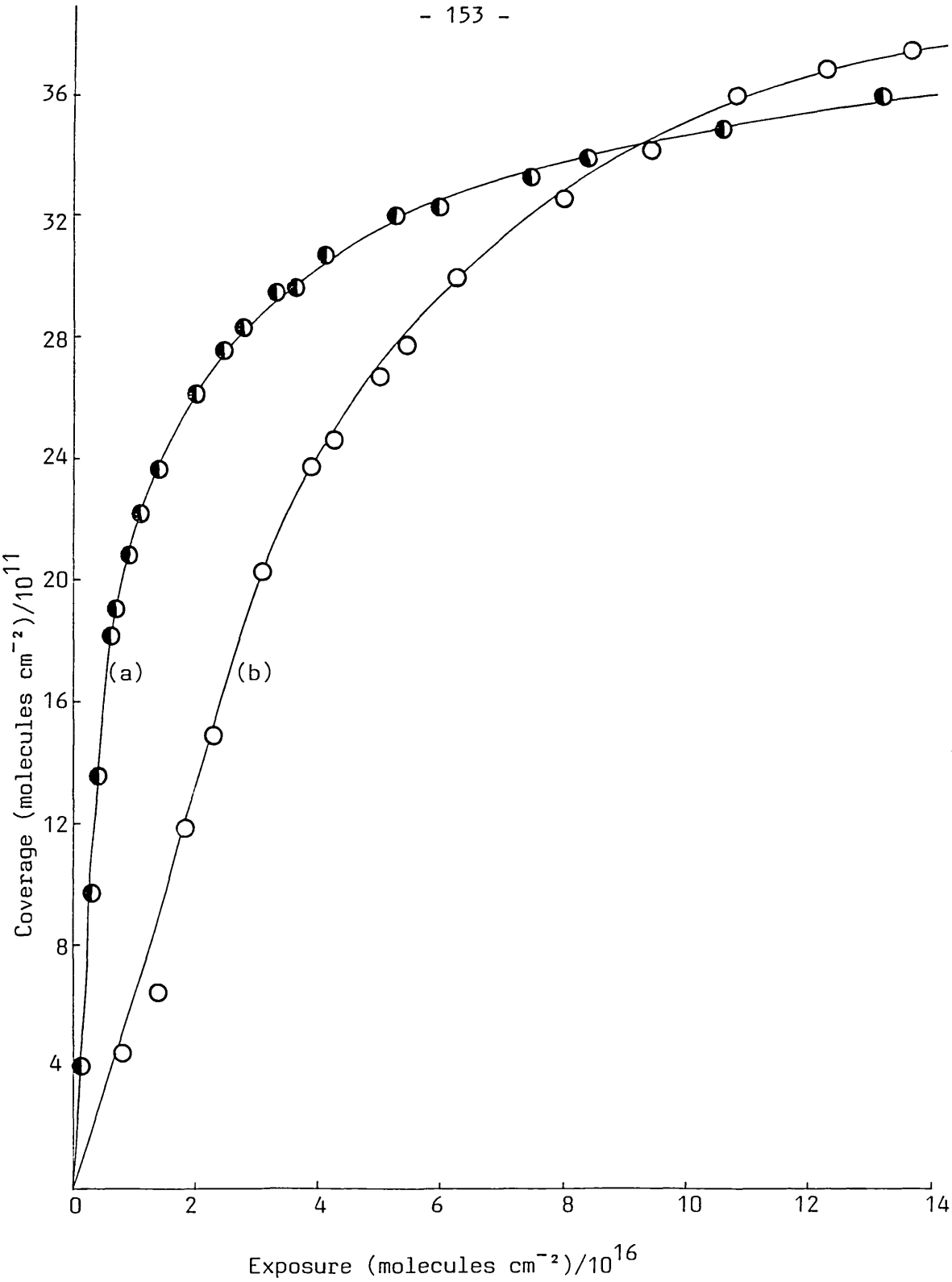

FIG. 37: Coverage versus exposure plots for the high temperature desorption peak of room temperature ammonia adsorption on (a) cleaned, air-cleaved mica and (b) vacuum-cleaved mica.

desorption could still be first order). In general, however, first order desorption kinetics points to an undissociated form of ammonia.

TABLE 5: Some features of ammonia adsorption on mica

Low Temperature State		High Temperature State	
Saturation Coverage /molecules cm^{-2}	Initial Sticking Probability	Saturation Coverage /molecules cm^{-2}	Initial Sticking Probability
AIR-CLEAVED MICA			
2.4×10^{13}	2.8×10^{-3}	3.6×10^{12}	3.9×10^{-4}
VACUUM-CLEAVED MICA			
1.8×10^{13}	7.8×10^{-5}	3.9×10^{12}	6.5×10^{-5}

The adsorption state of ammonia on mica which desorbs with a peak maximum at 310-325K is obviously very weakly held on the surface. Possibly this represents ammonia bonded to weakly acidic sites. The other state of ammonia on mica has quite a high binding energy shown by its desorption at temperatures in excess of 450K. It is most likely that strong acid sites are involved in this state. Since the high temperature state has a saturation coverage which is only about one-tenth of that for the low temperature state, one must conclude that the number of weak acid sites is far in excess of the number of strong acid sites on the mica surface.

Acidic sites might arise through the hydroxylation of some of the bridged oxygen atoms in the mica structure, as proposed in the

previous section. The process may occur in two stages: (i) replacement of some potassium ions by hydroxonium (H_3O^+) ions and (ii) subsequent dehydration on heating. The scheme is shown below:

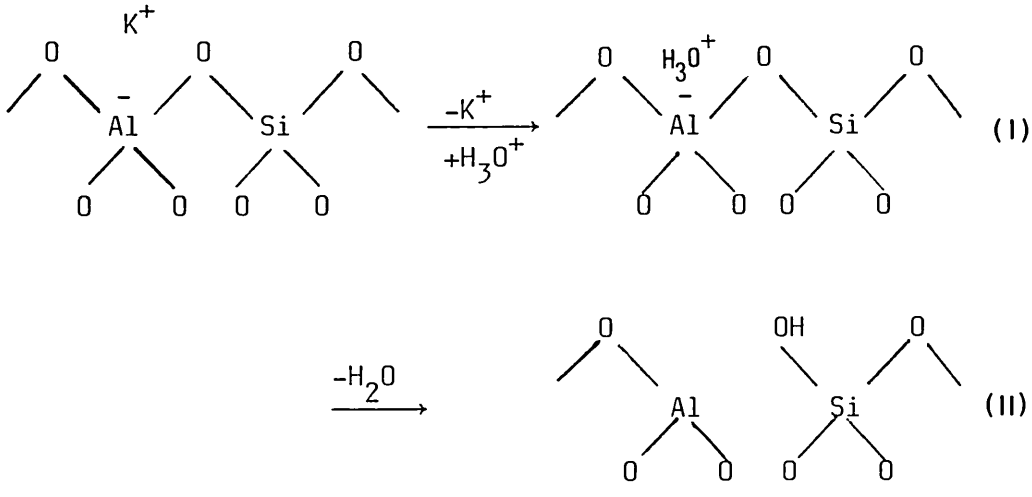

Hydrogen atom bombardment is also likely to cause further hydroxylation.

Although removal of potassium from both the surface and the bulk has been observed by many workers, the mechanism of removal is still not clear. One possibility is that hydrated potassium ions are removed from the surface as KOH, leaving protons, which then form hydroxonium ions:-

$$K^+(H_2O) \rightarrow KOH + H^+ \xrightarrow{H_2O} H_3O^+ + KOH$$

The energy and other thermodynamic parameters for such transformations on the mica surface are uncertain. Ward (1968) has proposed such a scheme for existence of acidic sites on alkaline earth zeolites while Angell and Schaffer (1965) showed that acidic hydroxyl groups could be generated even in alkali metal zeolites by partial hydrolysis of the alkali metal ions in a similar way.

Uytterhoeven, Christner and Hall (1965) have shown that the trivalent aluminium in structure (II) above may act as a Lewis acid depending on its accessibility to a base. In mica, the oxygens form a hexagon of area about $24\mathring{A}^2$ and the aluminium atom thus should be accessible to small molecules like ammonia through the hexagonal hole. Ammonia can therefore adsorb in the following way:

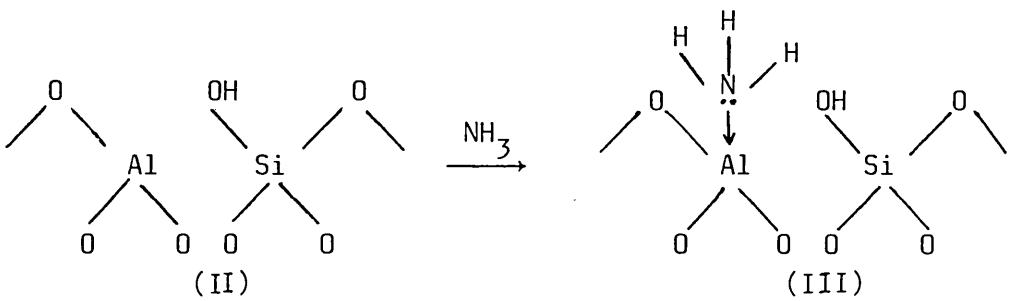

(II) (III)

On desorption (III) will revert back to (II).

On the other hand, structure (I) can behave as a Brönsted acid and ammonia adsorption is possible through formation of an ammonium ion:-

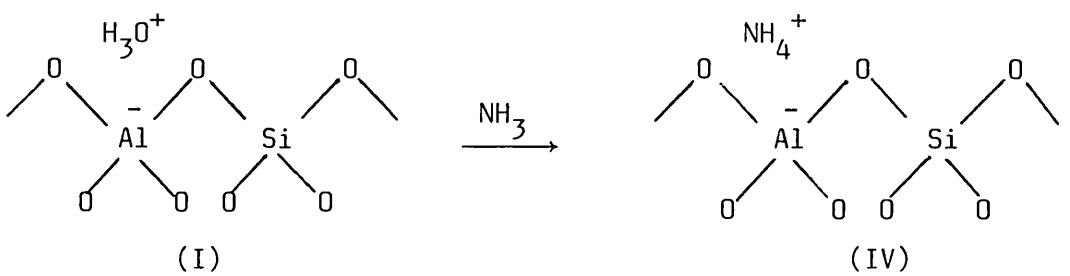

(I) (IV)

Desorption of ammonia follows through the release of a proton which may either be hydrated to form a hydroxonium ion or attack a bridged oxygen forming structure (II).

It needs to be pointed out that both (III) and (IV) represent only a single state of adsorbed ammonia on mica since one form can be transformed into the other by a relatively small movement of a hydrogen atom. Which form of adsorption exists depends on the relative stability of structures (III) and (IV).

A second kind of acid site is possible through dehydroxylation of structure (II), as in the case of the zeolites:

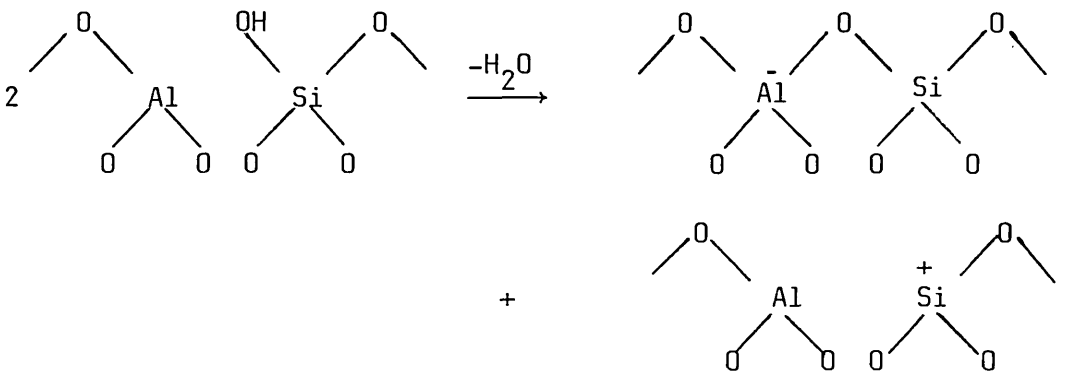

(V)

Dehydroxylation requires a temperature of nearly 800K for the zeolites and the resulting positively charged silicon has been proposed as a strong Lewis acid site. Although mica was generally not heated above 600K, some dehydroxylation cannot be ruled out. The hydrogen-atom bombardment was also likely to remove some of the bridged oxygen atoms leaving behind trivalent aluminium and trivalent silicon. Evolution of a large amount of water vapour during the hydrogen-atom bombardment may be an indication of dehydroxylation.

Ammonia is expected to adsorb strongly on (V) as shown below:

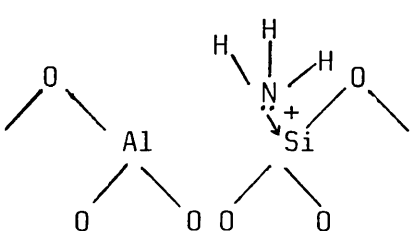

(VI)

Ammonia adsorbed in the form of either (III) or (IV) is likely to be loosely held. In (III), for example, electrically neutral trivalent aluminium atom constitutes only a weak Lewis acid site. On the other hand, the positively charged trivalent silicon in (VI) will have strong electron-accepting properties and ammonia is likely to be held very strongly. On this basis the low temperature state of

ammonia on mica can be attributed to adsorption on sites of type (I) or (II) and the high temperature state of adsorption on sites of type (V). This is supported by the much larger ammonia uptake into the low temperature state as compared to that into the high temperature state. Obviously the mica surface can be expected to have very few dehydroxylated sites (type V) while the number of sites of type (I) or (II) may be quite high. It should be pointed out that the number of type (I) or (II) sites will be equal to the number of potassium ions replaced from the surface by hydroxonium ions.

Significantly it was observed that a freshly vacuum-cleaved surface before any treatment adsorbed ammonia only in the low temperature state. This is consistent with the above conclusions because while the vacuum-cleaved surface is likely to have some type (I) or (II) sites, no dehydroxylated site of type (V) can be expected.

Another form of weak adsorption of ammonia on mica should be considered. Ammonia, being a small molecule, can readily diffuse into the interior of mica and interact via dipole-dipole interactions or hydrogen bonding. Very little is known about this mode of interaction and it is therefore difficult to assess its importance.

Very few kinetic data for TPD of ammonia on materials comparable to mica are available. Topsøe et al (1981) obtained three chemisorbed states of ammonia on ZSM-5 zeolites at 333-373, 423-473 and 693-773K, labelled respectively α, β and γ states. All three followed first order desorption kinetics with activation energies of 84.8, 97.0 and 163.0 $kJmol^{-1}$ respectively. No definite assignment was made for the α and β states although various possibilities were considered including the interaction of ammonia with surface oxygen or hydroxyl groups by hydrogen-bonding. The γ-state was assigned to strong,

structural Brönsted and/or Lewis acid sites. Hidalgo et al. (1984) have reported two states of chemisorbed ammonia on mordenite, ZSM-5, Y-faujasite and various other cation-exchanged and dealuminated zeolites by adsorbing ammonia at 373K. The TPD peak maxima were around 420 and 680K respectively with activation energies of 67 and 145 $kJmol^{-1}$. Both the states obeyed first order desorption kinetics. The assignment of the peaks to specific acid or other sites was again uncertain although in the case of the 680K peak, adsorption at strongly acidic hydroxyl groups was proposed with some confidence.

It is thus evident that the TPD technique on its own cannot be used to relate the strong and weak acid sites to discrete positions in the lattice. The technique is however useful for estimating the acid strength of a solid from ammonia desorption data and in particular for characterizing the different acid sites in terms of their relative acid strengths. From the value of the activation energy of desorption for the high temperature state of ammonia on mica (122 $kJmol^{-1}$), the corresponding sites appear to be quite strongly acidic. The desorption maxima at 450-465K for this state on mica show some similarity to the β-state of Topsøe et al. for ammonia on ZSM-5 zeolites and to the low temperature state (at 420K) of Hidalgo et al. for NH_3 on different types of zeolites. It was not possible to verify the existence of any other high temperature state of ammonia on mica because of heating limitations.

Finally it is necessary to point out that carbon residue on a solid surface is known to behave as an acidic site. Cant and Hall (1972), and many others have pointed out that the carbonaceous residue formed on oxide surfaces catalyzes hydrocarbon transformations, which are known to be acid-catalyzed. Poutsma (1976) has commented that

the role of such a residue cannot be totally ignored in the commercial cracking catalysts which often function with a finite coke level. Poutsma has proposed that the carbon residue may consist of large adsorbed aromatic carbonium ions which by some not-too-well defined mechanism act as proton-donors. For ammonia adsorption on mica, such a situation is unlikely to arise. Ammonia activity is almost equal on both the air-cleaved and vacuum-cleaved mica surfaces both of which had undergone extended hydrogen-atom bombardment. Also the major part of carbon contamination in mica is expected to be of a carbonate-bicarbonate type, which is not known for the above type of behaviour.

3.3.6 ADSORPTION OF OTHER GASES ON MICA SURFACES

In the glass adsorption/desorption apparatus, adsorption of hydrogen, oxygen, carbon monoxide, water vapour, methanol, pyridine and 1-butene were also investigated mainly on the air-cleaved and hydrogen-atom bombarded mica surfaces. No chemisorption of hydrogen and oxygen was detected in agreement with the works of Poppa and Elliot (1971) and Dowsett et al.(1977). In the early investigations of the adsorption of carbon monoxide on mica, a broad TPD peak was obtained in the mass 28 spectrum with the peak maximum corresponding to a mica temperature of 400K. At high exposures this peak developed a shoulder at temperatures above 420K. However, in the blank tests, with the mica removed from the cell, a desorption peak for mass 28 was obtained in almost the same position, although the peak appeared sharper and was without a shoulder. It seems likely, therefore, that the mass 28 peak was caused by desorption from the filament or from the walls of the cell. With

the existing heating arrangement, it was found difficult to analyse any possible desorption of carbon monoxide from mica surfaces and no conclusion could be drawn. However, since in these experiments the tungsten filament was in contact with the mica, it was likely that some parts of the mica reached a much higher temperature than that indicated by the thermocouple. Appreciable dehydroxylation of the mica surface was thus likely and adsorption of carbon monoxide on this dehydroxylated surface could not be ruled out. No possible mechanism could, however, be put forward without further work.

The TPD after exposure to water vapour was also uninformative. A rise in the partial pressure of mass 18 was observed almost from the beginning of the heating cycle and the rise continued to the end of the heating cycle (~600K). This can be attributed to water vapour, present in the space between the layers of the mica, continually diffusing to the surface and desorbing. If there was a chemisorbed state, it was completely masked by the continuous evolution of water. No chemisorbed state of water on the mica within the temperature range 298-600K was therefore detected.

The TPD with respect to methanol was done by monitoring the partial pressures of both masses 31 and 32. Again no chemisorbed state was detected up to a temperature of 600K. Use of methanol as a weak acid to probe for strongly basic sites has recently been receiving a lot of attention. The fact that it does not chemisorb on mica perhaps indicates the absence of strongly basic sites on the mica surface.

No adsorption of pyridine or 1-butene was observed on mica surfaces at room temperature. These molecules are quite large and therefore their adsorption is likely to be governed by steric factors. Since the potassium ions on the mica surface can hardly act as the

adsorption sites, the adsorbate molecules will have to enter into the tetrahedral layer through vacant potassium positions. While this is possible for a small molecule like ammonia, the same may not be true of pyridine and 1-butene. However, if the chemisorbed state were strongly bonded with a desorption temperature above 600K, it would not have been possible to detect it in the present investigation.

CHAPTER FOUR

STUDY OF A MODEL REACTION CATALYSED BY MICA

The catalytic activity of mica was tested by observing the rate of isomerization of cyclopropane to propene in a micro-reactor system. The study was mainly qualitative in nature and therefore no attempt was made to determine the surface area and other physical characteristics of the mica sample used as a catalyst for the reaction.

The catalyst sample was prepared from very fine mica flakes made with a sharp razor blade from a piece of Grade 5 muscovite mica. Under an optical microscope, the mica flakes appeared to be small platelets about 10-20μ wide in either direction. An XPS characterization of the sample, both before and after the reaction was studied, showed that the surface composition of the mica flakes was identical to that of an air-exposed mica surface. Even after the use of the mica flakes as a catalyst in the micro-reactor for a large number of runs at temperatures up to 700K, the photoelectron spectrum revealed no essential difference in the surface composition of mica excepting some depletion of potassium. The mica flakes also did not lose their crystallinity.

4.1 THE MICRO-REACTOR SYSTEM

4.4.1 THE REACTOR

The reactor itself and the system as a whole are shown schematically in Fig. 38. The reactor consisted of a pyrex tube

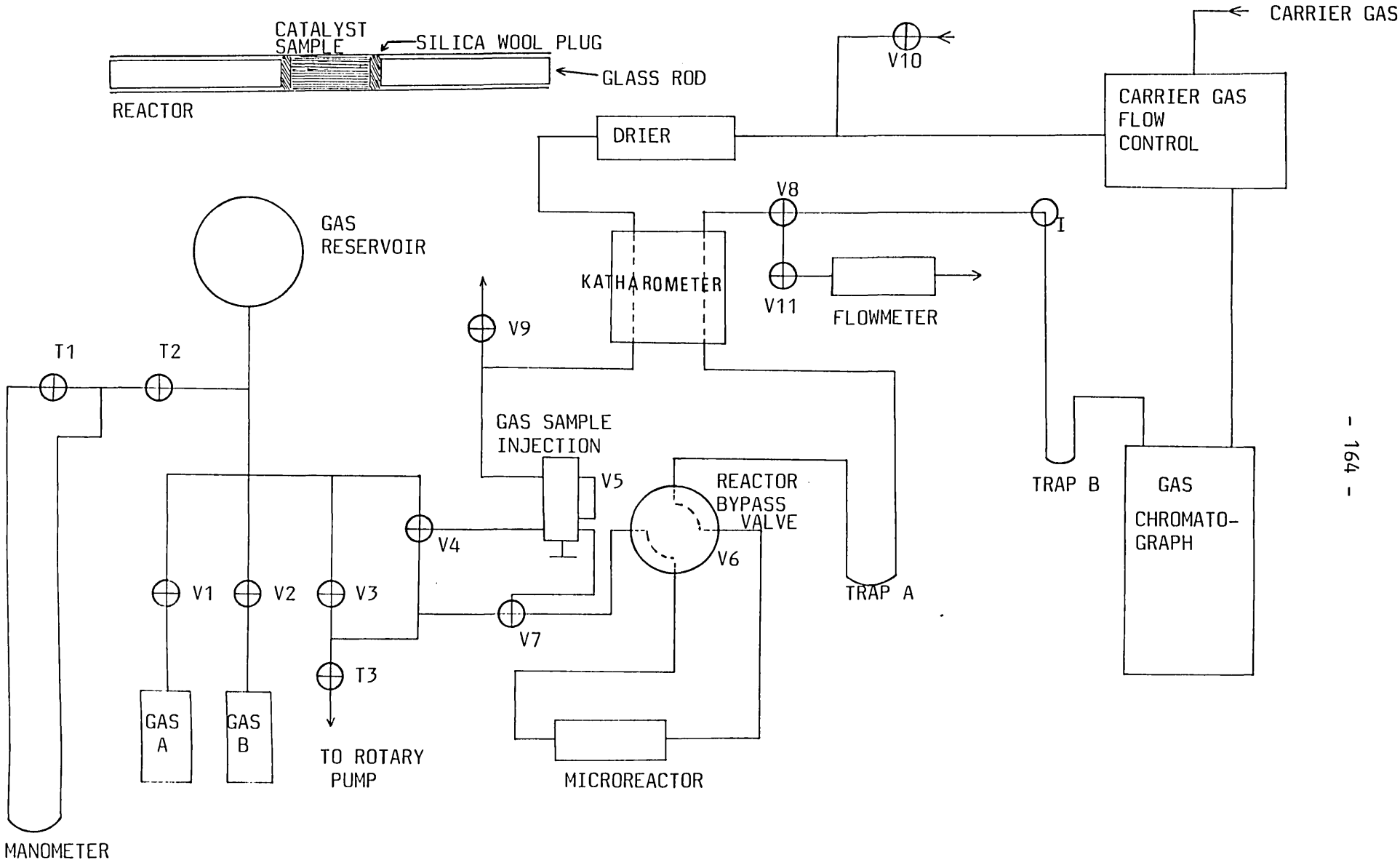

FIG. 38: The microreactor system.

of length 20cm and internal diameter 3.5mm. A small amount of the catalyst was placed in the middle of this tube and was held between inert silica wool plugs. The sample was packed so as not to restrict the flow of the carrier gas through it. The void spaces of the reactor tube at both ends were filled with glass rods to reduce the system dead space. This precaution was necessary to prevent broadening of the chromatographic peaks. The reactor tube was mounted between moveable Gyrolock fittings with teflon ferrules.

The reactor was surrounded by a small ceramic electric furnace which was operated by means of a variable transformer power supply. A chromel-alumel thermocouple was placed at the middle of the outside wall of the reactor and it read the reactor temperature to within ±1° accuracy. The variable power supply controlled the temperature of the reactor satisfactorily to with ±2°. As a continuous variation of temperature was not required during the present investigation, this arrangement of heating and temperature measurement was adequate.

4.1.2 THE DETECTION SYSTEM

The detection system consisted of a Perkin-Elmer F11 gas chromatograph with a hot wire type detector. The chromatographic column was 2 metres long and 6mm in diameter, and was packed with 13.5% bis-2-methoxy ethyl adipate with 6.5% di-2-ethyl hexyl sebacate on chromosorb P, mesh 80-100. During a measurement, the column was kept at 100°C. The detector response could be calibrated against known amounts of the reactant gases without the reactor in the system.

Products of a reaction could be analysed by trapping them in

one of the two traps, A and B, which were cooled in liquid nitrogen. A condensible reaction product could be trapped in this way and introduced later to the gas chromatograph as a concentrated pulse by warming the trap rapidly. Products of a reaction were identified by passing known chemicals directly into the chromatograph by syringe injection through a septum inserted at I in the figure.

The katharometer hot-wire detector, located between the reactor and the gas chromatograph, was not used during the present work.

4.1.3 EVACUATION, GAS-HANDLING AND FLOW-CONTROL

The reactor and all the other parts of the system could be evacuated to rough vacuum ($\sim 10^{-3}$ torr) by means of an Edwards ES100 rotary pump connected at T3. The gas-handling line was made from pyrex glass, while the rest of the system was constructed from 3mm internal diameter copper tubing with Gyrolock fittings.

The reactant gas was introduced through either V1 or V2 to the gas reservoir and the gas pressure was read from the mercury manometer. A mixture of two gases could be prepared by introducing the gases consecutively to the reservoir through V1 and V2. The injection valve, V5, could be used to introduce a volume of 1.1 ± 0.1 cm^3 of the reactant gas to the carrier gas-flow. The bypass valve V6 allowed the reactor to be bypassed so that the reactant gas went directly to the detection system.

The flow rate of the carrier gas to the reactor and to the gas chromatograph could be adjusted with a Perkin-Elmer flow control unit which had been calibrated with a soap bubble flow meter.

The flow rate, however, needed to be corrected for the pressure drop between the reactor and the flowmeter. The carrier gas was dried by passing it through a column of previously outgassed zeolite-13X molecular sieve. A second gas could be added to the carrier gas flow at V10. This was used to introduce oxygen or hydrogen to the carrier gas for respectively oxidizing or reducing the catalyst.

Research Grade cyclopropane of 99% purity supplied by the British Oxygen Company was used as the reactant gas without further purification. The carrier gas was high purity helium (BOC, 99.99% purity). Research Grade propene (BOC, 99% purity) was also used for the purpose of identification of peaks in the chromatograms.

4.2 EXPERIMENTAL PROCEDURES

About 0.2g of the mica flakes was packed into the reactor tube to be used as the catalyst. The system was then pumped down to rough vacuum and the mica sample was outgassed at 700K for approximately 30 minutes with the carrier gas flowing through the reactor at a constant flow rate of $1cm^3$ per second. After this, the catalyst sample was allowed to cool to the desired reaction temperature. The gas reservoir was then filled up to about 30cm pressure of cyclopropane and a sample of the reactant was injected into the carrier gas flow. The condensible products of reaction emerging from the reactor were trapped in the liquid nitrogen cooled cold trap B whilst the incondensible part of the products was monitored in the gas chromatograph. After all the condensible gases were trapped, the trap was rapidly warmed with a hot air-blower and the chromatogram of the released gases was taken.

During this process, the reactor was bypassed and the carrier gas flowed directly through the trap to the gas-chromatograph.

To verify that the isomerization was taking place on the surface of the mica, and not on any other parts of the system, a few blank experiments were carried out with the reactor packed with silica wool and glass rods alone. Chromatographic peaks were identified by obtaining chromatograms for known gases under identical conditions.

4.3 RESULTS AND DISCUSSION

The condensible products formed during the outgassing of the mica at 700K were collected in a cold trap and the chromatogram obtained after the cold trap was warmed is shown in Fig. 39(a). Zero time on the time scale corresponds to the moment when warming of the cold trap commenced. The two peaks, which can be seen in the chromatogram, were later found to be due to water and carbon dioxide respectively. This was established by taking chromatograms for water and carbon dioxide separately condensed in the cold trap and warmed in a similar way. A considerable length of time was needed to raise the temperature of the catalyst sample to 700K and any incondensible gas given off was likely to be produced slowly over a long period. Thus chromatographic identification of the incondensible part of the outgassing products of mica was not possible.

After the first heating, the mica was allowed to cool to room temperature before being heated to 700K a second time, the cold trap again being used to trap condensible gases released by the mica. The chromatogram of the trapped gas, shown in Fig. 39(b), indicates

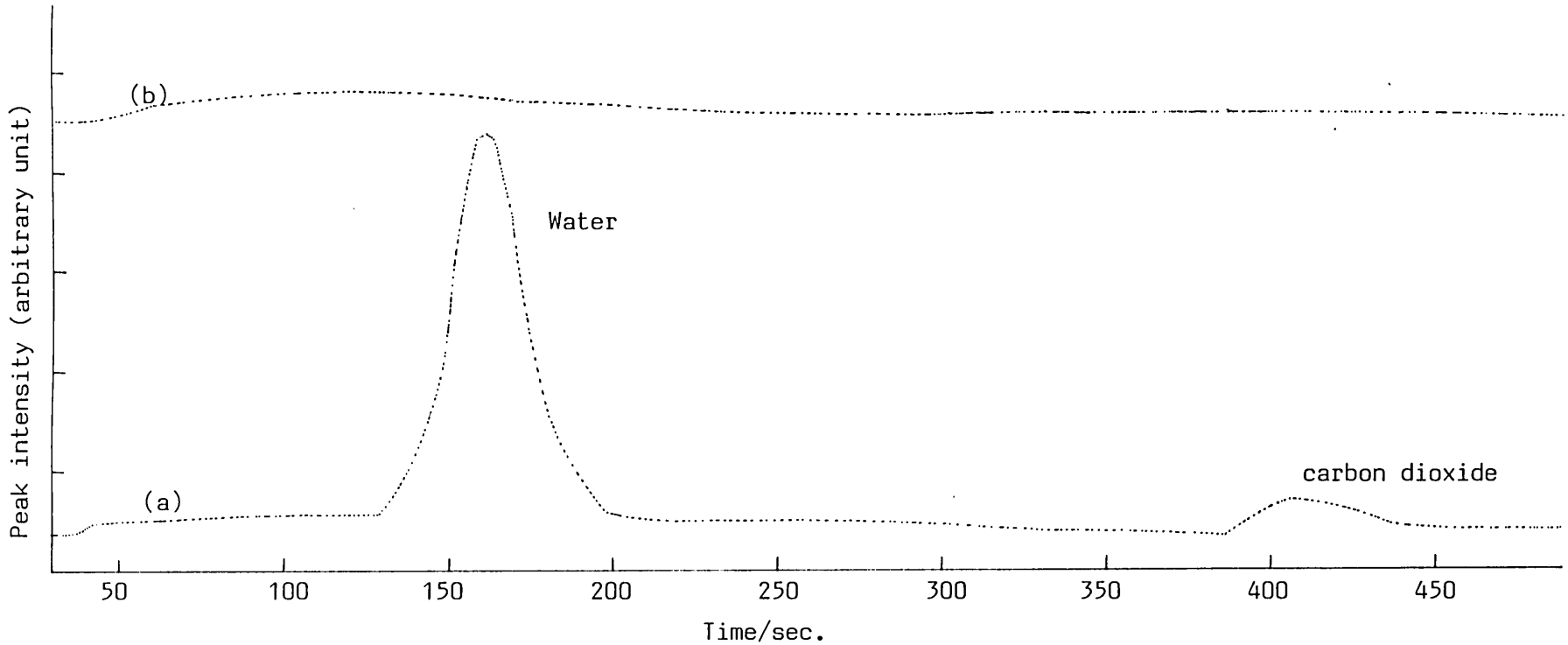

FIG. 39: Chromatograms of condensible outgassing products of mica flakes, (a) heating for the first time and (b) heating immediately after (a). Time scale starts from the moment of warming of the cold trap in which outgassing products were condensed.

that some water vapour was still coming off but no other gas was detected.

Before commencing a study of the isomerization of cyclopropane over mica it was necessary to determine the retention times for known gases in the chromatographic column after a cold trap containing the gases was warmed up. In each case, the gas was injected into the carrier gas in the usual way and flowed through the reactor at room temperature before being trapped in product trap B. After allowing sufficient time for collection, the reactor was bypassed and the cold trap was warmed to get a chromatogram. Results for cyclopropane, propene and a mixture of the two gases are shown in Fig. 40. All the chromatograms showed a broad peak during collection of condensible gases in the cold trap. This was thought to be due to the presence either of non-condensible impurities in the carrier gas or of a small leak in the system. When air was deliberately let into the carrier gas flow, a peak was obtained almost in the same position.

Isomerization of cyclopropane was observed when a dose of the gas was introduced into the carrier gas flow passing over a heated mica sample. The best conversion was obtained with the mica at a temperature of 670K, although propene could be detected at temperatures as low as 470K. The chromatograms obtained by warming the cold trap after a single dose of cyclopropane had passed over the mica catalyst at temperatures of 620 and 670K respectively are shown in Fig. 41. The figure also shows the non-condensible part of the gas which passed through the cold trap whilst the reaction was taking place. In the chromatograms, a small but distinct propene peak can be seen with two additional peaks, one in the condensible part and the other in the non-condensible part. The non-condensible product of the reaction

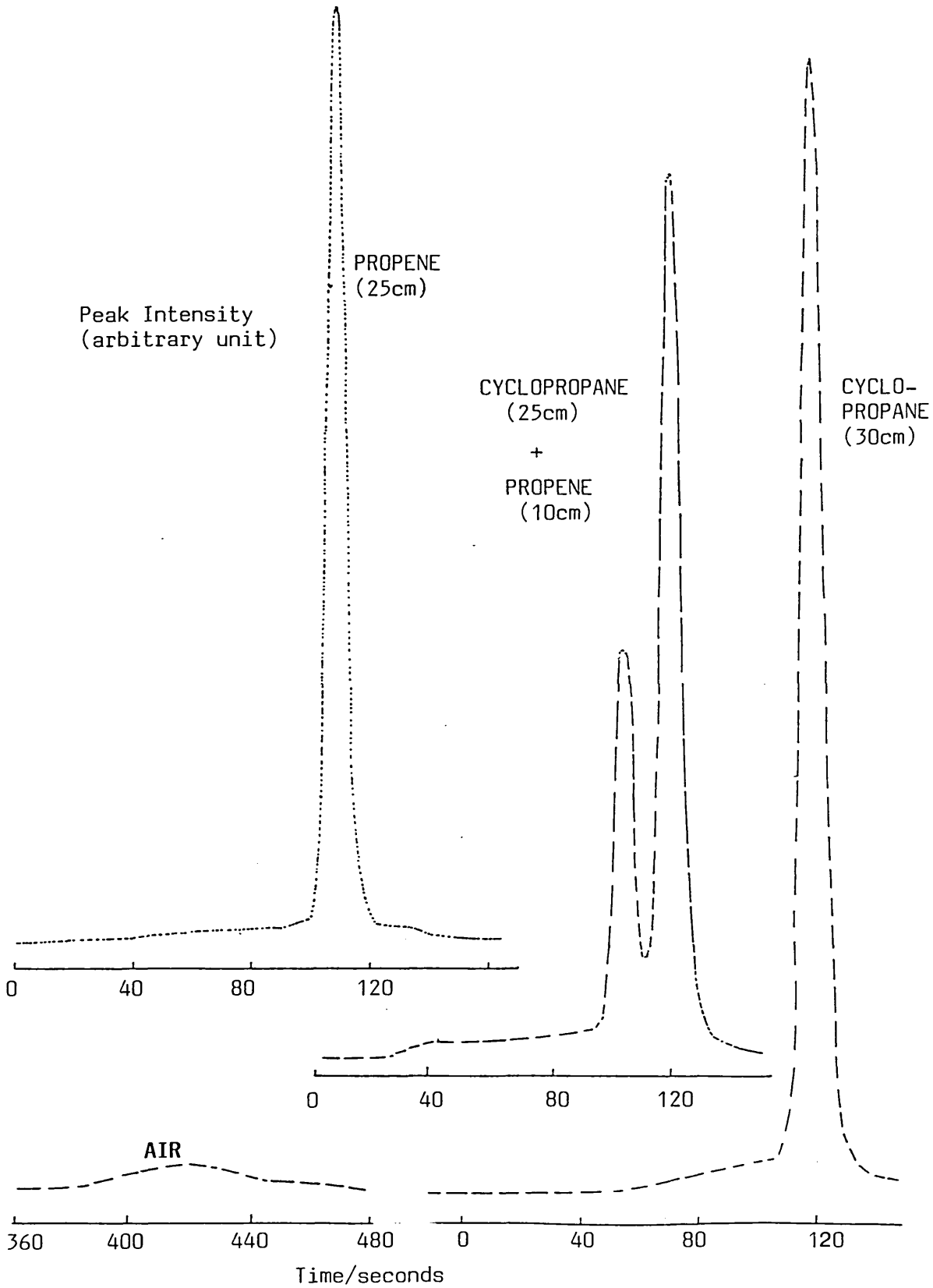

FIG. 40: Chromatograms for cyclopropane, propene and a mixture of the two. The air peak appeared before warming of the cold trap. Time scale for the air peak starts from the moment of gas-sample injection while for all other peaks it starts from the moment of warming of the cold trap.

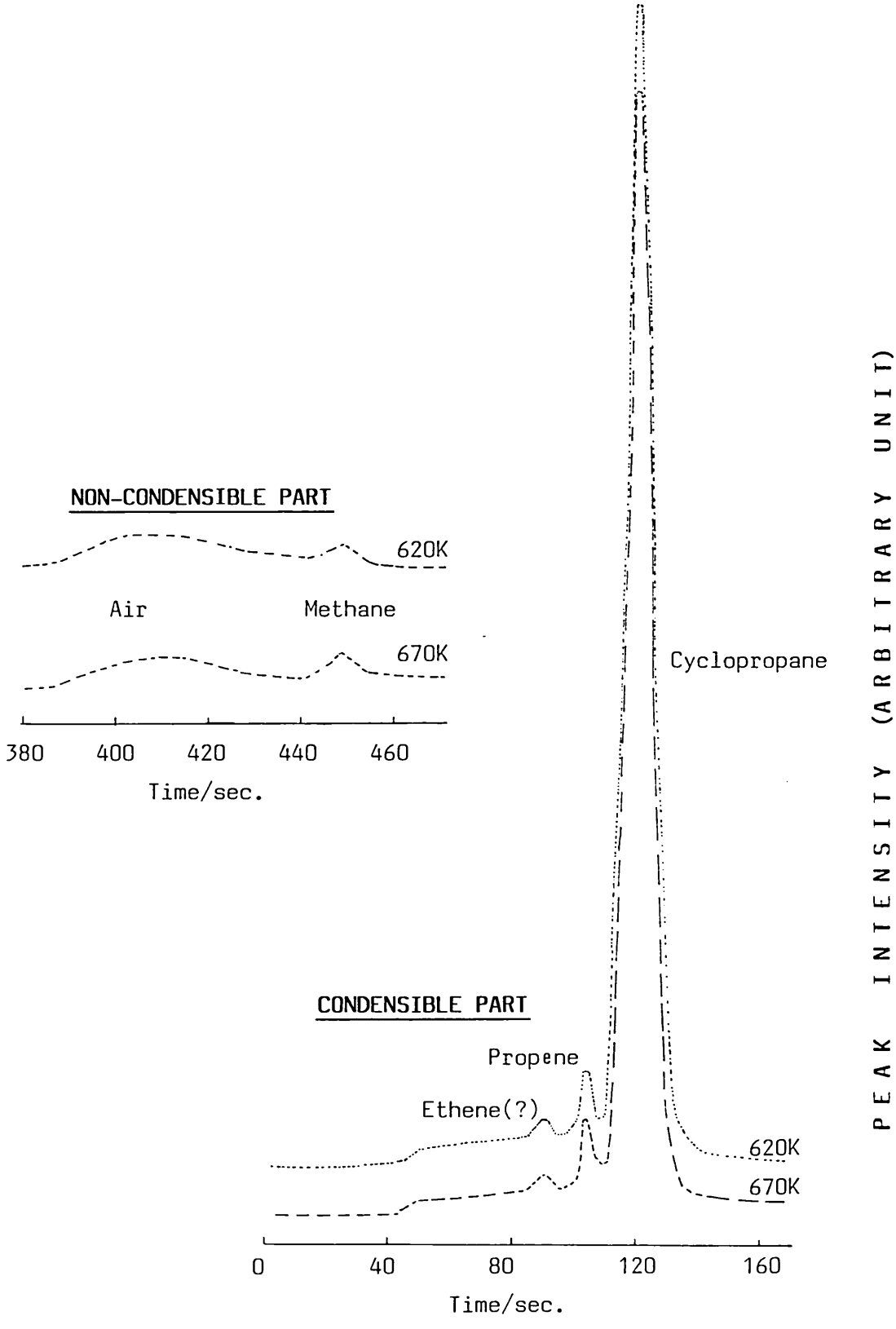

FIG. 41: Chromatograms for isomerization of cyclopropane on mica surface at 620 and 670K. Time scale for the non-condensible part of the reaction products starts from the moment of injection of reactant sample while for the condensible part, it starts from the moment of warming of the cold trap.

was definitely identified as methane from a chromatogram obtained by injecting methane into the carrier gas flow in a separate experiment. It was not possible to identify definitely the peak appearing just before propene although it was likely to be ethene. It would thus appear that the mica sample was active in the isomerization reaction despite the fact that the rate of conversion was low and the reaction was accompanied by decomposition to lower hydrocarbons.

Previously, Prada-Silva et al. (1979) have found that small amounts of oxygen promote conversion of propene to methane and ethene in approximately equal quantities. On the other hand, Krivanek and co-workers (1971), working with bismuth-molybdenum oxide catalysts, found that the presence of oxygen converted propene to acrolein, which became the major desorbed product under these conditions.

It is thus likely that in the present work, traces of air were responsible for the production of methane and possibly ethene. If there was thermal decomposition of propene, the products would have been methane and acetylene. Because of the uncertainty associated with the identification of the 'ethene' peak, it is not possible to rule out any thermal decomposition of propene.

Bassett and Habgood (1960), as well as Hightower and Hall (1968) and many others, have shown that the sensitivity of chromatographic detectors to propene and cyclopropane are almost equal. The relative amounts of propene and cyclopropane in a chromatogram with constant flow rate of the carrier gas can therefore be determined from the products of peak heights and widths at half height. On this basis, the fractional conversion over mica at a temperature of 670K was found to be 3.7×10^{-2}, which is reasonable.

No conversion of cyclopropane to propene was noticed in blank

experiments in which the reactor was packed with glass rods and silica wool rather than mica flakes. Even at temperatures as high as 670K, propene was undetectable in the gas emerging from the reactor. This temperature is not far below the temperature of 770K at which Chambers and Kistiakowsky (1934) observed the onset of the homogeneous, non-catalytic isomerization of cyclopropane. It seems clear that the mica surface was responsible for the conversion observed.

The decomposition of part of the cyclopropane and the corresponding uncertainty in the nature of the products formed made it difficult to quantitatively evaluate the kinetic parameters of the isomerization reaction. The work was also limited by the simple design of the microreactor system, which did not allow sufficient control over the experimental parameters. It was however sufficient to show that the isomerization of cyclopropane could be catalysed over mica surfaces and that fine mica flakes could be used as a model catalyst for similar reactions.

The ring opening of cyclopropane has been a favourite test reaction for studying the catalytic activity of silica-aluminas following the works of Hall et al. (1965, 1968). It has equally been used to characterize zeolite surfaces by Bassett and Habgood (1960), George and Habgood (1970), Tam et al. (1976), Kiricsi et al. (1980). Förster and Seebode (1983), Schobert and Ma (1981), and many others. The order of the reaction was found to be between 1 and 2, and in most of these studies Brönsted acidsites have been proposed as the active sites. While the mechanism of the reaction has not been established conclusively, it is thought that the isomerization proceeds through a 'face on' or 'edge on' protonated cyclopropane molecule, the so-called non-classical carbonium ion. Some authors

however propose a significant role for the exchangeable cations of the zeolite structure. For example, Förster and Seebode (1983) postulate polarization of the π-electron system of the cyclopropane molecule by the electrical field of the cations. This is thought to promote transfer of a hydrogen atom from one carbon atom to another and to cause rearrangement of the bonding electrons. It is thus not possible to propose a clear-cut mechanism for the cyclopropane isomerization over mica.

From a molecular beam study of the isomerization of cyclopropane on a mica surface, Prada-Silva et al. (1979) concluded that the adsorption of cyclopropane was activated. No evidence for activated adsorption was found in the present study. On the contrary a small amount of cyclopropane was found to adsorb on the mica surface even at room temperature. This was demonstrated by injecting a dose of cyclopropane into the carrier gas and passing it over the mica at room temperature. Subsequently the mica was warmed to 425K and any gas desorbed by the mica was collected in a cold trap. On warming the trap the chromatograph showed a small peak due to cyclopropane.

A conceivable mechanism for the isomerization can be proposed involving an 'edge on' carbonium ion formation on the small number of Brönsted acid sites on a mica surface, discussed in the preceding chapter, as follows:

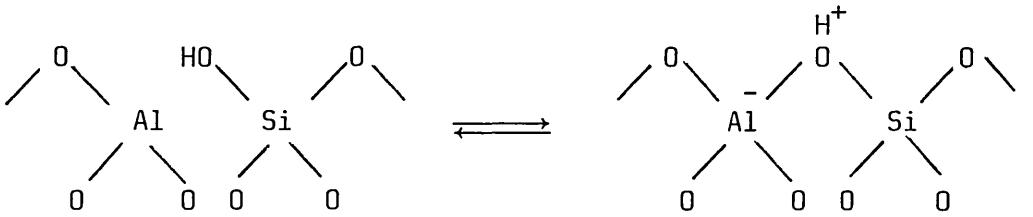

Hydroxylated tetrahedral layer of mica

Brönsted acid

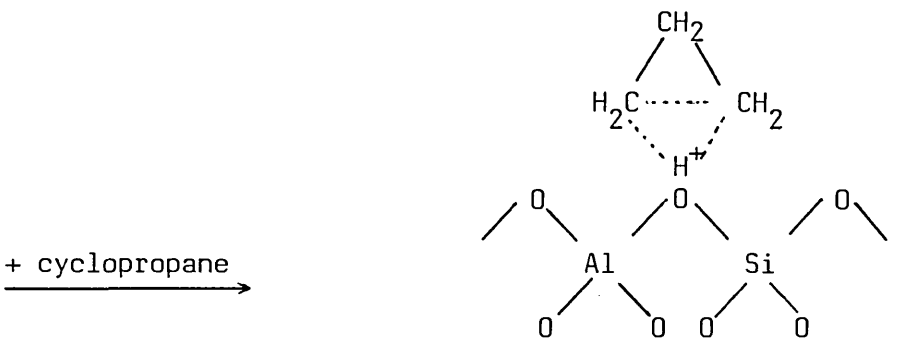

Protonated complex with cyclopropane

This would be followed by breaking of a C-C bond and rearrangement of the bonding electrons to form propene which perhaps remain adsorbed on the surface before being desorbed.

It must be pointed out,however, that much more data will be needed to verify the mechanism and the associated propositions.

CHAPTER FIVE

SURFACE CHARACTERIZATION AND ADSORPTION EXPERIMENTS IN THE ESCALAB SYSTEM

5.1 THE ESCALAB-MK II SYSTEM

5.1.1 GENERAL DESCRIPTION

The ESCALAB-MK II is a stainless steel, multi-purpose surface analysis system made by the Vacuum Generators Ltd. It has facilities for X-ray Photoelectron Spectroscopy (XPS), Ultraviolet Photoelectron Spectroscopy (UPS), Auger Electron Spectroscopy (AES), Secondary Ion Mass Spectroscopy (SIMS), Ion Scattering Spectroscopy (ISS) and Low Energy Electron Diffraction (LEED).

The main body of the instrument can be divided into three sections:-

(a) the Analysis Chamber,

(b) the Preparation Chamber, and

(c) the Fast Entry Airlock.

The general outline of the instrument is shown in Fig. 42. A photograph of the instrument is presented in Fig. 43. All the surface techniques are contained in the Analysis Chamber excepting the LEED facility which is on an extension of the Preparation Chamber. The Preparation Chamber also contains an argon ion gun for sample cleaning through bombardment, metal evaporators for depositing thin films on samples, and a linear motion drive (henceforth referred to as the

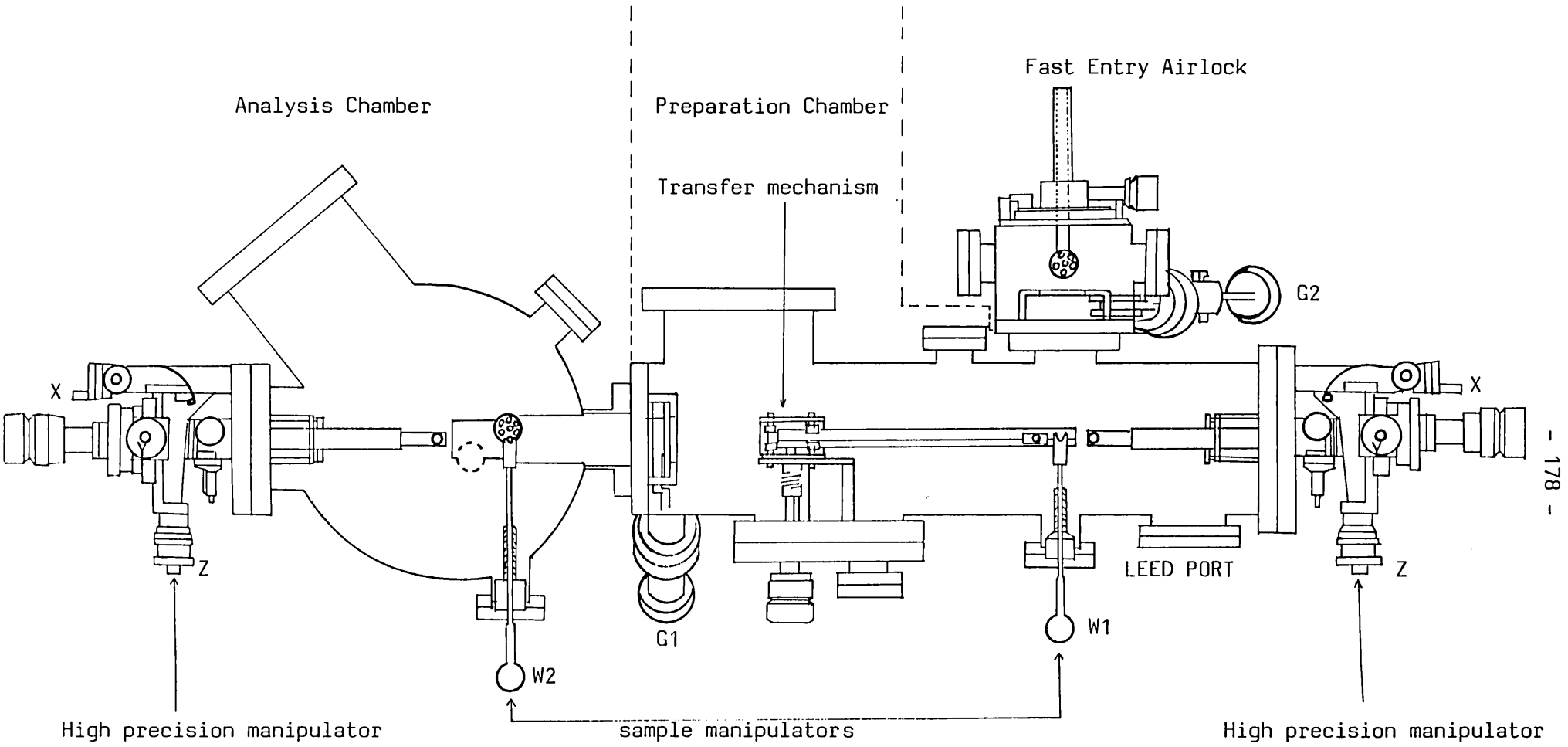

FIG. 42: Plan view of the ESCALAB.

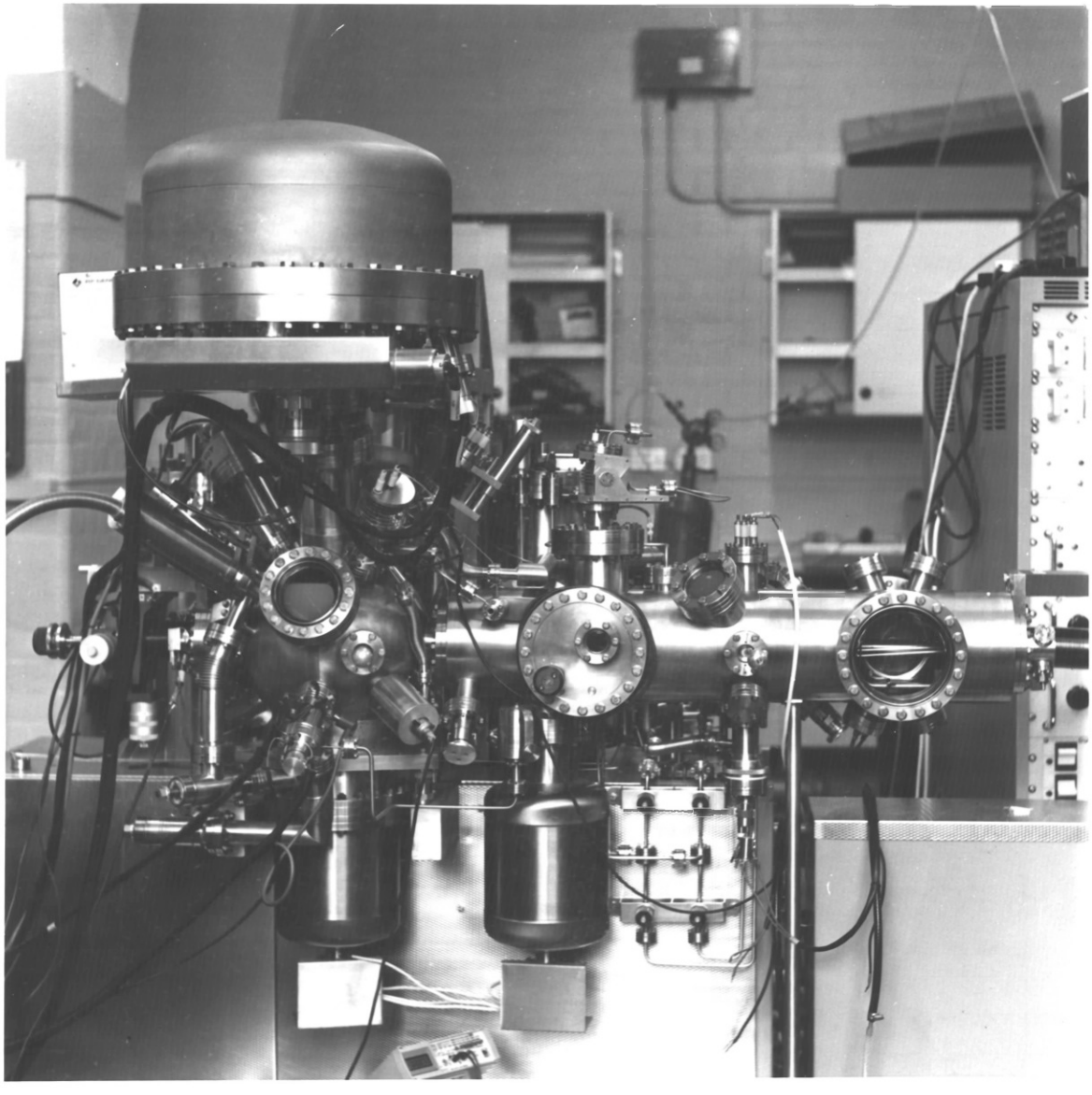

Fig. 43 Front view of the ESCALAB-MK II system. The Analysis Chamber with the hemispherical analyser and other attachments can be seen on the left side of the photograph. The high precision manipulator connected to the end of the Preparation Chamber (on the right side of the photograph) is not seen here.

P8 probe) with facilities for heating and cooling samples.

5.1.2 SAMPLE INTRODUCTION AND TRANSFER MECHANISM

Two UHV compatible gate valves, G1 and G2, isolate the Preparation Chamber respectively from the Analysis Chamber and the Fast Entry Airlock. Samples are mounted on special metal holders, referred to as stubs, which can be transferred from one operating position to another by means of various transfer devices. The stub-mounted samples are placed initially on a carousel in the Fast Entry Airlock which is then pumped to rough vacuum. The gate valve G2 is then opened and the carousel moved by a rotary drive system into the Preparation Chamber where the sample can be picked up with a bellows-mounted wabble stick W1. It can then be placed either on the P8 probe for cleaning and other sample preparation processes or on the transfer train which operates along the main axis of the instrument. After opening G1 the train can be moved into the Analysis Chamber and, with the help of the wabble stick W2, the sample can be transferred to the operating position for various experiments. Alternatively, the sample can be stored in one of the two carousel holders provided for the purpose in the Analysis Chamber.

There are two high precision sample manipulators, one at each end of the main body of the instrument. Both of these have linear motion in three perpendicular directions as well as rotational motion about the x-axis. The manipulator in the Preparation Chamber has an extra long x-motion and is used for positioning the sample for LEED.

Two types of stub holders are in use for sample mounting. With the simpler type, heating of the sample can be done only on the P8 probe which has its own heater. The other type has an integral heater with a small contact pin at its base which makes it possible to pass current through the heater while the stub is on the high precision manipulators.

5.1.3 THE X-RAY SOURCE

ESCALAB has facilities for both monochromated and unmonochromated XPS, but only the unmonochromated X-ray source was used in the present investigation. This has a twin anode source with magnesium on one side and aluminium on the other. Thus, two independent X-ray lines at 1253.6 ($MgK\alpha_1,\alpha_2$) and 1486.6 ($AlK\alpha_1,\alpha_2$) eV are available. The source is operated with the filament at earth potential and the anode at a positive potential of up to 15kV. A maximum emission of 100mA is possible, but normally 40mA is not exceeded for the aluminium source and 20mA for the magnesium source. The X-ray gun is mounted on a linear motion drive which allows it to be moved away from the sample during sample manipulation. When taking an XPS spectrum, the gun is wound fully inward to put the X-ray source as near as possible to the sample.

5.1.4 THE ELECTRON FLOOD GUN

An electron Flood Gun, V.G. model LEG 51, is positioned at right angles to the X-ray gun in the Analysis Chamber just above the high

precision manipulator. The Flood Gun is useful for neutralizing surface charges which may build up on insulating samples during XPS, SIMS and ISS measurements. The Gun can be operated in two modes: in mode 1, which is used in XPS measurements, low energy electrons up to an energy of 12 volts are produced; in the other mode, useful for SIMS and ISS measurements, an electron beam of about 500V energy is generated.

5.1.5 THE ANALYSER AND THE DETECTION SYSTEM

The electron spectrometer consists of a 150° spherical sector analyser. It serves as a narrow pass filter allowing only electrons with an energy equal to HV electron volts to pass through it, where V is the potential difference between inner and outer hemispheres and H is a constant dependent upon the dimensions of the analyser. .

In XPS, the electrons collected at the exit of the analyser are equivalent typically to a current in the region of 10^{-16} to 10^{-14} amperes. This extremely small signal can be detected only by the pulse counting technique. The detection system consists of a Mullard B419AL bakeable, channel electron-multiplier. It has a typical gain of 1.7×10^{8} at 2.5kV, a resistance of 3×10^{9} ohms and a maximum operating voltage of 3.5kV. The pulses from the channeltron pass through a series of pulse shaping and amplifying circuits, followed by a discriminator, before being fed into the ratemeter, which records the signal.

The inlet and exit slits of the analyser can be changed by the external operation of a rotary drive. Seven pairs of different slits are available. Normally 6mm slits were selected for both inlet and exit apertures of the analyser.

5.1.6 PUMPING

The Analysis Chamber is pumped by a titanium sublimation pump and an Edwards E04 diffusion pump containing polyphenyl ether pumping fluid. The line is backed by an E2M5 Edwards rotary pump and incorporates a CCT 100 liquid nitrogen cold trap. The Preparation Chamber has a similar pumping line but the diffusion pump is valved so that it can also be used for differentially pumping the UV source, the SIMS gun and the ISS gun. The X-ray source has its own ion-pump for keeping it under UHV even when it is isolated from the diffusion pump of the Analysis Chamber. A series of interlocks and safety trips provide the system with necessary safeguards against different kinds of mechanical failures. The system can be baked at 150-180°C without the monochromator and at 80-100°C with the monochromator.

5.1.7 GAS HANDLING AND DATA ACQUISITION

A schematic diagram of the gas-handling section is shown in Fig. 44. This section consists of two manifolds each with connections for four gas-bottles. Each manifold can be pumped and used independently. Rough pumping is done by a separate rotary pump but better vacuum can be obtained through the Preparation Chamber diffusion pump. The manifolds and the all-metal gas inlet valves are bakeable. Each manifold has a mixing volume and gas from one manifold can be transferred to the other. The upper manifold is generally used to handle gases for the SIMS and ISS guns as well as for the argon-ion gun for cleaning purposes. The UV source has its own separate gas-handling line. The lower manifold is reserved for gases used in adsorption and surface

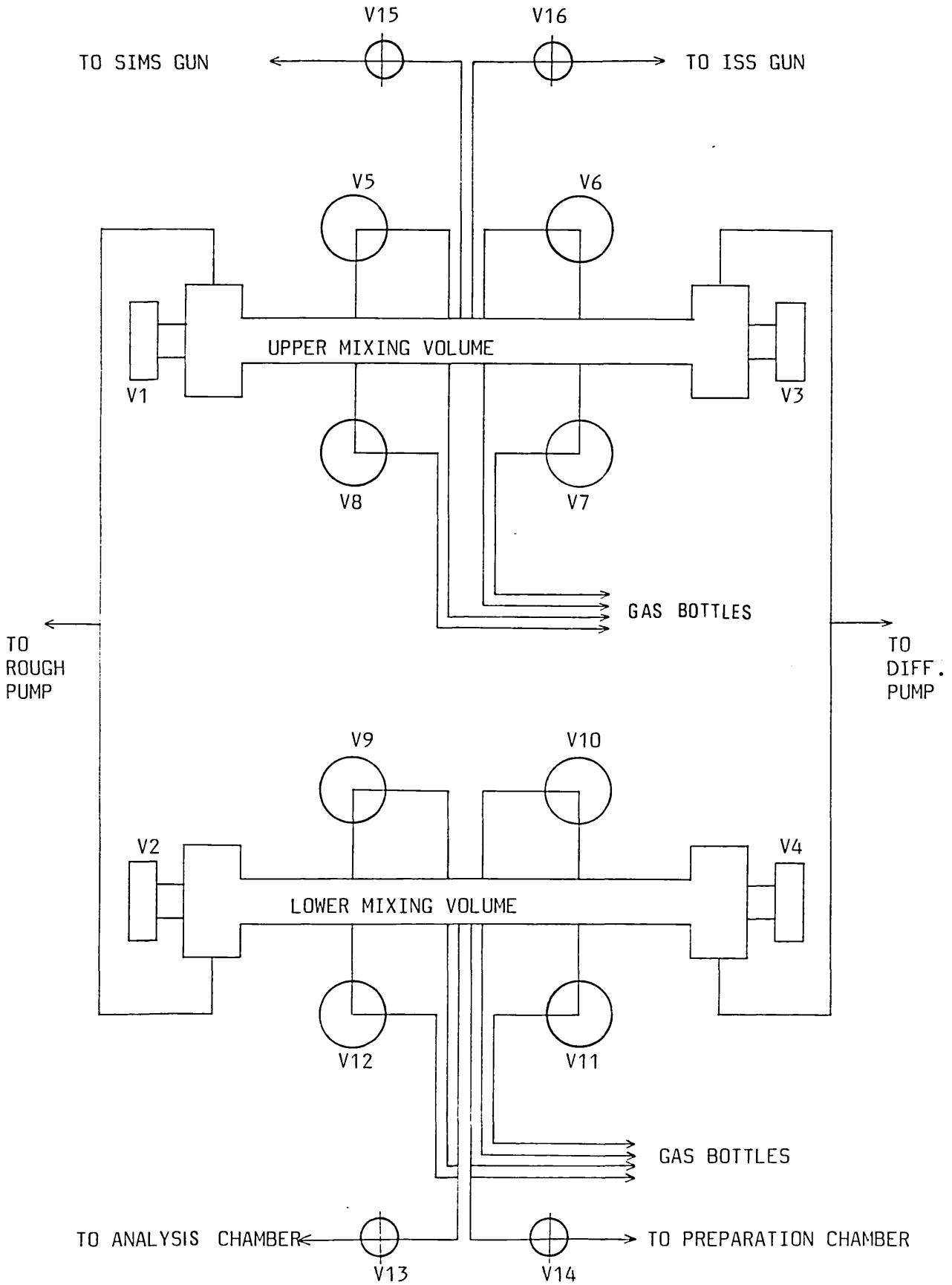

FIG. 44: Gas handling section of the ESCALAB. V1 to V16 are all stainless steel bakeable valves.

reaction studies. This manifold has connections to both the Analysis and Preparation Chambers through high precision leak valves.

Data acquisition and treatment were carried out with an APPLE 2e microcomputer equipped with a VGS 1000 data system. The electron spectrometer can also be operated manually.

5.2 EXPERIMENTAL PROCEDURE

5.2.1 GENERAL POINTS

The Analysis Chamber of the ESCALAB was routinely maintained at pressures in the 10^{-10} torr region. The pressure in the Preparation Chamber tended to be higher, in the 10^{-9} - 10^{-8} torr region, because of constant use of this chamber for cleaning samples. The mica samples were normally stored in the Analysis Chamber and were transferred to the Preparation Chamber only for annealing, exposure to gases and for LEED experiments. Because of ease of introducing samples, a fresh mica sample was used for each different set of experiments.

5.2.2 SAMPLE MOUNTING AND CLEAVING

1cm squares were cut from sheets of Grade 5 muscovite mica which had been freshly cleaved in air. The thickness of the samples varied but was always less than 0.25mm. On one side of each sample the corners were cut away to leave a raised octagonal area in the middle as illustrated in Fig. 45. This central area could be cleaved with the aid of a loop of fine silver wire attached through a hole to one edge. Care was taken in fixing this loop to the sample to avoid

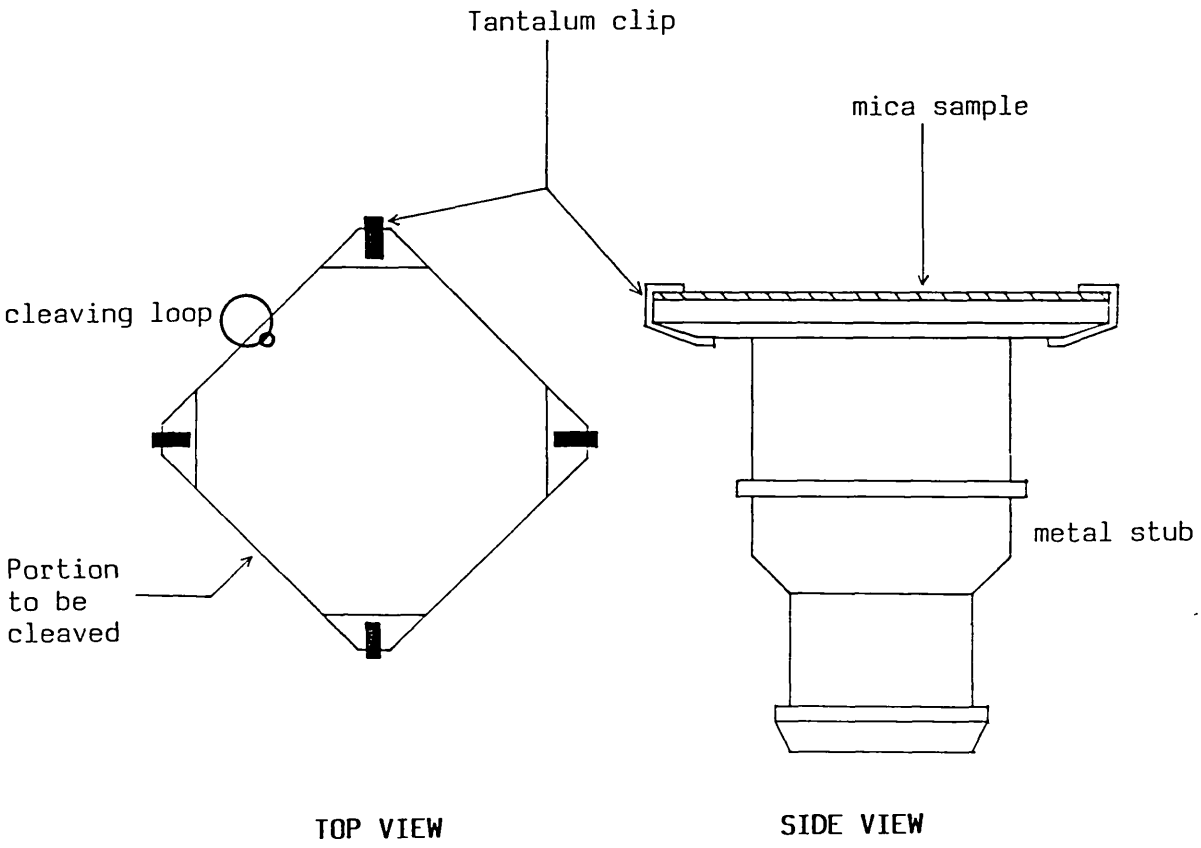

FIG. 45: Mica sample and holder for experiments in the ESCALAB.

lifting the edge beyond what was absolutely necessary.

The sample was then fixed to a nickel stub with four tantalum clips spotwelded to the top-plate of the stub. The clips were just long enough to hold the sample at the four corners.

The mica could be cleaved in either the Analysis Chamber or the Preparation Chamber. After the stub holder had been locked onto one of the high precision manipulators, a wabble stick was used to lift off the front face of the sample with the help of the wire loop. In these positions, sufficient force for cleaving could be applied without difficulty. Only one cleaving could be done at a time in this type of arrangement and if another freshly vacuum-cleaved surface was needed, a new sample had to be introduced.

The mica was heated by placing the stub holder on the P8 probe of the Preparation Chamber. The temperature was read with the help of a chromel-alumel thermocouple attached to the base plate of the heater. A temperature difference of approximately 50° was found to exist between the heater plate and the mica surface. Although correction was made for this temperature difference, the temperatures quoted for the mica surface are still only approximate values.

5.2.3 SURFACE ANALYSIS WITH THE ESCALAB

Of all the techniques available, X-ray Photoelectron Spectroscopy (XPS) was the most useful for characterizing mica surfaces. The achromatic AlKα source was mainly used but the MgKα source was also used sparingly for specific purposes. The sources were operated at an energy of 10-12kV with an emission current of 5, 10 or 20mA.

Monochromatic X-radiation was not used because the signals obtained with it for mica surfaces were too small to be meaningful.

In taking a photoelectron spectrum of the mica surface, charging of the sample created some uncertainty in the interpretation of the binding energies corresponding to various peaks. The Flood Gun was found not to be completely effective in neutralizing the charge possibly due to differential charging of the mica surface. The imperfect alignment of the beam of low energy electrons from the Flood Gun with respect to the sample surface may be another reason. Most data were collected without the use of the Flood Gun and therefore the energies needed to be corrected for the apparent shifts caused by charging. This will be discussed in the next section.

All the data were collected with the sample holder earthed. If the earth was removed the photoelectron peaks shifted to apparently higher binding energies due to further charging of the sample. Two positions of the sample were used: in the 'normal emission' position, the analyser collects all the photoelectrons ejected normal to the surface while in the 'grazing emission' position, only photoelectrons ejected at an angle of 5-15° to the surface enter the analyser.

The following procedure was normally used to obtain a photoelectron spectrum. The sample was placed in either the 'normal' or 'grazing' emission position in front of the X-ray source, and the signal corresponding to the most prominent XPS peak (O1s peak for mica) was obtained manually. The sample position was then adjusted by moving the high precision manipulator in x, y and z-directions to get the maximum possible signal. If the Flood Gun was used, the electron energy and the emission current were adjusted to optimize the signal

and also to reduce the charging shift as much as possible. The analyser was operated in the Constant Analyser Energy (CAE) mode with a 6mm slit and the channeltron voltage was set at between 2.5 and 3kV.

Once the signals were optimized through a manual scan, the microcomputer was set for collection of data. XPS data from a large number of scans were collected and accumulated until a reasonable signal-to-noise ratio was obtained. Wide scans were done with 50eV CAE for increased sensitivity whilst narrow regions were scanned at 20eV CAE or less for better resolution of multiplet peaks. The number of channels and the count numbers were automatically selected by the computer from the chosen step-size. The data could be later processed and subjected to various operations such as background subtraction, smoothing, deconvolution, curve-fitting, etc.

5.2.4 OTHER TECHNIQUES

LEED patterns of both air-cleaved and vacuum-cleaved mica surfaces were taken using the standard procedure. Because of surface charging, it was found that the electron beam energy was very critical for getting a good, stable pattern. No pattern could be seen if the energy of the electron beam was less than 70V. Well defined LEED patterns were seen between 90 and 150V beam energy.

Low energy Ion Scattering Spectroscopy (ISS), Secondary Ion Mass Spectroscopy (SIMS) and Ultraviolet Photoelectron Spectroscopy (UPS) were also used to a very limited extent to characterize mica surfaces. In all cases, standard operating procedures were followed. Without the Flood Gun, no SIMS pattern could be obtained; this showed

the very high surface charging in mica during a SIMS experiment. The Flood Gun was also used in the ISS measurements, but even so it was not possible to set the Flood Gun so that the ISS peaks appeared at their expected positions. High purity helium (BOC, 99.99%) was used in ISS and UPS while high purity argon (BOC, 99.99%) was used in SIMS.

5.2.5 EXPOSURES TO GASES

Most of the exposure experiments were done in the Preparation Chamber at pressures in the range 10^{-6} to 10^{-5} torr. After gas exposure the chamber was pumped down to the 10^{-8} torr region and the sample was transferred to the Analysis Chamber for XPS and other measurements. This procedure helped to keep the ultra-high vacuum section free of the gases, particularly the condensible ones, used in the experiments on mica.

Carbon dioxide (grade X) was supplied by BOC Ltd. Ammonia and pyridine were generated respectively from ammonia solution (BDH AnalaR grade, about 35% NH_3) and from pyridine (BDH General Purpose reagent) by the freeze-pump-thaw process, described earlier for the glass system.

A few experiments were carried out in the Fast Entry Airlock by exposing the sample to a condensible gas under its own vapour pressure. In this case a cold finger containing the condensible gas was directly connected to the fast-entry airlock and, after pumping to rough vacuum, the cold finger was allowed to warm up to room temperature so that the chamber became filled with the gas at its own vapour pressure.

5.3 RESULTS AND DISCUSSION

5.3.1 SAMPLE CHARGING AND CHOICE OF A REFERENCE IN XPS

The ejection of photoelectrons from a sample after irradiation with X-rays leaves the sample positively charged. In a conducting sample this charge is readily neutralized by a flow of electrons from the spectrometer earth, to which the sample holder is electrically connected. The Fermi levels of the sample and the spectrometer chamber are then equal and the kinetic energies of the photoelectrons are measured with respect to this Fermi level. In the case of a poor conductor or an insulating sample, like mica, the charge cannot be neutralized in this way. There is, however, a second means of charge neutralization in operation. For an achromatic source of X-rays the bremsstrahlung component produces a background of low energy electrons (<5 eV) by striking the X-ray gun window and the walls of the chamber. These electrons partially neutralize the surface charge and within a few seconds of X-rays hitting the surface, an equilibrium steady-state static charge is established.

The nature of the residual static charge and its effects on XPS measurements made with non-conducting samples have been dealt with by Siegbahn et al. (1967), Evans (1977), Lewis and Kelly (1980), Swift (1982), Swift, Shuttleworth and Seah (1983), Kohiki and Oki (1984), and many other authors. Besides reducing the kinetic energies of the photoelectrons, the surface charging tends to make the peaks in a photoelectron spectrum very broad. This is particularly prominent in a sample where differential charging occurs due to the different insulating properties of the constituents. For an insulator an apparent binding energy, E_B' , measured by XPS, is related to the true

binding energy, E_B, by the relation

$$E_B = E_B' - C \qquad (5.1)$$

where C is the apparent shift in binding energy due to the steady-state surface charging. Because the Fermi level of the insulator is not coupled to the Fermi level of the spectrometer chamber there is an uncertainty in E_B. The binding energy recorded by the spectrometer is measured with respect to the vacuum level of the insulator rather than to the Fermi level as happens with a conducting material.

Several methods have been devised either to eliminate C or to estimate its value. Use of a low energy electron flood gun to neutralize the residual charge has been described by Huchital and McKeon (1972), Müller (1976) and Hunt et al. (1981). However, as mentioned earlier, this method was found to be only partially effective in the case of mica samples in the present system.

Another method frequently employed is to refer the XPS peaks of an insulator to the binding energy of a well-established constituent. The C1s peak of an adventitious hydrocarbon overlayer formed from pump oil contamination is widely used as the reference. This corresponds to a binding energy in the range 284.4 - 284.8eV. However, many workers, including Brandt et al. (1978), Bird and Swift (1980), Wagner (1980) and Swift (1982), have shown that the C1s standard suffers from a number of uncertainties arising from the chemical state of the carbon contamination and particularly the thickness of the carbon overlayer. For mica, the C1s standard is unsuitable because all air-cleaved surfaces contain some carbon contamination which is perhaps in a different chemical state from that of the adventitious carbon. The

vacuum-cleaved surface, on the other hand, has almost no carbon contamination.

Another common practice has been to deposit a thin layer of gold or other noble metal on to the insulator surface. The binding energy values are then corrected with respect to the binding energy of a particular metal level, e.g. Au4f, which is assumed to be affected by the charging in a similar way to the insulator levels. Ebel and Ebel (1974), Grinnard and Riggs (1974) and Uwamine et al. (1981) have discussed the use of the Au4f level as a reference and have shown that the thickness of the deposited layer is very important for accurate calibration. However some doubts have been expressed as to the good electrical contact between the deposited layer and the substrate and also to the possibility of chemical interaction between the metal and the substrate.

For zeolites, silica-aluminas and clay-minerals, the practice has been to use the core level of a constituent (most commonly the Si2p level) as an internal standard to calibrate the binding energies of all other levels. The energy of this level is determined with respect to Au4f or any other level of a deposited metal layer. Ogilvie and Wolberg (1972), Clark and Thomas (1976), and Defossé and Canesson (1976) have demonstrated the advantages of using the Si2p reference level over either C1s or Au4f levels. As an alternative, Seyama and Soma (1984) have used the Si2s level for binding energy calibration in montmorillonites. Other reference levels have also been used. Kantschewa, Albano, Ertl and Knözinger (1983) have shown that the insensitivity of the potassium energy levels to chemical shifts makes it possible to use the $K2p_{3/2}$ level as a reference as was done in their study of the

$K_2CO_3/\gamma\text{-}Al_2O_3$ system.

The XPS data in the present work were also calibrated with respect to the $K2p_{3/2}$ level. The energy of the reference level was determined by evaporating platinum on to the mica surface and then estimating the apparent binding energy shift experienced by Pt $4f_{5/2}$ and $4f_{7/2}$ levels due to charging. The Si2p level was not used because this level was seen to have split after platinum evaporation.

Platinum was evaporated on to both air-cleaved and vacuum-cleaved mica surfaces from a platinum source heated by electron bombardment. Evaporation was continued for 12 minutes with 8mA emission current and 2kV accelerating potential. The evaporation source was previously calibrated to give a deposit of one monolayer of platinum on a nickel single crystal under identical conditions. The binding energies of the Pt $4f_{7/2}$ and $4f_{5/2}$ levels were determined from the platinum deposited on nickel to be respectively 71.1eV and 74.3eV. The apparent binding energies of the platinum 4f levels from the deposited layers on air-cleaved and vacuum-cleaved mica surfaces are shown in Table 6. The platinum peaks were shifted by between 6 and 7eV due to charging, the effect being greater for grazing emission than for normal emission. The mean value of the apparent shifts of the Pt $4f_{7/2}$ and $4f_{5/2}$ levels was used to correct the $K2p_{3/2}$ binding energy giving it a value of 293.75 ± 0.2eV for both air-cleaved and vacuum-cleaved surfaces. The binding energies of principal constituents of mica on the basis of $K2p_{3/2}$ reference level are shown in Table 7, together with the few published data that are available for muscovite mica. Considering the uncertainties associated with charging, the agreement among the values is reasonable. Other reported values are mainly

TABLE 6: Shift of platinum 4f peaks on mica due to charging

PLATINUM LEVELS	PLATINUM ON AIR-CLEAVED MUSCOVITE				PLATINUM ON VACUUM-CLEAVED MUSCOVITE			
	NORMAL EMISSION		GRAZING EMISSION		NORMAL EMISSION		GRAZING EMISSION	
	Apparent B.E./eV	Shift C/eV	Apparent B.E./eV	Shift C/eV	Apparent B.E./eV	Shift C/eV	Apparent B.E./eV	Shift C/eV
$4f_{5/2}$	80.30	6.00	81.25	6.95	80.50	6.20	81.50	7.20
$4f_{7/2}$	77.20	6.10	78.00	6.90	77.40	6.30	78.25	7.15

NB: The shifts are calculated on the basis of Pt $4f_{5/2}$ and $4f_{7/2}$ binding energies of 74.3 and 71.1eV respectively. The apparent binding energies were determined without the use of the Flood Gun. From several measurements the values are found to have a variance ±0.3eV.

TABLE 7: Binding energies of principal constituents of muscovite mica obtained with Al Kα X-rays with K $2p_{3/2}$ = 293.75 ± 0.2eV as the reference. Comparison with published data.

Study	Aluminium 2p B.E./eV	Aluminium 2s B.E./eV	Silicon 2p B.E./eV	Silicon 2s B.E./eV	Oxygen 1s B.E./eV	Carbon 1s B.E./eV
Present work[a]	74.40	119.45	102.65	153.50	531.65	285.55
Wagner et al.[b] (1982)	74.05	-	102.16		531.23	284.60
Schultz et al.[c] (1974)	-	-	108.30	159.50		
Castle et al.[d] (1979)	74.50	103.70*	-	-	533.20	284.80

a - The binding energies are mean values obtained from a number of measurements on both air-cleaved and vacuum-cleaved mica surfaces. The individual values do not differ by more than 0.3eV.

b - Reference here was to C1s = 284.60eV.

c - These values were not corrected for charging.

d - The binding energies were determined with respect to a constant shift of about 7.5eV due to charging.

* - This appears to be a wrong value.

for the zeolites. Tempere et al. (1975) reported Al 2s and Si 2p energies in zeolites to be respectively in the ranges 119.3 - 119.9 and 102.1 - 103.5eV with reference to C1s = 285eV. Similarly Barr (1983) has shown that for a large number of zeolites and clay-minerals the Al 2p and Si 2p energies (referred to C1s = 284.4eV) lie respectively in the ranges 73.20 - 74.60eV and 100.90 - 103.35eV.

Some uncertainty seems to be inevitable in assigning binding energies to mica and other insulators and therefore it seems impossible to determine very small chemical shifts in the core electron energy levels of these materials.

5.3.2 XPS CHARACTERIZATION OF THE MICA SURFACE

The wide scan photoelectron spectrum of a sample of muscovite mica which was air-cleaved immediately before introduction into the system is shown in Fig. 46. The spectrum was taken in the grazing emission mode with the aluminium X-ray source operated at 11kV energy and 10mA emission. All the major constituents of mica can be seen to produce photo-emission peaks. Some magnesium and sodium could also be detected in the spectrum from the appearance of X-ray induced Auger peaks corresponding to these elements. This agrees well with the generally accepted view that small amounts of sodium and magnesium respectively replace potassium in the inter layer positions and aluminium in the octahedral positions. The spectrum also shows a satellite for each of the prominant peaks. The satellite is due to $K\alpha_{3},\alpha_{4}$ components of the X-radiation and it appears about 10eV below the main peak which results from the predominant $K\alpha_{1},\alpha_{2}$ radiation.

The existence of the Auger peaks in the photoelectron spectrum was verified by taking the spectrum with the magnesium X-ray source when these peaks were displaced by 233eV to the lower binding energy side.

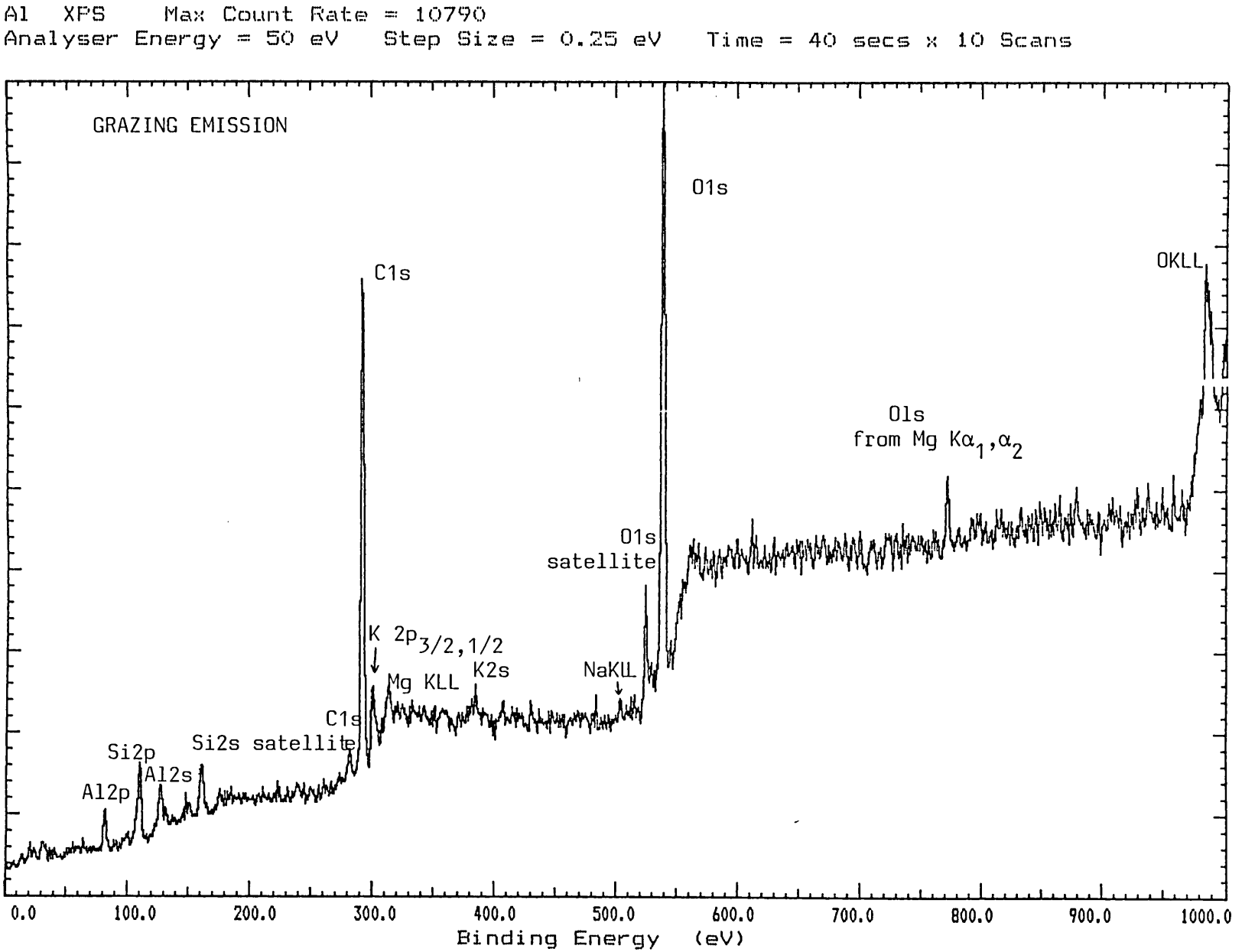

FIG. 46: Photoelectron spectrum of an air-cleaved muscovite mica surface (Binding energies are uncorrected, signal-to-noise ratio 223:1).

One of the most prominent features of the spectrum is the massive carbon peak. It was not possible to determine the absolute C1s binding energy corresponding to this peak, but on the basis of K $2p_{3/2}$ = 293.75eV, the C1s peak position varied from 285.25 to 285.85eV. the width of the peak at half maximum (FWHM) was found to be between 1.65 and 2eV from different measurements. The C1s peak due to a hydrocarbon contaminant is generally assigned a binding energy in the range 284.4 to 284.8eV by various authors. On this basis, it can be assumed that the C1s peak from air-cleaved mica has at least some contribution from a carbon species other than a hydrocarbon.

The wide scan spectrum taken immediately after cleaving the same specimen of mica at 2×10^{-10} torr is shown in Fig. 47. The spectrum was again taken in the grazing emission mode under conditions identical to that of Fig. 46. The reduction in the C1s peak is very evident. As the X-ray beam has a diameter of almost 1cm, some carbon signal may have originated from the air-cleaved corners of the sample. This could explain the small carbon peak still visible in the spectrum of the vacuum-cleaved surface. All the other peaks became more pronounced after the cleaving which showed that the carbon contamination was responsible for some degree of screening of the XPS signals in the case of the air-cleaved surface. The vacuum-cleaved surface also revealed some iron which may be in either tetrahedral or octahedral positions of the muscovite lattice.

The problems which arise when photoelectron spectra are used to give quantitative information about relative abundance of constituent elements are well-known. These have been dealt with in detail, particularly for the silica-aluminas, zeolites and clay-minerals,

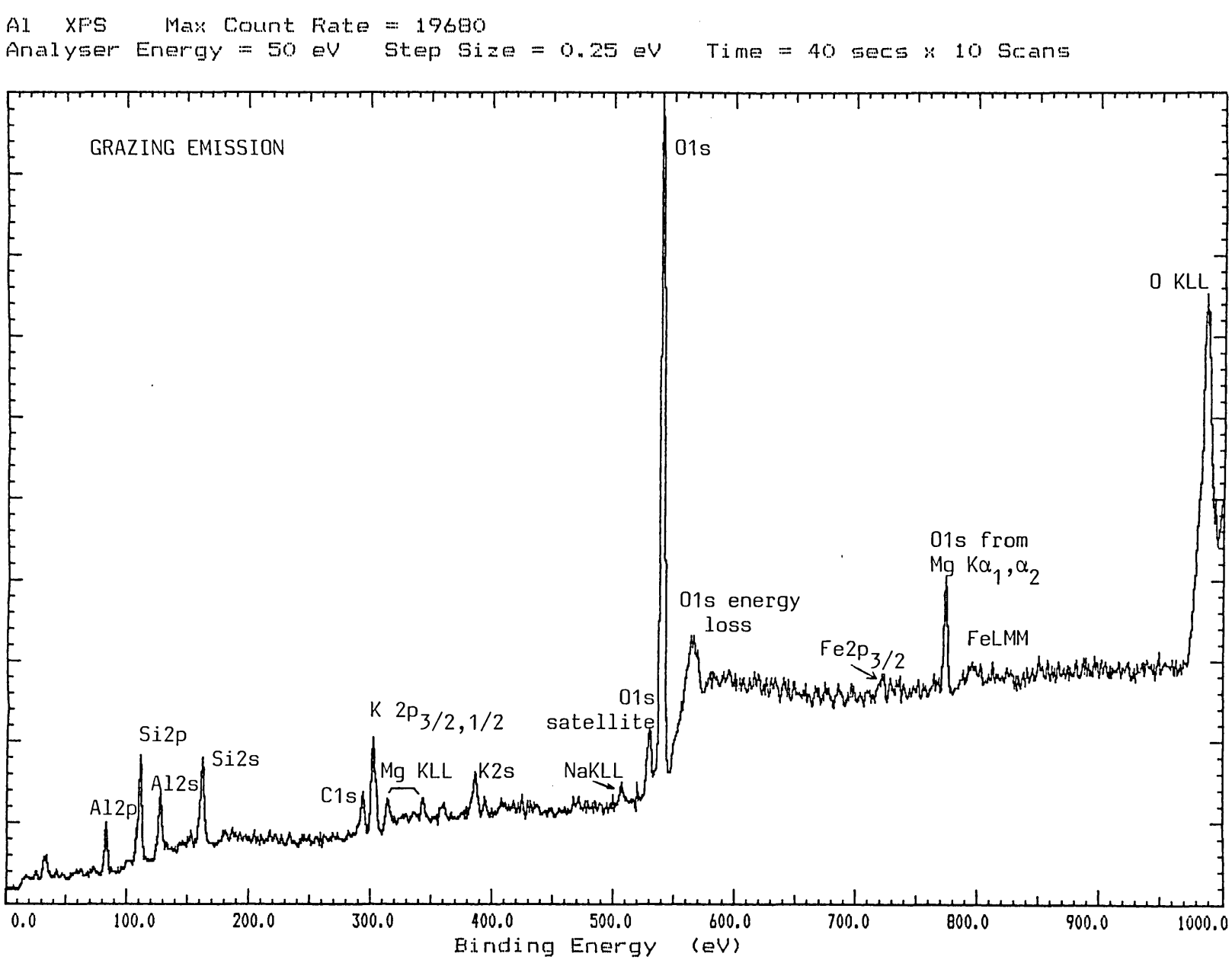

FIG. 47: Photoelectron spectrum of the muscovite mica surface immediately after cleaving in vacuum. (Binding energies are uncorrected, signal-to-noise ratio 634:1).

by Koppelman (1976, 1980), Adams et al. (1977), Defosse and Rouxhet (1980) and a large number of other authors. Despite the limitations, peak area ratios are widely used to characterize these solids. Relative concentrations of any two elements, A and B, can be compared using the following elementary relation:-

$$\frac{C_A}{C_B} = \frac{I_A}{I_B} \times \frac{S_B}{S_A} \qquad (5.2)$$

where C_A and C_B are the concentrations of the two elements, I_A and I_B are the intensities of their prominent XPS peaks, and S_A and S_B are the relative sensitivities for those peaks with the spectrometer used.

The intensity of an XPS line is obtained from the peak area after the background has been subtracted and allowance has been made for sweep width, number of scans and time taken for each scan. Various normalized peak area ratios for air-cleaved and vacuum-cleaved muscovite surfaces have been calculated using relation (5.2) and the results are given in Table 8. Background subtraction and peak area determination were carried out using a VGS computer programme. Each peak was scanned separately at the same beam energy under identical conditions, these being sweep width 10eV, CAE 20eV, step size 0.05eV, scan time 10 seconds and number of scans 25. The relative sensitivity data for the ESCALAB-MkII were not determined however and instead the relative sensitivity data of Wagner et al. (1981) were used for the calculations. The values used are shown below:

F1s : 1.00 as the standard
C1s : 0.25
Al2p : 0.185
Si2P : 0.27
K2p : 0.83 .

The table also shows the data for XPS at normal emission which should be more representative of the bulk composition of the mica whereas the grazing emission data should represent the surface composition.

TABLE 8: Normalised peak area ratios in muscovite mica from XPS intensity data

Normalised peak area ratios	XPS AT NORMAL EMISSION		XPS AT GRAZING EMISSION	
	air-cleaved surface	vacuum-cleaved surface	air-cleaved surface	vacuum-cleaved surface
$\frac{\text{Al 2p}}{\text{Si 2P}}$	0.54	0.57	0.30	0.69
$\frac{\text{K 2p}_{3/2}}{\text{Si 2p}}$	0.34	0.35	0.24	0.30
$\frac{\text{C1s}}{\text{Si 2p}}$	4.54	0.15	3.29	0.25
$\frac{\text{Al 2p air}}{\text{Al 2p vac.}}$	0.33		0.26	
$\frac{\text{Si 2p air}}{\text{Si 2p vac.}}$	0.34		0.60	
$\frac{\text{K 2p}_{3/2}\text{ air}}{\text{K 2p}_{3/2}\text{ vac.}}$	0.34		0.48	
$\frac{\text{C1s air}}{\text{C1s vac.}}$	10.64		7.93	

N.B. Al 2p air/Al 2p vac., ... etc., are peak area ratios for the same element respectively in the air-cleaved and in the vacuum-cleaved mica surfaces.

In order to interpret the data given in Table 8 some consideration must first be given to the mean free path of the photoelectrons in mica.

According to Cox et al. (1982) the mean free path, λ, of electrons in a whole variety of insulating and semiconducting oxides tends to follow the approximate relationship

$$\lambda = 0.35 \times \sqrt{E} \qquad (5.3)$$

where E is the kinetic energy of the electron in eV and λ is given in Å. On this basis λ would be approximately 13Å for the electrons contributing to the Si 2p and Al 2p peaks and approximately 12Å for the electrons contributing to K $2p_{3/2}$ peak.

For normal emission the attenuation of photoelectrons originating at a distance D below the surface will be equal to $\exp(-D/\lambda)$. Thus at a depth of 10Å, which corresponds to the distance between cleavage plains in mica, the attenuation will be 0.50. Although this attenuation is considerable, detailed calculations show, that the photoelectron spectra taken at normal emission should be fairly representative of the bulk structure of mica as far as the Al 2p, Si 2p and K $2p_{3/2}$ peaks are concerned. In keeping with this conclusion, the experimental K $2p_{3/2}$/Si 2p ratio of 0.34 - 0.35 is close to the elemental ratio of 0.30 for bulk muscovite mica. However, there is a large discrepancy between the experimental Al 2p/Si 2p ratio of ~0.55 and the bulk composition ratio of 0.87.

The reasons for the above discrepancy are not clear but the following possibilities should be considered:

(i) the relative sensitivity factor given for Al 2p by Wagner et al. (1981) may not be applicable to mica. A large part of the aluminium in muscovite mica is in octahedral coordination, a type of bonding not found in the reference compounds used in determining the relative sensitivity data.

(ii) The attenuation of photoelectrons originating from the octahedral layer at normal emission may be greater than supposed because of steric blocking by the tetrahedral layer of atoms immediately above.

(iii) There may be genuine depletion of aluminium in the surface layers, although it is difficult to understand how this might come about and also such an interpretation is in conflict with the data to be discussed below.

The grazing emission data from the vacuum-cleaved surface show an enhanced Al 2p/Si 2p ratio of 0.69. Under these conditions, the photoelectrons leave the surface at an angle of approximately 10° to the surface plane and the attenuation will be equal to $\exp(-\frac{D}{\lambda \sin 10^{o}})$. Even at a depth of 3Å below the surface the attenuation is already equal to 0.26 and the photoelectrons will effectively come from the top two layers of atoms. Thus only the tetrahedrally coordinated layer of the mica structure with its associated potassium ions would be detected in grazing emission. For this layer the elemental ratios are Al/Si = 0.29 and K/Si = 0.30. Once again the K/Si ratio is close to the experimental K $2p_{3/2}$/Si 2p value but there now appears to be an excess, rather than a depletion of aluminium in the surface layer. This anomalous result may be due to steric blocking arising from the particular

structure of mica. Although the silicon and aluminium atoms occur in the same tetrahedral environment there is a slight distortion in the muscovite structure which causes the aluminium atoms to be approximately 0.12Å closer to the surface than the silicon atoms. Thus photoelectrons emerging at grazing angles from the silicon atoms may be blocked by the aluminium atoms but not vice versa.

The effect of a layer of carbon on the mica surface can be seen by comparing results for the vacuum- and air-cleaved mica surfaces. At normal emission the intensities of all the photoemission peaks are reduced by a factor of three. Such a large attenuation in signal is hard to explain. A layer of carbon about 10Å thick would normally be required to give such a tremendous effect but a comparison of the C1s peak with the platinum photoemission peaks obtained after controlled evaporation of the metal on to the mica surface indicated that the carbon contamination consisted of no more than a monolayer. It could be that the carbon atoms sit directly above the Al, Si and K atoms in such a way as to block photoelectrons emitted from these atoms at normal incidence.

The effect of carbon contamination on the photoelectron spectra taken at grazing emission is rather different. Whereas for normal emission there is a uniform attenuation of peak intensities, the effects of grazing emission are more selective. Thus the Al 2p peak intensity drops by a factor of four whilst the Si 2p and K $2p_{3/2}$ peak intensities are much less affected. It is significant that the Al 2p/Si 2p ratio for the carbon contaminated surface (at grazing emission) is almost equal to the elemental ratio for the tetrahedral layer. This could be explained if the presence of the carbon contamination caused the tetrahedrally coordinated atoms to relax so that the aluminium and silicon atoms were in the same plane equidistant from the surface.

An interesting phenomenon was observed after cleaving the mica sample in vacuum. It was noticed that all peaks shifted to still apparent higher binding energies. Also it was found that the apparent shift increased when the sample was heated and decreased when it was exposed to water vapour (or to ammonia). Generally, the apparent shift of binding energies oscillated between 4.5 and 7.0eV depending upon the history of the mica surface. The apparent and corrected binding energies of the principal peaks for a few differently treated mica surfaces are given in Table 9. Also recorded is the full width at half maximum for these peaks. XPS data were collected in the grazing emission mode for the following surfaces in sequence:

A - Air-cleaved surface,

B - Vacuum-cleaved surface,

C - Surface after heating to 600K for 30 mins.,

D - Surface exposed to 1800L water vapour, ($1L = 10^{-6}$ torr sec.),

E - Surface reheated to 600K for 30 mins.

Each peak was scanned individually under an identical set of conditions, i.e. 10eV sweep width, 20eV CAE, 25 scans each with a time of 10 seconds, and the same X-ray beam energy. Repeating the above sequence over again produced similar results.

The peaks corresponding to mica surfaces A, B and C are shown in Fig. 48 after subtraction of the nonlinear background in each case. The apparent shifts are clearly visible for each peak. The surfaces D and E produced peaks in almost the same positions as B and C respectively. The potassium $2p_{3/2,1/2}$ doublet was well resolved with an energy difference of ~3 eV. The Si 2p peak showed a shoulder on the

TABLE 9: Apparent shift of binding energies of muscovite XPS peaks depending upon surface treatment

MICA SURFACE	C1s B.E./eV	FWHM/eV	Al 2p B.E./eV	FWHM/eV	Si 2p B.E./eV	FWHM/eV	K $2p_{3/2}$ B.E./eV	FWHM/eV	K $2p_{1/2}$ B.E./eV	FWHM/eV	O1s B.E./eV	FWHM/eV
A	290.35 (285.55)	1.65	79.20 (74.40)	2.85	107.45 (102.65)	2.05	298.55 (293.75)	1.85	301.4 (296.6)	1.90	536.45 (531.65)	2.30
B	292.05 (286.00)	1.65	80.50 (74.50)	1.65	108.60 (102.55)	2.00	299.80 (293.75)	1.80	302.65 (296.6)	1.90	537.55 (531.50)	2.35
C	292.55 (285.60)	2.20	81.40 (74.45)	1.80	109.50 (102.55)	2.05	300.70 (293.75)	1.80	303.40 (296.45)	1.85	538.55 (531.60)	2.30
D	291.70 (285.80)	1.90	80.30 (74.40)	1.85	108.50 (102.60)	2.05	299.65 (293.75)	1.80	302.45 (296.55)	1.85	537.45 (531.55)	2.35
E	292.70 (285.90)	2.05	81.45 (74.45)	1.90	109.65 (102.65)	2.05	300.75 (293.75)	1.85	303.50 (296.50)	1.85	538.65 (531.65)	2.35

N.B. All data refer to grazing emission. The Flood Gun was not used. The binding energies inside parentheses represent the corrected values with respect to K $2p_{3/2}$ energy = 293.75eV as the reference.

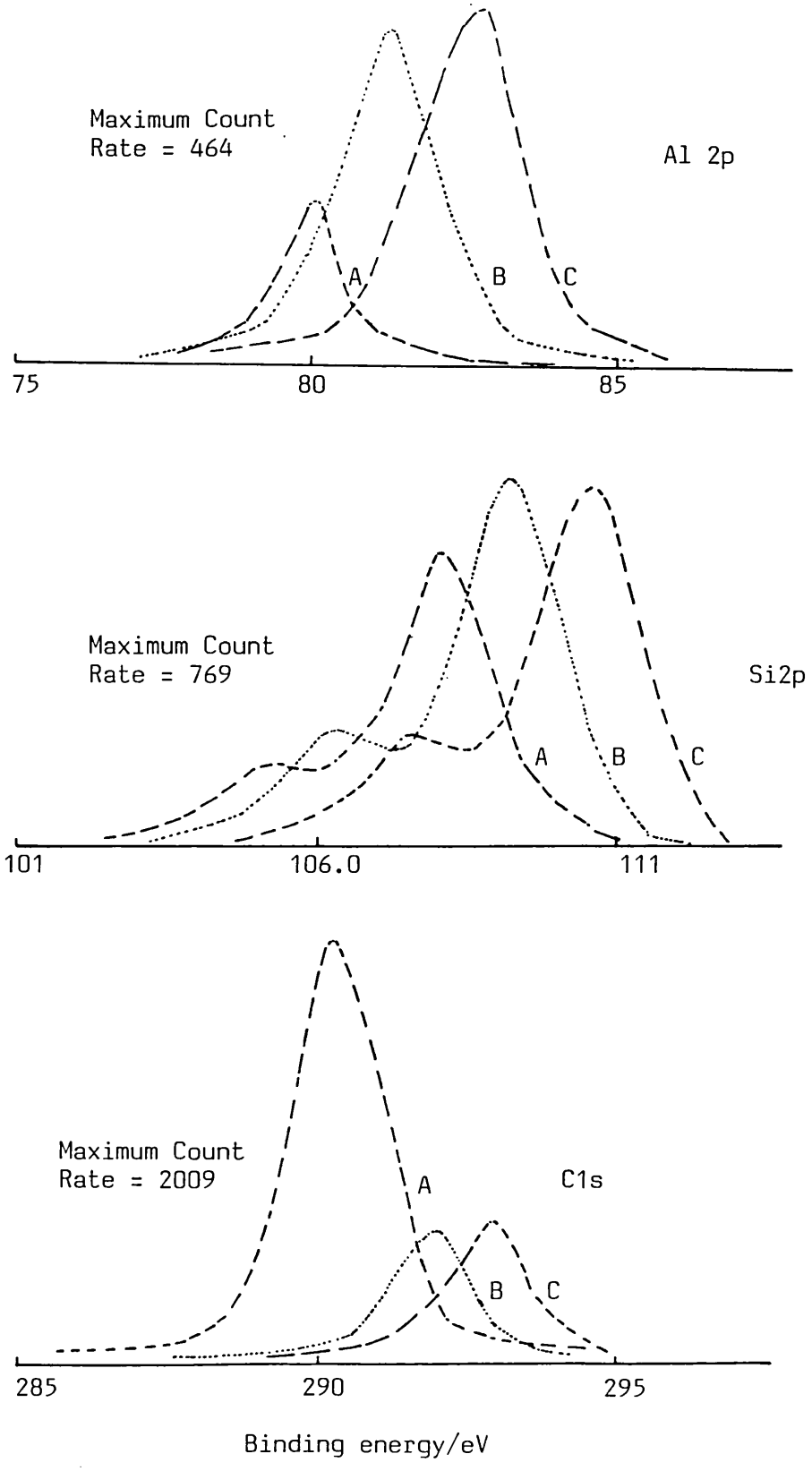

FIG. 48: Apparent shift of XPS peaks of muscovite mica due to variable amount of charging.

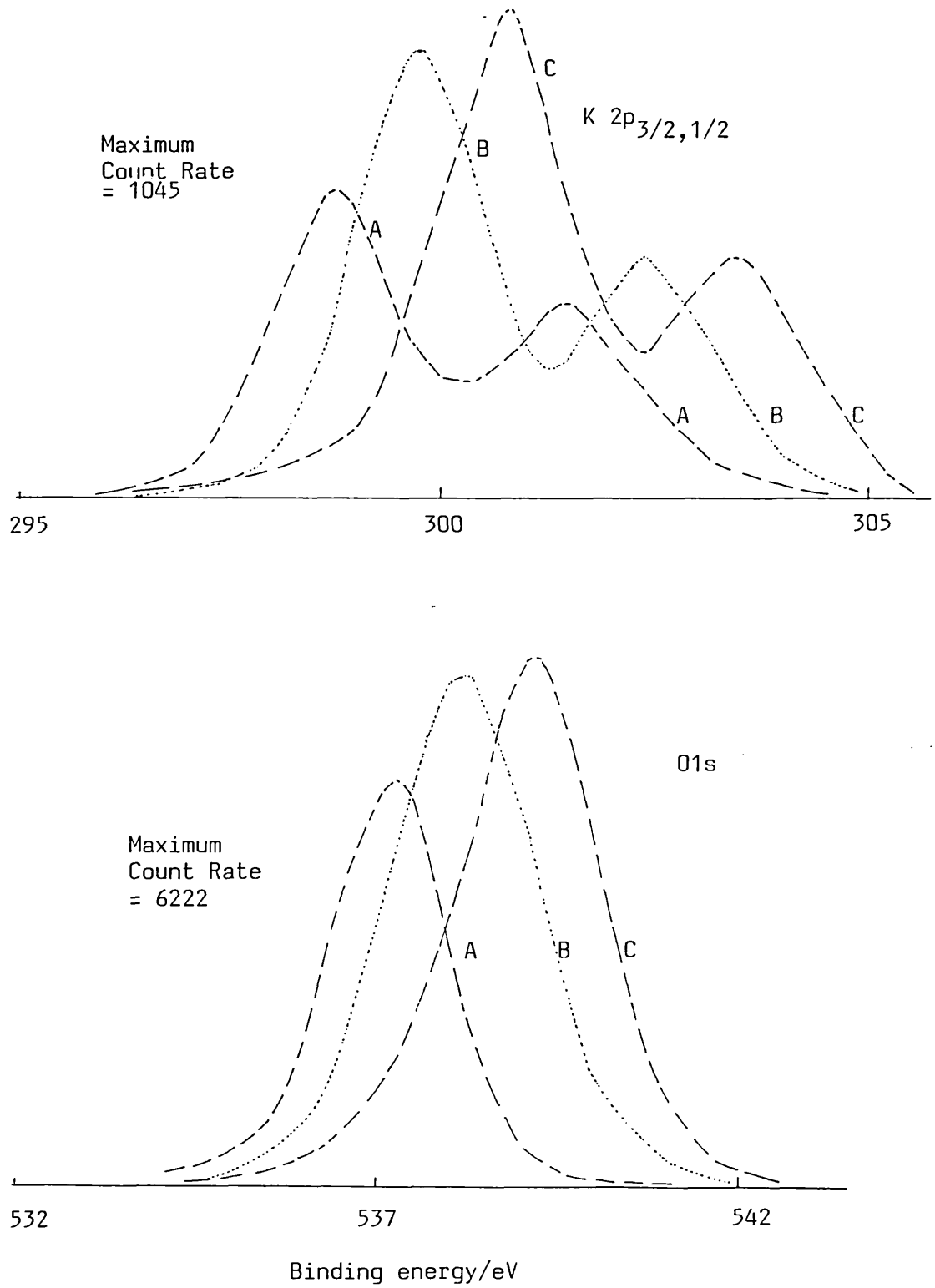

FIG. 48: Apparent shift of XPS peaks of muscovite mica due to variable amount of charging.

low binding energy side with an energy difference of more than 3eV from the principal peak. After correction of the apparent shift, this peak could be assigned an apparent binding energy of ~98eV. This is an Al $KL_{2,3}L_{2,3}$ Auger peak induced by the bremsstrahlung component of the X-radiation (the characteristic lines of an aluminium X-ray source are too near to the kinetic energy of an aluminium $KL_{2,3}L_{2,3}$ electron to excite this Auger transition). Such bremstrahlung-induced Auger peaks appearing in the photoelectron spectrum from an achromatic X-ray source have been discussed by Wagner and Taylor (1980). In the present case, the appearance of this aluminium Auger peak at ~98eV apparent binding energy was further proved by recording the photo-electron spectrum with the magnesium X-ray source, when this peak disappeared. As the difference in photon energy between the aluminium and the magnesium sources is ~233eV, the aluminium Auger peak would be displaced to the hypothetical negative binding energy side in case of the magnesium XPS.

The shifts in the apparent binding energies appear to be associated with the presence or absence of adsorbed layers on the mica surface. Thus the large increase in apparent binding energy which occurs for all the photoemission peaks when the mica surface is cleaved may be due to the difference in carbon contamination between the air- and vacuum-cleaved surfaces. If this interpretation is correct the carbon layer is responsible for a drop of approximately 1.2eV in the binding energies of Al 2p, Si 2p, K $2p_{3/2,1/2}$ and O1s core electrons. Similarly one can interpret the rise in apparent binding energy of approximately 1.0eV which occurs when the vacuum-cleaved surface is heated as due to the removal of water from the surface. Readsorption of water causes this process to be reversed and the apparent binding energy is restored

more or less to its previous value.

Two possibilities should be considered to explain this change in apparent binding energy:

(i) It is conceivable that the presence of an adsorbed layer on the surface could cause some change in the steady state charge present on the surface during the photo-ionization process. This might come about by a change in the rate of neutralization of the positive charge by the stray electrons generated by the bremsstrahlung component of the X-radiation.

(ii) A more likely explanation is that the shift in apparent binding energy is brought about by changes in the dipole layer of the surface. This will cause a change of potential inside the mica and hence a shift of binding energies. Quite large dipole fields can be expected at the surface of mica because of the presence of potassium ions with the corresponding negative charge residing on the tetrahedral aluminium atoms. Dipole fields at the mica surface have been considered previously by Müller and Chang (1969). Molecules adsorbing on the surface will therefore be in a strong field and may become polarised, thus reducing the potential drop across the double layer. Alternatively adsorption might cause some movement of the potassium ions with a resultant change in dipole moment.

Since the position of the potassium ions relative to the aluminium atoms is not definitely known for a mica surface, it is not possible to calculate the potential drop arising from the dipole layer. However a rough calculation shows that the potential drop can be considerable. If the dipole layer is treated as a parallel plate condenser, the potential drop is given by the formula

$$\Delta V = \frac{\sigma d}{\epsilon_o \epsilon_r} \qquad (5.4)$$

where σ is the charge density, d is the separation of opposite charges, ϵ_o is the permittivity of vacuum and ϵ_r is the relative permittivity of the medium. There are about 2×10^{18} potassium ions per m^2 in a mica surface. With d equal to $1\mathring{A}$ and ϵ_r taken as unity, the potential drop across the dipole layer is calculated to be 3.6 volts. Hence a change of 1.0 - 1.2 volts caused by adsorption is quite feasible.

With this model both carbon contamination and water have to be adsorbed so as to make the outer end of the dipole layer more positive. If the molecules were merely polarised in the surface field this would require the initial fields to be negative outwards i.e. for the potassium ions to lie deeper in the surface than the corresponding negative charge. On the other hand a small relaxation of the potassium ions outwards, induced by adsorption, would produce the desired result, irrespective of the initial direction of the field.

All the photoemission peaks have a FWHM much larger than in a conducting sample. The Si 2p, O1s and K $2p_{3/2,1/2}$ peaks were found to have a constant FWHM value but this is not true of the C1s and Al 2p peaks. The Al 2p peak for the air-cleaved surface was very small and broad (FWHM = 2.85eV). The C1s peak was also very small after cleaving and it tended to broaden after the sample was heated. The oxygen and silicon peaks appeared exceptionally broad indicating that they might be composite peaks.

It has not been possible to resolve the Si $2p_{3/2,1/2}$ and Al $2p_{3/2,1/2}$ doublets because of the closeness of their binding energies (~1eV difference). The Al 2p and Al 2s peaks might be expected to be split because aluminium occurs in two environments, tetrahedral and octahedral.

However, in all cases (including normal emission spectra), only single aluminium 2p and 2s peaks were observed.

Tetrahedrally co-ordinated silicon also occupies two types of site, as already discussed in Chapter 2, one with an aluminium neighbour and the other without. Photoionization is expected to distinguish between the two sites. Once again, however, silicon 2p and 2s levels produced single peaks only.

Attempts to deconvolute the Al 2p and Si 2p peaks using an iterative computer program supplied by the VG Scientific Limited were not very successful in resolving the peaks.

A qualitative study of the extent of charging on other insulator surfaces was conducted using powdered samples of 13X-molecular sieve, potassium carbonate and silicon carbide. In each case, a thin layer of the sample was pressed on to a rhenium foil which was held by four metal tags spotwelded to a stub-holder. It was found that the powdered samples suffered a binding energy shift of between 0.5 and 2eV depending upon the thickness of the layer. It does appear, therefore, that the sheet structure of mica is a significant factor in obtaining a substantial amount of surface charge during the photoionization. The amount of charging in mica did not particularly depend on the thickness of the sample; the removal of the front face on cleaving actually increased the charging.

The XPS measurements showed that the carbon contamination of the air-cleaved mica surface could be reduced by prolonged heating at a temperature of 600K. However the initial effect of such heating was actually to increase the C1s peak. The result after a 19 hour heating period at 500K is shown in Fig. 49. The decrease in the intensity of

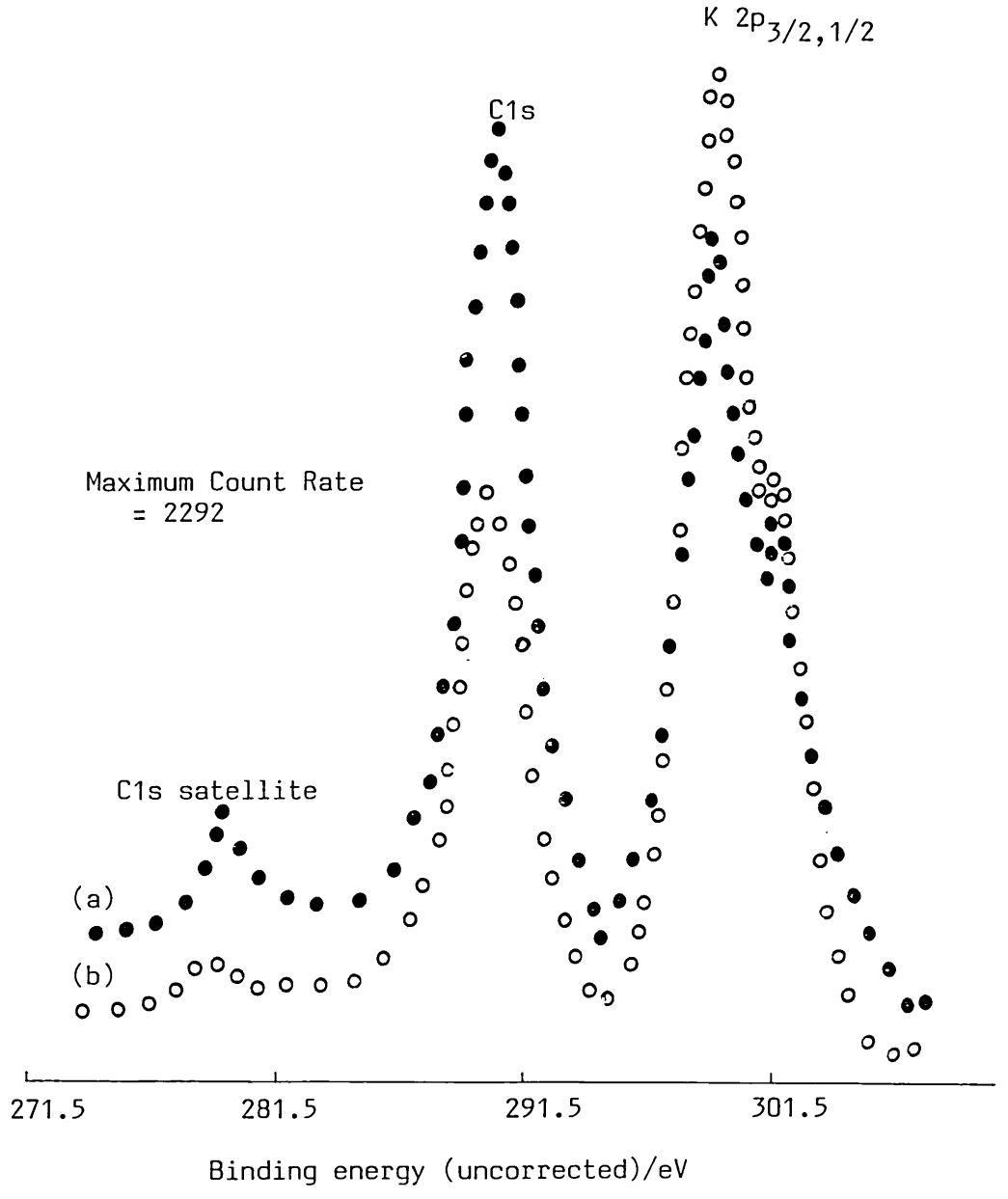

FIG. 49: Reduction of C1s intensity on heating the air-cleaved mica at 500K for 19 hours. (Nonlinear background subtracted). Data taken at normal emission with CAE = 50eV, step size = 0.25eV, 50 scans x 40 seconds, (a) before heating and (b) after heating.

C1s signal was accompanied by a small increase in K $2p_{3/2,1/2}$ intensity which showed that the carbon layer had been screening the potassium signal.

The effect of hydrogen-atom bombardment on the carbon overlayer of air-cleaved mica surfaces was repeated in the ESCALAB. The sample was placed on the P8 probe and was kept at a temperature of about 400K during bombardment at a hydrogen pressure of 2×10^{-6} torr. However the arrangement for atomisation was not very satisfactory because the filament was at an obtuse angle to the mica surface and was positioned more than 6cm away. The result was still impressive as is shown in Fig. 50. The C1s peak became very broad after bombardment but it was reduced by at least 5 times after a 30 minute bombardment period.

The used muscovite sample from the glass system was also subjected to XPS measurements and the photoelectron spectrum at grazing emission is shown in Fig. 51. It shows some remarkable differences from the spectrum for an ordinary air-cleaved mica surface which has been shown in Fig. 46. The surface was depleted very appreciably of potassium and a comparison of the silicon and aluminium peaks show some depletion of aluminium as well. This is in agreement with the observations of many workers, already discussed, who have observed a gradual depletion of potassium from the mica surface after long heating periods. From the relative areas of K $2p_{3/2}$ peaks for this used surface and a fresh air-cleaved surface, it was estimated that the surface depletion of potassium was more than 30 per cent. The depletion of the aluminium, on the other hand, was less marked, the Si/Al ratio for the used surface being 3.65 compared to 3.36 for the fresh, air-cleaved surface.

The C1s peak of the mica surface used in the glass system is

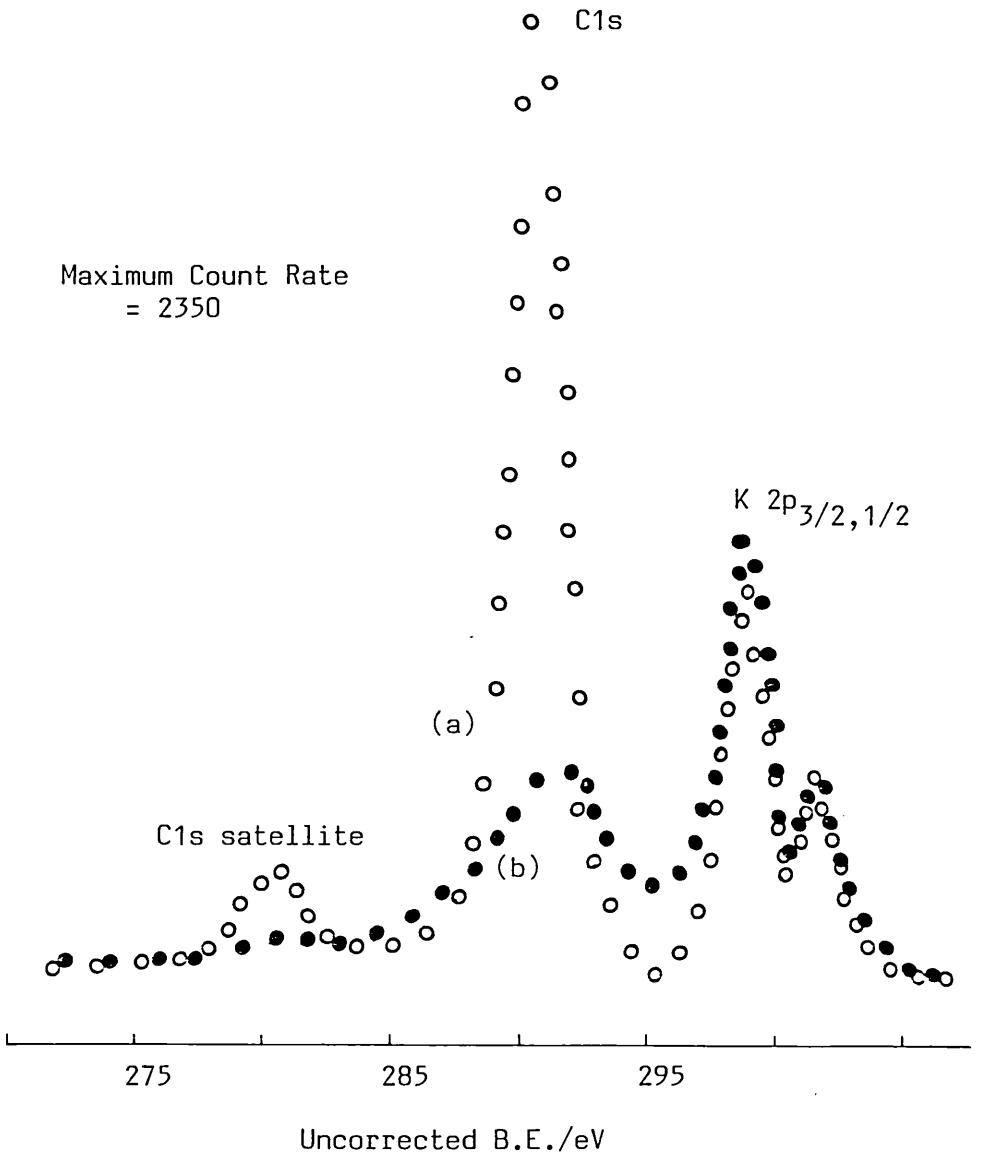

FIG. 50: Effect of hydrogen-atom bombardment on the intensity of C1s peak, (a) before bombardment and (b) after bombardment. Data collected at grazing emission with CAE = 50eV, step size = 0.25eV, 20 scans x 20 seconds. (Nonlinear background subtracted).

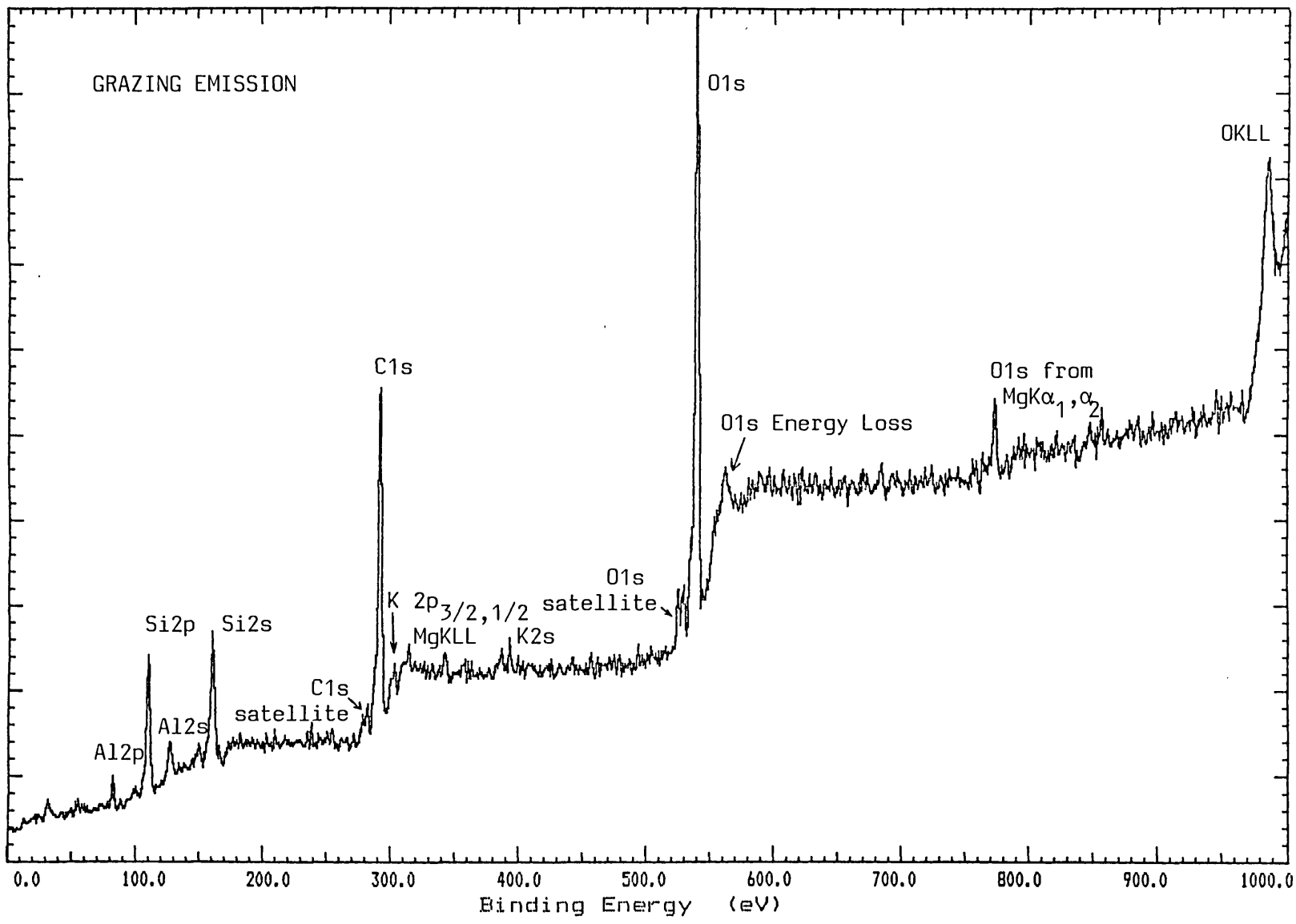

FIG. 51: Photoelectron spectrum of the worked out muscovite sample from the glass system. (Binding energies are uncorrected, signal-to-noise ratio 219:1).

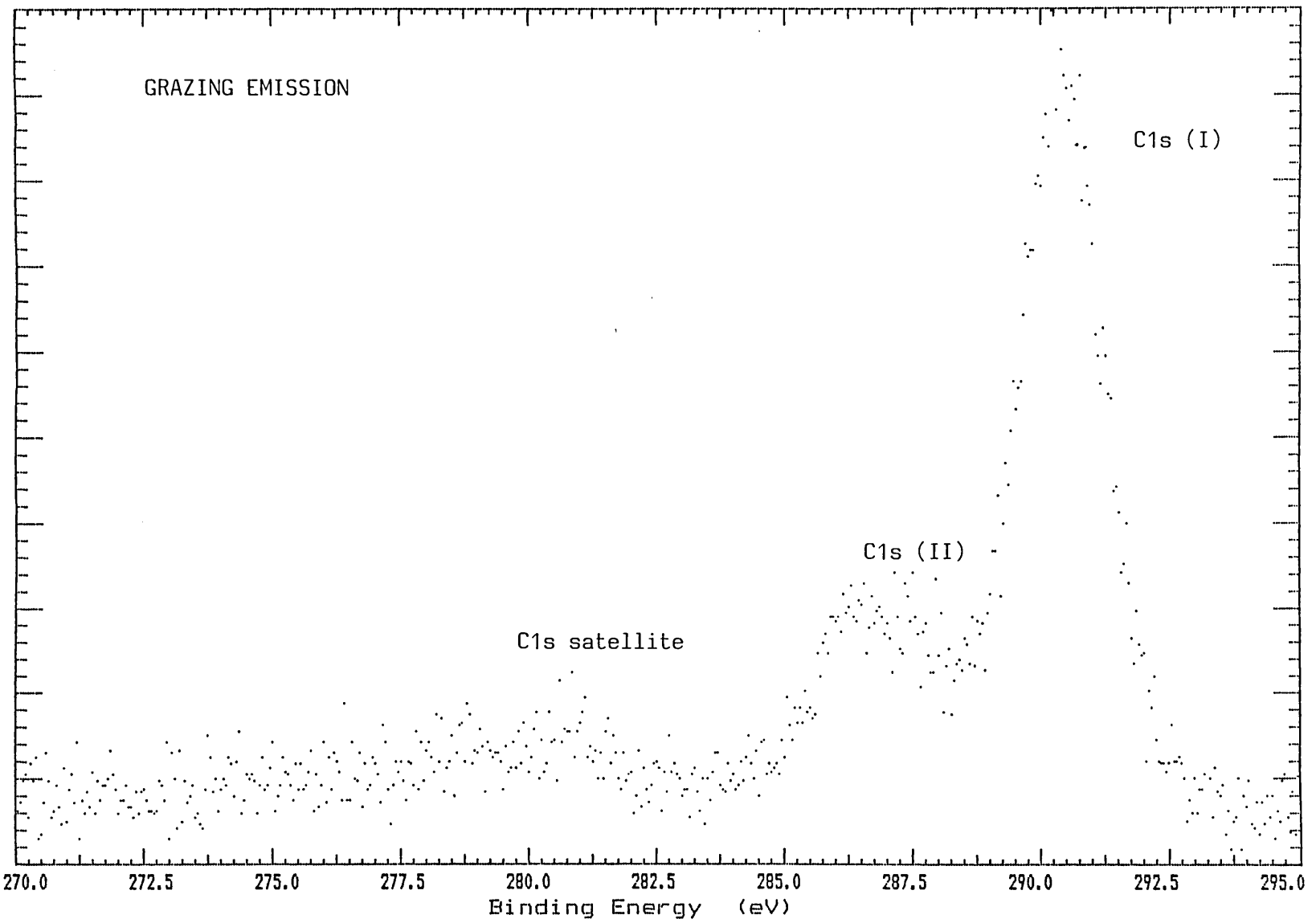

FIG. 52: C1s peaks in the photoelectron spectrum of the mica sample from the glass system (Binding energy uncorrected).

definitely composite consisting of at least two peaks. The result of the narrow scans of this peak with a sweep width of 25eV is shown in Fig. 52. The two carbon 1s peaks are separated by an energy of ~4.13eV and after correction the binding energies corresponded to 285.15 and 281.12eV respectively. The carbon peak with low binding energy has never been observed on freshly air-cleaved surfaces and it must be assumed that this state results from the treatment given to the mica surface in the glass system.

5.3.3 CHARACTERIZATION OF MICA SURFACES BY LOW ENERGY ELECTRON DIFFRACTION AND OTHER TECHNIQUES

The charging of the mica surface was a major problem in the LEED experiments as there was no arrangement for charge neutralization in the LEED chamber. The energy of the electron beam was very critical and it was found that LEED patterns could only be obtained with electron beam energies greater than 70V.

Despite many attempts it proved impossible to get a good LEED pattern from the air-cleaved mica surface. Some patterns could be seen but they were very faint and could not be photographed. Annealing the surface to a temperature of 700K did not improve the LEED pattern. The carbon contamination layer of the mica might be responsible for this.

The best LEED patterns were obtained when the mica sample was cleaved in flowing argon at atmospheric pressure and immediately introduced into the LEED Chamber. The patterns are shown in Fig.53(a), (b), (c) and (d) respectively for beam energies of 90, 100, 115 and 135V.

(a)

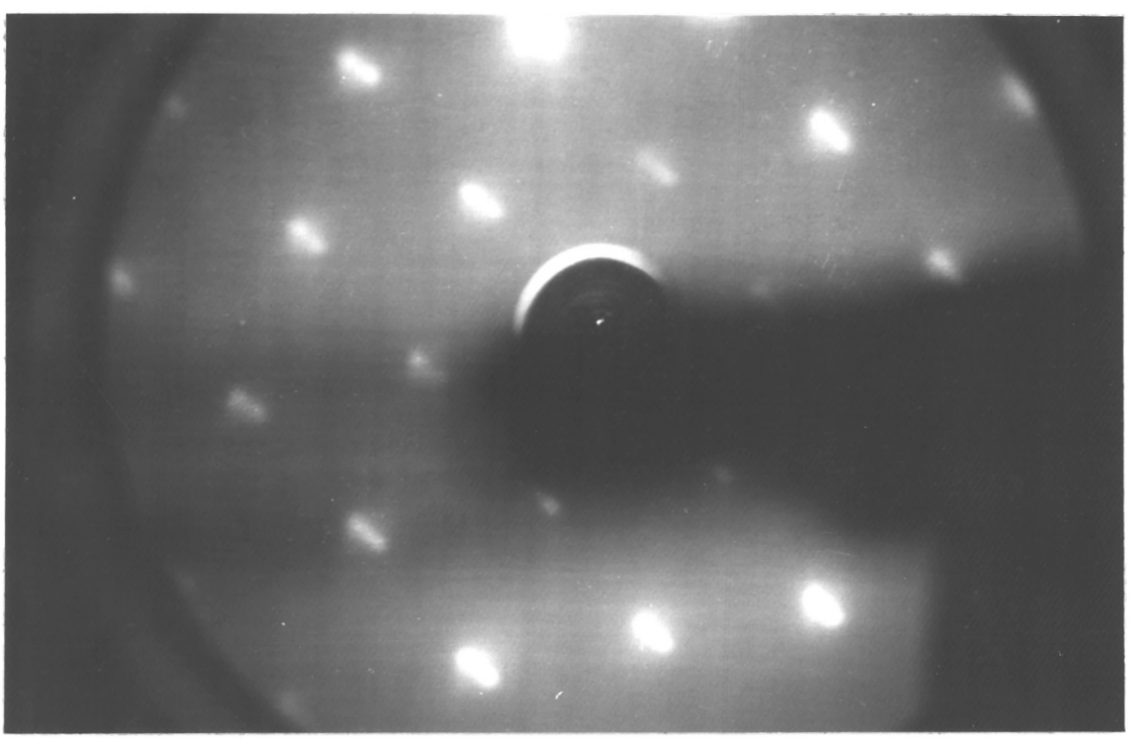

(b)

FIG. 53: LEED patterns from a muscovite mica surface cleaved in 1 atmosphere of argon at beam energy (a) 90V and (b) 100V.

(c)

(d)

FIG. 53: LEED patterns from a muscovite mica surface cleaved in 1 atmosphere of argon at beam energy (c) 115V and (d) 135V.

All these LEED patterns have a hexagonal structure which can be attributed to the basal plane of the tetrahedral layer with the surface oxygen atoms arranged in hexagons. The spots, however, appear as doublets and the separation and orientation of each doublet varies with beam energy. Spot splitting is normally associated either with anti-phase domains or with surface steps but such an explanation cannot apply here because the orientation of the doublets is not constant. The splitting would appear rather to be connected with electrical fields at the surface which cause slight deflection of the back-scattered electrons. There is experimental evidence for two types of electrical fields at mica surfaces. The first has been observed by Deryagin and Metsik (1960) and consists of a mosaic of positive and negative charge density probably induced by a non-uniform distribution of potassium ions. A different type of field, arising from aligned dipoles in the surface, has been proposed by Müller and Chang (1969).

The fact that all the spots in any one pattern are split in the same direction shows that the electrical field is uni-directional across the area covered by the electron beam. It is not clear, however, why the direction of splitting should change as the beam energy is raised. It is known that the extent of surface charging diminishes at high beam energies and this may explain why normal circular spots are observed at the highest beam energy used, namely 135V. Regular patterns with circular spots have also been reported by Müller (1966), Deville et al. (1967) and Müller and Chang (1968, 1969) for air-cleaved mica surfaces.

It should be noted that all the above patterns had disappeared when further LEED experiments were performed after the sample had remained for a few days in the system under UHV conditions.

Immediately after cleaving the sample in a vacuum of 2×10^{-9} torr, some good LEED patterns were seen again. Two of the patterns taken at 90 and 120V are shown in Fig. 54(a) and (b) respectively. The patterns are similar but the one taken at the lower binding energy has more diffuse spots and very pronounced streaking.

These patterns from the fresh, vacuum-cleaved surface appear to be distorted hexagonal arrays in which the spots on certain azimuths are shifted outwards relative to the other spots. From measurements of the diffraction pattern, it can be shown that the first order array of six spots must be obscured by the sample manipulator and the array of eight bright spots seen in the photograph are second order spots, four of which are still obscured. This would seem to indicate that a complex electrical field exists at the surface causing different effects in different directions.

These patterns are quite different from the only other LEED patterns observed for the vacuum-cleaved surface, namely those of Müller and Chang (1969). These authors have found a regular hexagonal array with spots split into triplets. As here, they attributed their findings to the effect of surface electrical fields.

Triplets were observed in the present work only after the vacuum-cleaved surface had been outgassed at a temperature of 500K for 19 hours. The LEED patterns became blurred with a high background intensity. The best pattern obtained is shown in Fig. 54(c) which shows the triplets arranged in a triangle, all triangles being oriented similarly. The pattern became fainter and fainter with time and two days after cleaving, the pattern appeared to consist of very faint triangles as shown in Fig. 54(d). The orientation of the spots also changed. Finally, no pattern could be seen three days after cleaving the sample in

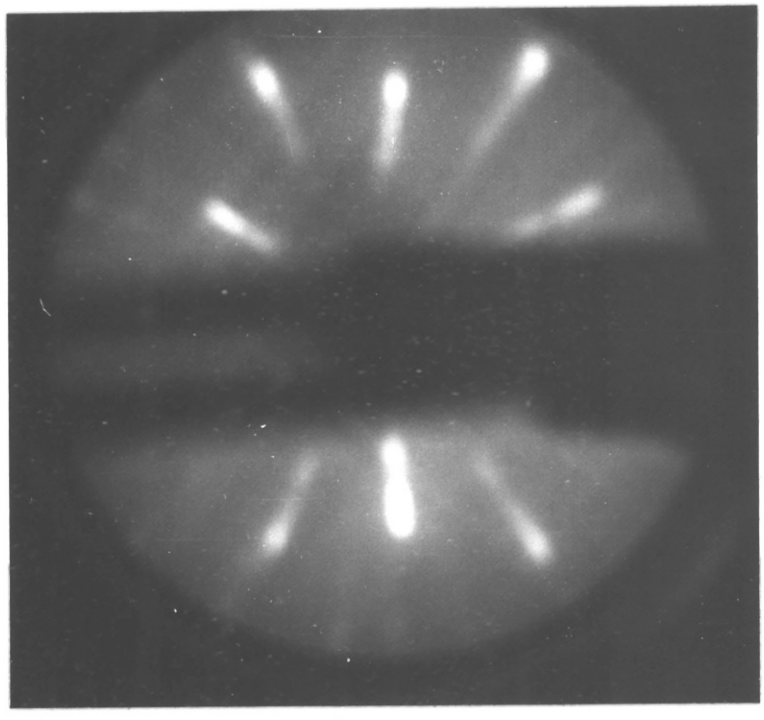

(a)

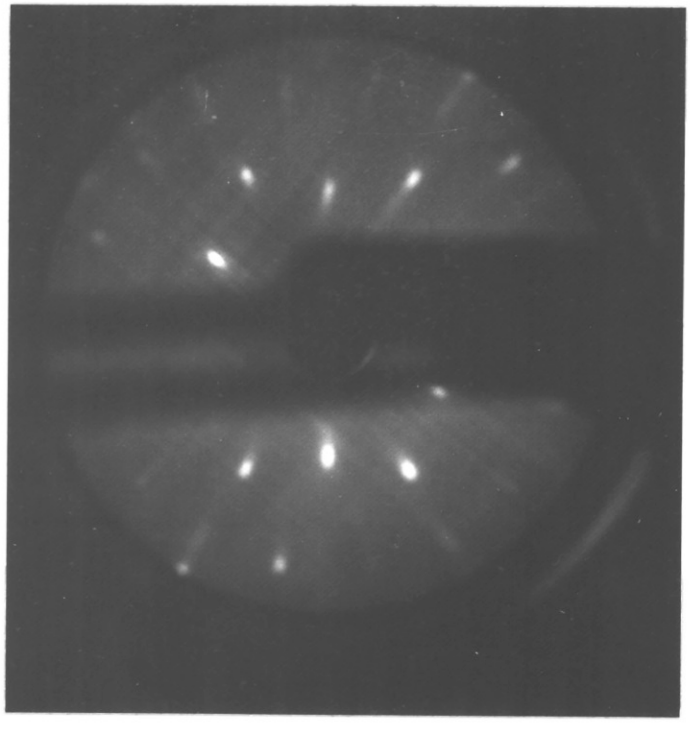

(b)

FIG. 54: LEED patterns for a fresh, vacuum-cleaved muscovite mica surface at beam energy (a) 90V and (b) 120V.

(c)

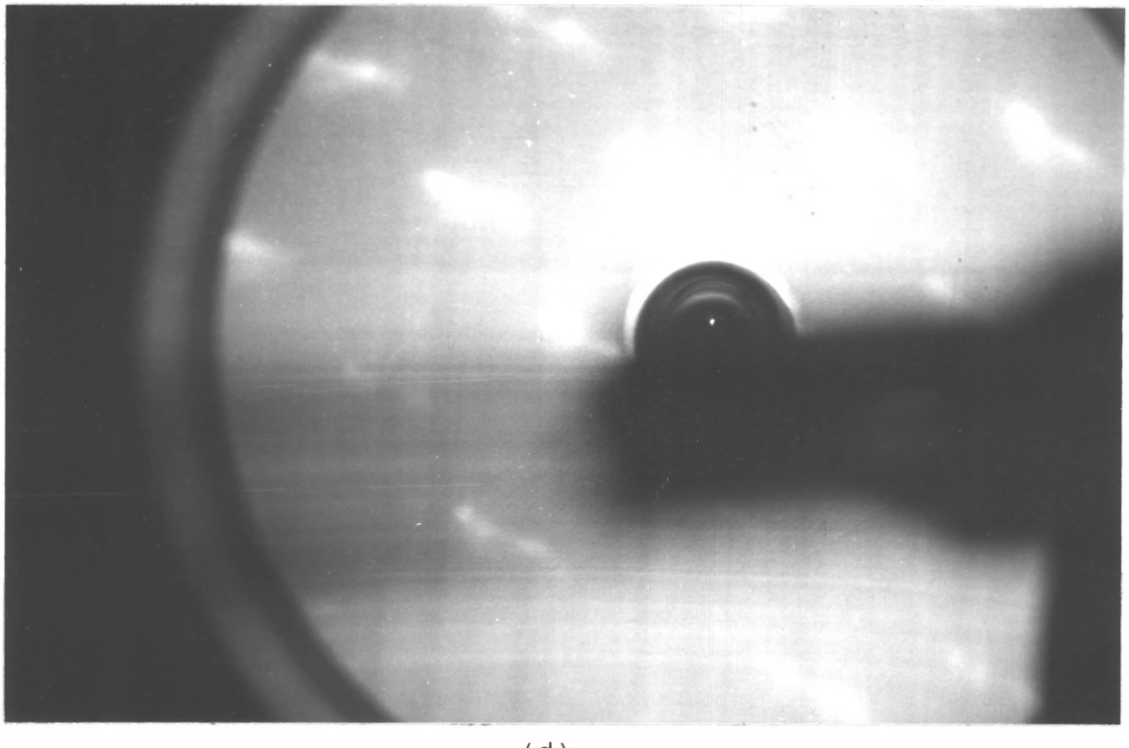

(d)

FIG. 54: LEED patterns for a vacuum-cleaved muscovite mica surface at 120V beam energy: (c) after outgassing at 500K for 19 hours and (d) two days after cleaving in vacuum.

vacuum.

After cleaving, only half a monolayer of potassium ions remain on the mica surface and therefore half the oxygen hexagons are empty. The position of the potassium ions on the surface depends on the site of the corresponding negative charge, namely, the aluminium atoms of the tetrahedral layer. Because of lack of ordering of these aluminium atoms, the potassium ions are likely to have a random distribution and they are unlikely to contribute to the LEED pattern. Müller and Chang have made a similar observation.

SIMS was used to see which elements were present in the mica surface but no quantitative SIMS analysis was undertaken. The SIMS pattern could be obtained only after the surface charge had been partially neutralized with the use of the Flood Gun. The positive ion SIMS of the air-cleaved surface is shown in Fig. 55. It has peaks corresponding to potassium (m/e 39), magnesium (m/e 24), sodium (m/e 23), silicon (m/e 28), aluminium (m/e 27) and other peaks at m/e ratios of 25, 29, 37, 38, 40, 41, 54, 58, etc., which corresponds to various carbonaceous fragments. The potassium peak was very intense compared to all other peaks. The negative ion SIMS spectrum was extremely difficult to obtain and it showed a massive oxygen peak (m/e 16) with all other peaks dwarfed.

Ion scattering spectra were taken for muscovite mica but the results were difficult to interpret because of the non-uniform shift of the peaks due to charging. Without a proper charge neutralization arrangement, the ISS data were fairly meaningless although the spectra produced the correct number of peaks corresponding to the main constituents of muscovite mica.

The Ultraviolet Photoelectron Spectra for the air-cleaved and the

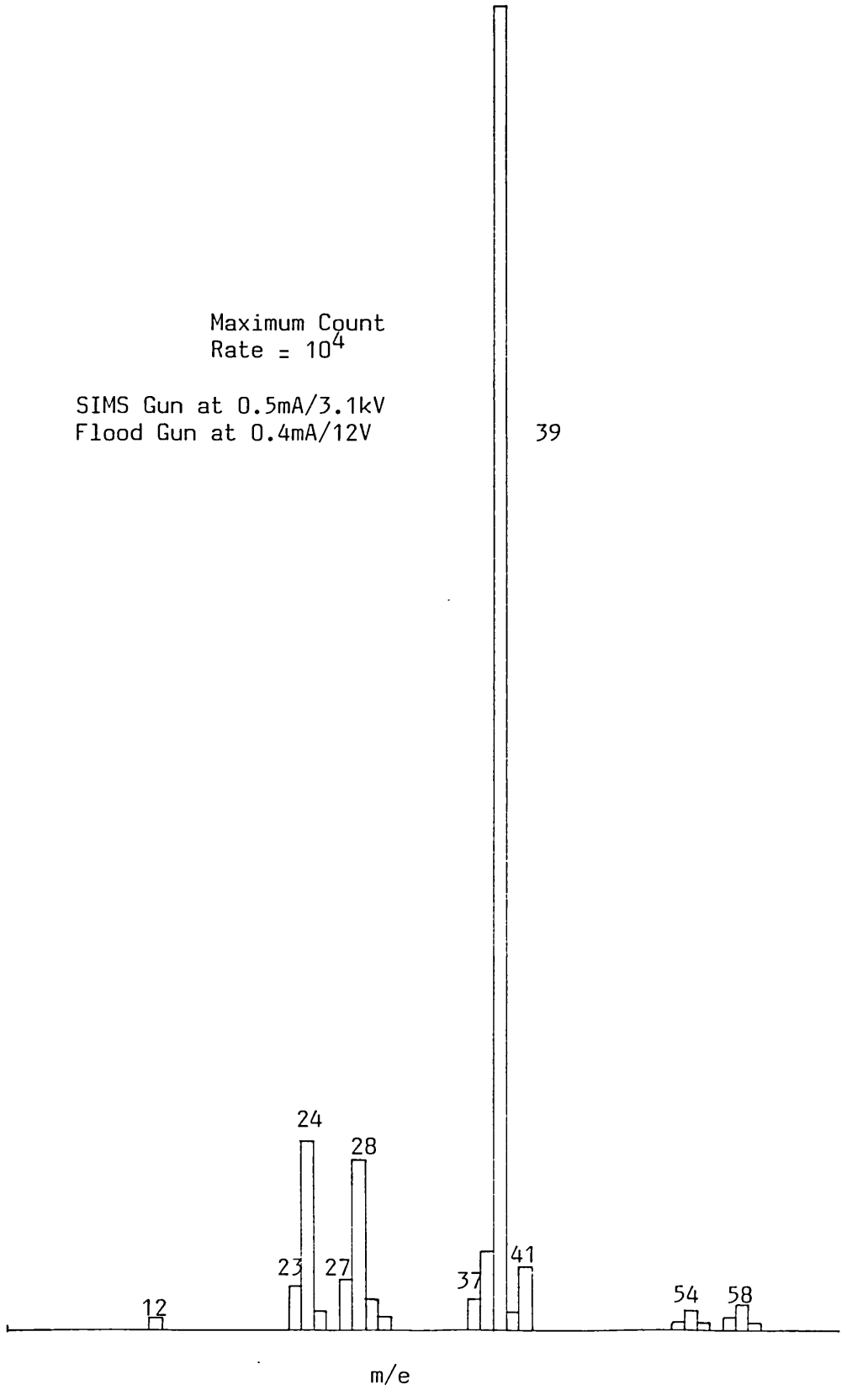

FIG. 55: Positive ion SIMS spectrum of air-cleaved muscovite mica.

vacuum-cleaved surfaces of mica showed remarkable differences in the overall spectra but each spectrum on its own was devoid of much structure. Again, because of uncertainty in the position of the Fermi level in an insulator, not much useful information could be extracted from the UPS measurements of mica.

5.3.4 ADSORPTION OF CARBON DIOXIDE

Exposure of the untreated air-cleaved surface of mica to carbon dioxide up to a pressure of 10^{-5} torr did not cause any increase in the carbon 1s peak intensity nor was any other carbon state observed. The carbon contamination layer already existing on the mica surface was presumed to have precluded any further adsorption of carbon dioxide. However very small amount of adsorption would have been undetectable because of the very large carbon peak already present.

No exposure experiments were carried out on the hydrogen-atom bombarded mica surface for two reasons: (i) the arrangement for atomisation was not available for the most part of the work and (ii) the filament finally used was made of tantalum and this proved unsuitable because some tantalum was evaporated on to the mica surface at the temperature used for atomisation.

It was shown earlier that the XPS spectrum of vacuum-cleaved mica had a small C1s peak which might conceivably come from the air-cleaved corners. The binding energy of this peak after correction for charge-shift appeared to be 285.7 ± 0.3eV. When the vacuum-cleaved surface was exposed to carbon dioxide, the intensity of this peak increased. One typical result obtained after an exposure to 600L

(1L = 10^{-6} torr sec.) of carbon dioxide is shown in Fig. 56. After subtraction of the nonlinear background, the carbon 1s peak is found to have increased in area by three times. Only a part of this gain by the C1s could be removed on heating to a temperature of 670K.

In a separate experiment, it was found that a mica sample which had been vacuum-cleaved and subsequently exposed to the air showed a C1s peak as big as the one obtained from an air-cleaved surface. However it was not possible to produce an equally big carbon peak by simply exposing the vacuum-cleaved surface to carbon dioxide. It was thought that water vapour in the atmosphere might in some way promote carbon dioxide adsorption. Exposure of the vacuum-cleaved surface to a mixture of carbon dioxide and water did not, however, generate the desired result.

Some other factor thus appears to be involved in the interaction of carbon dioxide from the atmosphere with mica surface to produce the large carbon contamination of an air-cleaved surface. The C1s peak, which appears at a binding energy of 285.7 ± 0.3eV, must be identified with the carbon dioxide species studied in the desorption experiments in the glass system. However the XPS data show that only a part of the carbon is removed by heating to a temperature of 670K. This shows that although there is a single photoemission peak, some adsorbed species are more strongly held than others.

When discussing the second order kinetics found for desorption of carbon dioxide it was proposed that the adsorbed species was a carbonate formed by interaction with a surface hydroxyl group:

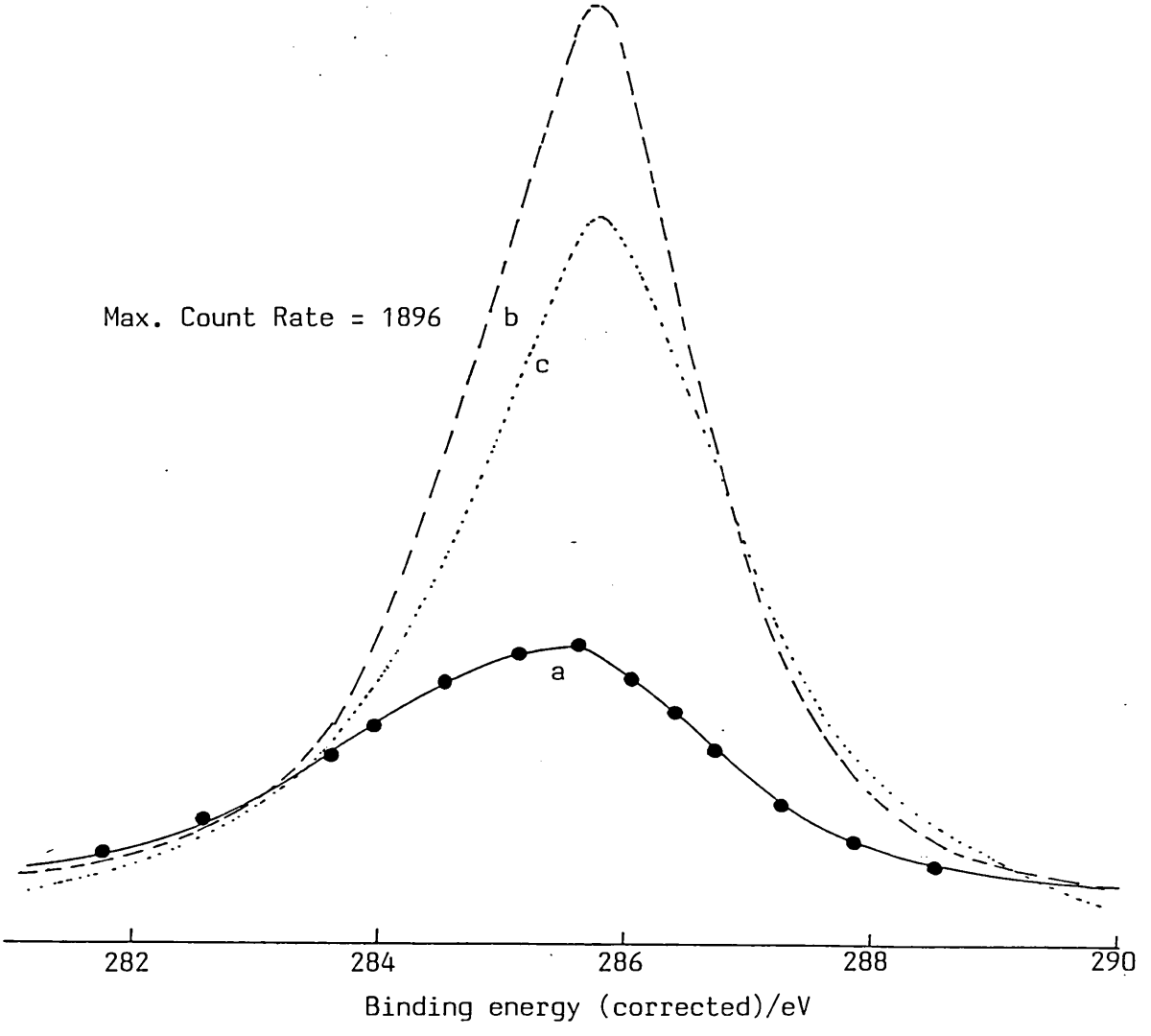

FIG. 56: Change in C1s peak intensity after the vacuum-cleaved mica surface was exposed to carbon dioxide,

a - C1s peak before exposure,
b - C1s peak after exposure to 600L CO_2,
c - C1s peak after heating to 670K.

(Grazing emission with CAE =20eV, step size = 0.05eV, 10 secs. x 25 scans).

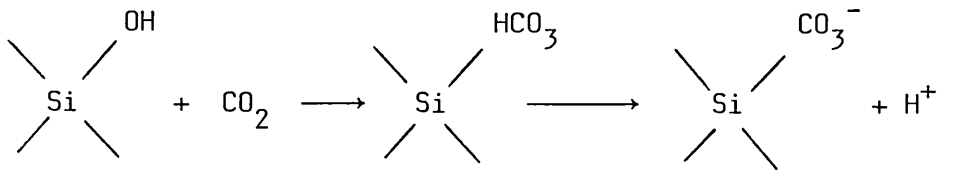

The protons become trapped at basic sites as shown earlier and desorption can occur only by migration of the protons back to the carbonate complex. There is likely to be a variety of basic sites in the mica surface at some of which the protons may be very strongly held. Thus insufficient protons may be available to cause the desorption of all the carbon dioxide leaving a residue of irreversibly adsorbed carbonate species on the surface.

The binding energy of the C1s peak is somewhat lower than the values reported in the literature for carbonate species. Kantschewa, Albano, Ertl and Knözinger (1983) have observed two C1s peaks in their study of the $K_2CO_3/\gamma\text{-}Al_2O_3$ system, one occurring at 285.7 ± 0.2eV and the other at 291eV binding energy. The first peak was found to be resistant to heating while the second peak almost disappeared above 520K. These authors have assigned the peak at 291eV to carbon in carbonate form while the peak at 285.7eV was assigned to an unspecified carbon contamination. In the case of mica, the potassium $2p_{3/2}$ peak (B.E. 293.75eV) was very broad and any small peak due to a species with a C1s binding energy in the region of 291eV would have been very difficult to detect.

There are considerable variations in the values of binding energy reported in the literature for carbonyl carbon atoms. Barteau and Madix (1983), for example, reported a C1s binding energy of 287.7eV

for an adsorbed = CO_3 species and 287.2eV for an adsorbed - CO_2 species, both formed when carbon dioxide was adsorbed on preadsorbed oxygen on a silver surface. Bonzel and Krebs (1981) on the other hand reported a value of 290.7eV for the binding energy of a carbonate carbon. Gelius et al. (1970) have carried out a detailed investigation of the theoretical and experimental binding energy shifts of the C1s level in a large number of compounds and have concluded that the shifts are predominantly influenced by the nearest neighbours and that the influence of hybridization of the carbon atom is negligible. No XPS data for adsorption of carbon dioxide on zeolites, silica-aluminas or clay-minerals could be found in the literature and it is thus not possible to arrive at a definite conclusion regarding the state of carbon on the mica surface but a carbonate complex certainly cannot be ruled out.

A completely unexpected result was obtained when the muscovite sample was cleaved in 10^{-5} torr pressure of carbon dioxide. Two very prominent carbon peaks appeared in the grazing emission spectra with binding energies of 285.75 and 279.55eV and there was another small peak at 289.50eV. The spectra, after background subtraction, are shown in Fig. 57. It is interesting to note that the peak at 279.55eV was very much attenuated in the normal emission spectra, appearing with only one tenth of the intensity of the peak in the grazing emission. On heating to 570K the peaks at 285.75 and 279.55eV came down in intensity by almost equal amounts and the peak at 289.50eV almost disappeared. When the sample was reexposed to carbon dioxide (~600L) all three peaks showed an increase in intensity, but the low binding energy C1s peak showed a much more enhanced intensity. On the other hand, after a day in the Analysis Chamber at a pressure of 5×10^{-11}

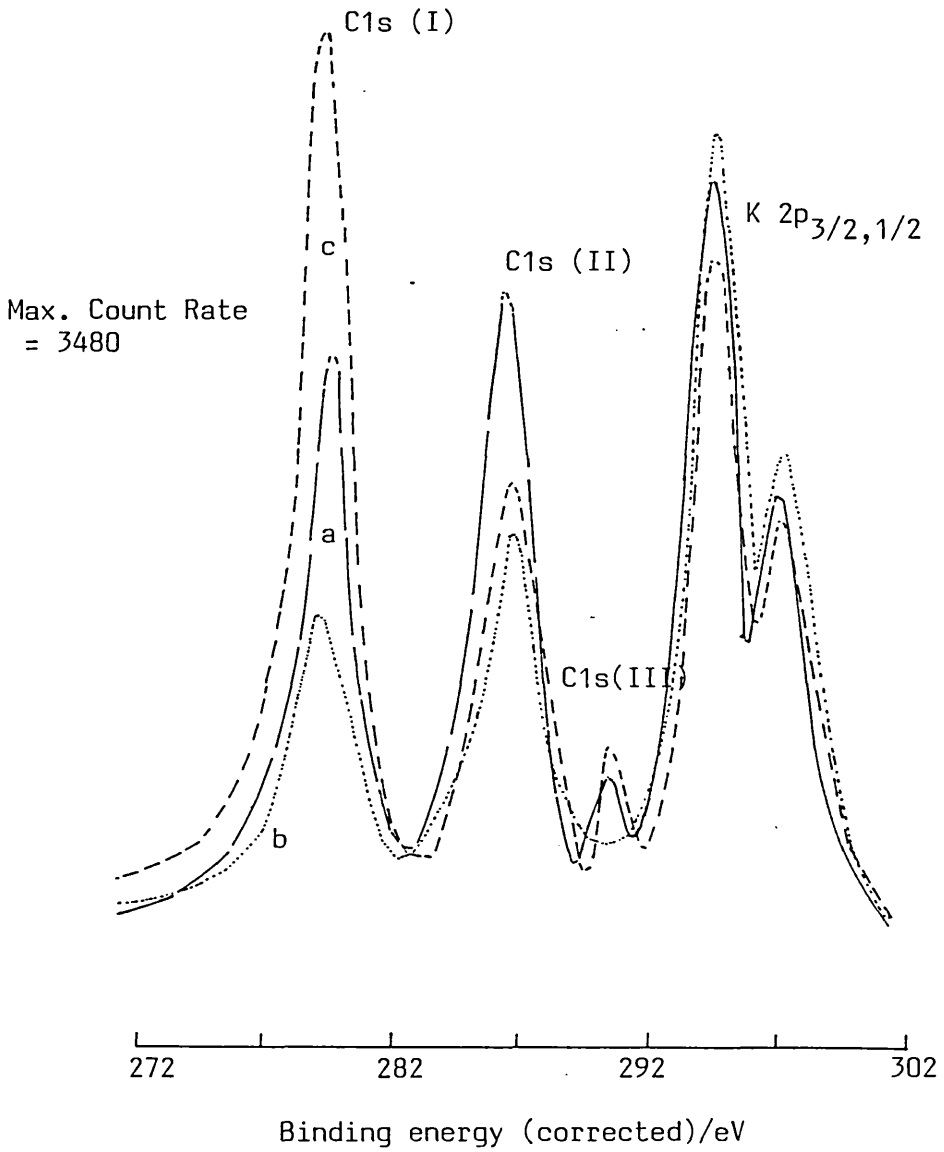

FIG. 57: C1s and K $2p_{3/2,1/2}$ XPS peaks from the photoelectron spectrum of a mica surface cleaved in 10^{-5} torr CO_2,

a - Immediately after cleaving.
b - After outgassing at 570K for 15 mins.
c - After re-exposure to 600L CO_2.

(Grazing emission XPS with CAE = 50eV, step size = 0.25eV, 10 secs. x 10 scans).

torr, the peaks at 279.55 and 289.50eV disappeared and only the peak at 285.75eV remained.

The appearance of two main carbon peaks cannot be attributed simply to the effect of gross surface charging since no splitting was observed for any of the other peaks of mica. The peak at 279.55eV was apparently a negatively charged carbon species. No C1s peak with a binding energy as low as this has been found in the literature although carbidic carbon is known to give low binding energies. For example, Ramqvist et al. (1969) measured the C1s binding energies for the covalent carbides of Group 4b, 5b and 6b metals and found that hafnium carbide had the lowest C1s binding energy with a value of 281.0eV (referenced to adventitious C1s = 285eV). Recently Tanaka et al. (1984) have reported a value of 281.2eV for the C1s binding energy in titanium carbide. No data has been found concerning the C1s binding energies of ionic carbides and acetylides (C_2^{-2}) of alkali and alkaline earth metals. From XPS measurements on silicon carbide in the present work, two C1s peaks were obtained with a binding energy difference of 4eV. If the adventitious carbon is assigned a C1s binding energy of 284.6eV then that for the carbidic carbon would be 280.6eV.

Although a carbidic form of carbon cannot be ruled out, the mechanism of its formation is hard to understand. The most likely explanation would be a carbide or acetylide of potassium formed by decomposition of carbon dioxide on some local excess of potassium ions immediately after cleaving. Such a species is likely to produce a C1s binding energy of quite low value. Alkali metal carbides and acetylides are also known to be relatively unstable. The problem with this type of model is to find a suitable location for the oxygen atoms, bearing in mind that part of the adsorption is reversible. One also has to

give a convincing explanation for the lack of such dissociative adsorption of carbon dioxide when the mica is cleaved in vacuum and the gas is added subsequently.

There is some evidence that the C1s peaks may arise from the same state of adsorption existing in different electrical environments. Thus both peaks (at binding energies 279.55 and 285.75eV) diminish at approximately the same rate when the mica is heated, showing that they have similar adsorption energies. A degree of interchangeability also appears to exist between the two carbon states. Initial adsorption of carbon dixoide during cleavage of mica produced peaks of approximately equal intensity but after desorption and readsorption there was a transfer of intensity from the high binding energy peak to the low binding energy peak. The opposite effect was observed when the mica sample was left in ultra-high vacuum for a few days, the whole of the intensity being transferred to the high binding energy peak.

It is significant that the abnormal carbon peak (binding energy 279.55eV) appeared only when the sample was cleaved in carbon dioxide. The actual process of cleaving was thus a significant factor in its formation. After cleaving, although each face of the sample possesses half a monolayer of potassium ions to maintain electrical neutrality, there is evidence that some regions of the mica surface remain potassium-rich and others potassium-deficient. Such non-uniform distribution of potassium ions produces patch fields on the surface. It may be that carbon dioxide adsorbs preferentially on patches which are deficient in potassium. If the excess negative charge on such patches is sufficient to lower the electrical potential by a few volts, this would give an adequate explanation of the anomalously low binding energy found for the carbon peak. It would also explain the slow disappearance of

this peak over a period of days as the potassium ions rearranged to give a more uniform surface distribution. The situation envisaged may be as follows:

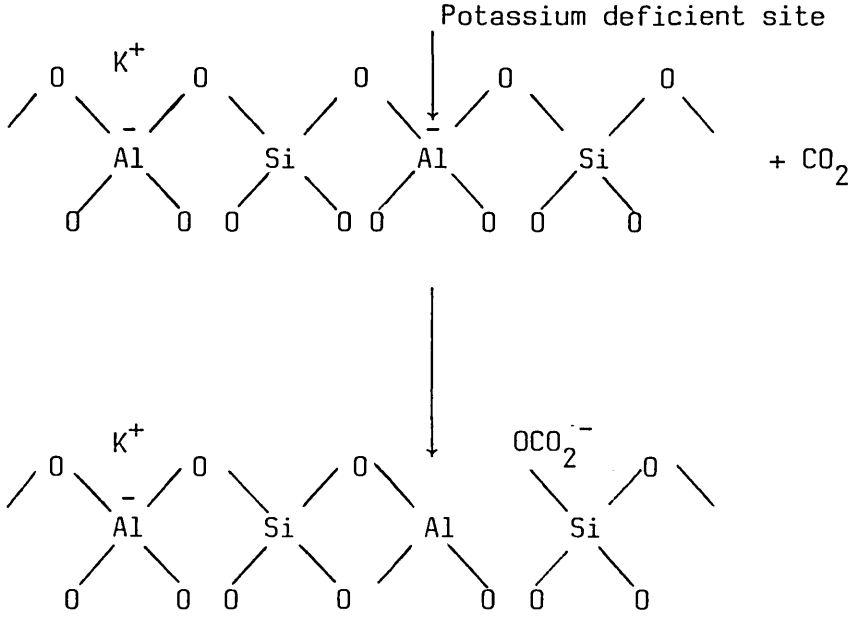

Although the normal carbonate species is formed there is now no nearby compensating positive charge and the carbon atom will be in a highly negative potential.

5.3.5 ADSORPTION OF AMMONIA

No ammonia adsorption could be detected by XPS measurement on the air-cleaved mica surface even after exposure to ammonia under its own vapour pressure. This result was hardly surprising since the air-cleaved surface could not be expected to show any reactivity with the large carbonaceous overlayer present. The air-cleaved surface had to be outgassed for more than 18 hours at a temperature of 500K under UHV conditions before ammonia adsorption could be detected. The wide-

scan photoelectron spectrum of the mica surface after room temperature exposure to 600L of ammonia is shown in Fig. 58. Ammonia was introduced to the mica sample in the Preparation Chamber. This chamber had subsequently to be evacuated to a pressure of approximately 10^{-8} torr before the sample could be transferred to the Analysis chamber for XPS measurement. Thus, any weakly held ammonia species would be removed from the mica surface before measurements were made. It is therefore possible that the first of the two states found during desorption experiments in the glass apparatus might not be observed in XPS. The N1s peak was very small and broad and it did not increase in intensity after the surface was given larger exposures. The C1s peak was still very big even after outgassing for 18 hours.

Ammonia adsorption was also investigated on the vacuum-cleaved mica surface after it had first been heated at a temperature of 500K for 30 minutes to get rid of adsorbed water vapour. A narrow 10eV scan of the N1s peak on the vacuum-cleaved surface after subtraction of the nonlinear background is shown in Fig. 59. The peak is almost as big as the one observed on the air-cleaved mica surface. Because of the small signal to noise ratio (~26:1) and the very broad nature of the N1s peak, it was not possible to determine accurately the FWHM value, but it must be around 5eV. The binding energy of the peak was calculated to be between 399.75 and 400.00eV with respect to the K $2p_{3/2}$ binding energy reference.

After exposure to ammonia, the following binding energies could be assigned to the main constituents of mica:

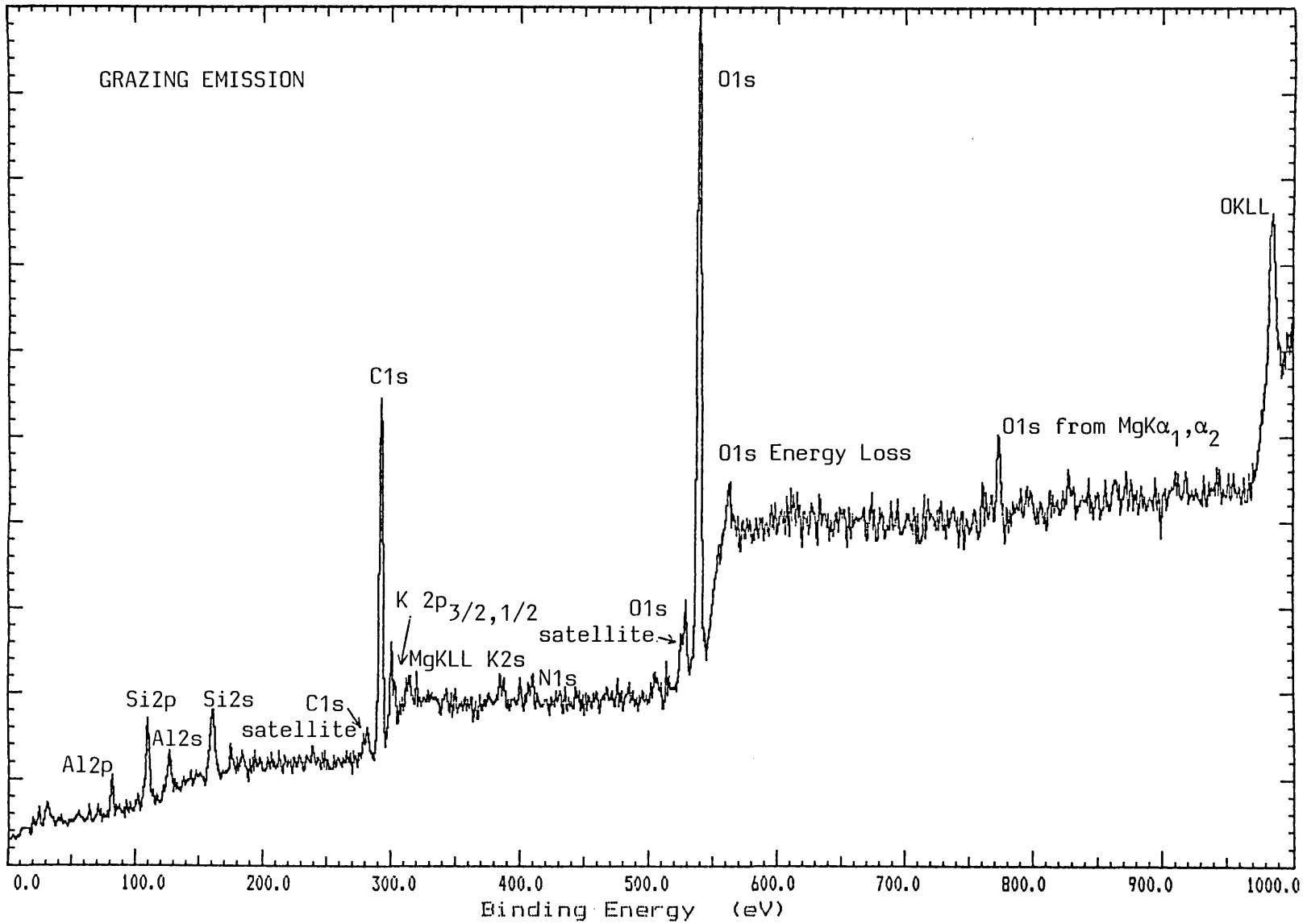

FIG. 58: Photoelectron spectrum of an air-cleaved, outgassed mica surface exposed to 600L ammonia vapour.(Binding energies uncorrected, signal-to-noise ratio 205:1).

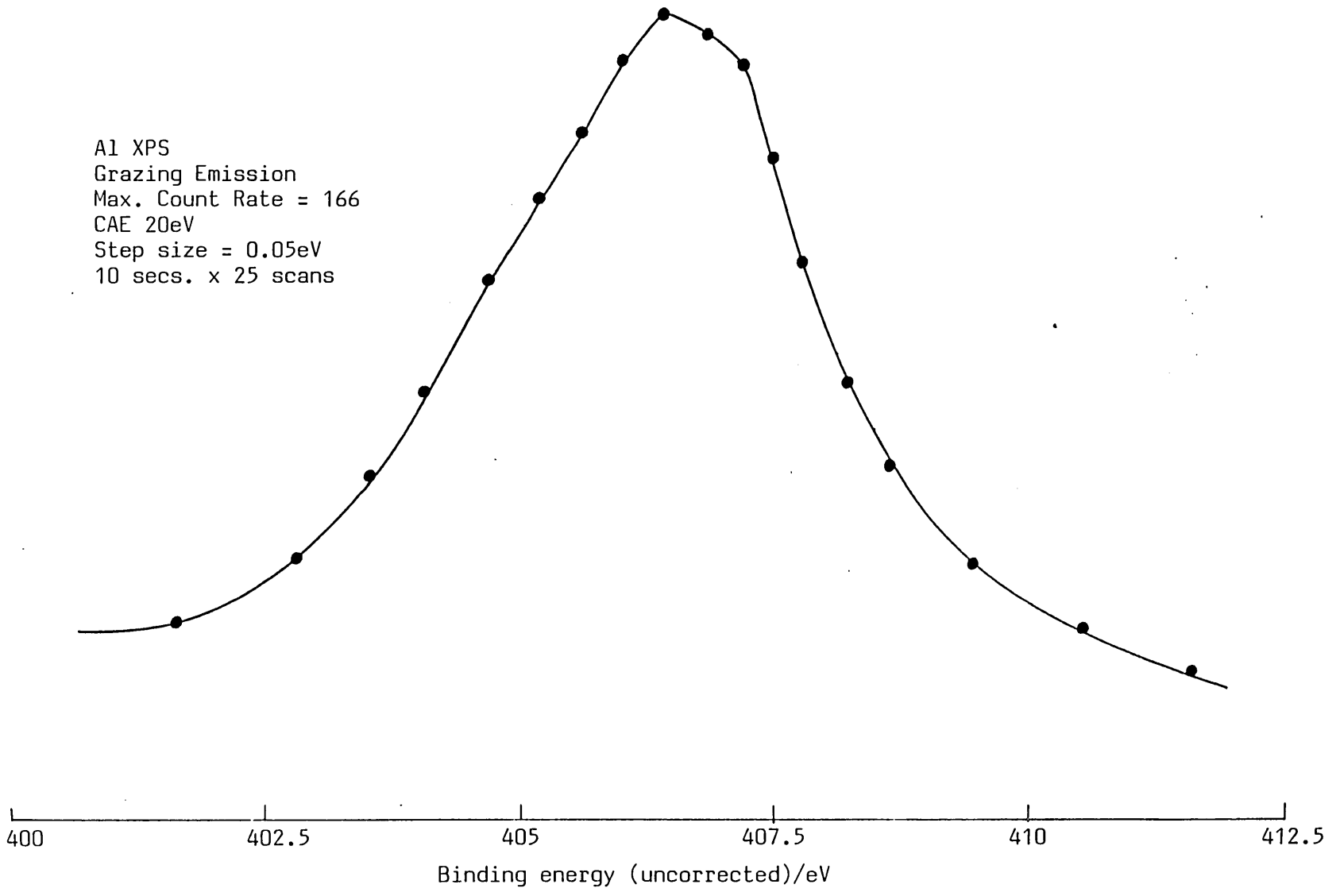

FIG. 59: The N1s peak after the vacuum-cleaved mica surface was exposed to 600L ammonia vapour.

Al 2p	74.75eV
Si 2p	102.70eV
C1s	285.60eV
K $2p_{3/2}$	293.75eV (reference level)
O1s	531.80eV

No significant shift in the peaks is noticeable excepting the Al 2p peak which appeared at a slightly higher binding energy compared to the adsorbate-free surface. This might indicate a specific interaction between aluminium and ammonia although the binding energy shift is in the opposite direction to that expected if there is a donation of electrons to the aluminium.

The N1s peak disappeared when the surface was heated to a temperature of 470K in agreement with the desorption data given in Chapter 3. However when gas exposure was carried out at a temperature of 370K, a small N1s peak could still be detected.

Very few XPS measurements have been made of ammonia adsorbed on the so-called acidic solids. Rogers et al. (1980) found a N1s peak at 400.3eV for ammonia adsorbed on an oxidized aluminium surface. The peak was attributed to molecularly held ammonia. If ammonia dissociates on adsorption into $-NH_2$ or =NH groups or it adsorbs on Brönsted acid sites, the binding energy of N1s electron is expected to be higher. On this basis and from infra-red measurements, Rogers et al. have precluded the existence of Brönsted acid sites on an oxidized aluminium surface. However, such a conclusion cannot be based entirely on the binding energy of the N1s electron. Defosse and Canesson (1976) studied the adsorption of pyridine on NH_4-Y zeolites activated at temperatures above 570K. Two N1s photoemission peaks were observed with

binding energies in the ranges 397.5 - 398.3eV and 399.5 - 400.5eV. The lower binding energy peak was attributed to adsorption at Lewis acid sites and the higher binding energy peak to adsorption at Brönsted acid sites. If this assignment is accepted there is insufficient reason for rejecting Brönsted acid sites simply because the N1s binding energy is around 400eV, although some allowance must be made for the different nitrogen environments in pyridine and ammonia.

On mica the N1s peak was too broad to allow specific characterization to be made but the peak maximum at ~400eV is close to the upper N1s binding energy found for pyridine. This may indicate the existence of some Brönsted as well as Lewis acid sites. The large FWHM value could point to a distribution of acidic sites over a wide range of acid strengths.

Mica surfaces were also exposed to pyridine under its own vapour pressure, but no N1s XPS signal was seen nor was there any change in the C1s signal. It may be that the pyridine molecule is too large to adsorb at the tetrahedral aluminium sites which lie inside the mica surface.

5.3.6 REACTIVITY OF MICA SURFACES TOWARDS A VARIETY OF SOLVENTS

The reactivity of mica surfaces and particularly their ion-exchange properties were investigated in aqueous solutions of ammonia, sodium hydroxide, lithium chloride and sulphuric acid. The usual procedure was to cleave the mica while it was immersed in the liquid and to keep the freshly cleaved portions under the liquid for 3-4 hours. The sample was then thoroughly washed with deionized water and dried before being introduced into the ESCALAB system. Sufficient time was allowed for the sample to outgass under UHV conditions before XPS measurements were taken.

The photoelectron spectrum of a mica surface after the above treatment had been carried out with aqueous ammonia solution (~35% NH_3) is shown in Fig. 60. The spectrum is remarkable in several respects, namely,

(i) the potassium peaks had almost disappeared,

(ii) the nitrogen 1s peak was more prominent than when the surface was exposed to ammonia vapour,

(iii) the silicon peaks were very much reduced in intensity compared to the aluminium peaks, and

(iv) the silicon and aluminium peaks were very broad, with FWHM values more than 5eV and both Al 2p and Al 2s peaks were split. The C1s peak also appeared to be composed of two peaks.

It was difficult to assign binding energies to the peaks. The K $2p_{3/2}$ and $2p_{1/2}$ peaks were indistinguishable and were unsuitable for use as a reference. The silicon and aluminium peaks also cannot be used for the reasons stated above. If a binding energy of 285.6eV is assigned

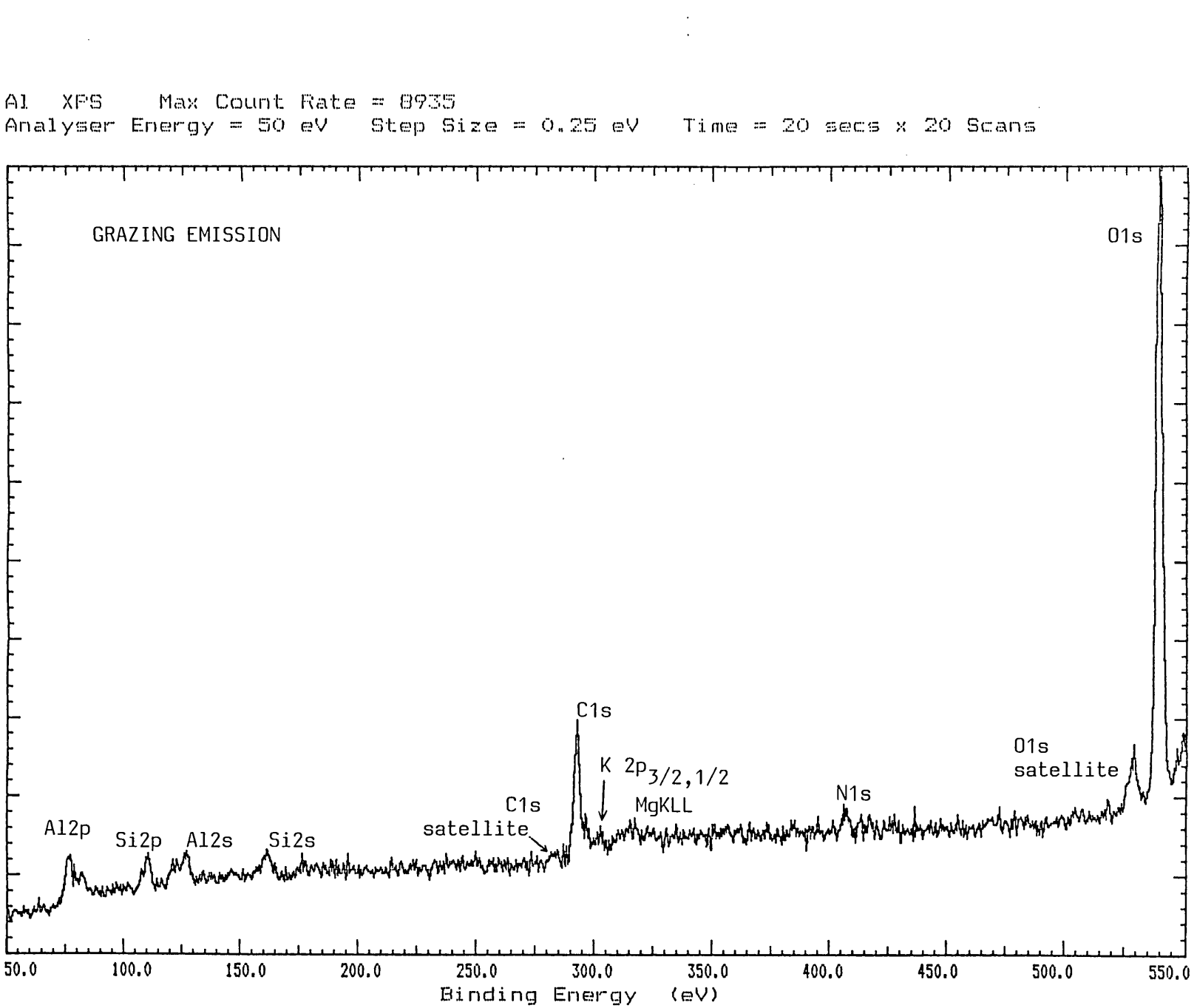

FIG. 60: Photoelectron spectrum of a mica surface cleaved under aqueous ammonia and kept immersed for 6 hours.(Binding energies are uncorrected, signal-to-noise ratio 226:1).

to the main C1s peak, the N1s peak is found to appear at 400.6eV. This value is ~0.6eV higher than the binding energy of the N1s peak in case of the mica surface exposed to ammonia vapour.

More detailed information concerning the shape of the N1s peak was obtained from narrow scans with a sweep width of 10eV. The spectrum after subtraction of the nonlinear background is shown in Fig. 61. The peak was very broad with a FWHM of ~3.8eV. Since most of the potassium ions appear to have been removed from the mica surface on treatment with aqueous ammonia, the obvious conclusion is that ammonium ions replace potassium as interlayer ions in at least the top layers of mica, giving an ammonium form of the muscovite mica as shown below,

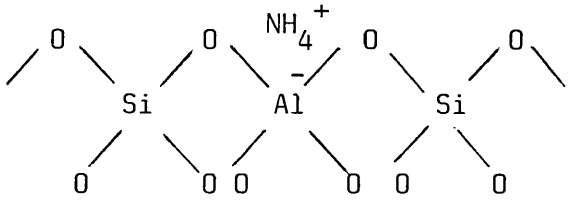

Ammonium form of the tetrahedral layer of mica

The two Al 2p photoemission peaks were found to have a separation of ~4.5eV. Such a large shift cannot easily be explained. It seems that the ammonium ions have caused a drastic modification of the environment around some of the aluminium atoms. This could be brought about by the neutralization of the ammonium ion according to the following process:

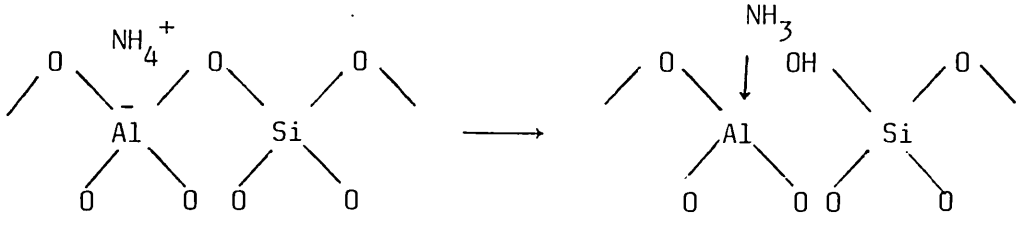

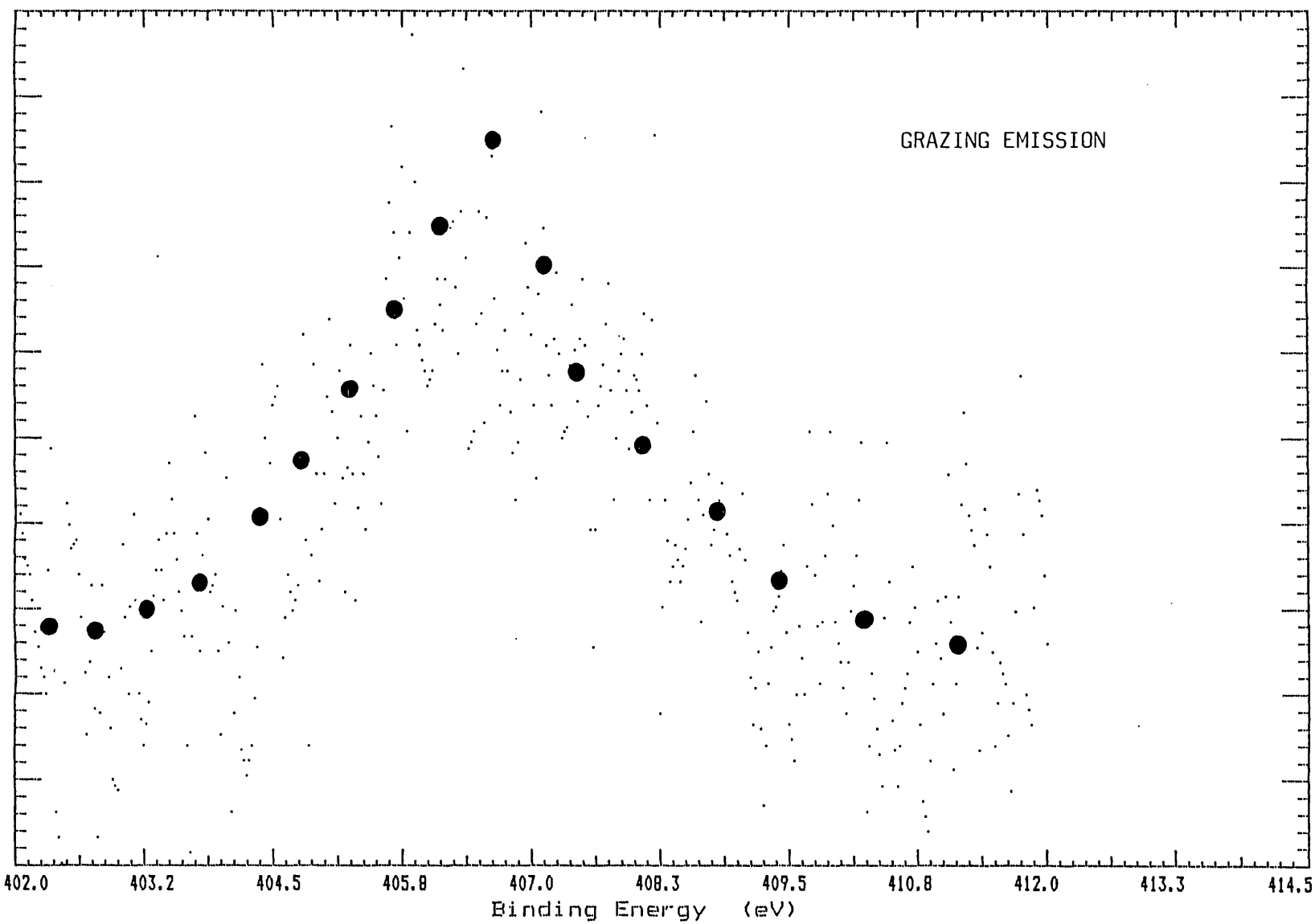

FIG. 61: The N1s peak from a mica surface cleaved under aqueous ammonia and kept immersed for 6 hours. (The actual noise level is shown).

It is not clear, however, whether such a change is sufficient to account for the large shift in the Al 2p binding energy. It might be argued that a similar splitting of the Al 2p peak should have been observed after adsorption of ammonia from the vapour phase on the mica surface. The reason why such a splitting was not observed may be that insufficient ammonia was adsorbed to produce a detectable effect on the Al 2p peak.

The splitting of the aluminium XPS peaks could not be explained away as due to gross charging of the sample because the equivalent effect was not seen for the other peaks. A small, additional C1s peak was shown by the photoelectron spectrum at a binding energy about 4eV greater than the usual carbon peak seen on the air-cleaved mica surface. This may represent some form of interaction between carbon dioxide and the ammonium ions in the surface.

Prada-Silva et al. (1979) have described an acidic mica surface obtained by treating mica with aqueous ammonia followed by heating, but no characterization of the surface was reported. The present investigation definitely demonstrates the exchangeability of potassium ions with ammonium ions. Much work, however, will be necessary to characterize the ammonium form of mica and to categorise its chemical activity towards various substances. The 'acidic surface' to be obtained by calcination of the ammonium form of mica holds important possibilities as an attractive model for an acidic catalyst.

Attempts were also made to exchange the potassium ions with sodium and lithium ions but these experiments were unsuccessful. After cleavage under a 1N solution of either sodium hydroxide or sodium chloride, followed by 6 hours immersion, the mica surface gave an XPS spectrum which was more or less identical to the one obtained from the air-cleaved surface. No appreciable change in the Na KLL peak or in any other

constituent peak of mica was observed. It appears that the sodium ions are too small to provide an effective exchange with potassium ions in the mica surface.

Although no exchange was observed when mica was cleaved under a 1N LiCl solution, the XPS measurements did show significant changes. The intensities of all the peaks were reduced by at least four-fold and the silicon and aluminium peaks became very broad. It is thought that the strongly corrosive LiCl solution had attacked the mica surface to some extent destroying the structure of the top layers.

Mica samples were also cleaved under 1N sulphuric acid. The photoelectron spectrum of the resulting surface was similar to that of an air-cleaved mica surface with one important difference. The C1s signal was now split into two peaks with binding energies of 285.85 and 282.25eV with respect to the K $2p_{3/2}$ binding energy of 293.75eV. The C1s peaks after background substraction are shown in Fig. 62 for grazing emission. It was likely that during the washing and drying operations of the acid-treated surface another carbon species was formed on the mica surface. The exact structure of the carbon species at the binding energy of 282.2eV is again uncertain. There may be some connection between this species and the one observed earlier when a mica sample was cleaved in carbon dioxide, although the binding energies do not match. Also there was a C1s signal at low binding energy in the photo-electron spectrum of the worked-out surface of mica from the glass system.

The acid was most likely to protonate the mica surface with a consequent loss of some potassium. The protons might then attack the bridged oxygen sites of the tetrahedral layer according to the following scheme:

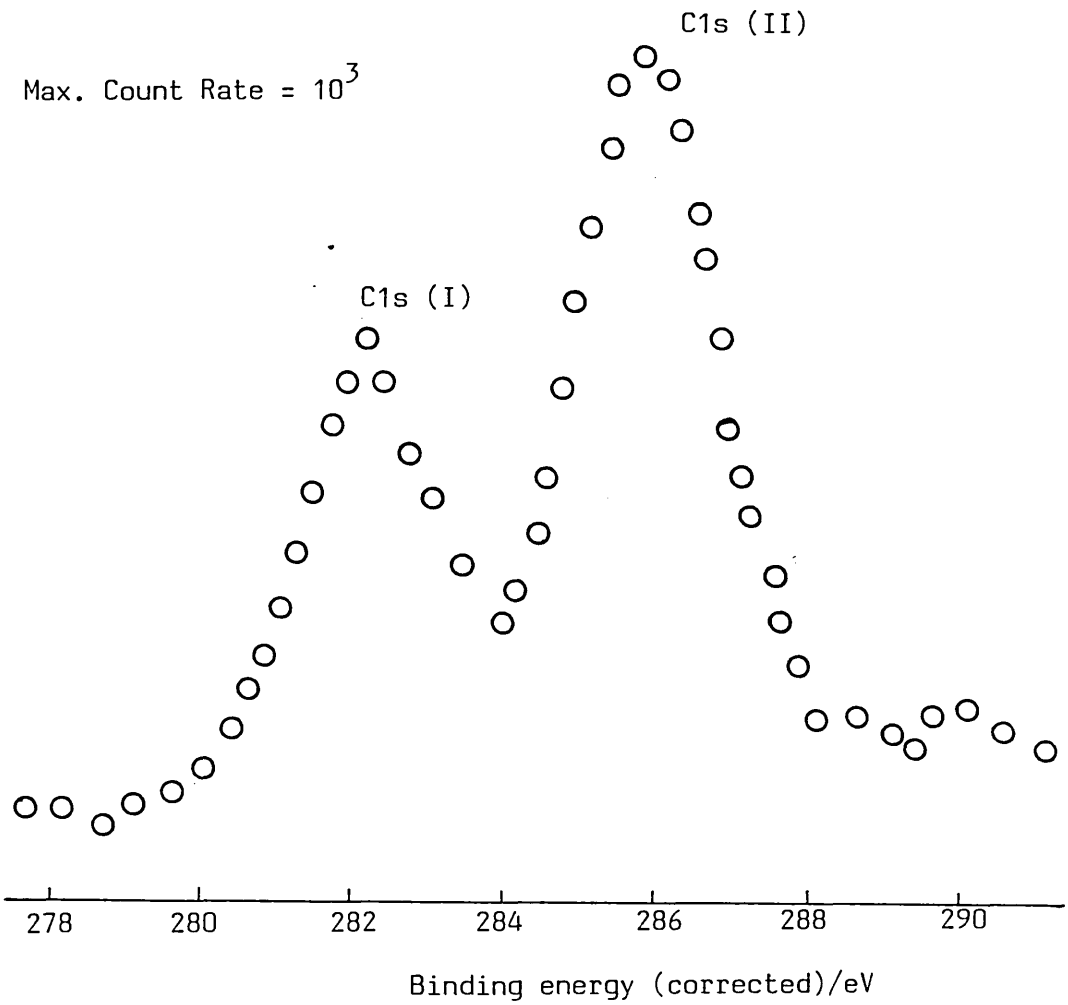

FIG. 62: Splitting of the C1s photoemission peak on an acid-treated muscovite surface (Grazing emission, CAE 20eV, manual scan).

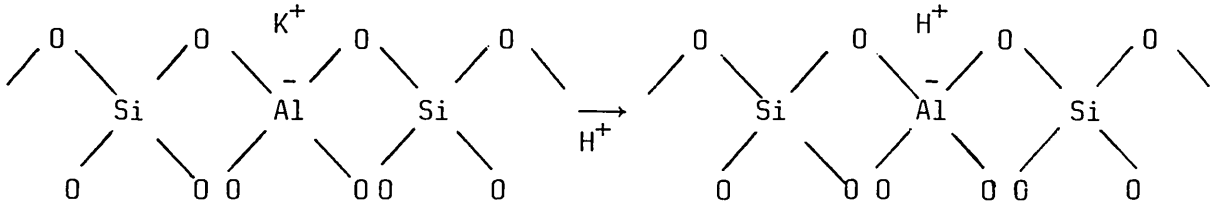

Tetrahedral layer Protonated layer

Hydroxylated surface

The hydroxylated surface could react with atmospheric carbon dioxide forming bicarbonate or carbonate species as outlined in Chapter 3. Thus both the C1s peaks are assigned to negatively charged carbonate species, the essential difference being the positioning of the compensating positive charge. In the normal mica surface the potassium ion provides this charge but in the potassium deficient surface, the charge resides on a proton which may migrate some distance from the carbon species.

Mica surfaces were also treated with methanol, acetone or pyridine using the procedure described above. In all the cases, XPS measurements gave spectra similar to those obtained from an air-cleaved mica surface. Also no significant change was observed after treatment with water. However any change in the state of hydroxylation of the surface would not have been detected because of the presence of the very intense oxygen peak in all photoelectron spectra taken with mica samples.

CHAPTER SIX

CONCLUSION

In this work clean mica surfaces have been shown to be chemically reactive towards both ammonia and carbon dioxide. The normal chemical inertness of the surface must therefore be due to the carbonaceous overlayer which is always present on the air-cleaved surface. Since carbon dioxide has been shown to react with clean mica surfaces it seems reasonable to suppose that this carbon overlayer is formed largely through the action of carbon dioxide present in air. However it has not been possible to generate the same amount of carbon on a vacuum-cleaved mica surface simply by exposing the surface to carbon dioxide. It would seem that some other constituent of air is important in promoting the carbon layer although the actual constituent and its mode of operation have not been discovered. More research is clearly needed in this area.

The carbon contamination must be removed to make the mica surface chemically active. Prolonged heating at 500K in ultra-high vacuum reduces the carbon appreciably but to remove all the carbon the mica has to be heated to temperatures at which it begins to decompose. XPS measurements have shown that an undesirable effect of prolonged heating is a severe depletion of potassium in the surface layer. A more efficient way of removing carbon is by bombardment with hydrogen-atoms and this method has the advantage that it does not remove the surface potassium ions. However, the best method of cleaning is undoubtedly through cleavage.

Characterization of the mica surface by XPS has produced some

interesting results. Abnormal elemental ratios have been obtained from XPS intensity data which are explicable in terms of distortions in the mica structure. The photoelectrons in an insulator have quite a small mean free path and therefore the sampling depth is much less than in a conducting sample. It should thus be possible to use XPS at various angles of emission to determine not only elemental ratios at certain depths but also to locate the position of atoms with respect to the surface level. The photoemission spectra also show some very interesting shifts in apparent binding energy when the mica surface is exposed to various gases. These shifts have been interpreted in terms of changes in the dipole field existing at the surface. These apparent shifts may be very useful in comparing the strengths and direction of electrical fields at insulator surfaces.

The LEED patterns of the muscovite mica have been found to be very irregular. Such irregular patterns have been reported previously for a mica surface cleaved in vacuum. In the present work, irregular LEED patterns have been shown to be produced by a mica surface cleaved in one atmosphere of argon. The air-cleaved surface on the other hand did not give a stable pattern whilst the vacuum-cleaved surface produced further distortion in the pattern. These abnormal patterns have been attributed to surface electrical fields and also to the variable amount of surface charge depending upon the energy of the electron beam.

The clean mica surface has been shown to adsorb both carbon dioxide and ammonia. The adsorption site is thought to be located in the tetrahedral layer of silicon and aluminium atoms and the site appears to be generated by a process analogous to the generation of acidic sites in zeolites, silica-aluminas and other clay-minerals. It has been shown that some depletion of potassium ions is a necessary pre-requisite to

adsorption activity. Normally the missing potassium ions will be replaced by hydroxonium ions. The impossibility of completely removing water from the mica surface supports the formation of hydroxonium ions. These can attack some of the bridged oxygen sites of the tetrahedral layer causing partial hydroxylation and creating both Brönsted and Lewis acid sites.

The measured uptakes of ammonia and carbon dioxide on mica were small and therefore unlikely to have been detected in large, conventional stainless steel systems by volumetric measurement. The limited extent of adsorption is in agreement with the idea that adsorption occurs only at special acid sites since these will have a relatively low concentration in the surface. Ammonia has been shown to have two adsorption states on a mica surface and both follow first order desorption kinetics. For carbon dioxide, the reversible state of adsorption has been discovered with second order kinetics of desorption. A mechanism involving initial formation of a surface bicarbonate followed by transformation into a carbonate and migration of the proton has been proposed to account for the second order kinetics. XPS measurements have shown that only part of the carbon 1s photoemission peak, obtained when the clean mica surface is exposed to carbon dioxide, can be removed by heating, indicating that there is also a stronger, irreversible adsorption of carbon dioxide.

A surprising result has been the additional C1s photoemission peaks observed when mica was cleaved in carbon dioxide as compared to experiments in which the carbon dioxide was added subsequently. The question arises as to whether these additional C1s peaks represent distinctively different carbon species or whether they merely reflect a change in the surrounding electrical environment. This kind of problem is peculiar

to insulating materials in which measured binding energies of the photoemission peaks are not referenced to the Fermi level of the electron energy analyser. Any interpretation of the data must account for the fact that these anomalous carbon peaks disappear when the mica surface is left in vacuum for a long time, leaving only the normal carbon peak, which reaches its intensity similar to that found on the air-cleaved mica surface. It would seem that some slow, activated surface re-arrangement is responsible for these changes, most probably a diffusion of potassium ions across the surface to give a more uniform distribution. The shift in apparent binding energy of the C1s peak can then be accounted for in terms of charge mosaics formed on the surface during the act of cleavage. However the details of this process still need to be worked out.

The existence of small number of acidic sites on a well-outgassed mica specimen was further verified by its ability to catalyse the isomerization of cyclopropane. As already mentioned, the number of acidic sites can be increased by removing the potassium ions from the surface. It was also seen that the potassium ions could be exchanged with ammonium ions by cleaving the mica surface under aqueous ammonia. There was not time to study this surface in detail but it is expected to be highly active, especially after ammonia has been removed by heating, leaving what should be a highly active acidic surface.

The mica surface was found not to be affected much by acid and alkali; the XPS measurements did not show any drastic change in the surface composition. However, sulphuric acid treatment promoted the formation of a second species of carbon (binding energy = 282.25eV) on the surface which indicates that the reactivity of the acid-treated surface towards atmospheric carbon dioxide differed from that of the

vacuum-cleaved surface.

It must be said in conclusion that there is no reason why a suitably treated mica surface should not be used as a model for the acidic catalysts used in cracking and other processes. 'Ammonium-mica' would be particularly useful as a model for the synthetic mica-montmorillonites because of the remarkable structural similarities between the two. Much more work will be needed however to establish the ammonium form of mica as a viable catalyst.

REFERENCES

Adams, C.E., Kimberlin, C.N. Jr., Shoemaker, D.P., Proc. 3rd Int. Cong. Catal., Amsterdam 1964, Vol.2, Wiley, N.Y., 1965, p.1310.

Adams, J.M., Evans, S., Reid, P.I., Thomas, J.M. and Walters, M.J., Anal. Chem., 49, 2001, 1977.

Adams, J.M., Evans, S. and Thomas, J.M., J. Am. Chem. Soc., 100, 3260, 1978.

Amenomiya, Y. and Cvetanovic, R.J., J. Phys. Chem., 67, 114, 1963.

Amenomiya, Y., Chenier, J.H.B. and Cvetanovic, R.J., J. Phys. Chem., 68, 52, 1964.

Anganer, R.J. and Landolt, G.R., U.S. Patent 3702886, 1972.

Angell, C.L. and Schaffer, P.C., J. Phys. Chem., 69, 3463, 1965.

Angell, C.L. and Howell, M.V., Can. J. Chem., 47, 3831, 1969.

Bailey, S.W. in "Crystal Structure of Clay Minerals and Their X-ray Identification", (G.W. Brindley and G.Brown, eds.), Mineralogical Society, London 1980, Chapter 1, Structure of Layer Silicates.

Bailey, S.W., Clays and Clay Minerals, 32, 81, 1984.

Ballivet, D., Barthomeuf, D. and Pichat, P., J.C.S., Faraday Trans.1, 68, 1712, 1972.

Barr, T.L., Appl. Surf. Sci., 15, 1, 1983.

Barrer, R.M. in "Zeolites and Clay Minerals as Sorbents and Molecular Sieves", Academic Press, N.Y., 1978, p.414.

Barteau, M.A. and Madix, R.J., J. Electron Spectrosc. Rel. Phen., 31, 101, 1983.

Barthomeuf, D. in "Zeolites: Science and Technology", (F.R. Ribeiro et al. eds.), NATO ASI Series 1984a, p.317.

Barthomeuf, D., J. Phys. Chem., 88, 42, 1984b.

Basila, M.R., Kantner, T.R. and Rhee, K.H., J. Phys. Chem., 68, 3197, 1964.

Bassett, D.W. and Habgood, H.W., J. Phys. Chem., 64, 769, 1960.

Baun, W.L., Surf. Interface Anal., 2, 145, 1980.

Baun, W.L. and Solomon, J.S., Govt. Rep. Announce Index (U.S.), 80(14), 2638, 1980.

Benesi, H.A., J. Am. Chem. Soc., 78, 5490, 1956.

Benesi, H.A., J. Phys. Chem., 61, 970, 1957.

Benesi, H.A., J. Catal., 8, 368, 1967.

Benesi, H.A., J. Catal., 28, 176, 1973.

Benesi, H.A. and Winquist, B.H.C., Adv. Catal., 27, 97, 1978.

Bercik, P.G., Metzger, K.J. and Swift, H.E., Ind. Eng. Chem., Prod. Res. Dev., 17, 214, 1978.

Bertsch, L. and Habgood, H.W., J. Phys. Chem., 67, 1621, 1963.

Bierenbaum, H.S., Chiramongkol, S. and Weiss, A.H., J. Catal., 23, 61, 1971.

Bird, R.J. and Swift, P., J. Electron Spectrosc. Rel. Phen., 21, 227, 1980.

Bonzel, H.P. and Krebs, H.J., Surf. Sci., 109, L527, 1981.

Bourne, K.H., Cannings, F.R. and Pitkethley, R.C., J. Phys. Chem., 74, 2197, 1970.

Bragg, L., Claringbull, G.F. and Taylor, W.H. in "Crystal Structure of Minerals", Cornell University Press, 1965, Chapter 13, p.253.

Brandt, E.S., Untereker, D.F., Reilley, C.N. and Murray, R.W., J. Electron Spectrosc. Rel. Phen., 14, 113, 1978.

Breck, D.W. in "Zeolite Molecular Sieves", Wiley Interscience, N.Y., 1974.

Brown, G. and Norrish, K., Min. Mag., 29, 929, 1952.

Brown, H.C. and Johanneson, R.B., J. Am. Chem. Soc., 75, 16, 1953.

Brown, H.C. and Kanner, B., J. Am. Chem. Soc., 75, 3865, 1933.

Bryant, P.J. Trans. 9th Nat. Vac. Symp., Macmillan Co., N.Y., 1962, p.311.

Bryant, P.J., Taylor, L.H. and Gutshall, P.C., Trans. 10th Nat. Vac. Symp., Macmillan Co.,N.Y., 1963, p.21.

Cant, N.W. and Hall, W.K., J. Catal., 25, 161, 1972.

Castle, J.E., Hazell, L.B. and West, R.H., J. Electron Spectrosc. Rel. Phen., 16, 97, 1979.

Chambers, T.S. and Kistiakowsky, G.B., J. Am. Chem. soc., 56, 399, 1934.

Chao, K., Chiou, B., Cho, C. and Jeng, S., Zeolites, 4, 2, 1984.

Chappell, R. and Hayward, D.O., J. Vac. Sci. Technol., 9, 1052, 1972.

Chu, P., J. Catal., 43, 346, 1976.

Clark, D.T. and Thomas, H.R., J. Polym. Sci., 14, 1671, 1976.

Clark, A., Holm, V.C.F. and Blackburn, D.M., J. Catal., 1, 244, 1962.

Collins, R.H. and Turnbull, J.C., Vacuum, 11, 119, 1961.

Cox, P.A., Egdell, R.G., Harding, C., Patterson, W.R. and Tavener, P.J., Surf. Sci., 123, 179, 1982.

Davidtz, J.C., J. Catal., 43, 260, 1976.

Deer, W.A., Howie, R.A. and Zussman, J. in "Rock-forming Minerals", Vol.3, (Sheet Silicates), Longman, London,1962.

Defosse, C. and Canesson, P., J.C.S., Faraday Trans. 1, 72, 2565, 1976.

Defosse, C. and Rouxhet, P.G., in "Advanced Chemical Methods for Soil and Clay Minerals Research", (J.W. Stucki and W.L. Banwart, eds.), D. Reidel, 1980, p.169.

Deryagin, B.V. and Metsik, M.S., Soviet Physics Solid State, 1, 1393, 1960.

Deville, J.P., Eberhardt, J.P. and Goldsztaub, S., Compt. Rend. (Paris), 264, 124, 1967a and 264, 289, 1967b.

Dowsett, M.J., King, R.M. and Parker, E.H.C., J. Vac. Sci. Technol., 14, 711, 1977 and Surf. Sci., 71, 541, 1978.

Drushel, H.V. and Sommers, A.L., Anal. Chem., 38, 1723, 1966.

Dushmann, S. in "The Production and Measurement of High Vacuum", Gen. Elec. Rev., 1922.

Eastwood, S.C., Drew, R.D. and Hartzell, F.D., Oil Gas J., 60, 152, 1962a.

Eastwood, S.C. with Elliott, K.M., Oil Gas J., 60, 142, 1962b.

Ebel, M.F. and Ebel, H., J. Electron Spectrosc. Rel. Phen., 3, 169, 1974.

Elliot, A.G., Surf. Sci., 44, 337, 1974.

Evans, S., Pritchard, R.G. and Thomas, J.M., J. Phys. C10, 2483, 1977 and J. Electron Spectrosc. Rel. Phen., 14, 341, 1978.

Evans, S., Raftery, E. and Thomas, J.M., Surf. Sci., 89, 64, 1979a.

Evans, S., Adams, J.M. and Thomas, J.M., Phil. Trans. Roy. Soc., 292, 563, 1979b.

Evans, S. and Raftery, E., Clay Minerals, 17, 443, 1982.

Fink, P., Z. Chem., 7, 324, 1967.

Finster, J. and Lorenz, P., Chem. Phys. Lett., 50, 223, 1977.

Forni, L., Catal. Rev., 8, 65, 1974.

Förster, H. and Seebode, J., Zeolites, 3, 63, 1983.

Frenkel, M., Clays and Clay Minerals, 22, 435, 1974.

Frenkel, M., and Heller-Kallai,L., Clays and Clay Minerals, 31, 92, 1983.

Freude, D., Oehme, W., Schmiedel, H. and Staudte, B., J. Catal., 32, 137, 1974.

Fripiat, J.J., Catal. Rev., 5, 269, 1971.

Gaede, Ann. Physik, 6, 129, 1913.

Gaines, G.L. and Tabor, D., Nature, 178, 1304, 1956.

Ganguly, A.K., Soil Sci., 71, 239, 1951.

Gati, G. and Knözinger, H., 5th Int. Cong. Catal., Miami Beach, Florida 1972, 1, 819, 1973.

Gatineau, L. and Méring, J., Clay Min. Bull., 3, 238, 1958.

Gay, I.D. and Liang, S., J. Catal., 44, 306, 1976.

Gelius, U., Hedén, P.F. Hedman, J., Lindberg, B.J., Manne, R., Nordberg, R., Nordling, C. and Siegbahn, K., Physica Scripta, 2, 70, 1970.

George, Z.M. and Habgood, H.W., J. Phys. Chem., 74, 1502, 1970.

Gerberich, H.R. and Hall, W.K., J. Catal., 5, 99, 1966.

Ghorbel, A., Hoang-Van, C. and Teichner, S.J., J. Catal., 33, 123, 1974.

Giannetti, J.P. and Fisher, D.C., Amer. Chem. Soc. Div. Pet. Chem. Prepr., 20(2), 52, 1975.

Goldstaub, S. et al., C.R. Acad. Sci., (Paris), 262, 1718, 1966.

Goldstein, M.S. in "Experimental Methods in Catalytic Research", Academic Press, N.Y., 1968, p.361.

Goldstein, M.S. and Morgan, T.R., J. Catal., 16, 232, 1970.

Gregory, J.C., Ph.D. Thesis, University of London, 1967.

Grinnard, C.R. and Riggs, H.M., Anal. Chem., 46, 1306, 1974.

Gross, T., Lohse, U., Engelhardt, G., Richter, K.H. and Patzelová, V., Zeolites, 4, 25, 1984.

Güven, N., Clays and Clay Minerals, 19, 159, 1971.

Haag, W.O., Lago, R.M. and Weisz, P.B.,Nature, (London), 309 (5969), 589, 1984.

Hall, W.K., Leftin, H.P., Chiselke, F.J. and O'Reilley, D.E., J. Catal., 2, 506, 1963.

Hall, W.K., Lutinski, F.E. and Gerberich, H., J. Catal., 3, 512, 1964.

Hall, W.K. with Larson, J.G. and Gerberich, H.R., J. Am. Chem. Soc., 87, 1880, 1965.

Hansford, R.C., Adv. Catal., 4, 17, 1952.

Hattori, H., Milliron, D.L. and Hightower, J.W., J. Am. Chem. Soc., Div. Pet. Chem. Prepr., 28, 33, 1973.

Haynes Jr., H.W., Catal. Rev. Sci. Eng., 17, 290, 1978.

Hayward, D.O. and Taylor, N., J. Sci. Instr., 43, 762, 1966.

Hayward, D.O. and Walters, M.R., Proc. 2nd Int. Conf. on Solid Surfaces, Jap. J. Appl. Phys. Suppl. 2, part 2, 1974, p.587.

Heinemann, H. in "Catalysis: Science and Technology" (J.R. Anderson and M. Boudart, eds.), Springer-Verlag, Berlin, 1981, p.1.

Heinerman, J.J.L., Freriks, I.L.C., Gaaf, J., Pott, G.T. and Coolegem, J.G.F., J. Catal., 80, 145, 1983.

Herz, H., Conrad, H. and Küppers, J., J. Phys. E, Sci. Instrum., 12, 369, 1979.

Hidalgo, C.V., Itoh, H., Hattori, T, Niwa, M. and Murakami, Y., J. Catal., 85, 362, 1984.

Hightower, J.W. and Hall, W.K., J. Am. Chem. Soc., 90, 851, 1968.

Hindlin, S.G. and Weller, S.W., J. Phys. Chem., 16, 1501, 1956.

Hines, R.L., J. Phys., 25, 134, 1964.

Hirschler, A.E., J. Catal., 2, 428, 1963.

Holm, V.C.F. and Clark, A.J., J. Catal., 2, 16, 1963.

Huchital, D.A. and McKeon, R.T., Appl. Phys. Lett., 20, 158, 1972.

Hughes, T.R. and White, H.M., J. Phys. Chem., 71, 2192, 1967.

Hunt, C.P., Stoddart, C.T.H. and Seah, M.P., Surf. Interface Anal., 3, 157, 1981.

Ito, M., Matsura, K., Yoshii, Y., Igarashi, K. and Suzuki, A., 1969 from "Solid Acids and Bases", by K. Tanabe, Kodansha, Tokyo, 1970, p.46.

Itoh, H., Hidalgo, C., Hattori, T., Niwa, M. and Murakami, Y., J. Catal., 85, 521, 1984.

Jackson, W.W. and West, J., Z. Kristallogr., 76, 211, 1930 and 85, 160, 1933.

Jaeger, H., Mercer, P.D. and Sherwood, R.G., Surf. Sci., 6, 309, 1967.

Johnson, O., J. Phys. Chem., 59, 827, 1965.

Kantschewa, M., Albano, E.V., Ertl, G. and Knözinger, H., Appl. Catal., 8, 71, 1983.

Kawakami, H., Yoshida, S. and Yonezawa, T., J.C.S. Faraday Trans. 2, 80, 205, 1984.

Kerr, G.T., Miale, J.N. and Mikovksy, R.J., U.S. Patent 3, 493, 519, 1970.

Khulbe, K.C., Mann, R.S. and Manoogian, A., Zeolites, 3, 360, 1983.

King, D.A., Surf. Sci., 47, 384, 1975.

Kiricsi, I., Hannus, I., Varga, K. and Fejes, P., J. Catal., 63, 501, 1980.

Knecht, J. and Stork, G., Z. anal. chemie 283, 105, 1977; 286, 44, 1977, and 286, 47, 1977.

Knözinger, H. and Ratnasamy, P., Catal. Rev. Sci. Eng., 17, 31, 1978.

Kohiki, S. and Oki, K., J. Electron Spectrosc. Rel. Phen., 33, 375, 1984.

Koppelman, M.H., in "Advanced Chemical Methods for Soil and Clay Minerals Research" (J.W. Stucki and W.L. Banwart, eds.), D. Reidel, 1980, p.205.

Kotsarenko, N.S., Karakchiev, L.G. and Dzisko, V.A., Kinetika i Kataliz, 9, 158, 1968.

Krivanek, M., Jiru, P. and Strnad, J., J. Catal., 23, 259, 1971.

Kubokawa, Y., J. Phys. Chem., 67, 769, 1963.

Kuhl, G.H., J. Phys. Chem. Solids, 38, 1259, 1977.

Lawson, R.W., Vacuum, 12, 145, 1962.

Leck, J.H. in "Pressure Measurement in Vacuum Systems", Chapman & Hall, London, 1964.

Leftin, H.P. and Hobson Jr., M.C., Adv. Catal., 14, 115, 1963.

Leonard, A.J., Ratnasamy, P., Declerek, F.D. and Fripiat, J.J., Discuss. Faraday Soc., 52, 98, 1971.

Lercher, J.A., Colombier, C. and Noller, H., J.C.S. Faraday Trans. 1, 80, 949, 1984.

Lerot, L., Poncelet, G., Debru, M.L. and Fripiat, J.J., J. Catal., 37, 396, 1975.

Lewis, B. and Anderson, J.C. in "Nucleation and Growth of Thin Films", Academic Press, N.Y., 1978, p.29.

Lewis, R.T. and Kelly, M.A., J. Electron Spectrosc. Rel. Phen., 20, 105, 1980.

Löffler, D., Haller, G.L. and Fenn, J.B., J. Catal., 57, 96, 1979.

Loper, B.H., Oil Gas J., 53(51), 115, 1955.

Lunsford, J.H., Zingery, L.W. and Rosynek, M.P., J. Catal., 38, 179, 1975.

Madema, J., Van Bokhoven, J.J.G.M. and Kuiper, A.E.T., J. Catal., 25, 238, 1972.

Mapes, J.E. and Eischens, R.P., J. Phys. Chem., 58, 1059, 1954.

Mauguin, C., C.R. Acad. Sci., (Paris), 185, 288, 1927 and 186, 879, 1928, and 186, 1131, 1928.

Mercer, P.D., Vacuum, 17, 267, 1967.

Minchev, K.M. and Isakov, Y.I. in "Zeolite Chemistry and Catalysis", ACS Monograph 171, Amer. Chem. Soc., Washington D.C., 1976, (J.A. Rado, ed.), p.552.

Mirodatos, G., Pichat, P. and Barthomeuf, D., J. Phys. Chem., 80, 1335, 1976a.

Mirodatos, C., Abou Kais, A., Vedrine, J.C. Pichat, P. and Barthomeuf, D., J. Phys. Chem., 80, 2366, 1976b.

Mirodatos, C. and Barthomeuf, D., J.C.S., Chem. Commun., 2, 39, 1981.

Mizuno, K., Take, J. and Yoneda, Y., Bull. Chem. Soc. (Japan), 49, 634, 1976.

Mochida, I., Uchino, A., Fujitso, H. and Takeshita, K., J. Catal., 51, 72, 1978.

Morimoto, T., Imai, J. and Nagao, M., J. Phys. Chem., 78, 704, 1974.

Morrow, B.A. and Cody, I.A., J. Phys. Chem., 79, 761, 1975; 80, 1995, 1976a and 80, 1995, 1976b.

Morterra, C., Zecchina, A., Coluccia, S. and Chiorino, A., J.C.S. Faraday Trans. 1, 73, 1544, 1977.

Morterra, C., Chiorino, A., Chiotti, G. and Garrone, E., J.C.S. Faraday Trans. 1, 75, 271, 1979.

Mortland, M.M., Fripiat, J.J., Chaussidon, J. and Uytterhoeven, J., J.Phys. Chem., 67, 248, 1963.

Mortland, M.M., 9th Int. Cong. Soil Sci., 1, 691, 1968a.

Mortland, M.M. and Raman, K.V., Clays and Clay Miner. 16, 393, 1968b.

Müller, K., Z. Physik, 195, 105, 1966.

Müller, K. and Chang, C.C., Surf. Sci., 8, 455, 1968 and 14, 39, 1969.

Müller, G., Appl. Phys., 10, 317, 1976.

Myers, C.G., Rope, B.W. and Garwood, W.E., U.S. Patent 3, 384, 572, 1968.

Nguyen, T.T., Cooney, R.P. and Curthoys, G., J. Catal., 44, 81, 1976.

Ogilvie, J.J. and Wolberg, A., Appl. Spectrosc., 26, 401, 1972.

Palmer, D.A. and van Eldik, R., Chem. Rev., 83, 651, 1983.

Parkyns, N.D., J. Phys. Chem., 75, 526, 1971.

Parra, C.F., Ballivet, D. and Barthomeuf, D., J. Catal., 40, 52, 1975.

Parry, E.P., J. Catal., 2, 371, 1963.

Pauling, L., Proc. Nat. Acad. Sci., 16, 123, 1930.

Pearson, R.M., J. Catal., 46, 279, 1977.

Peri, J.B., J. Phys. Chem., 69, 231, 1965 and 70, 3168, 1966.

Pines, H. and Haag, W.O., J. Am. Chem. Soc., 82, 2471, 1960a and 82, 2488, 1960b.

Plank, C.J., Rosinsky, E.J. and Hawthorne, W.P., Ind. Eng. Chem., Prod. Res. Devel., 3, 165, 1964.

Poppa, H. and Elliot, A.G., Surf. Sci., 24, 149, 1971.

Poppa, H. and Lee, E.H., Thin Solid Films, 32, 223, 1976.

Post, J.G. and van Hooff, J.H.C., Zeolites, 4,9, 1984.

Poutsma, M.L. in "Zeolite Chemistry and Catalysis", ACS Monograph 171 (J.A. Rabo, ed.), Am. Chem.Soc., Washington D.C., 1976, p.437.

Prada-Silva, G., Löffler, D., Halpern, B.L., Haller, G.L. and Fenn, J.B., Surf. Sci., 83, 453, 1979.

Rabo, J.A., in "Zeolites: Science and Technology", NATO ASI Ser., Ser.E, 80, 291, 1984.

Radoslovich, E.W., Nature (London) 183, 253, 1959; Acta Crystallogr., 13, 919, 1960 and Amer. Min., 47, 617, 1962a.

Radoslovich, E.W. and Norrish, K., Amer. Min., 47, 599, 1962b.

Radoslovich, E.W., Proc. Int. Clay Conf., Stockholm, Pergamon Press, 1963, p.3.

Ramqvist, L., Hamrin, K., Johansson, G., Fahlman, A. and Nordling, C., J.Phys. Chem. Solids, 30, 1835, 1969.

Redhead, P.A., Vacuum, 12, 203, 1962.

Reed, A.P.C. and Lambert, R.M., J. Phys. Chem., 88, 1954, 1984.

Rhodin, T.N. and Adams, D.L. in "Treatise on Solid State Chemistry", Vol. 6A, Surfaces I (N.B. Hannay, ed.), Plenum Press, 1976, p.374.

Robschlager, K.H.W., Emeis, C.A. and van Santen, R.A., J. Catal., 86, 1, 1984.

Rogers Jr., J.W., Campbell, C.T., Hance, R.L. and White, J.M., Surf. Sci., 97, 425, 1980.

Ryland, L.B., Tamele, M.W. and Wilson, J.N. in "Catalysis", Vol. VII, (P.H. Emmett, ed.), Reinhold Publishing Corp., N.Y., 1960, p.1.

Salmeron, M. and Somorjai, G.A., J. Phys. Chem., 84, 341, 1982.

Satterfield, C.N. and George, C.T., Amer. Inst. Chem. Engineers J., 20, 522, 1978

Schobert, M.A. and Ma, Y.H., J. Catal., 70, 111, 1981.

Schultz, H.D., Vesely, C.J. and Langer, D.W., Appl. Spectrosc., 28, 374, 1974.

Schwarz, J.A., J. Vac. Sci. Technol., 12, 321, 1975.

Schwarz, J.A., Russell, B.G. and Hamberger, H.F., J. Catal., 54, 303, 1978.

Seyama, H. and Soma, M., J.C.S. Faraday Trans. 1, 80, 237, 1984.

Shiba, T., Sato, M., Hattori, H. and Yashida, K., 1964, from "Solid Acids and Bases" by K. Tanabe, Kodansha, Tokyo, 1970, p.59.

Siegbahn, K., Nordling, C., Fahlman, A., Nordberg, R., Hamrin, K., Hedman, J., Johansson, G., Bergmark, T., Karlsson, S.E., Lindgren, I. and Lindberg, B.J., Nova Acta Regiae Soc. Sci., Upsaliensis, Ser. IV, Vol. 20, 1967.

Smith, J.V. and Yoder, H.S., Min. Mag., 31, 209, 1956.

Solomon, D.H., Swift, J.D. and Murphy, A.J., J. Macromol. Sci. Chem., A5, 587, 1971.

Solomon, D.H. and Murray, H.H., Clays and Clay Minerals, 20, 135, 1972.

Somorjai, G.A., Proc. 9th Int. Conf. on Atomic Spectroscopy, XXII CSI, Tokyo, 1981, Pure and Applied Chem.

Spencer, M.S. and Whittam, T.V., Specialist Periodical Reports, The Chemical Society, Catalysis, Vol.3, 1980, p.208.

Staib, P., Radiation Effects, 18, 217, 1973.

Suib, S.L., Stucky, G.D. and Blattner, R.J., J. Catal., 65, 174, 1980.

Swift, H.E. and Black, E.R., Ind. Eng. Chem., Prod. Res. Devel., 13, 106, 1974.

Swift, P., Surf. Interface Anal., 4, 47, 1982.

Swift, P., Shuttleworth, D. and Seah, M.P., in "Practical Surface Analysis by Auger and X-ray Photoelectron Spectroscopy", (D. Briggs and M.P. Seah, eds.), John Wiley & Sons Ltd., 1983, p. 437.

Takahashi, M., Iwasawa, Y. and Ogasawara, S., J. Catal., 45, 15, 1976.

Takeda, H. with Ross, M. and Wones, D.R., Science, N.Y., 151, 191, 1966.

Takeda, H. and Sadanga, R., Mineralogy J., 5, 434, 1969.

Takeda, H., Am. Miner., 56, 1042, 1971.

Take, J., Nomizo, Y. and Yoneda, Y., Bull. Chem. Soc. Japan, 46, 3568, 1973.

Tam, N.T., Cooney, R.P. and Curthoys, G., J. Catal., 44, 81, 1976.

Tamele, M.M., Discuss. Faraday Soc., 8, 270, 1950.

Tanabe, K,., "Solid Acids and Bases", Kodansha, Tokyo, 1970.

Tanaka, K., Miyahara, K. and Toyashima, I., J. Phys. Chem., 88, 3504, 1984.

Tempere, J.F., Delafosse, D. and Contour, J.P., Chem. Phys. Lett., 33, 95, 1975.

Thomas, C.L., Ind. Eng. Chem., Prod. Res. Devel., 41, 2564, 1949.

Tolansky, S. in "Multiple Beam Interferometry of Surfaces and Films", Clarendon Press, 1948.

Topsøe, N.Y., Pederson, K. and Derouane, E.G., J. Catal., 70, 41, 1981.

Uwamine, Y., Ishizuka, T. and Yamatera, H., J. Electron Spectrosc. Rel. Phen., 23, 55, 1981.

Uytterhoeven, J.B., Christner, L.G. and Hall, W.K., J. Phys. Chem., 69, 2117, 1965.

Vedder, W. and Wilkins, R.W.T., Amer. Miner., 54, 482, 1969.

Vinek, H., Noller, H., Ebel, M. and Schwarz, K., J.C.S. Faraday Trans. 1, 73, 734, 1977.

Vinek, H., Latzel, J., Noller, H. and Ebel, M., J.C.S. Faraday Trans. 1, 74, 2092, 1978.

Vit, Z., Vala, J. and Malek, J., Appl. Catal., 7, 159, 1983.

Wagner, C.D., "Applied Surface Analysis", ASTM STP 699, American Society for Testing Materials, Philadelphia, 1980.

Wagner, C.D. and Taylor A.T., J. Electron Spectrosc. Rel. Phen., 20, 83, 1980.

Wagner, C.D., Davis, L.E., Zeller, M.V., Taylor, J.A., Raymond, R.M. and Gale, L.H., Surf. Interface Anal., 3, 211, 1981.

Wagner, C.D., Passoja, D.E., Hillery, H.T., Kinisky, T.G., Six, H.A., Jansen, W.T. and Taylor, J.A., J. Vac. Sci. Technol., 21, 933, 1982.

Walling, C., J. Am. Chem. Soc., 72, 1164, 1950.

Walters, M.R., Ph.D Thesis, University of London, 1973.

Ward, J.W. and Habgood, H.W., J. Phys. Chem., 70, 1178, 1966.

Ward, J.W., J. Catal., 9, 225, 1967.

Ward, J.W., J. Catal., 11, 259, 1968.

Ward, J.T. and Hansford, R.C., J. Catal., 13, 154, 1969.

Ward, J.W. in "Zeolite Chemistry and Catalysis", (J.A. Rabo, ed.), ACS Monograph 171, Amer.Chem.Soc., Washington, D.C., 1976, p.118.

West, P.B., Haller, G.L. and Burwell, R.L., J. Catal., 29, 486, 1973.

Weston, G.F., Vacuum, 29, 290, 1979.

Whitmore, F.C., Ind. Eng. Chem., 26, 94, 1934.

Wright, A.C., Granquist, W.T. and Kennedy, J.V., J. Catal., 25, 65, 1972.

Yoder, H.S. and Eugster, H.P., Geochim. Cosmochim. Acta, 8, 225, 1955.

Young, G.J., J. Colloid Sci., 13, 67, 1958.

Zhixing, C., Zhengwu, W., Ruiya, H. and Yala, Z., J. Catal., 79, 271, 1983.